University of Neuchâtel

Centre of Hydrogeology

Origin and Behaviour of Microorganisms and Particles in Selected Karst Aquifer Systems

PhD thesis presented to the Faculty of Sciences of the University of Neuchâtel
to satisfy the requirements of the degree of Doctor of Philosophy in Science

by

Michiel Pronk

Thesis defence date: 27 November 2008
Public presentation date: 6 March 2009

PhD thesis evaluation committee:

Prof. François Zwahlen	University of Neuchâtel, Switzerland	Thesis director
Dr. Nico Goldscheider	University of Neuchâtel, Switzerland	Thesis co-director
Prof. Peter Germann	University of Bern, Switzerland	Jury member
Dr. Ronald Kozel	Federal Office for the Environment, Switzerland	Jury member
Prof. Jacques Mudry	University of Franche-Comté, France	Jury member
Dr. Jakob Zopfi	University of Lausanne, Switzerland	Jury member

Université de Neuchâtel unine

FACULTE DES SCIENCES
Secrétariat-Décanat de la faculté
- Rue Emile-Argand 11
- CP 158
- CH-2009 Neuchâtel

IMPRIMATUR POUR LA THESE

Origin and behaviour of microorganisms and particles in selected karst aquifer systems

Michiel PRONK

UNIVERSITE DE NEUCHATEL

FACULTE DES SCIENCES

La Faculté des sciences de l'Université de Neuchâtel,
sur le rapport des membres du jury

MM. F. Zwahlen (directeur de thèse),
J. Zopfi, N. Goldscheider, J. Mudry (Besançon F),
R. Kozel (Berne) et P. Germann (Berne)

autorise l'impression de la présente thèse.

Neuchâtel, le 20 février 2009

Le doyen :
F. Kessler

UNIVERSITE DE NEUCHATEL
FACULTE DES SCIENCES
Secrétariat - décanat de la faculté
Rue Emile-Argand 11 - CP 158
CH-2009 Neuchâtel
felix Kessler

■ Téléphone : +41 32 718 21 00 ■ E-mail : secretariat.sciences@unine.ch ■ www.unine.ch/sciences

This research project was funded by the Swiss National Science Foundation (grants n°: 200020-105427 and 200020-113609). It was carried out at the Centre of Hydrogeology (CHYN) and the Laboratory of Microbiology (LAMUN) of the University of Neuchâtel (Switzerland).

Remerciements

Quelques quatre années après le début de ce projet de recherche, j'en arrive à cette difficile et ultime tâche de rédaction des remerciements. A travers ces quelques lignes, je tiens à exprimer ma profonde gratitude à mes collègues et amis qui ont contribué à la réussite de ce travail.

Je commence tout naturellement par Nico Goldscheider, co-directeur de cette thèse, qui est à la base de ce projet de recherche et de la réussite de ce travail. Je le remercie vivement pour la confiance qu'il a su montrer à mon égard pendant toutes ces années de recherche et pour ses encouragements et conseils en permanence, tout en me laissant une grande liberté dans la réalisation de ce projet.

Je tiens tout particulièrement à remercier Jakob Zopfi pour m'avoir appris tout les secrets de la microbiologie et pour sa grande disponibilité. Les longues discussions « microbio-hydrogéologiques » que nous avons eues tout au long de ces quatre ans ont été plus que constructives, enrichissantes et passionnantes.

Je tiens ensuite à exprimer mes sincères remerciements et toute mon admiration à François Zwahlen, directeur de cette thèse et surtout directeur du CHYN.

J'aimerais également remercier le Prof. Peter Germann de l'Université de Berne, le Dr. Ronald Kozel de l'Office fédéral de l'environnement et le Prof. Jacques Mudry de l'Université de Franche-Comté, qui ont accepté d'être membres du jury de thèse.

Toute ma gratitude va aussi à Marie-Eve Wyniger, laborantine au CHYN, ainsi qu'à toutes les personnes du labo de microbiologie (LAMUN), en particulier Vanessa Di Marzo, Nicole Jeanneret, Alexis Walter, Sylvia Humbert et Sonia Tarnawski, qui m'ont toujours précieusement conseillé.

Un grand merci également à toutes les personnes qui m'ont accompagné sur le terrain. Je ne saurais oublier ces mythiques journées passées sur le terrain avec François Gainon (vive la Passion Forêt!), toujours un agréable moment de détente. Je remercie aussi Ludovic Savoy pour m'avoir fait découvrir les sites de Vers-chez-le-Brandt, Grand-Bochat et Gänsbrunnen. Les durs départs sur le terrain à 04h00, les grillades de midi, ainsi que les rentrées à 02h00 le lendemain resteront d'excellents souvenirs.

Je tiens également à remercier chaleureusement mes collègues et amis du fameux bureau E210 pour la bonne ambiance tout au long de ces années: Jaouher Kerrou (les apéros au bureau dans la phase finale de la rédaction de ce manuscrit resteront de grands souvenirs), Alessandro Comunian, Antoine Baillieux et Denis Blant.

Je remercie aussi tous mes collègues du CHYN, d'une part pour la très agréable ambiance de travail qui y règne, et d'autre part pour les nombreux coups de mains sans lesquels cette thèse ne serait probablement pas ce qu'elle est. A savoir, Pierre Schnegg et Roberta Costa (pour le développement du fameux fluorimètre de terrain), François Bourret (pour toutes les installations d'appareils de mesure et son immense « know-how » du karst), Ellen Milnes (pour sa patience et ses précieuses corrections), ainsi que tous les doctorants, notamment Romain Ducommun, Pascale Ducommun, Xanthippe Boutsiadou, Vincent Badoux, Domagoj Babic, Vivian Gremaud, Daniel Bouchard, Alain Pochon, Michael Sinreich et Rob de Rooij.

Mes remerciements vont également au Service des Energies de la ville d'Yverdon-les-Bains (SEY), et tout particulièrement à Olivier Flueckiger. Leur soutien financier et logistique ainsi que leur intérêt porté à cette étude ont su me motiver tout au long de ces années.

Ma sincère reconnaissance va aussi à Pascal Piguet, pour les nombreux « cafés'scientifiques » qui ont permis à cette thèse d'avancer, ainsi qu'à mes amis de longue date Julien Tschirren, Lukas Bitter, Jeremy Blatti, Juan Bravo et Gérard Meystre.

Mes parents, Karel et Christa, ainsi que ma sœur Caroline, que je ne saurais assez remercier pour leur inestimable soutien apporté durant toutes ces années d'études.

Enfin, « *last but not least* », je tiens à sincèrement remercier Fanny. Cette thèse doit énormément à son soutien et ses encouragements tout au long de ces quatre années de travail.

Abstract

Karst aquifers represent an important groundwater resource world-wide. They are, however, highly vulnerable to contamination due to fast transport and limited contaminant attenuation processes encountered in such systems.

Pathogenic microorganisms are among the most frequent and problematic contaminants in groundwater from karst aquifers. It is generally accepted that the presence of faecal indicator bacteria, such as *Escherichia coli* and enterococci, in groundwater indicates the possible presence of pathogenic bacteria, protozoa and viruses. Monitoring microbial water quality relies, however, on sterile water sampling and subsequent laboratory analyses. Moreover, the sampling intervals and the relatively long time lag between sampling and results are often too long to prevent microbially polluted water entering the distribution network. Therefore, establishing a correlation between the microbial water quality and parameters that can easily be measured online – using it as an "early-warning" parameter – constitutes the first main objective of this work.

Most microorganisms in groundwater are harmless. Enumeration of pathogenic and water quality indicator bacteria thus provides an incomplete picture of the microbial assemblages. These microbial communities are of growing interest, as aquifers, which include habitats for a wide range of organisms, are increasingly considered as ecosystems harbouring their proper biocenoses. These ecosystems have to be better understood in order to ensure the sustainable management of groundwater resources. Furthermore, as bacteria are abundant and ubiquitous, thriving even in extreme habitats, the potential use of microbial communities for groundwater biomonitoring has been raised. However, the understanding of microbial diversity, their distribution patterns and their dynamics in karst aquifer ecosystems are actually still in an early stage and rather sparse and constitute therefore the second main objective of this research project.

The occurrence, dynamics and transport processes of suspended matter and faecal indicator bacteria were investigated at two karst aquifer systems (the Yverdon-les-Bains and Noiraigue test sites, Switzerland), which are characterised by allochthonous point recharge, and several shallow cave sites located in the unsaturated zone of karst aquifers (the Vers-chez-le-Brandt, Grand-Bochat and Gänsbrunnen test sites, Switzerland). Classical hydrogeological parameters, such as discharge, temperature, electrical conductivity, organic carbon and turbidity, were monitored continuously online, along with event-based, high-frequency analyses of *Escherichia coli* and enterococci. In order to gain more insight into the origin and behaviour of suspended particles in karst groundwater, particle-size distribution (PSD) was also monitored continuously.

Results demonstrated that suspended particles in karst spring water either originated from the remobilisation and scouring of intrakarstic particulate material due to increasing flow velocities (i.e. autochthonous turbidity) and / or the transfer of particles from land surface and sinking

streams (i.e. allochthonous turbidity), which entered the system following rainfall events. These allochthonous turbidity events coincided with increased faecal indicator bacteria and organic carbon levels. PSD allowed distinguishing both types of turbidity: autochthonous turbidity consisted of particle concentration increases over a wide range of particle sizes (from colloidal sizes up to 0.1 mm), whereas allochthonous turbidity periods were characterised by a predominance of finer particles (0.9 to 10 µm). PSD is therefore proposed as surrogate indicator for possible microbial contamination of groundwater from karst aquifers.

The structure, diversity and temporal variability of microbial communities from a swallow hole draining agricultural land and two connected karst springs (Yverdon-les-Bains karst aquifer system) were investigated using molecular microbiological methods (PCR-DGGE and cloning / sequencing) and related to hydrological and physico-chemical parameters. Storm responses and an annual hydrological cycle were monitored to determine the short- and long-term variability, respectively, of bacterial communities.

Statistical analysis of bacterial genetic fingerprints (16S rDNA PCR-DGGE profiles) of spring water samples revealed several clusters that corresponded well with different levels of the allochthonous swallow hole contribution. Microbial communities in spring water samples highly affected by the swallow hole showed low similarities among them, reflecting the high temporal variability of the bacterial communities in the water entering the swallow hole. Conversely, high similarities among spring water samples with low allochthonous contribution provided evidence for a stable autochthonous endokarst microbial community. This autochthonous endokarst microbial community was characterised by a high diversity with only a few dominant species. *δ-Proteobacteria*, *Acidobacteria* and *Nitrospira* species were important members of this community. The high percentage of unknown sequences (i.e. sequences revealing similarities lower than 97 % to already known sequences) suggests that many karst aquifer bacteria are still undiscovered. Moreover, it highlights that karst aquifers are rarely studied, unique habitats and that sequences from shallow subsurface ecosystems are currently underrepresented in databases.

In conclusion, the high sensitivity of PSD analysis allows consequently proposing it as an “early-warning” surrogate for real-time monitoring of possible microbial contamination of groundwater from karst aquifers. The method permits optimising water treatment and identifying periods when spring water must be rejected. Furthermore, this study represents a first step towards a better understanding of the microbial ecology in karst aquifer systems and may serve as a starting point for developing biomonitoring tools.

Keywords: karst hydrology; total organic carbon; turbidity; particle-size distribution (PSD); faecal indicator bacteria; unsaturated zone; subsurface microbiology; ecology; PCR-DGGE; cloning / sequencing.

Origin and Behaviour of Microorganisms and Particles in Selected Karst Aquifer Systems

Table of contents

1

Introduction

1.1 BACKGROUND

Karst aquifers are among the most important drinking water resources throughout the world, supplying about 25 % of the global population (Ford and Williams 1989). In some European countries, carbonate aquifers even contribute to as much as 50 % of the total drinking water supply (e.g. Austria and Slovenia). Despite their important contribution to freshwater supply, karst aquifers – because of their specific hydrological and hydrogeological features – are particularly vulnerable to contamination (e.g. Zwahlen 2004). In contrast to other types of aquifers, the effectiveness of many of the natural contaminant attenuation processes is reduced in karst aquifers. During recharge periods, chemical and microbiological contaminants, which originate principally from industrial and agricultural activities, may be introduced into the aquifer, either diffusely by infiltration and percolation through shallow soils and the unsaturated zone or concentrated via sinking streams. These contaminants may then be rapidly transported in the saturated zone, through the active conduit networks of karst systems, towards water abstraction points.

1.2 AIM AND STRUCTURE OF THE THESIS

Pathogenic microorganisms in drinking water represent not only a major health risk in developing countries (e.g. Montgomery and Elimelech 2007) but are also a concern in developed nations (e.g. Herwaldt *et al*. 1992; Kramer *et al*. 2001). In groundwater from karst aquifers, microbial pathogens are among the most frequent and problematic contaminants (Auckenthaler and Huggenberger 2003). Although most microorganisms are harmless, the presence of faecal "index" or "indicator" bacteria (e.g. *Escherichia coli* and enterococci) in groundwater indicates the possible presence of pathogenic bacteria, protozoa and / or viruses (Auckenthaler *et al*. 2002). However, monitoring microbial water quality relies on sterile water sampling and subsequent laboratory analyses. The sampling intervals and the time lag between sampling and results are, due to the generally rapid and strong variations of flow conditions and water quality in karst aquifers (e.g. Hunkeler and Mudry 2007), often too long to prevent microbially polluted water entering the distribution network. Conversely, various hydrological and physico-chemical properties can easily be measured *in situ* and continuously. If correlations between these "easy-to-

measure" parameters and microbial water quality were established, they could be used as indicators for the presence of microbial pathogens. This issue has caught the attention of many drinking water purveyors and scientists.

Suspended and dissolved matter in karst groundwater is either derived from the aquifer itself (autochthonous origin) or from outside, i.e. the land surface (allochthonous origin). In rural karst areas, faecal and pathogenic bacteria often originate from agricultural activities, such as cattle pasturing and the application of manure (Drew and Hötzl 1999), and are thus strictly of allochthonous origin. In groundwater, bacteria are mainly transported together with or attached to suspended particles (e.g. Hipsey *et al*. 2006; Mahler *et al*. 2000). Several authors therefore proposed turbidity as being an indicator of microbial contamination (e.g. Nebbache *et al*. 1997; Ryan and Meiman 1996). However, turbidity events occurring at karst springs may either result from the resuspension and scouring of intrakarstic particulate material, i.e. autochthonous turbidity, and / or the direct transfer of particles from the soil or sinking surface streams, i.e. allochthonous turbidity (Mahler and Lynch 1999; Massei *et al*. 2003). Consequently, turbidity monitoring alone does not allow identifying the origin and type of suspended particles; turbidity is therefore not always a reliable water quality indicator. More recently, Stadler *et al*. (2008) proposed total organic carbon (TOC) as an "early-warning" surrogate for real-time monitoring of faecal input. TOC principally originates from the soil and surface waters and is thus typically of allochthonous origin. However, as TOC behaves similarly to solutes in karst aquifers (e.g. Savoy 2007), their signals at karst springs often trail behind the faecal bacteria signals (Auckenthaler *et al*. 2002), whereas an ideal indicator should react simultaneously or even precede the contamination event.

Establishing a correlation between such "easy-to-measure" parameters and microbial water quality – using it as an "early-warning" parameter – forms the fundamental backcloth of this thesis. For that purpose, the occurrence, dynamics and transport processes of faecal indicator bacteria, suspended matter and various physico-chemical parameters in karst aquifers were investigated to identify a surrogate parameter.

It is increasingly recognised that aquifers should be considered as ecosystems harbouring their proper biocenoses (Danielopol *et al*. 2003; Hancock *et al*. 2005). These ecosystems have to be better understood in order to ensure the sustainable management of groundwater resources. This reasoning is also reflected in the Swiss Water Protection Ordinance (GSchV 1998), which demands, in order to improve water-quality standards, that the biocenoses in groundwater should be in a natural state, adapted to the habitat and characteristic of water that is not or only slightly polluted. Yet ecological studies in karst aquifers mainly dealt with invertebrates and larger animals (e.g. Vervier and Gibert 1991), microbial ecology research in such subsurface environments has mostly focused on caves within the unsaturated zone (e.g. Barton and Northup 2007) and on the role of specific bacteria in geochemical processes (e.g. Canaveras *et al*. 1999). However, as bacteria are abundant and ubiquitous, thriving even in extreme habitats such as contaminated, anoxic or thermal aquifers (e.g. Cho and Kim 2000; Engel *et al*. 2003; Kimura *et al*. 2005), the potential use of microbial communities for groundwater biomonitoring has been raised (Goldscheider *et al*. 2006; Steube *et al*. 2009).

Today's understanding of microbial diversity, their distribution patterns and their dynamics in karst aquifer ecosystems are, however, still in an early stage and rather sparse. This is why another objective of this research project was to investigate the structure, diversity and dynamics of microbial communities in karst aquifers.

The main body of the present thesis consists of four chapters. All four chapters are self-contained and are based on papers that have been published in peer-reviewed journals.

Chapter 2: **From quantitative tracer tests towards a conceptual flow model of the Yverdon-les-Bains karst aquifer system**. This chapter proposes a conceptual model of the functioning of the Yverdon-les-Bains karst aquifer system (Switzerland), based on results of several quantitative tracer experiments along with monitoring of physical, chemical and microbiological parameters. It will essentially provide the hydrogeological background of the investigated karst aquifer system, which will serve as a base for further investigations on the characterisation and dynamics of particles and microorganisms in karst aquifers (Chapters 3 and 5).

Chapter 3: **Particle-size distribution as indicator for faecal bacteria contamination of groundwater from karst springs**. This chapter investigates the occurrence and dynamics of suspended matter and faecal indicator bacteria in the Yverdon-les-Bains karst aquifer system. Additional monitoring of specific hydrological events undertaken at the Noiraigue karst aquifer system (Switzerland) is also presented. Autochthonous and allochthonous turbidity events occurring in the active conduit network of karst aquifers are identified and characterised by particle-size distribution (PSD) measurements. The contribution of PSD monitoring to assess microbial contamination occurring at karst groundwater abstraction points is demonstrated. Furthermore, the characterisation of suspended matter by PSD measurements allowed several aspects of particle transport and deposition processes in the saturated zone of karst aquifers to be inferred.

Chapter 4: **Percolation and particle transport in the unsaturated zone of karst aquifers**. This chapter focuses mainly on water percolation and the associated transport of particles and faecal indicator bacteria in the unsaturated zone of karst aquifers. The study was carried out at the Grand-Bochat and Vers-chez-le-Brandt cave sites and the artificial galleries near Gänsbrunnen (Switzerland). The monitoring of the responses of the water outlets in the caves to natural rainfall events and artificial irrigation experiments enabled a "phase-by-phase" conceptual flow model to be proposed; allowed differentiating the components contributing to percolation in the unsaturated zone; and allowed investigating the temporal variations of sediment particles in this zone, with the main focus on the mobilisation and transfer of particles and the associated microbial contaminants. This chapter provides furthermore observations on transport and exclusion mechanisms of particles in the unsaturated zone.

Chapter 5: **Microbial communities in karst groundwater and their potential use for biomonitoring**. This chapter investigates the structure, diversity and temporal variability of microbial communities in the Yverdon-les-Bains karst aquifer system using molecular microbiological methods. Changes in microbial communities at the springs are related to hydrological and physico-chemical parameters in order to differentiate between allochthonous bacteria from the land surface and autochthonous endokarstic bacteria. The autochthonous

endokarst microbial community is then characterised by identifying the most abundant bacterial components. Furthermore, the potential use of microbial communities for biomonitoring is discussed.

Chapter 6 summarises the main conclusions from the foregoing chapters and discusses the limitations and future perspectives.

The methodology relevant for each chapter is described in the respective "Material and methods" section. All calibration curves (e.g. stage-discharge rating curves, temperature and electrical conductivity calibration curves, etc.) are illustrated in appendix A. Appendices B, C, D and E are related to chapters 2, 3, 4 and 5, respectively.

1.3 STUDY AREAS

The five experimental sites that have been investigated within the framework of this study are located in western and north-western Switzerland (Fig. 1.1). The main test site is a karst aquifer system near the city of Yverdon-les-Bains. This karst aquifer system covers an area of roughly 40 km^2 astride on the Swiss Plateau and the south-east slope of the Jura Mountains. The Noiraigue karst aquifer system is located about 15 km west of the city of Neuchâtel, covering an area of 60 to 70 km^2 in the Jura Mountains. The small Vers-chez-le-Brandt and Grand-Bochat cave sites and the artificial galleries of Gänsbrunnen are located near the villages of Les Verrières, Les Ponts-de-Martel and Gänsbrunnen, respectively, also in the Jura Mountains.

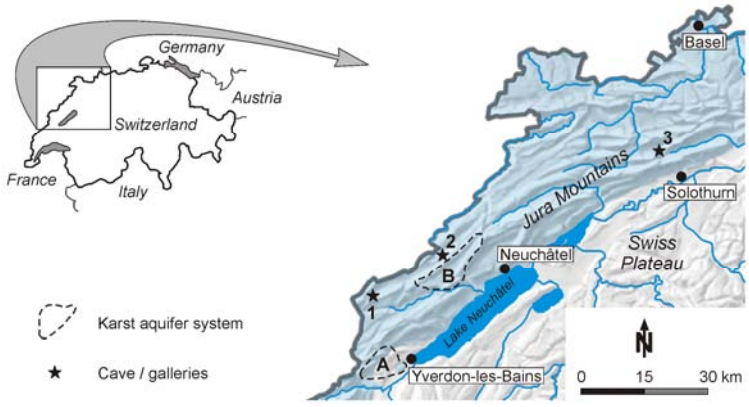

Fig. 1.1 Location of the study areas. **A**: Yverdon-les-Bains karst aquifer system; **B**: Noiraigue karst aquifer system; **1**: Vers-chez-le-Brandt cave site; **2**: Grand-Bochat cave site; **3**: Gänsbrunnen artificial galleries.

The Yverdon-les-Bains karst aquifer system being the main test site investigated during this study, its geological and hydrogeological setting is therefore described in detail below. The main geological and hydrogeological features of the other test sites are only briefly discussed here.

1.3.1 Yverdon-les-Bains karst aquifer system

The Yverdon-les-Bains karst aquifer system is located between two major landscape units: the Jura Mountains and the Swiss Plateau (Fig. 1.2). The Jura Mountains reach altitudes of more than 1500 m near the test site, while the altitude of the Swiss Plateau ranges between 430 and 600 m. Lake Neuchâtel forms the regional hydrologic base level at an altitude of approximately 430 m. Mean annual precipitation ranges between 900 mm on the Plateau and 1700 mm in the mountains.

This contrast in landscape also reflects the contrast between two major geological units: the folded Jura Mountains and the Molasse Basin. The Jura Mountains consist of Jurassic and Cretaceous limestone and marl. The strata were folded and thrusted at the end of the alpine orogenesis in the Miocene and Pliocene. The fold axes strike SW – NE. Towards the south-east, the strata plunge under the Molasse Basin, which is the northern foreland basin of the Alps and formed during the Oligocene and Miocene. In the study area, the Molasse is mainly composed of Chattian and Burdigalian marl and sandstone. Glacial and postglacial deposits cover wide areas of the Swiss Plateau. Two series of transpressive faults structure the region of Yverdon-les-Bains: E – W trending right-lateral thrust faults, which form the Pipechat – Chamblon – Chevressy (PCC) fault zone; and N – S trending left-lateral thrust faults, such as the Rances-Pipechat thrust fault and the western Chamblon thrust fault. This complex arrangement of faults along with the folding raised two hills (Pipechat and Mont de Chamblon), exposing in this way Jurassic and Cretaceous carbonate rocks within the Molasse zone (Jordi 1993; Muralt *et al*. 1997; Sommaruga 1997).

Overlying the impermeable Argovian marls, Upper Jurassic (Malm) limestones with a total thickness of about 400 m form the main regional karst aquifer. The Valanginian and Hauterivian

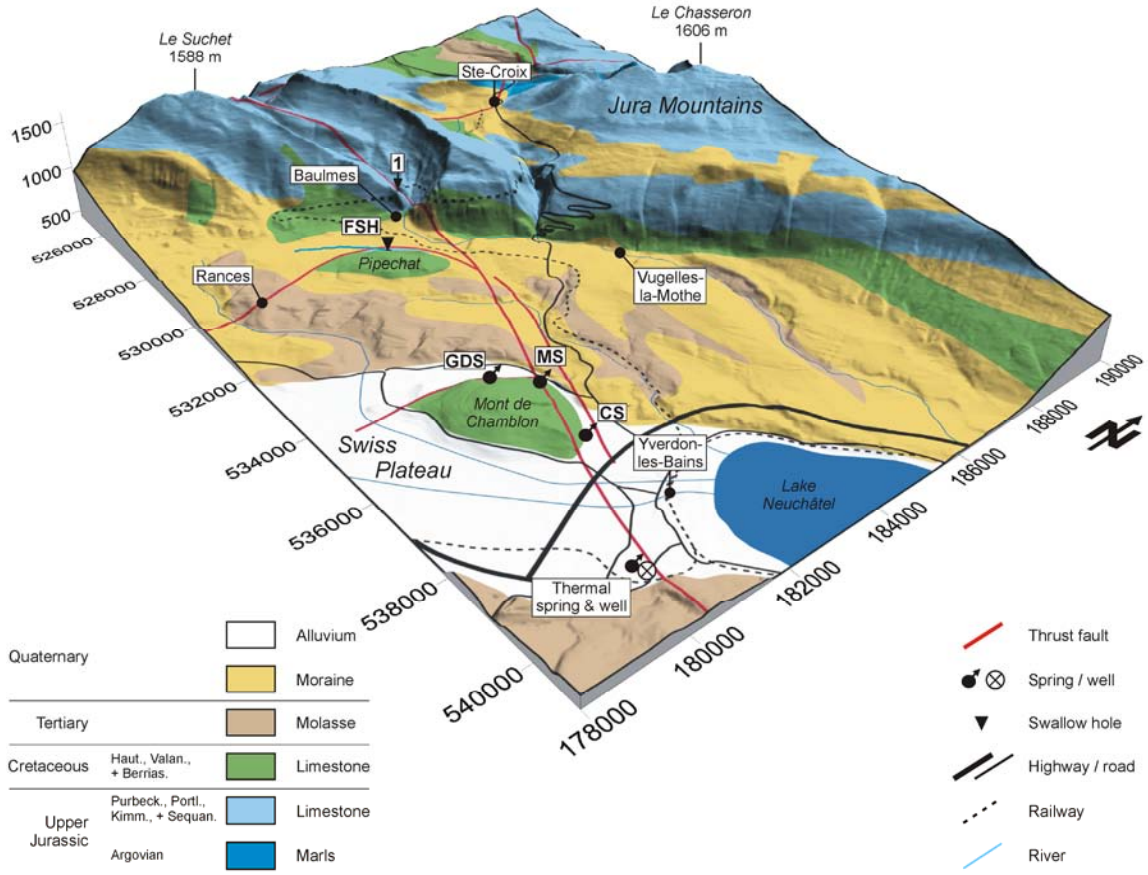

Fig. 1.2 Geological map of the Yverdon-les-Bains area (modified after Gainon 2008). **FSH**: Feurtille swallow hole; **CS**: Cossaux spring; **MS**: Moulinet spring; **GDS**: Grange-Décoppet spring; **1**: La Côte, injection point of regional tracer test (see Section 2.4.4). Latitudes and longitudes are given in Swiss coordinates in m. Altitudes are given in m (vertical exaggeration 2:1).

(Cretaceous) limestones, which are both approximately 30 – 60 m thick, are also karstified. These aquifers are separated by thin marl aquicludes. On the Swiss Plateau, the low-permeable Molasse marls and sandstones confine these aquifers. This is also attested by the presence of large karst springs at the foot of the Jura Mountains (e.g. Fontanney spring at Vugelles-la-Mothe). The vertical displacement of the PCC fault zone, estimated at about 700 m (Jordi 1993), separates the region in two hydrogeological systems (Muralt 1999), from which the southern compartment corresponds to the Yverdon-les-Bains karst aquifer system.

The south-east slope of the Jura Mountains between Le Suchet and the village of Baulmes, where the limestones crop out, is the most important autogenic recharge area of the Yverdon-les-Bains karst aquifer system (Muralt 1999). Large parts of this zone are forested, and recharge mainly occurs diffusely through the soil. There are consequently few contamination problems, resulting from some local cattle pasture. Further to the south-east, on the Swiss Plateau, where the Molasse sediments confine the karst aquifer system, the above mentioned hills act as hydrogeological windows. These hills allow, through the intermediate of the PCC fault zone, for water exchange between the land surface and the karst aquifer system.

The Feurtille swallow hole (Swiss coordinates: x: 530’575 / y: 181’840; Fig. 1.3a) is located at an altitude of 605 m at the western of these two hills (Pipechat), at the contact between the Molasse (covered with Quaternary sediments) and the Portlandian – Purbeckian (Malm) limestone. The stream sinking into this swallow hole drains an agricultural area of about 3 km² (Fig. 1.3b) and is frequently contaminated with high levels of turbidity, organic carbon, nitrate, faecal bacteria and probably other contaminants that were not analysed. The flow rate of the sinking stream ranges from 0 to more than 1000 L/s. Recharge via the swallow hole can be classified as allogenic point recharge.

About 5 km to the east, two major karst springs – the Cossaux and Moulinet springs – and several less important outlets are located at the northern base of the eastern hill (Mont de Chamblon) and discharge from Valanginian and Hauterivian limestones.

- The Cossaux spring (x: 536’860 / y: 181’545; Fig. 1.3c), which contributes to the drinking water supply of Yverdon-les-Bains, is located at an altitude of approximately 440 m. The spring is captured by means of eight radial, inclined drillings of 100 to 150 m length. The total discharge ranges from 42 to 90 L/s. The Cossaux spring is classified as subthermal as its temperature varies between 12.3 and 13.6 °C. The water quality is generally good, although turbidity, TOC and faecal bacteria sometimes cause problems.

- The Moulinet spring (x: 535’375 / y: 181’810; Fig. 1.3d, e, f and g), located about 1.5 km west of the Cossaux spring, discharges at an altitude of about 450 m. The spring consists of eight individual outlets: 6A, 6B and 7A – F. The two captured outlets (6A and 6B) were used for the drinking water supply of Yverdon-les-Bains during the first half of the 20th century, but they were then abandoned because of frequent microbial and chemical contamination. Outlets 6A, 6B and 7B are permanent, while the others sometimes run dry. Physical, chemical and microbiological water characteristics are, however, identical for all outlets (unpublished report by Mautner 1978). The total discharge of this group of outlets varies between 19 L/s and approximately 750 L/s, and the temperature ranges from 8.6 to 11.9 °C.

Fig. 1.3 Photographs of (**a**) the Feurtille swallow hole, (**b**) the agricultural area drained by the stream sinking into the Feurtille swallow hole, (**c**) the Cossaux spring, (**d**, **e** and **f**) the outlets 6A, 6B and 7A, respectively, of the Moulinet spring and (**g**) the Moulinet spring discharge monitoring point (junction of all eight Moulinet outlets).

- The small Grange-Décoppet spring (x: 534’530 / y: 181’050) is located approximately 1.2 km south-west of the Moulinet spring and discharges at an altitude of about 460 m. The spring is used for the water supply of several fountains of a near located village. Spring discharge varies between 2 and 40 L/s, and water characteristics are identical to those of the Moulinet spring (Muralt 1999; unpublished report by Mautner 1978). Furthermore, several minor outlets, among which Les Uttins (x: 537’040 / y: 181’370), Praz Barbey (x: 536’810 / y: 181’630) and Gruvy (x: 536’500 / y: 181’700), are located close to the Cossaux spring. The discharges of these outlets vary between 0 and 2 L/s.

Finally, about 4 km east of the Mont de Chamblon, where the Cretaceous and Jurassic rocks are locally close to the surface and where, consequently, the low-permeable Molasse sediments are nearly absent, thermal water of 18 – 22 °C discharges at a spring (x: 539’690 / y: 180’325). In 1982, in order to obtain higher temperatures and flow rates for the thermal centre of Yverdon-les-Bains, a well was drilled to a depth of 598 m. The artesian well (x: 539’675 / y: 180’335) catches a 28 °C water, mainly between 400 and 500 m depth (Kimmeridgian limestone).

Muralt (1999) provided, through detailed hydrochemical and isotopic investigations, a general conceptual model of groundwater flow in the Yverdon-les-Bains karst aquifer system (Fig. 1.4). Groundwater discharging at the Mont de Chamblon karst springs consists essentially of three different components:

A. a slow, deep and warm groundwater component from several hundred meters of depth, circulating probably in the deeper part of the Upper Malm limestone (Kimmeridgian). This component has rather stable water characteristics, and its temperature was evaluated at about 18 °C. The thermal spring and well are also partially fed by this component. This component will be referred to as the “*deep and warm groundwater component*” or the “*thermal groundwater component*”;

B. a rapid, cold and slightly contaminated groundwater component infiltrating on the forested south-east slope of the Jura Mountains and circulating through karst conduits in the shallow

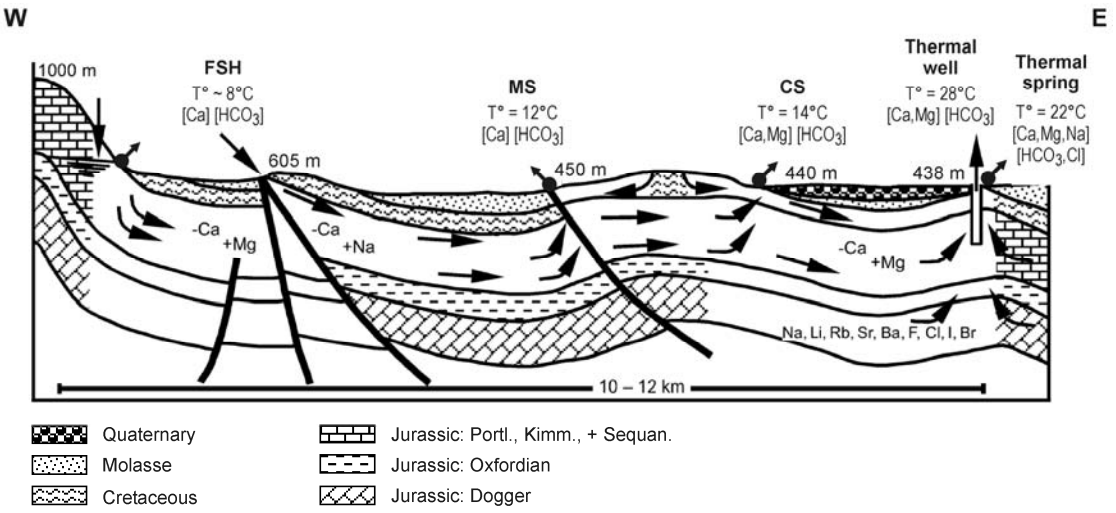

Fig. 1.4 Conceptual model (W – E cross-section) of the Yverdon-les-Bains karst aquifer system (after Muralt 1999). **FSH**: Feurtille swallow hole; **MS**: Moulinet spring; **CS**: Cossaux spring.

part of the Upper Malm limestone (Portlandian). This component will be referred to as the "*karst groundwater component*";

C. a rapid, cold and frequently contaminated water component sinking into the Feurtille swallow hole. Several tracer tests, which were carried out at the end of the 19th century and in 1989, proved the underground connection between the swallow hole and the Cossaux, Moulinet and Grange-Décoppet springs (unpublished reports by Looser 1990; Schardt 1910, 1920). This component will be referred to as the "*Feurtille swallow hole component*".

The karst groundwater component (component ***B***) and the deep and warm groundwater component (***A***) are the main components flowing in the karst aquifer system and discharging at the springs. Based on the aforementioned tracer tests, the Feurtille swallow hole component (***C***) was estimated to contribute about 5 and 1 % during low-flow, 20 and 10 % during medium-flow and 35 and 5 % during high-flow conditions to the discharges of the Moulinet and Cossaux springs, respectively (unpublished reports by Schardt 1910, 1920). A local contribution of water infiltrating on the Mont de Chamblon has also been proposed and was later verified by tracer tests (unpublished report by CSD 1976). However, this local groundwater component participates only very slightly to the water discharging at the springs (unpublished reports by Blanc 1995; Gagnebin *et al*. 1936; Schardt 1910, 1920) and may thus be neglected.

Despite the same origins for the waters feeding the springs, the Cossaux spring shows significant differences in its physical, chemical and microbiological composition compared to the Moulinet and Grange-Décoppet springs. This is explained by an additional inflow of the deep and warm groundwater component (***A***) at the Cossaux spring, resulting in lower contamination levels and a 2 – 4 °C higher water temperature (Muralt 1999).

1.3.2 Noiraigue karst aquifer system

The geological and hydrogeological setting of the Noiraigue karst aquifer system is described in detail elsewhere (e.g. Atteia *et al*. 1996; Burkhard *et al*. 1998; Gillmann 2007; Gogniat 1995; Sommaruga 1997; Valley *et al*. 2004) and will therefore only briefly be discussed here.

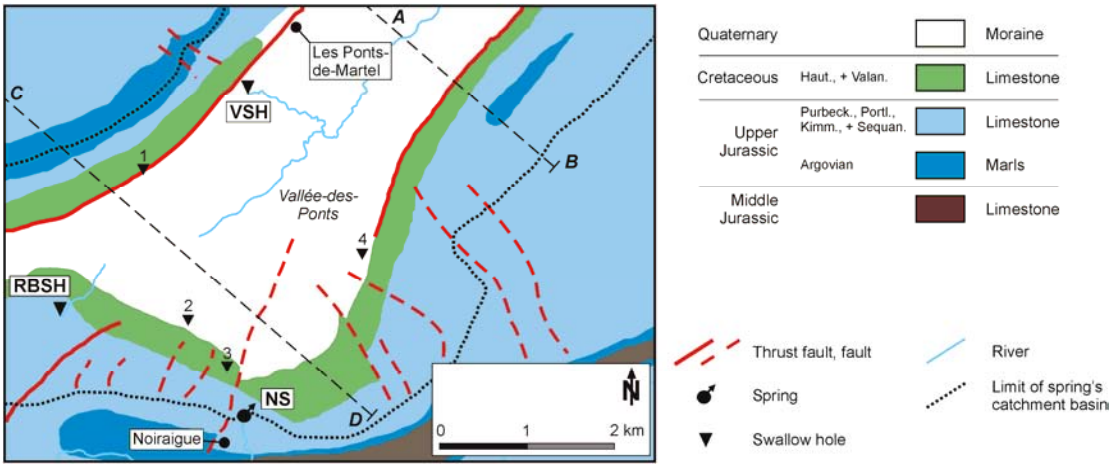

Fig. 1.5 Geological map of the southern part of the Noiraigue karst aquifer system (modified after Gillmann 2007 and Sommaruga 1997). **VSH**: Voisinage swallow hole; **RBSH**: Roche Berthoud swallow hole; **NS**: Noiraigue spring; **1-4**: other sinkholes.

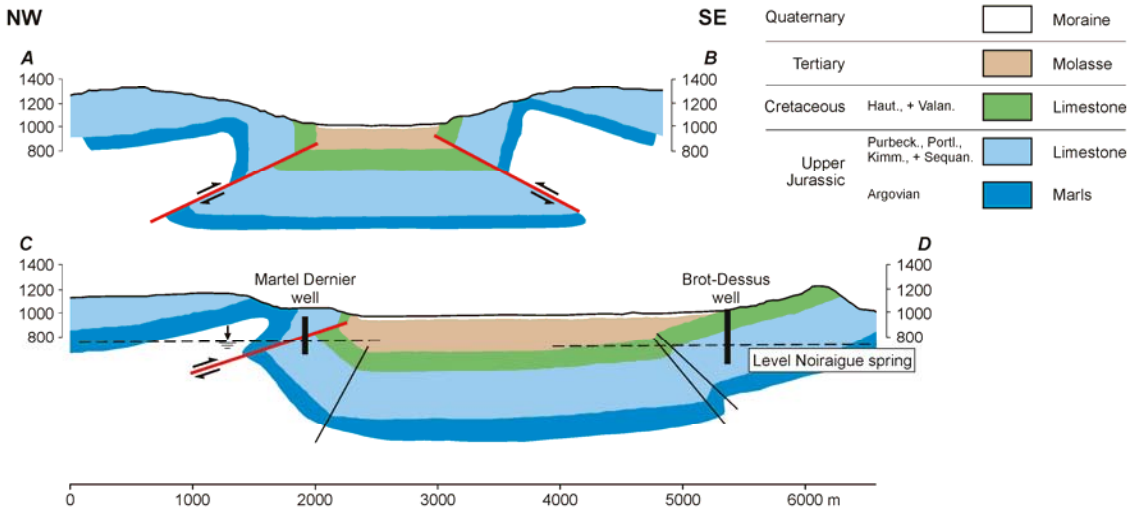

Fig. 1.6 Geological cross sections through the Noiraigue karst aquifer system (after Atteia *et al*. 1996). See Fig. 1.5 for locations of the cross sections.

The Noiraigue karst aquifer system extends over an area of 60 to 70 km^2 at an altitude ranging from 750 to 1300 m. The region receives a mean annual precipitation of 1500 mm. The aquifer, delimited at its base by the Argovian marl aquiclude, consists of an approximately 500 m thick karstified Upper Jurassic and Lower Cretaceous limestone syncline, bordered by two thrusting anticlines (Fig. 1.5 and 1.6). Low-permeable Tertiary and Quaternary sediments cover the limestone in the centre of the valley over an area of about 20 km^2 with a thickness up to 300 m.

The perennial Bied brook, which drains the major part of the intensively cultivated valley, sinks into the Voisinage swallow hole (x: 545’725 / y: 204’900). The discharge of the Bied brook ranges from 30 to 600 L/s. Further to the south-west, a second perennial brook, which has a discharge varying between 1 and 100 L/s, sinks into the Roche Berthoud swallow hole (x: 543’640 / y: 202’270). Several other sinkholes, principally located on the border of the valley at the contact zone between the low-permeable sediments and the Cretaceous limestone, are temporarily active, especially following rainfalls (Gogniat 1995).

The Noiraigue spring (x: 545’690 / y: 200’960), discharging from Sequanian (Upper Jurassic, Malm) limestone at an altitude of 740 m, is the only outlet of the closed basin. Spring discharge ranges from 200 L/s to more than 14 m³/s. Tracer tests revealed connections between all sinkholes and the spring. Transit times from the Voisinage swallow hole to the spring varied from 15 d during low-flow conditions to 60 h during high-flow conditions, while transit times from the Roche Berthoud swallow hole to the spring varied between 6 d and 33 h, respectively (Atteia *et al*. 1996; Gillmann 2007).

1.3.3 Vers-chez-le-Brandt and Grand-Bochat cave sites

The small Vers-chez-le-Brandt and Grand-Bochat cave sites are both located in the uppermost part of an approximately 300-m-thick unsaturated zone (Gigon 1976; Müller 1982). Ready access and the simple settings make these caves suitable sites to study the role of the unsaturated zone in karst aquifers. Both cave sites have been extensively investigated within the last decade, mainly by tracer tests and irrigation experiments, for the characterisation of conservative transport and

biodegradation processes (Madec 1999; Perrin 2003; Puech and Bourret 1998; Savoy 2007; unpublished report by Pochon 2004).

The nearly horizontal Vers-chez-le-Brandt cave (x: 526'490 / y: 198'980) is developed in Upper Jurassic (Malm) limestone beneath relatively flat pasture land. About 1 to 2 m of soil / loess and 30 m of unsaturated limestone overlie the 200-m-long cave. The monitored perennial vadose flow issuing from a fracture at the cave roof has a base flow of about 0.6 L/min. The recharge area of this outlet is approximately 500 to 600 m² (unpublished report by Pochon 2004).

The Grand-Bochat cave (x: 544'590 / y: 206'590), which has a development of about 20 m, is located beneath flat forested land. The cave is overlaid by approximately 15 m of unsaturated Upper Jurassic (Malm) limestone and a soil cover of less than 0.3 m. The monitored outlet is a perennial epikarst flow issuing from a fissure in the cave wall. Base flow of this outlet is approximately 0.1 L/min; its catchment area was estimated at 400 m² (unpublished report by Pochon 2004). Flow in this unsaturated zone is essentially controlled by the dip of the bedding planes (N/12°).

1.3.4 Gänsbrunnen artificial galleries

The artificial galleries of the Gänsbrunnen test site (x: 602'050 / y: 234'820) are located beneath a forested hilltop formed by Upper Jurassic (Malm) limestone. The artificial nature of these galleries implies that the 10-m-thick overlying limestone is less affected by karstification processes than natural caves (Savoy 2007; unpublished report by Pochon 2004). This is particularly illustrated by the existence of numerous water outlets activated during precipitation events and running rapidly dry. Soil cover is nearly absent in the catchment area of the galleries, which is about 200 m².

REFERENCES

Atteia O., Gogniat S. and Kozel R. 1996. Apport de l'hydrologie, de la géophysique et des essais de traçage à la connaissance de l'aquifère karstique de la Noiraigue, Jura neuchâtelois, Suisse. Bulletin d'Hydrogéologie 15: 33-61.

Auckenthaler A. and Huggenberger P. 2003. Pathogene Mikroorganismen im Grund- und Trinkwasser. Transport – Nachweismethoden – Wassermanagement. Birkhäuser, Basel.

Auckenthaler A., Raso G. and Huggenberger P. 2002. Particle transport in a karst aquifer: natural and artificial tracer experiments with bacteria, bacteriophages and microspheres. Water Science and Technology 46 (3): 131-138.

Barton H.A. and Northup D.E. 2007. Geomicrobiology in cave environments: past, current and future perspectives. Journal of Cave and Karst Studies 69 (1): 163-178.

Burkhard M., Atteia O., Sommaruga A., Gogniat S. and Evard D. 1998. Tectonique et hydrogéologie dans le Jura neuchâtelois. Eclogae Geologicae Helvetiae 91 (1): 177-183.

Canaveras J.C., Hoyos M., Sanchez-Moral S., Sanz-Rubio E., Bedoya J., Soler V., Groth I., Schumann P., Laiz L., Gonzales I. and Sainz-Jimenez C. 1999. Microbial communities associated with hydromagnesite and needle-fiber aragonite deposits in a karstic cave (Altamira, northern Spain). Geomicrobiology Journal 16 (1): 9-25.

Cho J.C. and Kim S.J. 2000. Increase in bacterial community diversity in subsurface aquifers receiving livestock wastewater input. Applied and Environmental Microbiology 66 (3): 956-965.

Danielopol D.L., Griebler C., Gunatilaka A. and Notenboom J. 2003. Present state and future prospects for groundwater ecosystems. Environmental Conservation 30 (2): 104-130.

Drew D. and Hötzl H. 1999. Karst hydrogeology and human activities. Impacts, consequences and implications. International Contributions to Hydrogeology (IAH), Balkema, Rotterdam.

Engel A.S., Lee N., Porter M.L., Stern L.A., Bennett P.C. and Wagner M. 2003. Filamentous "*Epsilonproteobacteria*" dominate microbial mats from sulfidic cave springs. Applied and Environmental Microbiology 69 (9): 5503-5511.

Ford D. and Williams D.W. 1989. Karst geomorphology and hydrology. Unwin Hyman, London.

Gainon F. 2008. Les isotopes radioactifs de la série de l'uranium-238 (^{222}Rn, ^{226}Ra, ^{234}U et ^{238}U) dans les eaux thermales de Suisse. Sites d'Yverdon-les-Bains, Moiry, Loèche-les-Bains, Saxon, Val d'Illiez, Bad Ragaz, Delémont, Lavey-les-Bains, Brigerbad et Combioula. PhD thesis, Centre of Hydrogeology, University of Neuchâtel, Switzerland.

Gigon R. 1976. Inventaire spéléologique de la Suisse. I. – Canton de Neuchâtel. Commission de Spéléologie de la Société helvétique des Sciences Naturelles, Neuchâtel.

Gillmann A. 2007. Etude du comportement des substances particulaires et solubles dans le système karstique de la source de la Noiraigue. MSc thesis, Centre of Hydrogeology, University of Neuchâtel, Switzerland.

Gogniat S. 1995. Etude des infiltrations rapides de l'aquifère de la Noiraigue, Neuchâtel, Suisse. Postgraduate diploma thesis, Centre of Hydrogeology, University of Neuchâtel, Switzerland.

Goldscheider N., Hunkeler D. and Rossi P. 2006. Review: Microbial biocenoses in pristine aquifers and an assessment of investigative methods. Hydrogeology Journal 14 (6): 926-941.

GSchV. 1998. Water Protection Ordinance, SR 814.201, Swiss Federal Law, Bern.

Hancock P.J., Boulton A.J. and Humphreys W.F. 2005. Aquifers and hyporheic zone: towards an ecological understanding of groundwater. Hydrogeology Journal 13 (1): 98-111.

Herwaldt B.L., Craun G.F., Stokes S.L. and Junanek D.D. 1992. Outbreaks of waterborne disease in the United States – 1989-90. Journal American Water Work Association 84 (4): 129-135.

Hipsey M.R., Brookes J.D., Regel R.H., Antenucci J.P. and Burch M.D. 2006. In situ evidence for the association of total coliforms and *Escherichia coli* with suspended inorganic particles in an Australian reservoir. Water Air and Soil Pollution 170 (1-4): 191-209.

Hunkeler D. and Mudry J. 2007. Hydrochemical methods. In: Goldscheider N. and Drew D. (eds.) Methods in karst hydrogeology. International Contributions to Hydrogeology (IAH), Balkema, Rotterdam.

Jordi H.A. 1993. Tectonique du basin molassique et de son substratum jurassique-crétacé dans la region Orbe-Yverdon-Grandson. Bulletin de la Société vaudoise des Sciences Naturelles 82 (3) : 279-299.

Kimura H., Sugihara M., Yamamoto H., Patel B.K.C., Kato K. and Hanada S. 2005. Microbial community in a geothermal aquifer associated with the subsurface of the Great Artesian Basin, Australia. Extremophiles 9 (5): 407-414.llllp

Kramer M.H., Quade G., Hartemann P. and Exner M. 2001. Waterborne diseases in Europe 1986-1996. Journal American Water Works Association 93 (1): 48-53.

Madec G. 1999. Etude des écoulements dans l'épikarst. Approche géophysique, hydraulique et hydrochimique sur le site de Grand-Bochat. Postgraduate diploma thesis, Centre of Hydrogeology, University of Neuchâtel, Switzerland.

Mahler B.J. and Lynch F.L. 1999. Muddy waters: temporal variation in sediment discharging from a karst spring. Journal of Hydrology 214 (1-4): 165-178.

Mahler B.J., Personné J.C., Lods G.F. and Drogue C. 2000. Transport of free and particulate-associated bacteria in karst. Journal of Hydrology 238 (3-4): 179-193.

Massei M., Wang H.Q., Dupont J.P., Rodet J. and Laignel B. 2003. Assessment of direct transfer and resuspension of particles during turbid floods at a karstic spring. Journal of Hydrology 275 (1-2): 109-121.

Montgomery M.A. and Elimelech M. 2007. Water and sanitation in developing countries: including health in the equation. Environmental Science & Technology 41 (1): 17-24.

Müller I. 1982. Multitraçage des eaux souterraines karstiques dans le bassin de la source de l'Areuse (Jura neuchâtelois, Suisse). Bulletin d'Hydrogéologie 4: 7-40.

Muralt R. 1999. Processus hydrogéologiques et hydrochimiques dans les circulations profondes des calcaires du Malm de l'arc jurassien (zones de Delémont, Yverdon-les-Bains, Moiry, Genève et Aix-les-Bains). Beiträge zur Geologie der Schweiz, Geotechnische Serie, Lieferung 82, Schweizerischen Geotechnischen Kommission, Zürich.

Muralt R., Vuataz F.D., Schonborn G., Sommaruga A. and Jenny J. 1997. Integration of hydrochemical, geological and geophysical methods for the exploration of a new thermal water resource. Case of Yverdon-les-Bains, foot of the Jura range. Eclogae Geologicae Helvetiae 90 (2): 179-197.

Nebbache S., Loquet M., Vinceslas-Akpa M. and Feeny V. 1997. Turbidity and microorganisms in a karst spring. European Journal of Soil Biology 33 (2): 89-103.

Perrin J. 2003. A conceptual model of flow and transport in a karst aquifer based on spatial and temporal variations of natural tracers. PhD thesis, Centre of Hydrogeology, University of Neuchâtel, Switzerland.

Puech V. and Bourret F. 1998. Mesure du débit de percolation dans les grottes de Vers-chez-le-Brandt et du Grand-Bochat. Cavernes 42 (1) : 22-24.

Ryan M. and Meiman J. 1996. An examination of short-term variations in water quality at a karst spring in Kentucky. Ground Water 34 (1): 23-30.

Savoy L. 2007. Use of natural and artificial reactive tracers to investigate the transfer of solutes in karst systems. PhD thesis, Centre of Hydrogeology, University of Neuchâtel, Switzerland.

Sommaruga A. 1997. Geology of the central Jura and the Molasse Basin: new insight into an evaporate-based foreland fold and thrust belt. Mémoire de la Société neuchâteloise des Sciences Naturelles, tome XII.

Stadler H., Skritek P., Sommer R., Mach L., Zerobin W. and Farnleitner A.H. 2008. Microbiological monitoring and automated event sampling at karst springs using LEO-satellites. Water Science and Technology 58 (4): 899-909.

Steube C., Richter S. and Griebler C. 2009. First attempts towards an integrative concept for the ecological assessment of groundwater ecosystems. Hydrogeology Journal 17 (1): 23-35.

Valley B., Burkhard M. and Schnegg P.A. 2004. 3-D unfolding of the anticlines bordering the closed Vallée des Ponts syncline, Central Jura, Switzerland. Eclogae Geologicae Helvetiae 97 (2): 279-291.

Vervier P. and Gibert J. 1991. Dynamics of surface-water groundwater ecotones in a karstic aquifer. Freshwater Biology 26 (2): 241-250.

Zwahlen F. (ed.) 2004. Vulnerability and risk mapping for the protection of carbonate (karst) aquifers, COST action 620, final report. Office for Official Publications of the European Communities, Luxembourg.

2

From quantitative tracer tests towards a conceptual flow model of the Yverdon-les-Bains karst aquifer system*

ABSTRACT

The Yverdon-les-Bains karst aquifer system (Switzerland), which contributes to the drinking water supply of Yverdon-les-Bains, is mainly characterised by a stream sinking into a swallow hole (i.e. the Feurtille swallow hole) and two connected karst springs (i.e. the Cossaux and Moulinet springs) that often show periodical contamination by total organic carbon, nitrate and faecal indicator bacteria. The hydrogeological functioning of the karst aquifer system, and more specifically the swallow hole – springs relation, was investigated by means of five quantitative tracer experiments from the swallow hole and monitoring of natural physical, chemical and microbiological parameters. The tracer tests were carried out during different but stable flow conditions within the system. Transit times varied from 12 d during low-flow conditions to 24 h during high-flow conditions. Tracer recoveries increased at the Moulinet spring and decreased at the Cossaux spring with increasing flow conditions; total recovery remained, however, constant at about 30 %. Tracer test and monitoring results showed that the swallow hole is an important source of groundwater pollution. Moreover, the tracer experiments made it possible to design a conceptual model of the conduit structure of the karst aquifer system, and tracer recovery rates permitted quantifying the flow rates within the system using water and mass balance equations. This in-depth characterisation of flow organisation in the Yverdon-les-Bains karst aquifer system has furthermore practical implications for the management of the groundwater resource.

2.1 INTRODUCTION

Effective management and protection strategies of karst groundwater resources are generally based on protection zoning, which are intended to protect the water abstraction point from contamination, and site-specific monitoring programs (continuous or sequential measurements) of natural parameters including also typical potential contaminants of allochthonous origin (e.g. nitrate and faecal indicator bacteria). To do so, detailed and reliable information on the

* This chapter is based on the paper:

Pronk M., Goldscheider N. and Zopfi J. 2006. Dynamics and interaction of organic carbon, turbidity and bacteria in a karst aquifer system. Hydrogeology Journal 14 (4): 473-484.

hydrogeological functioning of the karst aquifer is needed. The high heterogeneity encountered in karst aquifers complicates, however, this characterisation.

Karst aquifers are usually characterised by a few high-permeability solution-enlarged conduits (conduit permeability) surrounded by a generally low-permeable fissured rock volume (matrix and fracture permeability; White 1988). While the latter generally accounts for the major part of total aquifer porosity and is therefore an important feature for groundwater storage, rapid groundwater flow is principally constrained to the conduits. This concentration of flow in conduits allows for large amounts of solute and particulate contaminants to be transferred rapidly towards water abstraction points (e.g. Vesper *et al*. 2003; White 2002). The hydrogeological characterisation of karst aquifers, and more particularly their active conduit networks, could thus further improve the management of these valuable groundwater resources (Perrin and Luetscher 2008).

Artificial groundwater tracing experiments have been extensively used in karst hydrogeology, as they deliver information on groundwater flow paths and contaminant transport in the aquifer (Käss 1998). Qualitative tracer tests are adequate for investigations that aim at identifying connections between injection and observation points, e.g. for the catchment area delineation of water abstraction points. However, information provided by such experiments is insufficient to infer the hydraulic properties of karst aquifers and the structure of the active conduit network. Quantitative tracing experiments have increasingly emerged in the last decades, facilitated by the development of new continuous on-site monitoring techniques (e.g. Schnegg and Doerfliger 1997). Such quantitative methods have proven to be of great help to infer the conduit structure of karst aquifers (e.g. Atkinson *et al*. 1973; Smart 1988; Perrin and Luetscher 2008).

The Yverdon-les-Bains karst aquifer system is mainly characterised by a stream sinking into the Feurtille swallow hole and the connected Cossaux and Moulinet karst springs, from which the Cossaux spring contributes to about one third of the water supply of Yverdon-les-Bains. The sinking stream, which drains an agricultural area and contains thus frequently high levels of turbidity, organic matter, nitrate and faecal bacteria, strongly impacts spring water quality. The present study aimed therefore at characterising the swallow hole component and at quantifying its contribution to the springs in order to improve the management of this groundwater resource. In order to achieve these goals, the study site was investigated by means of five quantitative tracer experiments along with monitoring of physical, chemical and microbiological parameters.

2.2 MATERIAL AND METHODS

2.2.1 Monitoring program of natural parameters

Discharge, water temperature, electrical conductivity, turbidity and total organic carbon (TOC) were monitored continuously (time step: 10 min) at several observation points of the Yverdon-les-Bains karst aquifer system from January 2005 till December 2007 (Table 2.1). Furthermore, from February 2005 till November 2006, samples were collected twice-monthly at the Feurtille swallow hole and the Cossaux and Moulinet springs for analyses of major ion chemistry and water quality indicator bacteria. The analysed ions included K^+, Na^+, Mg^{2+}, Ca^{2+},

Table 2.1 Overview of the monitoring program of continuously (time step: 10 min) on-site measured parameters at the Yverdon-les-Bains karst aquifer system.

Observation point		Q [a]	EC [b]	T° [c]	TOC [d]	Turb.[e]	Monitoring period
Feurtille swallow hole		•	•	•	•	•	Jan. 2005 – Dec. 2007
Cossaux spring		•	•	•	•	•	Jan. 2005 – Dec. 2007
Moulinet spring	Outlet 6A	•	•	•	•	•	Jan. 2005 – Dec. 2007
	Outlet 6B	•	•	•	•	•	Jan. 2005 – Dec. 2007
	Outlet 7D		•	•			May 2007 – Oct. 2007
	Outlet 7F		•	•			Nov. 2007 – Dec. 2007
	Junction of all outlets	•					Jan. 2005 – Dec. 2007
Grange-Décoppet spring		•	•	•	•	•	July 2007 – Dec. 2007

[a] Discharge
[b] Electrical conductivity
[c] Temperature
[d] Total organic carbon
[e] Turbidity

HCO_3^-, Cl^-, NO_3^- and SO_4^{2-}, while the indicator bacteria analyses focused on mesophilic aerobic bacteria, total coliforms, *E. coli* and enterococci.

2.2.2 Instrumentation and methodology

As the Cossaux spring is used for the drinking water supply of the city of Yverdon-les-Bains, the continuous monitoring of discharge, temperature, electrical conductivity, turbidity and TOC is part of the survey program and is managed by the SEY (Service des Energies d'Yverdon-les-Bains – Energy Service of Yverdon-les-Bains). Therefore, the standard industrial instruments installed at the Cossaux spring are differing from those of the other observation points. However, laboratory and field experiments showed the reliability of all methods and allowed cross-calibrating the instruments.

RAINFALL

Daily rainfall data were provided by MeteoSwiss. Three stations were considered in the area of the Yverdon-les-Bains karst aquifer system: the Yverdon-les-Bains station (station n°: 6130), which is located at an altitude of 433 m near the Mont de Chamblon; the Baulmes station (n°: 6180), located at an altitude of 642 m near the Feurtille swallow hole; and the L'Auberson station (n°: 6190), located at an altitude of 1110 m in the Jura Mountains (the main recharge area of the karst aquifer system).

DISCHARGE

At the Cossaux spring, the discharge was monitored using a flow meter (Endress + Hauser, Reinach, Switzerland), while the discharge of all other observation points was measured by means of weirs and pressure probes (DL/N 64, STS, Sirnach, Switzerland). Weir discharge formulas were not adapted as the upstream basins had not sufficient extensions. Therefore, salt dilution gauging allowed stage-discharge rating curves, which convert water level into discharge, to be

established (Fig. A.1 – A.5, Appendix A). Long-term stability of the pressure probes was controlled fortnightly by manual measurements of the water height (Fig. A.1 – A.5, Appendix A). The accuracy of discharge measurements is on the order of 10 %.

TURBIDITY AND TOTAL ORGANIC CARBON

Turbidity and total organic carbon (TOC) were monitored with GGUN-FL30 flow-through field fluorometers, developed by the Group of Geomagnetism of the University of Neuchâtel (Schnegg 2002, 2003), at all observation points, except at the Cossaux spring. The latter was equipped with standard industrial instruments: a WTM 500 turbidimeter and a ColorPlus bypass absorptiometer (Sigrist-Photometer, Ennetbürgen, Switzerland) for the monitoring of turbidity and TOC, respectively.

The turbidity sensors integrated in the field fluorometers were calibrated yearly with standards of formazine (according to standard ISO 7027) of 0, 1, 10 and 100 NTU (nephelometric turbidity unit). The WTM 500 turbidimeter is automatically and daily calibrated by the measurement of an integrated reference body. Previous on-site monitoring at the Moulinet spring showed the reliability of both instruments (Fig. A.6, Appendix A). The accuracy of turbidity measurements is on the order of 10 %.

The spectral absorbance coefficient at 254 nm is a widely accepted and efficient method for continuous on-site monitoring of TOC (e.g. Mrkva 1983; Reid *et al*. 1980). TOC dosage of Cossaux spring water samples, which were determined at the water and environment laboratory of Neuchâtel following a standard method (680 °C catalyst-aided combustion and non-dispersive infrared detection), allowed calibrating the absorptiometer (Fig. A.7, Appendix A).

The use of the fluorescence properties of organic matter to quantify its content has often been reported (e.g. MacCraith *et al*. 1993; Savoy 2007; Smart *et al*. 1976). Several studies investigated the fluorescence of TOC from different environmental samples such as soils and river, cave and spring waters (e.g. Baker 2001; Baker and Genty 1999; Batiot 2002; Senesi *et al*. 1991). Results showed that TOC is characterised by fluorescence emission between wavelengths of 350 and 500 nm for an excitation varying between 250 and 425 nm with a maximum intensity at excitation / emission wavelengths of 320-350 / 420-450 nm. The characteristics of the field fluorometer's excitation – detection system dedicated to the detection of tinopal are close to these wavelengths (excitation, about 365 nm, is performed by an UV LED combined with a filter, while emission is detected between 420 and 550 nm by a combination of a photodiode and a filter), allowing therefore to use the field fluorometers to monitor TOC. TOC dosage and maximum fluorescence intensities of water samples collected at the swallow hole and the springs allowed calibrating the field fluorometers (Fig. A.8 and A.9, Appendix A). Maximum fluorescence intensities were determined by synchronous excitation / emission scans using a spectrophotometer (LS 50 B, Perkin-Elmer, Waltham, USA). Specifications of the synchronous excitation / emission scans were chosen according to above-mentioned literature: fluorescence emission was detected between 350 and 500 nm at 0.5 nm steps, using a constant delta lambda of 100 nm. Finally, on-site monitoring at the Cossaux spring showed the reliability of both methods (Fig. A.10, Appendix A). The accuracy of TOC measurements is on the order of 10 %.

TEMPERATURE AND ELECTRICAL CONDUCTIVITY

Temperature and electrical conductivity were monitored by different instruments: a modified WTW 340i conductimeter (WTW, Weilheim, Germany) coupled to a DT50 datalogger (dataTaker, Rowville, Australia) at the Moulinet 6A outlet; a WTW tetracon probe (WTW) at the Cossaux spring; CTD diver probes (van Essen / Eijkelkamp, Delft, The Netherlands) at the Moulinet 7D and 7F outlets; and the latest genera of the aforementioned field fluorometers at the Feurtille swallow hole, the Moulinet 6B outlet and the Grange-Décoppet spring. Regular manual measurements using a reference WTW 340i conductimeter (WTW) were carried out in order to calibrate the different instruments and to verify their long-term stability (Fig. A.11 – A.16, Appendix A). Accuracies of the measurements, provided by the manufacturers, are 0.1 °C and 10 µS/cm for temperature and electrical conductivity, respectively.

MAJOR IONS

For major ion chemistry analyses, water was collected in 500 mL plastic bottles and transported to the laboratory in cooling boxes. Water samples were filtered through 0.45 µm pore size membranes (ME25 Mixed Cellulose Ester Circles, Whatman, Maidstone, UK). For cation preservation, samples were acidified to pH < 2 with HNO_3 suprapur. Bicarbonate concentrations were determined within 6 h following the sampling by titration with HCl 0.1 M to a pH of 4.3. Other major ions (K^+, Na^+, Mg^{2+}, Ca^{2+}, Cl^-, NO_3^- and SO_4^{2-}) were analysed by ion chromatography (IC DX-120, Dionex, Sunnyvale, USA) within the month following the sampling. Accuracies of bicarbonate and other ions analyses are 10 and 0.5 mg/L, respectively. Finally, major ion analyse quality was checked with the charge balance error equation. The analysis was considered acceptable if the error was less than 5 %.

WATER QUALITY INDICATOR BACTERIA

For microbiological analyses, water samples were collected in sterile 1 L Nalgene bottles, transported in cooling boxes to the laboratory and processed within 6 h. Water quality indicator bacteria, including mesophilic aerobic bacteria, total coliforms, *E. coli* and enterococci, were enumerated using standard cultivation techniques (APHA, AWWA and WEF 2005). Water samples were filtered on sterile 0.45 µm pore size membranes (ME25 Mixed Cellulose Ester Circles, Whatman), which were then incubated on different revivifying and selective cultivation media: (1) Trypcase Soy Agar (bioMérieux, Marcy l'Etoile, France) for 3±1 h at 37 °C and Coli ID (bioMérieux) for 48±2 h at 37 °C for total coliform enumeration; (2) Trypcase Soy Agar (bioMérieux) for 3±1 h at 37 °C and Tryptone Bile X-Glucuronide (Oxoid, Basingstoke, UK) for 22±2 h at 44 °C for *E. coli* enumeration; and (3) Slanetz-Bartley agar (Merck, Darmstadt, Germany) for 48±2 h at 37 °C and Bile Aesculin Azide Agar (Merck) for 3±1 h at 37 °C for enterococci enumeration. Enumeration of mesophilic aerobic bacteria was carried out by a direct inoculation of sampled water in Plate Count Agar (bioMérieux), which was then incubated for 24±2 h at 37 °C. All results are duplicate determinations.

2.2.3 Tracer tests

Within the framework of this study, several tracer experiments were conducted in the area of the Yverdon-les-Bains karst aquifer system. Five tracer tests were carried out, during different

flow conditions within the karst aquifer system, from the Feurtille swallow hole (on 1 September 2003, 21 March 2005, 2 June 2005, 22 April 2006 and 2 November 2007). For all these dye-tracing tests, 1 kg of uranine, dissolved in 10 L of water, was injected in the sinking stream about 10 m upstream of the swallow hole.

Moreover, a regional tracer test was carried out from a location on the south-east slope of the Jura Mountains: La Côte (x: 528'900 / y: 182'450), located at an altitude of 980 m at about 2 km north-west of the Feurtille swallow hole (see Fig. 1.2 for location). This regional tracer test was performed on 11 April 2007 by injecting 2 kg of sulforhodamine B, dissolved in 40 L of water, in an open fracture in the outcropping limestone. The injection was preceded and followed by flushing 1 and 7 m³ of water, respectively, in the fracture during approximately 1 h.

Tracer breakthrough monitoring at the springs consisted of continuous on-site measurements, discrete sampling and integrative sampling. The monitoring program for each tracer experiment is summarised in Table B.1 (Appendix B). The aforementioned field fluorometers allowed continuous dye concentrations to be monitored (Schnegg and Costa 2003). For the tracer tests performed from the Feurtille swallow hole, control water samples were collected automatically (6712C Sampler, Teledyne ISCO, Lincoln, USA) and / or manually at time steps varying from 1 to 3 h and 1 to 2 d, respectively. For the regional tracer test, samples were collected daily to weekly and additional charcoal bags were installed at the springs. Dye concentrations from water samples and charcoal bags were determined in the laboratory using a spectral fluorometer (LS 50 B, PerkinElmer), according to well-established methods (Käss 1998).

2.3 GENERAL CHARACTERISTICS OF THE YVERDON-LES-BAINS KARST AQUIFER SYSTEM

Physical, chemical and microbiological data recovered from the 3-year monitoring period allowed inferring some first statements regarding the relations between the springs, the swallow hole and the springs as well as the characterisation and behaviour of the Yverdon-les-Bains karst aquifer system. Summaries of all results are presented in Tables 2.2 and 2.3. Furthermore, a 3-month monitoring period is shown in Fig. 2.1 (complete data of the 3-year monitoring period are shown in Fig. B.1 – B.3, Appendix B), and temporal changes in major ion chemistry at the Moulinet and Cossaux springs are shown in Fig. 2.2.

During the investigation period, the discharge of the stream sinking into the Feurtille swallow hole was highly related to precipitation events and varied between 0 and more than 1 m³/s. While

Table 2.2 Overview of the continuously on-site monitored water characteristics of the Feurtille swallow hole and the Moulinet and Cossaux springs during the investigation period (Jan. 2005 – Dec. 2007).

Parameter	Unit	Feurtille swallow hole			Moulinet spring			Cossaux spring		
		Mean	Median	Range	Mean	Median	Range	Mean	Median	Range
Discharge	[L/s]	59	33	0 - 1300	157	111	20 - 737	54	48	43 - 88
Temperature	[°C]	10.6	10.2	3.4 - 23.9	10.6	10.7	8.6 - 11.6	13.2	13.3	12.3 - 13.6
EC [a]	[µS/cm]	722	719	76 - 1189	458	459	309 - 627	470	469	428 - 520
Turbidity	[NTU]	15.3	9.9	0.4 - 275	1.6	0.7	0.1 - 186	0.4	0.2	0.1 - 9.9
TOC	[mg/L]	4.3	3.7	0.5 - 18.6	1.4	1.1	0.2 - 10.8	0.7	0.6	0.3 - 3.2

[a] Electrical conductivity

Table 2.3 Summary of major ion and water quality indicator bacteria contents of the Feurtille swallow hole and the Moulinet and Cossaux springs during the investigation period (Feb. 2005 – Nov. 2006).

Parameter	Unit	Feurtille swallow hole			Moulinet spring			Cossaux spring		
		n [a]	Median	Range	n [a]	Median	Range	n [a]	Median	Range
Na^+	[mg/L]	53	4.1	2.8 - 9.0	53	1.4	0.9 - 2.6	53	1.6	1.1 - 3.1
K^+	[mg/L]	53	1.5	0.6 - 3.5	53	0.5	0.3 - 1.4	53	0.9	0.5 - 2.1
Mg^{2+}	[mg/L]	53	9.4	2.9 - 13.1	53	11.0	4.9 - 14.3	53	15.4	12.7 - 17.7
Ca^{2+}	[mg/L]	53	134	84 - 224	53	77	64 - 104	53	74	65 - 82
HCO_3^-	[mg/L]	49	379	301 - 452	49	270	236 - 293	49	282	251 - 299
Cl^-	[mg/L]	53	11.1	6.9 - 15.7	53	2.9	2.0 - 8.6	53	3.5	2.8 - 5.2
NO_3^-	[mg/L]	53	31.9	14.5 - 55.1	53	7.6	4.4 - 31.0	53	7.2	5.4 - 14.5
SO_4^{2-}	[mg/L]	53	31.0	13.0 - 133	53	11.3	7.3 - 44.1	53	14.6	12.6 - 22.1
MAB [b]	[CFU/mL]	33	548	80 - 10740	47	20	3 - 2564	44	8	1 - 1174
Tot. colif. [c]	[CFU/100 mL]	31	4300	600 - 65600	47	131	14 - 8680	44	37	2 - 2150
E. coli	[CFU/100 mL]	32	32	3 - 1990	46	3	0 - 648	43	1	0 - 183
Enterococci	[CFU/100 mL]	32	28	2 - 890	46	2	0 - 480	44	1	0 - 123

[a] Number of samples

[b] Mesophilic aerobic bacteria

[c] Total coliforms

during stable flow conditions all monitored parameters were rather stable, highly variable, fast and strong reactions were observed during rainfall events (Fig. 2.1a). Large amounts of TOC and turbidity, rising up to 18.6 mg/L and 275 NTU, respectively, entered the system during such periods. Furthermore, all water samples collected at the swallow hole during storm events showed also very high contents of nitrate, chloride and faecal indicator bacteria (Table 2.3).

The eight individual Moulinet outlets (outlets 6A, 6B and 7A – 7F) showed identical physical and chemical characteristics (Fig. B.4 – B.7, Appendix B), except the discharge. This group of eight outlets may thus be considered as a single spring: the Moulinet spring[*]. The typical karstic hydrographs monitored at the junction of all outlets, differing from the step-like discharge curves of permanent outlets 6A, 6B and 7B, further strengthen this assumption.

Discharge of the Moulinet spring varied from 20 to about 750 L/s during the investigation period. Water temperature, which is more or less inversely correlated to spring discharge at an annual cycle scale, varied between 8.6 and 11.6 °C. These slightly subthermal temperatures are explained by a contribution of the deep and warm groundwater component to the spring (Muralt 1999) and cannot be attributed to the daily variable temperature of water sinking into the swallow hole. Indeed, from September to December 2005, the temperature of the Moulinet spring increased progressively until 11.6 °C, whereas the temperature of water entering the swallow hole was decreasing (Fig. B.1, Appendix B). Electrical conductivity, which was rather stable at about 460 µS/cm during stable flow conditions, showed rather complex temporal changes during storm

[*] From this point in the manuscript, unless it is clearly mentioned, Moulinet spring data, excluding discharge data, correspond to those monitored at the Moulinet 6A outlet. The discharge of the Moulinet spring corresponds to the total discharge of all eight outlets, which was monitored at their junction (see Fig. 1.3g).

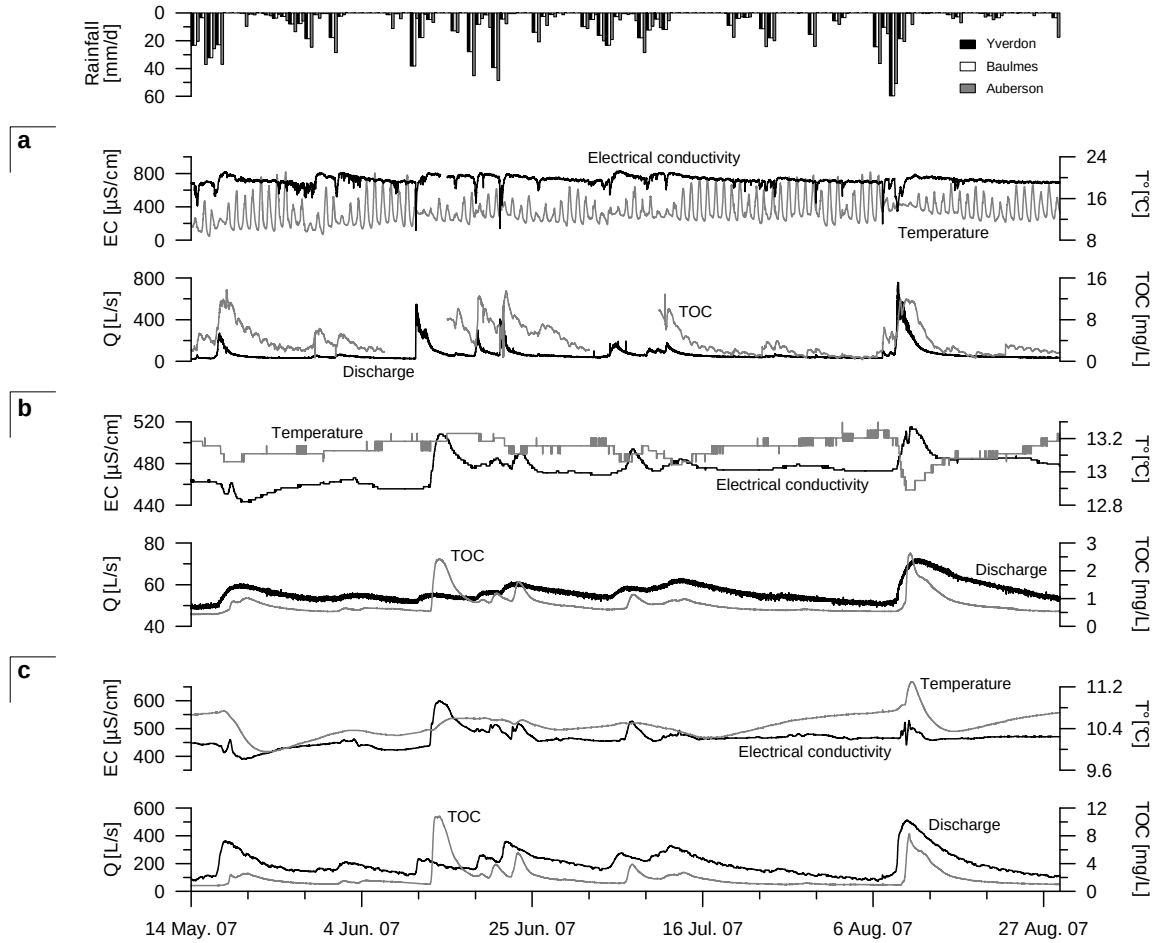

Fig. 2.1 Monitoring of natural parameters at the Yverdon-les-Bains karst aquifer system. (**a**) Feurtille swallow hole, (**b**) Cossaux spring and (**c**) Moulinet spring. Q: discharge; EC: electrical conductivity; T°: temperature.

events, comprising increases and decreases. This may reflect varying contributions of the three main components feeding the spring, especially following rainfall events. Electrical conductivity is therefore not a reliable tracer of any contributing component. TOC, which mainly originates from the soil and surface waters, was generally rather stable at a low level (0.2 – 0.8 mg/L) during stable flow conditions, but showed important increases following storm events (Fig. 2.1c). These high TOC content events provide evidence of an important contribution of the allochthonous swallow hole component. This contribution to spring water quality deterioration is also clearly discernable from chemical (e.g. nitrate, sulphate, chloride) and microbiological parameters (Table 2.3).

Temporal changes in physical, chemical and microbiological parameters at the Cossaux spring were highly similar to those of the Moulinet spring, whereas the absolute levels and amplitudes were differing (Fig. 2.1b and c). All parameters showed lower absolute levels and amplitudes at the Cossaux spring, except temperature and some major ions (in particular Mg^{2+}; Fig. 2.2). These latter also showed lower amplitude variations but always higher absolute levels (2 – 4 °C and 3 – 8 mg/L for temperature and Mg^{2+}, respectively). The Cossaux and Moulinet springs are thus outlets of the same flow system. However, the Cossaux spring receives an important additional

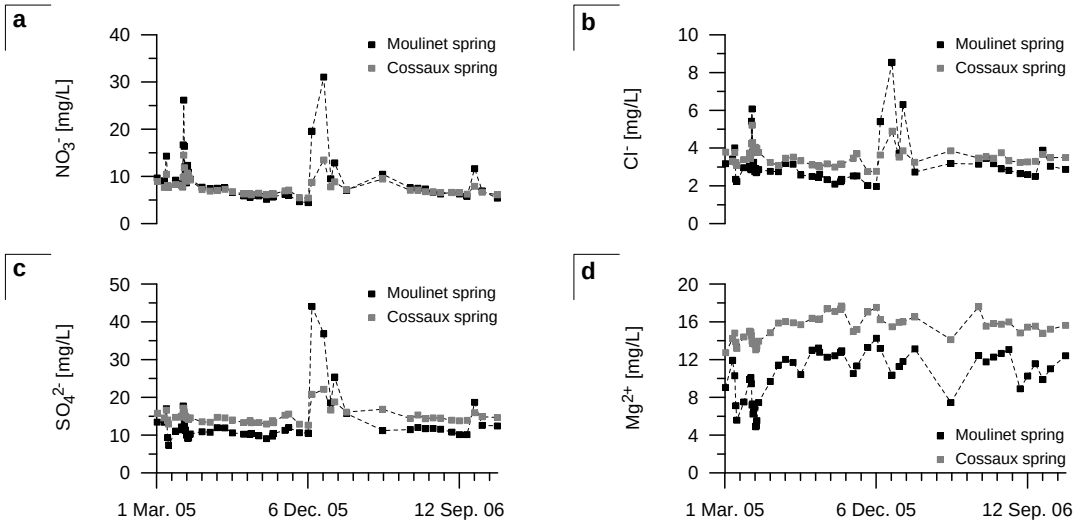

Fig. 2.2 Temporal changes in (**a**) NO_3^-, (**b**) Cl^-, (**c**) SO_4^{2-} and (**d**) Mg^{2+} at the Moulinet and Cossaux springs.

inflow of the deep and warm groundwater component (Muralt 1999), resulting in lower contamination levels and a 2 – 4 °C higher temperature. The important contribution of the slow, deep and warm groundwater component at the Cossaux spring is also reflected in the spring hydrographs, which showed wide low-amplitude shapes.

Finally, the small Grange-Décoppet spring showed identical physical and chemical characteristics to those of the Moulinet spring (Fig. B.8, Appendix B), proving that both springs are outlets of the same flow system and fed by an identical mixing of the different groundwater components. The discharge of the Grange-Décoppet spring, which varied between 3 and 40 L/s, is also closely linked to the discharge of the Moulinet spring (Fig. B.9, Appendix B). As the Moulinet and Grange-Décoppet springs are identical, further investigation will particularly focus on the relations between the Feurtille swallow hole and the Moulinet and Cossaux springs.

2.4 TRACER TESTS: QUANTIFICATION OF GROUNDWATER FLOW WITHIN THE SYSTEM

2.4.1 Swallow hole – springs tracer test during extreme low-flow conditions

On 1 September 2003, a first tracer test was carried out from the Feurtille swallow hole in order to infer its contribution to the springs. Summer 2003 was amongst the driest and warmest ever recorded in Switzerland. Consequently, the stream sinking into the swallow hole was dry during several weeks. However, a weak rainfall period occurred end of August 2003, generating by this way a very low discharge of the sinking stream of about 1 L/s at the moment of tracer injection. The discharges of the springs were extremely low and stable over a period of several months. The total discharge of the permanent outlets 6A, 6B and 7B of the Moulinet spring was about 19 L/s, while the other outlets were dry. The discharge of the Cossaux spring was about 43 L/s. All other monitored parameters (temperature, electrical conductivity, TOC and turbidity) showed also very stable levels. The September 2003 tracer test allowed thus observing the behaviour of the karst aquifer system during stable and extreme low-flow conditions (Fig. 2.3).

The distances from the swallow hole to the Moulinet and Cossaux springs are 4.8 and 6.3 km, respectively. Surprisingly the tracer first arrived at the Cossaux spring 259.8 h after injection and reached a maximum concentration of 8.7 µg/L after 311.9 h (Fig. 2.3a). At the Moulinet spring, the tracer was first detected after 292.4 h, the maximum concentration of 27.8 µg/L was measured 342.7 h after injection. Maximum linear groundwater flow velocities (calculated from the linear distance and the time of first arrival) were 16.4 m/h for the Moulinet spring and 24.4 m/h for the Cossaux spring. Dominant linear flow velocities were 14.0 and 20.3 m/h, respectively. However, these values do not represent real flow velocities in the conduit system.

After the first peak of the breakthrough curves, secondary uranine peaks were observed at the Cossaux (~ 400 – 500 h after injection) and Moulinet springs (~ 450 – 550 h after injection). This is explained by tracer remobilisation in the unsaturated zone near the injection point during the rainfall event of the 7th of September 2003 (154 h after tracer injection), which resulted in a small discharge increase to about 5 L/s of the sinking stream (Fig. 2.3a). Transit times corresponded well to those described above (261 h and 294 h for the Cossaux and Moulinet springs, respectively).

The similar behaviour among the eight outlets of the Moulinet spring, as well as the similar behaviour of the Moulinet and Grange-Décoppet springs, was also confirmed during the tracer test. The breakthrough curves at the three permanent Moulinet outlets (6A, 6B and 7B) were

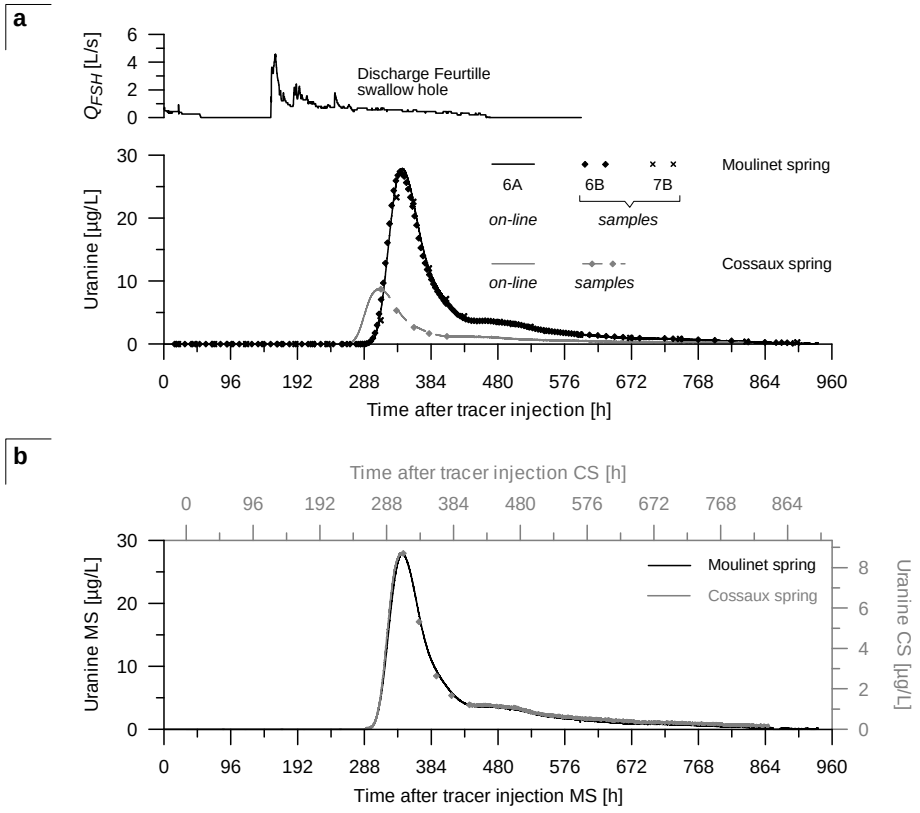

Fig. 2.3 (**a**) Uranine breakthrough curves at the Moulinet (MS) and Cossaux (CS) springs during the September 2003 tracer test (extreme low-flow conditions). (**b**) Similarity of the shapes of the uranine breakthrough curves.

almost identical. Furthermore, after heavy rainfall events, which occurred during the first week of October 2003, the non-permanent outlets (7A and 7C – F) started to discharge again. Identical uranine concentrations were subsequently measured at all outlets of this group. The daily samples collected at the small Grange-Décoppet spring (4.0 km away from the swallow hole) revealed similar tracer concentrations, with a delay of about 20 h, to those of the Moulinet spring.

The shape of the breakthrough curves of the Moulinet and Cossaux springs were remarkably similar (Fig. 2.3b). The time shift between the breakthrough curves was about 32 h, and the tracer concentrations at the Moulinet spring were approximately three times higher than at the Cossaux spring. This observation confirms that the Cossaux spring receives an additional contribution from another type of groundwater that is free of uranine (i.e. not affected by the swallow hole), causing dilution of the concentrations. The lower uranine concentrations at the Cossaux spring cannot be attributed to dispersion, double-porosity effects, adsorption, degradation or other processes, as its breakthrough at the Cossaux spring preceded the one of the Moulinet spring and as these processes would also change the shape of the breakthrough curve.

Tracer recovery rates were calculated based on the concentration-discharge-time data series. 12.3 % (123 g) of the tracer was recovered at the Cossaux spring. The recovery rates at the Moulinet outlets 6A, 6B and 7B were 3.7, 8.7 and 4.4 %, respectively. Recovery rates at the other outlets of this group were insignificant, because they were dry during the essential phase of the sampling period. The total tracer recovery at the Moulinet spring was thus 16.8 % (168 g), and the total tracer recovery at both springs was 29.1 %.

The rather rough breakthrough curve at the Grange-Décoppet spring, obtained from manual samples, did not allow the recovery rate to be calculated. Therefore, based on the similarity of the Grange-Décoppet and Moulinet springs and the relation between both springs' discharges, tracer recovery at the Grange-Décoppet spring was inferred from the data of the Moulinet spring. The recovery rate at the Grange-Décoppet spring was estimated at approximately 2 %.

Results of this first quantitative tracer test demonstrate that contaminated water sinking into the swallow hole may have a major impact on spring water quality, while its contribution to the water quantity (spring discharge) is insignificant during extreme low-flow conditions.

2.4.2 Conceptual flow model of the Yverdon-les-Bains karst aquifer system

The September 2003 tracer test made it possible, along with the observations resulting from the monitoring of natural parameters, to improve the existing conceptual flow model of the Yverdon-les-Bains karst aquifer system (Muralt 1999; see Fig. 1.4) and to quantify groundwater flow rates during extreme low-flow conditions. The model is based on the following observations and assumptions:

1. the tracer test proved a connection between the Feurtille swallow hole and the Mont de Chamblon springs;

2. geological and hydrological observations, as well as water temperature, chemical and isotopic data, suggest that the springs also receive large inflows from both the karst groundwater component and the deep and warm groundwater component (Muralt 1999). Local

groundwater from the Mont de Chamblon does not contribute significantly to the springs, and may thus be neglected;

3. the tracer breakthrough curves at both springs had a similar shape, but the concentrations at the Moulinet spring were higher than at the Cossaux spring. This behaviour, which was also observed for natural parameters, suggests that the Cossaux spring receives an additional inflow from groundwater that is free of uranine, i.e. the deep and warm groundwater component. Water temperature, chemical and isotopic data further confirm this assumption (Muralt 1999);

4. only about 29 % of uranine was recovered at the Moulinet and Cossaux springs. In a conduit system, uranine behaves nearly as a conservative tracer, i.e. there is no significant adsorption or degradation loss (Käss 1998). The proposed model thus assumes that most of the tracer that was not recovered at the springs discharged elsewhere: at the numerous minor outlets of the Mont de Chamblon such as the Grange-Décoppet spring; through subsurface outlets in the plain surrounding the Mont de Chamblon; or even flowed further down-gradient following the PCC fault zone. The presence of subsurface outlets was proven by the presence of uranine, during ulterior tracer experiments (April 2006 and November 2007 tracer tests), in an artificial conduit draining the plain about 500 m west of the Moulinet spring.

On this basis, it was possible to design a conceptual model showing the most important underground flow paths (Fig. 2.4). The model represents the simplest possible solution; the real system is almost certainly much more complicated. The flow rates inside the system were determined based on two types of equations: water balance and mass balance equations (Atkinson *et al*. 1973).

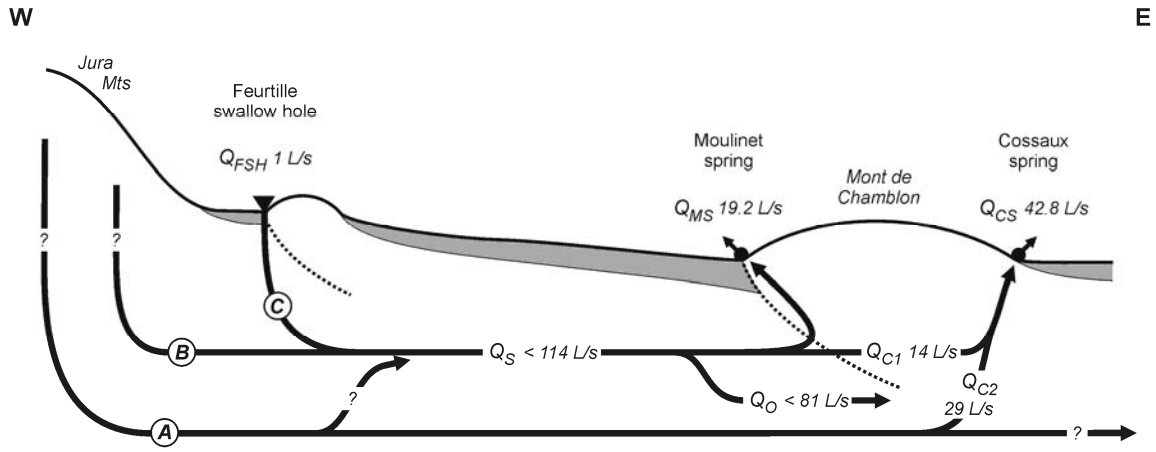

Fig. 2.4 Simplified conceptual flow model (schematic W – E cross-section) of the Yverdon-les-Bains karst aquifer system. The observed and calculated groundwater flow rates only apply for the hydrologic situation during the September 2003 tracer test. ***A***: deep and warm groundwater component; ***B***: karst groundwater component; ***C***: Feurtille swallow hole component; Q_{FSH}: Feurtille swallow hole discharge; Q_S: system discharge; Q_{MS}: Moulinet spring discharge; Q_{CS}: Cossaux spring discharge; Q_{C1}: discharge of Q_S feeding the Cossaux spring; Q_{C2}: discharge of the additional inflow of the deep and warm groundwater component at the Cossaux spring; Q_O: amount of groundwater not discharging at the Moulinet and Cossaux springs. Dotted lines symbolise major thrust faults, and grey shaded areas represent the low-permeability sediments confining the karst aquifer system.

Two water balance equations (Eq. 2.1 and 2.2) describe the flow organisation in the system, down-gradient of the Feurtille swallow hole contribution. Water flowing in the karst aquifer system between the swallow hole and the springs, which will be referred to as the system discharge Q_S, is composed of the deep and warm groundwater component (component *A*), the karst groundwater component (component *B*) and the Feurtille swallow hole component (component *C*). The system discharge Q_S is given by (Eq. 2.1):

$$Q_S = Q_{MS} + Q_{C1} + Q_O \tag{2.1}$$

where Q_{MS}, Q_{C1} and Q_O represent, respectively, the discharge of the Moulinet spring, the amount of Q_S discharging at the Cossaux spring and the amount of water discharging or flowing elsewhere. Furthermore, as mentioned before, the Cossaux spring discharge Q_{CS} results from two different inflows (Eq. 2.2):

$$Q_{CS} = Q_{C1} + Q_{C2} \tag{2.2}$$

where Q_{C2} corresponds to the additional inflow from the deep and warm groundwater component, which is not affected by the swallow hole component.

Following mass balance equations (Eq. 2.3 and 2.4), the observed Moulinet spring discharge Q_{MS}, along with the tracer recoveries at the Moulinet spring R_{MS} and Cossaux spring R_{CS}, allow the underground flow rates to be calculated. The system discharge Q_S is quantified according to (Eq. 2.3):

$$Q_S = Q_{MS} \cdot \left(100 / R_{MS}\right) \tag{2.3}$$

Similarly, Q_{C1} is calculated as follows (Eq. 2.4):

$$Q_{C1} = Q_{MS} \cdot \left(R_{CS} / R_{MS}\right) \tag{2.4}$$

Finally, Q_O and Q_{C2} are determined following Eq. 2.1 and 2.2, respectively.

The calculated flow rates only apply to the hydrologic conditions during the September 2003 tracer test. According to this calculation, the water sinking into the swallow hole (1 L/s, component ***C***) mixed with 113 L/s of groundwater in the karst aquifer (***A*** and ***B***). This flow split up into three pathways: 19 L/s discharged at the Moulinet spring, 14 L/s flowed to the Cossaux spring and 81 L/s discharged elsewhere or remained in the aquifer. The Cossaux spring received an additional inflow of 29 L/s from a deeper part of the aquifer system (***A***), which diluted the uranine concentrations. However, a small part of the tracer loss might be attributed to double-porosity effects or other processes; the long tail of the tracer breakthrough curve supports this assumption. The true flow rates inside the aquifer might thus be < 114 L/s up-gradient and < 81 L/s down-gradient from the springs.

2.4.3 Other swallow hole – springs tracer tests

Four additional quantitative tracer tests were carried out between the swallow hole and the springs during different but relatively stable flow conditions within the system. All other monitored parameters (temperature, electrical conductivity and TOC) remained also more or less stable during these tracer experiments. Main tracer test results, as well as the general hydrological conditions in which they were performed, are summarised below. Uranine breakthrough curves are shown in Fig. 2.5, and main properties (including those of the September 2003 tracer test) are given in Table 2.4.

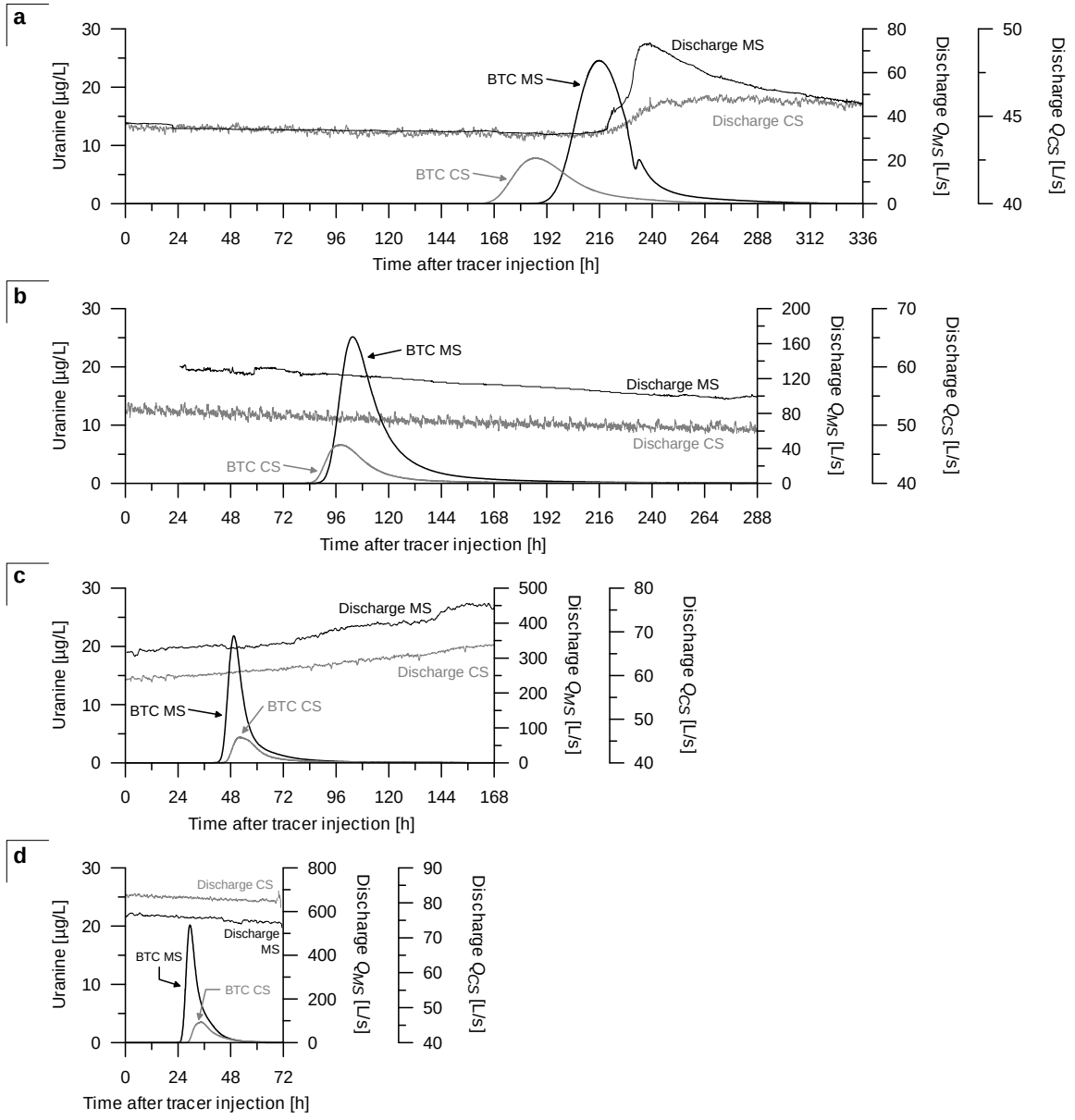

Fig. 2.5 Uranine breakthrough curves (BTC) at the Moulinet and Cossaux springs (MS and CS, respectively) during the (**a**) November 2007 (low-flow conditions), (**b**) June 2005 (medium-flow conditions), (**c**) March 2005 (high-flow conditions) and (**d**) April 2006 (extreme high-flow conditions) tracer experiments.

- The November 2007 tracer test (Fig. 2.5a) was carried out during low-flow conditions. The karst aquifer system was in a general recession period since August 2007. The discharge of the stream sinking into the Feurtille swallow hole at the moment of tracer injection was about 14 L/s, while the mean discharges of the Moulinet and Cossaux springs during the tracer test were 34 and 44 L/s, respectively. As during the September 2003 tracer test, uranine was first detected at the Cossaux spring after 159.1 h, against 183.3 h for the Moulinet spring. Tracer recoveries at the Moulinet and Cossaux springs were 21.1 and 8.6 %, respectively. The small rainfall event, which occurred on 11 November 2007 (about 220 h after tracer injection) and resulted in small discharge increases at the springs, only slightly affected the breakthrough curve at the Moulinet spring.
- The June 2005 tracer test (Fig. 2.5b) was conducted during medium-flow conditions. The heavy storm events of April 2005, combined with several less intense rainfall events during the month of May 2005, generated mean discharges at the Moulinet and Cossaux springs of about 130 and 50 L/s, respectively. The swallow hole flow rate was 21 L/s at the moment of

Table 2.4 Summary of swallow hole – springs tracer test results. Moulinet spring recovery rates (R_{MS}) were obtained from mean values of the Moulinet 6A and 6B outlet recovery rates.

Location	Property	Unit	Tracer injection date				
			1 Sept. 03	2 Nov. 07	2 June 05	21 Mar. 05	22 Apr. 06
Feurt. swallow hole (FSH)	Discharge Q_{FSH} [a]	[L/s]	1	14	21	52	103
Moulinet spring (MS)	Discharge Q_{MS} [b]	[L/s]	19	34	125	338	560
	$t_{\text{first detection}}$ [c]	[h]	292.4	183.3	86.9	40.3	23.7
	Peak concentration	[µg/L]	27.9	24.6	25.2	21.8	20.2
	$t_{\text{peak concentration}}$ [d]	[h]	342.8	215.8	103.5	49.4	29.4
	Flow velocity $_{\text{max. lin.}}$ [e]	[m/h]	16.4	26.2	55.2	119.1	202.5
	Flow velocity $_{\text{dom. lin.}}$ [f]	[m/h]	14.0	22.2	46.4	97.2	163.3
	Recovery R_{MS}	[%]	16.8	21.1	26.1	27.5	28.8
Cossaux spring (CS)	Discharge Q_{CS} [b]	[L/s]	43	44	52	61	81
	$t_{\text{first detection}}$ [c]	[h]	259.8	159.1	81.9	43.5	27.8
	Peak concentration	[µg/L]	8.7	7.8	6.6	4.5	3.5
	$t_{\text{peak concentration}}$ [d]	[h]	311.9	186.9	98.4	52.2	34.6
	Flow velocity $_{\text{max. lin.}}$ [e]	[m/h]	24.4	39.8	77.3	145.5	227.7
	Flow velocity $_{\text{dom. lin.}}$ [f]	[m/h]	20.3	33.9	64.3	121.3	182.9
	Recovery R_{CS}	[%]	12.3	8.6	3.2	1.6	1.1
	Q_{C1}	[L/s]	14	14	15	20	21
	Q_{C2}	[L/s]	29	30	37	41	60
MS + CS	Total recovery	[%]	29.1	29.7	29.3	29.1	29.9
Malm karst aquifer	System discharge Q_S	[L/s]	114	160	479	1229	1944

[a] Discharge at the moment of injection
[b] Mean discharge during the tracer test
[c] Time of first detection
[d] Time of peak concentration
[e] Maximum linear flow velocity
[f] Dominant linear flow velocity

tracer injection. Uranine was again first detected at the Cossaux spring after 98.4 h following tracer injection, preceding by 5 h its arrival at the Moulinet spring. Uranine recoveries were 26.1 and 3.2 % for the Moulinet and Cossaux springs, respectively.

- The March 2005 tracer test (Fig. 2.5c) was performed during high-flow conditions. A period of snowmelt on the Jura Mountains, which began about a week before the tracer experiment, resulted in high and stable (slightly increasing) flow rates within the system. Mean discharges of the Moulinet and Cossaux springs during the tracer experiment were approximately 340 and 60 L/s, respectively. At the moment of tracer injection, the swallow hole flow rate was about 50 L/s. Conversely to the aforementioned tracer experiments, uranine arrival was first detected at the Moulinet spring after 49.4 h, preceding the tracer arrival at the Cossaux spring by about 3 h. Tracer recoveries were 27.5 and 1.6 % for the Moulinet and Cossaux springs, respectively.
- Finally, the April 2006 tracer test (Fig. 2.5d) was carried out during extreme high-flow conditions. The combination of snowmelt and several heavy rainfalls, occurring begin April 2006, resulted in very high and stable discharges in the karst aquifer system: mean discharges of the Moulinet and Cossaux springs during the tracer experiment were approximately 560 and 80 L/s, respectively. The flow rate of the swallow hole was about 100 L/s. First tracer detection occurred again at the Moulinet spring after 23.7 h, preceding by about 4 h the first arrival at the Cossaux spring. Tracer recoveries were 28.8 and 1.1 % at the Moulinet and Cossaux springs, respectively.

During all tracer experiments, uranine was also detected at the Grange-Décoppet spring. However, as for the September 2003 tracer test, the irregular breakthrough curves did not allow the recovery rates to be calculated. Moreover, the continuous monitoring of the breakthrough curve during the November 2007 tracer experiment failed due to instrument defaults. Recovery rates at the Grange-Décoppet spring were thus inferred from the Moulinet spring results. The calculated tracer recoveries ranged between 2 and 3 % (March 2005: 2.4 %; June 2005: 2.7 %; April 2006: 2.0 %; November 2007: 1.9 %).

Results of these tracer experiments were in agreement with the earlier mentioned observations and assumptions, which allowed the conceptual flow model of the karst aquifer system to be established. Besides the proved hydrogeological connection between the swallow hole and the springs, tracer breakthrough curves at both springs had again very similar shapes and uranine concentrations were also always higher at the Moulinet spring. By this way, the additional inflow of the deep and warm groundwater component, which is not affected by the Feurtille swallow hole component, at the Cossaux spring is confirmed.

Flow rates within the karst aquifer system, which were quantified according to Equations 2.1 – 2.4, varied, however, highly from one tracer experiment to the other (Table 2.4). This is particularly marked by the system discharge Q_S, which ranged from 114 L/s during the September 2003 tracer test (extreme low-flow conditions) to about 2000 L/s during the April 2006 tracer test (extreme high-flow conditions). On this basis, it was possible to establish the relation between the Moulinet spring discharge Q_{MS} and the system discharge Q_S, which revealed a good linear correlation (Fig. 2.6). This relation allows thus quantifying the system discharge Q_S for any moment.

According to the conceptual model, it is suggested that these variable flow conditions within the karst aquifer system downstream of the swallow hole contribution, i.e. the system discharge Q_S, are governing the response of the swallow hole contribution at the springs. Tracer transit times between the swallow hole and the springs are function of the system discharge Q_S (Fig. 2.7a). This relation between system discharge and transit time may not be surprising, as the Yverdon-les-Bains karst aquifer system is confined by low-permeable sediments and thus fully saturated. An increasing discharge corresponds therefore to increasing flow velocities. The variable flow conditions in which the tracer experiments were performed also affected tracer recoveries at the springs (Fig. 2.7b). With increasing flow rates, tracer recoveries increased at the Moulinet spring and decreased at the Cossaux spring. Total recovery at both springs remained, however, constant at 29.4 ± 0.7 %. This behaviour suggests that the Moulinet spring acts as an overflow spring of the Cossaux spring. This may also be observed from the discharge data of both springs.

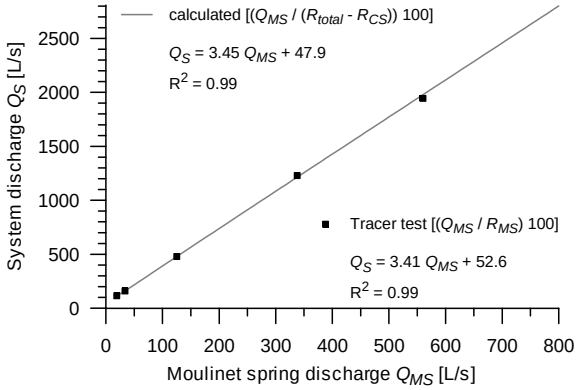

Fig. 2.6 Relation between the Moulinet spring discharge (Q_{MS}) and the system discharge (Q_S), obtained from tracer test results and calculated following the relation presented in Fig. 2.7b.

During low- and medium-flow conditions, uranine was first detected at the Cossaux spring, preceding the first arrival times at the Moulinet spring by 32.6, 24.2 and 5 h for the September 2003, November 2007 and June 2005 tracer tests, respectively. Conversely, during high-flow

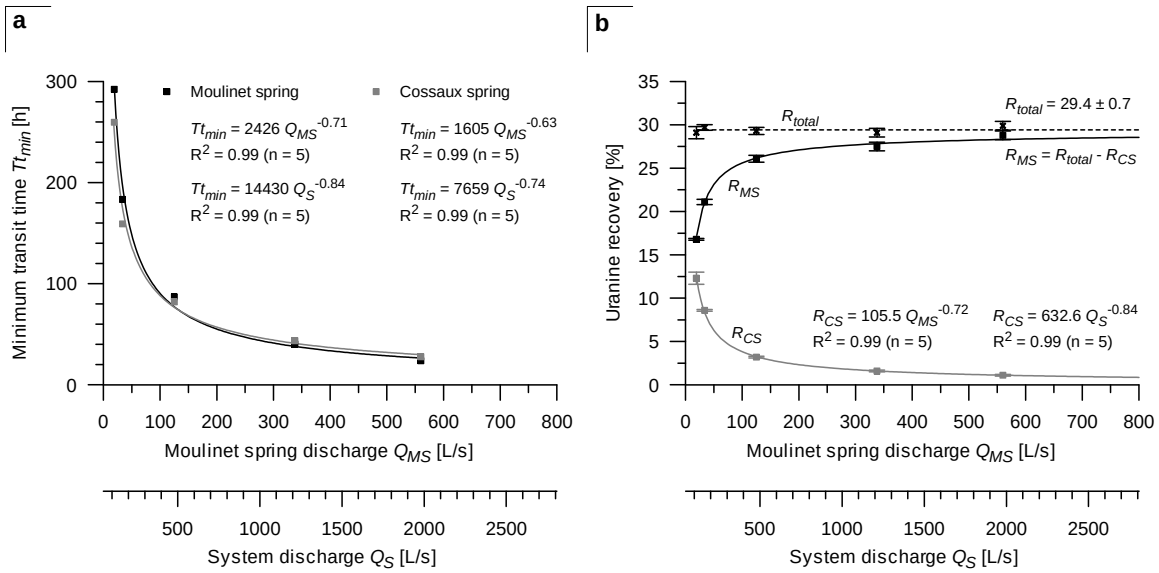

Fig. 2.7 (**a**) Minimum transit times (Tt_{min}) between the swallow hole and the springs as function of the system discharge (Q_S) or the Moulinet spring discharge (Q_{MS}), obtained from tracer test results. (**b**) Moulinet spring, Cossaux spring and total uranine recovery rates (R_{MS}, R_{CS} and R_{total}, respectively) as function of the system discharge or the Moulinet spring discharge.

conditions, uranine first appeared at the Moulinet spring, preceding first detection at the Cossaux spring by 3.2 and 4.1 h for the March 2005 and April 2006 tracer tests, respectively. This transit-time inversion is attributed to the variations of the hydraulic head in the recharge area, which affects the hydraulic gradient in the karst aquifer system, and the positioning (distance and altitude) of both springs with respect to the recharge area (Fig. 2.8). During low- and medium-flow conditions, the hydraulic gradient between the recharge area and the Cossaux is larger than the one between the recharge area and the Moulinet spring, resulting in an earlier breakthrough at the Cossaux spring. Conversely, during high-flow conditions, this relation is inverted. The latter case results in an earlier breakthrough at the Moulinet spring.

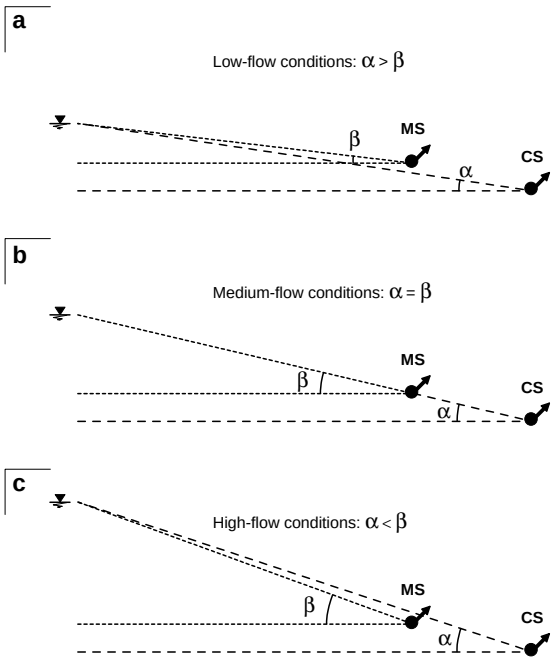

Fig. 2.8 Schematic illustration explaining the transit-time inversion. (**a**) low-flow conditions, (**b**) medium-flow conditions and (**c**) high-flow conditions. MS: Moulinet spring; CS: Cossaux spring.

2.4.4 Regional tracer test

The regional tracer test, which intended at identifying the main recharge area in the Jura Mountains (the injection point was approximately 2 km north-west of the Feurtille swallow hole; see Fig. 1.2) of the Mont de Chamblon springs, was not successful. All samples collected at the Cossaux, Moulinet and Grange-Décoppet springs, during a period of four months following the tracer injection, showed negative responses. However, analyses of the charcoal bags installed at the springs between June and July 2007 and August and September 2007 revealed very fine traces of sulforhodamine B of approximately 1 µg/L. Nevertheless, these results have to be handled with caution and do not allow establishing with certitude a hydrogeological connection between the injection point and the Mont de Chamblon springs. The regional tracer test did thus not allow further improving or refuting the conceptual flow model of the Yverdon-les-Bains karst aquifer system.

2.5 TOC: A NATURAL TRACER OF THE SWALLOW HOLE COMPONENT

A typical response of the Yverdon-les-Bains karst aquifer system to an intense rainfall event is shown in Fig. 2.9. As a long dry period of approximately two months preceded the rainfall event, the latter occurred in a general context of low-flow conditions. Discharge of the stream sinking into the Feurtille swallow hole increased rapidly from 20 to over 200 L/s (Fig. 2.9a), followed by rapid recession. During this event, large quantities of TOC entered the swallow hole (up to 14 mg/L).

Spring responses to precipitation events may generally be synthesised in the three following phases (Perrin 2003):

I. a lag phase, where rainfall has already occurred but the system shows no reaction. The duration of this phase is essentially dependent on the degree of saturation of the soil. Pre-storm conditions prevail during this phase;

II. a pulse-through phase (or piston phase), starting at the moment of flow increase and lasting until the arrival of runoff-event recharge. Water discharging at the springs during this phase results principally from the displacement of antecedent (i.e. pre-storm) water in the system;

III. a flow-through phase (or mixing phase), principally characterised by the arrival of storm-derived water that entered the system. Water discharging at the springs during this phase results from a mixing of waters from different origins (base-flow water, soil water and freshly infiltrated water).

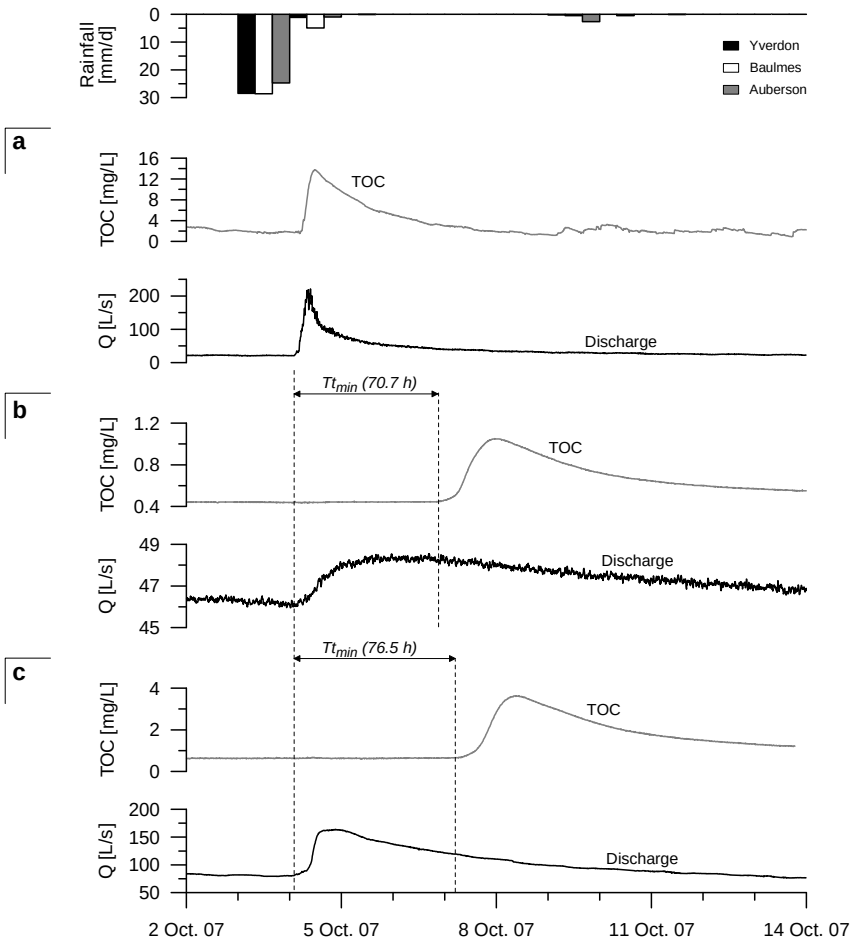

Fig. 2.9 Typical response of the Yverdon-les-Bains karst aquifer system to an intense rainfall event. (**a**) Feurtille swallow hole, (**b**) Cossaux spring and (**c**) Moulinet spring. Q: discharge; Tt_{min}: minimum swallow hole – spring transit time.

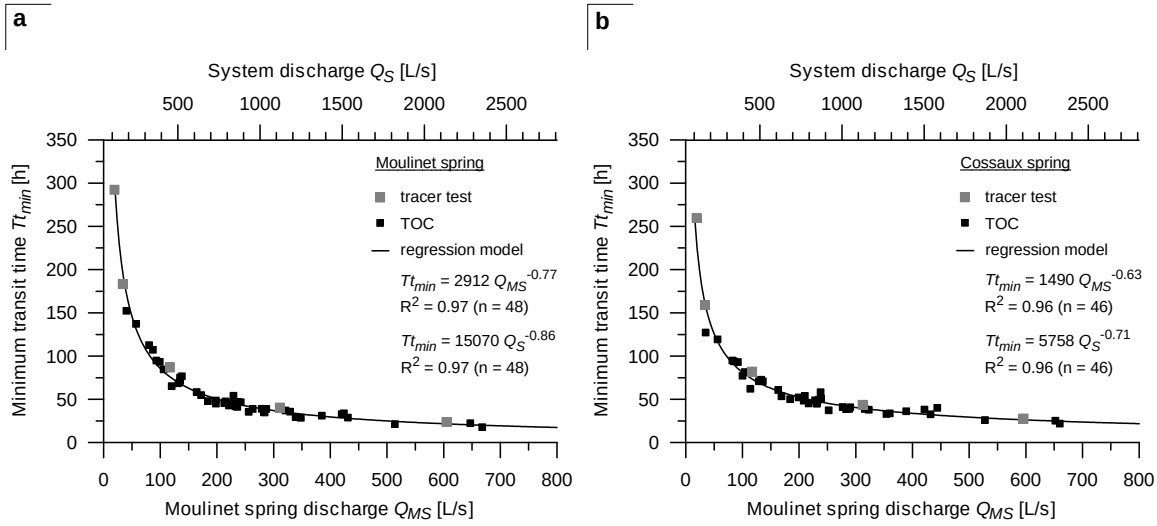

Fig. 2.10 Minimum transit times (Tt_{min}) between the swallow hole and the (**a**) Moulinet and (**b**) Cossaux springs as function of the system discharge (Q_S) or the Moulinet spring discharge (Q_{MS}), obtained from tracer tests and monitoring of TOC after rainfall events. Minimum transit times are spans of time between the moment of injection (artificial tracers), or discharge increase at the swallow hole (TOC), and the time when the respective parameter started to increase at the springs. The relative average absolute errors of the regression models are 8.1 and 7.6 % for the Moulinet and Cossaux springs, respectively.

During this study, it was not possible to clearly define the lag phase, as the resolution of precipitation data was too large (daily data). Nevertheless, preceding phase *II*, TOC and spring discharge were stable at low pre-storm levels at both the Moulinet spring and the Cossaux spring (Fig. 2.9b and c). This lag phase will thus further be described as the initial phase, representing

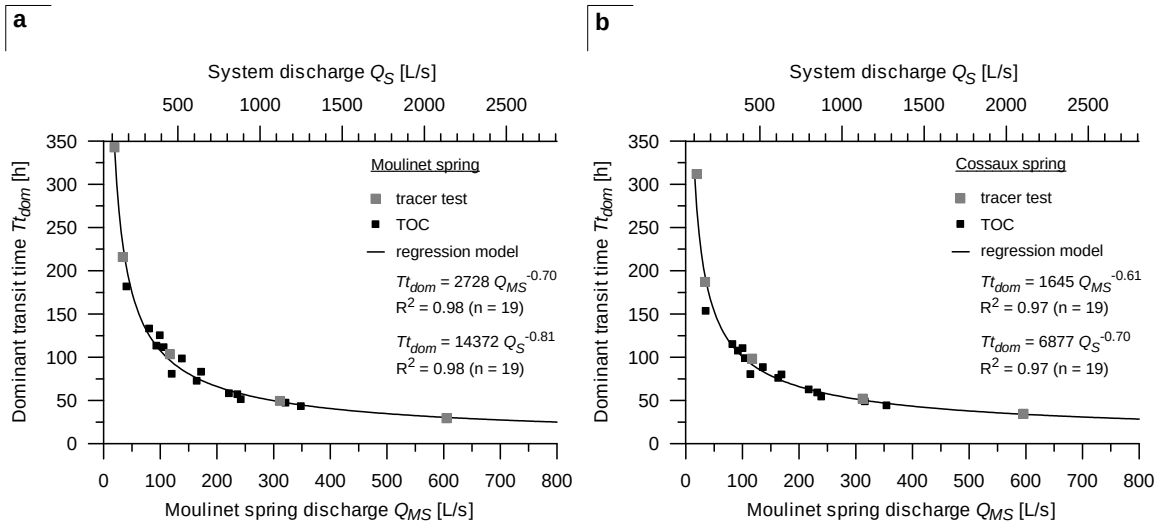

Fig. 2.11 Dominant transit times (Tt_{dom}) between the swallow hole and the (**a**) Moulinet and (**b**) Cossaux springs as function of the system discharge (Q_S) or the Moulinet spring discharge (Q_{MS}), obtained from tracer tests and monitoring of TOC after rainfall events. Dominant transit times are spans of time between the moment of injection (artificial tracers), or maximum discharge at the swallow hole (TOC), and the time when the respective parameter peaked at the springs. The relative average absolute errors of the regression models are 6.9 and 6.1 % for the Moulinet and Cossaux springs, respectively.

pre-storm conditions with low and stable values for all parameters and lasting until spring discharge increases. During phase *II* (pulse-though phase), the discharge of the Moulinet spring increased from approximately 80 to 170 L/s. The discharge of the Cossaux spring, which increased from about 46 to 48 L/s, was only slightly affected by the hydraulic pressure increase in the system. The fact that the Cossaux spring is mainly fed by the slow, deep and warm groundwater component explains this behaviour (see Section 2.4). At both springs, TOC remained stable at its pre-storm level during this phase, indicating that the water discharging at the springs corresponded to the displacement of antecedent water in the system.

About three days after the rainfall, when discharge was already in a recession stage, TOC increased abruptly. This is attributed to the arrival of TOC-rich, storm-derived water (phase *III*) that entered the Feurtille swallow hole. This is also corroborated by the time lags between the infiltration event at the swallow hole and the arrival at the springs (Tt_{min}), which corresponded well to the discharge-dependent transit times obtained during the tracer experiments (Fig. 2.10 and 2.11). These results showed that TOC is a typical natural tracer of the Feurtille swallow hole component.

2.6 ESTIMATION OF THE SWALLOW HOLE CONTRIBUTION TO THE SYSTEM DISCHARGE

The relation between Moulinet spring discharge and system discharge presented earlier (Fig. 2.6), along with the discharge of the stream sinking into the Feurtille swallow hole, allowed estimating on an annual basis the contribution of the swallow hole component (Q_{FSH}) to the system discharge (Q_S). The total volume of water entering the Feurtille swallow hole represented only about 6, 11 and 10 % of the total volume of groundwater flowing in the karst system for the years 2005, 2006 and 2007, respectively. By the way, this confirms that the largest part of groundwater discharging at the Mont de Chamblon springs is composed of the karst groundwater and the deep and warm groundwater components. However, it is obvious that the swallow hole contribution to the system discharge may vary at smaller time scales, and more especially during and following rainfall events.

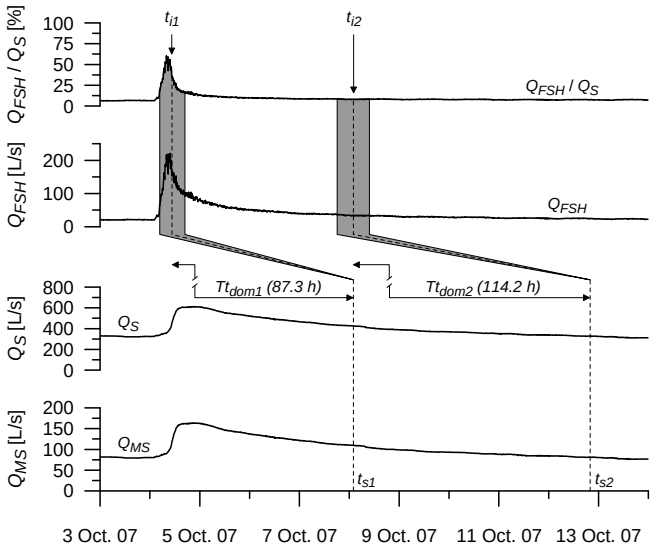

Fig. 2.12 Estimation of the Feurtille swallow hole contribution to the system discharge during the calculated infiltration time lag (Q_{FSH} / Q_S). Q_{MS}: Moulinet spring discharge; Q_S: system discharge; Q_{FSH}: discharge of the stream sinking into the swallow hole; Tt_{dom}: dominant transit time; t_s: sampling time; t_i: calculated infiltration time at the swallow hole. Grey shaded areas, representing the calculated infiltration time lag, were determined according to the relative average absolute errors of the discharge-dependent transit time relationship.

Based on the discharge-dependent transit time relationship,

along with the Moulinet spring discharge and system discharge relation, it was possible to estimate, for a sample collected at any moment at the springs, the contribution of the Feurtille swallow hole component (Q_{FSH}) to groundwater flow within the karst system (Q_S) at the moment of infiltration (Fig. 2.12). This moment of infiltration at the swallow hole (t_i) for a sample collected at time t_s was calculated according to the discharge-dependent dominant transit times (Eq. 2.5):

$$Tt_{dom} = t_s - t_i = a \cdot \left(\frac{\int_{t_i}^{t_s} Q_S \cdot dt}{t_s - t_i} \right)^b \tag{2.5}$$

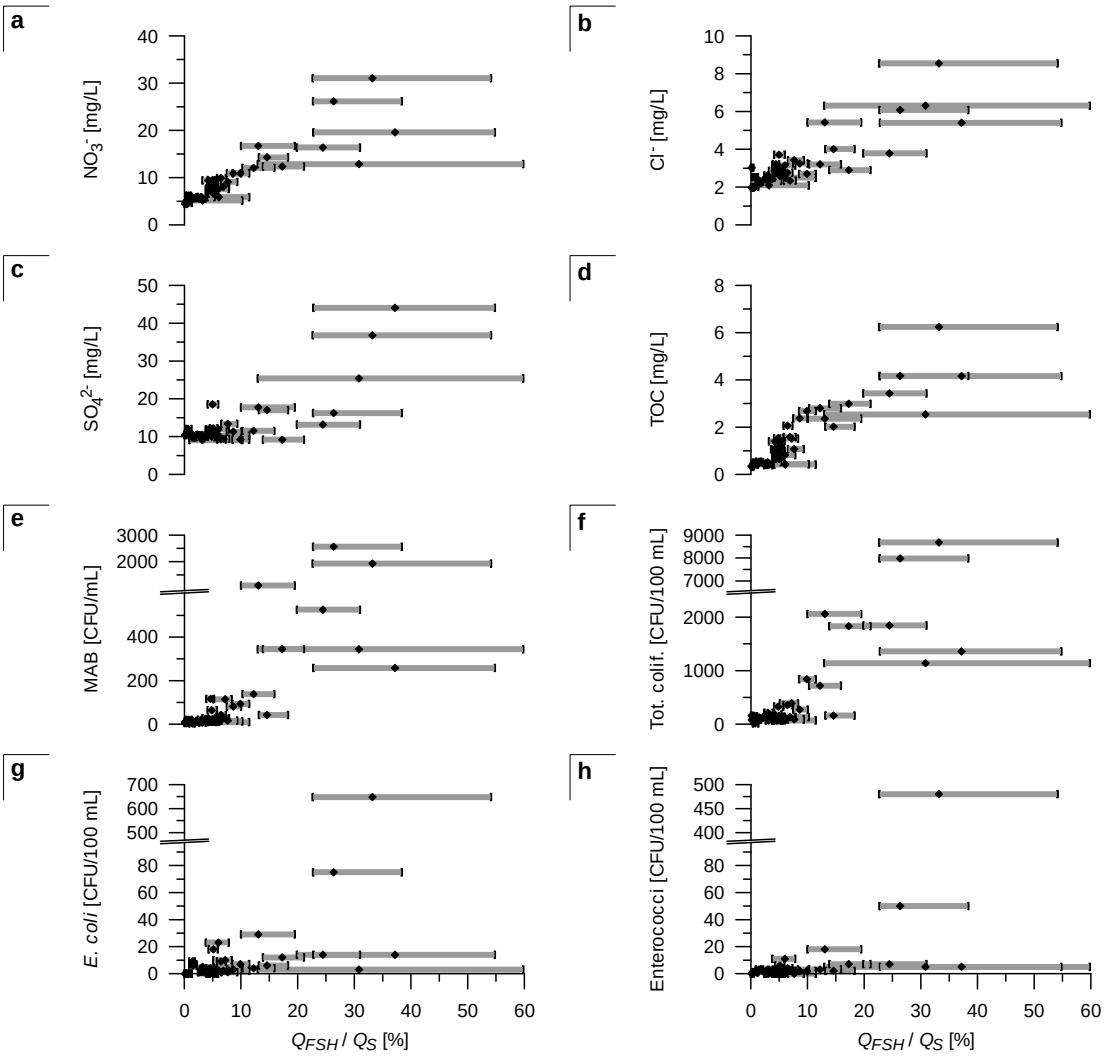

Fig. 2.13 Feurtille swallow hole contribution to the system discharge during the calculated infiltration time lag (Q_{FSH} / Q_S) versus major ion and water quality indicator bacteria contents of samples collected at the Moulinet spring: (**a**) NO_3^-, (**b**) Cl^-, (**c**) SO_4^{2-}, (**d**) TOC, (**e**) mesophilic aerobic bacteria (MAB), (**f**) total coliforms (Tot. colif.), (**g**) *E. coli* and (**h**) enterococci. Mean values (diamonds) with respective minimum and maximum values are shown. Similar data for the Cossaux spring are shown in Fig. B.10 (Appendix B).

where the equation in parentheses represent the mean system discharge during t_s and t_i, a is the intercept and b the slope of the regression model (see Fig. 2.11 for values). Knowing the moment of infiltration at the Feurtille swallow hole, it is thus possible to estimate its contribution to the system discharge at that time (Q_{FSH} / Q_S). For the example shown in Fig. 2.12, Q_{FSH} / Q_S varied between 16 and 59 % for the sample collected at time t_{s1}, against 8 and 9 % for the sample collected at time t_{s2}.

As these calculated Q_{FSH} / Q_S values may be correct during stable flow conditions, they are certainly overestimated during rainfall periods. It is suggested that during storm events, large amounts of water entering the Feurtille swallow hole may be stored in the unsaturated zone close to the swallow hole. This hypothesis is confirmed by the long tailing of TOC observed at the springs following rainfall events. Nevertheless, high calculated Q_{FSH} / Q_S values indicate a strong swallow hole impact. The effect of Q_{FSH} / Q_S estimates on major ion and water quality indicator bacteria contents of samples collected at the Moulinet spring is shown in Fig. 2.13. During low swallow hole contribution, low levels of typical allochthonous parameters are monitored at the spring. In contrast, high levels of allochthonous parameters reflect a strong impact of the swallow hole.

2.7 CONCLUSION

Results presented here demonstrated that quantitative tracer experiments performed during different hydrological conditions can lead to useful information on the structure of karst aquifer systems. The combination of the monitoring of physical, chemical and microbiological parameters and tracer tests allowed designing a conceptual flow model of the system and to quantify the flow rates within this system.

Concerning the Yverdon-les-Bains karst aquifer system, it was shown that the Feurtille swallow hole strongly impacts water quality of the Mont de Chamblon springs. While the annual contribution of the swallow hole to the groundwater flow within the system was approximately 10 %, the swallow hole contribution varied extremely at smaller time scales, particularly during and following storm events.

Finally, this in-depth characterisation of flow organisation in the Yverdon-les-Bains karst aquifer system, and more specifically the characterisation of the allochthonous swallow hole contribution, will allow further investigation on particle and faecal bacteria dynamics in karst aquifers (Chapter 3) and the characterisation of microbial communities in karst groundwater (Chapter 5).

REFERENCES

American Public Health Association, American Water Works Association and Water Environment Federation (APHA, AWWA and WEF). 2005. Standard methods for the examination of water and wastewater, 21st Edition. Water Environment Federation, Alexandria, VA.

Atkinson T.C., Smith D.I., Lavis J.J. and Whitaker R.J. 1973. Experiments in tracing underground waters in limestones. Journal of Hydrology 19 (4): 323-349.

Baker A. 2001. Fluorescence excitation – emission matrix characterization of some sewage-impacted rivers. Environmental Science & Technology 35 (5): 948-953.

Baker A. and Genty D. 1999. Fluorescence wavelength and intensity variations of cave waters. Journal of Hydrology 217 (1-2): 19-34.

Batiot C. 2002. Etude expérimentale du cycle du carbone en régions karstiques. Apport du carbone organique et du carbone minéral à la connaissance hydrogéologique des systèmes. PhD thesis, University of Avignon and Pays de Vaucluse, France.

Käss W. 1998. Tracing technique in geohydrology. Balkema, Rotterdam.

MacCraith B., Grattan K.T.V., Connolly D., Briggs R., Boyle W.J.O. and Avis M. 1993. Cross comparison of techniques for the monitoring of total organic-carbon (TOC) in water sources and supplies. Water Science and Technology 28 (11-12): 457-463.

Mrkva M. 1983. Evaluation of correlations between absorbance at 254 nm and COD of river waters. Water Research 17 (2): 231-235.

Muralt R. 1999. Processus hydrogéologiques et hydrochimiques dans les circulations profondes des calcaires du Malm de l'arc jurassien (zones de Delémont, Yverdon-les-Bains, Moiry, Genève et Aix-les-Bains). Beiträge zur Geologie der Schweiz, Geotechnische Serie, Lieferung 82, Schweizerischen Geotechnischen Kommission, Zürich.

Perrin J. 2003. A conceptual model of flow and transport in a karst aquifer based on spatial and temporal variations of natural tracers. PhD thesis, Centre of Hydrogeology, University of Neuchâtel, Switzerland.

Perrin J. and Luetscher M. 2008. Inference of the structure of karst conduits using quantitative tracer tests and geological information: example of the Swiss Jura. Hydrogeology Journal 16 (5): 951-967.

Reid J.M., Cresser M.S. and MacLeod D.A. 1980. Observations on the estimation of total organic-carbon from UV absorbance for an unpolluted stream. Water Research 14 (5): 525-529.

Savoy L. 2007. Use of natural and artificial reactive tracers to investigate the transfer of solutes in karst systems. PhD thesis, Centre of Hydrogeology, University of Neuchâtel, Switzerland.

Schnegg P.A. 2002. An inexpensive field fluorometer for hydrogeological tracer tests with three tracers and turbidity measurements. Proceedings of the XXXII IAH and VI ALHSUD Congress on Groundwater and Human Development, Mar de Plata (Argentina), 21-25 Oct. 2002, p. 1484-1488.

Schnegg P.A. 2003. A new field fluorometer for multi-tracer tests and turbidity measurement applied to hydrogeological problems. Proceedings of the 8th International Congress of the Brazilian Geophysical Society, Rio de Janeiro (Brazil), 14-18 Sept. 2003.

Schnegg P.A. and Costa R. 2003. Tracer tests made easier with field fluorometers. Technical note. Bulletin d'Hydrogéologie 20: 89-91.

Schnegg P.A. and Doerfliger N. 1997. An inexpensive flow-through field fluorometer. Proceedings of the 6th Conference on Limestone Hydrology and Fissured Media, La Chaux-de-Fonds (Switzerland), 10-17 Aug. 1997, p. 47-50.

Senesi N., Miano T.M., Provenzano M.R. and Brunetti G. 1991. Characterization, differentiation, and classification of humic substances by fluorescence spectroscopy. Soil Science 152 (4): 259-271.

Smart C.C. 1988. Artificial tracer techniques for the determination of the structure of conduit aquifers. Ground Water 26 (4): 445-453.

Smart P.L., Finlayson B.L., Rylands W.D. and Ball C.M. 1976. The relation of fluorescence to dissolved organic carbon in surface waters. Water Research 10 (9): 805-811.

Vesper D.J., Loop C.M. and White W.B. 2003. Contaminant transport in karst aquifers. Speleogenesis and Evolution of Karst Aquifers 1 (2): 11 p.

White W.B. 1988. Geomorphology and hydrology of karst terrains. Oxford University Press, New York.

White W.B. 2002. Karst hydrology: recent developments and open questions. Engineering Geology 65 (2-3): 85-105.

3

Particle-size distribution as indicator for faecal bacteria contamination of groundwater from karst springs*

ABSTRACT

Microbial contamination of drinking water from karst springs is still a major concern in many areas throughout the world. Therefore, the occurrence, dynamics and transport processes of suspended matter and faecal indicator bacteria in a karst aquifer system (Yverdon-les-Bains, Switzerland) were investigated. Classical hydrogeological parameters (e.g. discharge, turbidity, total organic carbon) and particle-size distribution (PSD) were monitored continuously, along with event-based, high-frequency analyses of *Escherichia coli* and enterococci, at a swallow hole draining agricultural land and two connected karst springs. Results demonstrated that suspended particles (turbidity) in karst spring water either originated from the remobilisation and scouring of intrakarstic particulate material due to increasing flow velocities (i.e. autochthonous turbidity) and / or the transfer of particles from land surface and sinking streams (i.e. allochthonous turbidity), which entered the system following rainfall events. These allochthonous turbidity events coincided with increased faecal indicator bacteria and total organic carbon levels. PSD allowed distinguishing both types of turbidity; autochthonous turbidity consisted of particle concentration increases over a wide range of particle sizes (from colloidal size up to 0.1 mm), whereas allochthonous turbidity periods were characterised by a predominance of finer particles (0.9 to 10 µm). PSD is therefore proposed as surrogate indicator for possible microbial contamination of groundwater from karst springs or other water abstraction points. The method permits optimising water treatment and identifying periods when spring water must be rejected. Furthermore, results from a second test site (Noiraigue karst aquifer system, Switzerland) confirmed the feasibility of this approach.

3.1 INTRODUCTION

Microbial pathogens in drinking water represent a major health risk in developing countries (e.g. Montgomery and Elimelech 2007) but are also a concern in developed nations (e.g. Herwaldt *et al*. 1992; Kramer *et al*. 2001; Lisle and Rose 1995). In many parts of the world, karst aquifers

* This chapter is based on the paper:

Pronk M., Goldscheider N. and Zopfi J. 2007. Particle-size distribution as indicator for fecal bacteria contamination of drinking water from karst springs. Environmental Science & Technology 41 (24): 8400-8405.

are among the most important freshwater resources (Ford and Williams 2007). Karst aquifers are, however, because of their unique hydrogeological features, particularly vulnerable to microbial and other contamination (Zwahlen 2004). Microbial contaminants, which have sizes ranging from the sub-micrometer to tens of micrometers, undergo only limited attenuation in such environments. Rapid infiltration through shallow soils or via sinking streams and fast transport in large conduit networks restrict deposition and removal mechanisms (mechanical filtration, straining, sedimentation) as auto-purification processes (Drew and Hötzl 1999; White 1988). Moreover, the often to short residence times reduce bacterial die-off (Personné *et al*. 1998).

Karst systems often drain towards springs, which are also preferred locations of drinking water abstraction. Springs often show strong and rapid variations of discharge and water quality in response to rainfall events. Indeed, microbial quality of karst spring water may deteriorate within hours (e.g. Ryan and Meiman 1996). Prolonged periods of good water quality may thus be interrupted by short microbial contamination events. Identifying those is therefore a major challenge in the use of karst water resources. Bakalowicz (2005) noted that karst aquifers are often avoided as drinking water resources because of their vulnerability and the perceived difficulties in exploitation. Better monitoring techniques and protection strategies could help to improve the use of these valuable resources.

Faecal "index" or "indicator" bacteria, particularly *E. coli* and enterococci, are widely accepted as indicators of the possible presence of pathogens (Edberg *et al*. 1997; Tallon *et al*. 2005). For example, good correlations were established between the occurrence of faecal indicator bacteria and pathogenic microorganisms such as *Cryptosporidium* oocysts and verotoxin-producing *E. coli* in karst spring waters (Auckenthaler *et al*. 2002). However, monitoring microbial water quality relies on sterile water sampling and subsequent laboratory analyses. Sampling intervals and time lags between sampling and results (generally larger than 24 h) are often too long to prevent contaminated water entering the distribution network. An "early-warning" parameter would thus be of high utility for drinking water purveyors.

Suspended and dissolved matter in karst groundwater either comes from the aquifer itself (autochthonous) or from outside (allochthonous), e.g. from the land surface. Faecal and pathogenic bacteria often originate from agricultural activities and enter the aquifer via sinking streams or through the soil; they are thus strictly allochthonous. In groundwater, bacteria are mainly transported together with or attached to suspended particles (e.g. Hipsey *et al*. 2006; Mahler *et al*. 2000). Several authors consequently proposed turbidity as an indicator of microbial contamination (Nebbache *et al*. 1997; Ryan and Meiman 1996). However, it is generally accepted that turbid events occurring at karst springs are complex signals resulting from the resuspension of sediments and scouring of particles inside conduits and fractures, i.e. autochthonous turbidity, and / or the direct transfer of particles from the soil or sinking surface streams, i.e. allochthonous turbidity (e.g. Amraoui *et al*. 2003; Lacroix *et al*. 2000; Mahler and Lynch 1999; Massei *et al*. 2003). Furthermore, small turbidity variations sometimes coincide with high faecal indicator bacteria levels, while large turbidity signals may occur without any microbial water contamination (Kralik 2001). Consequently, turbidity alone does not allow the identification of the origin and type of suspended particles and is therefore not always a reliable water quality indicator (Dussart-Baptista *et al*. 2003). Total organic carbon (TOC) in groundwater mainly originates from the soil and surface waters (allochthonous) and could thus complement turbidity as an indicator for faecal

contamination. However, TOC signals at karst springs often trails behind the faecal bacteria breakthrough due to their different transport behaviours (Auckenthaler *et al*. 2002), whereas an ideal indicator should react simultaneously or even precede the contamination event.

Turbidity is a bulk parameter, caused by the scattering of light by suspended particles, but it does not yield information about the number, the size and the size distribution of particles. Today, particle counters allow particle-size distribution (PSD) to be measured online and continuously. Therefore, PSD appears to be a promising parameter to gain more insight into the origin and behaviour of suspended particles in karst groundwater and, thus, a possible indicator for microbial contamination. Brookes *et al*. (2005) assessed the value of PSD as surrogate indicator for pathogens in lakes and reservoirs and found good correlations between specific particle-size classes, faecal indicator bacteria and selected pathogens. A similar approach has been applied to marine bathing waters, where PSD measurements revealed a correlation between dinoflagellates and a specific particle-size class (Ahn and Grant 2007).

Atteia and co-workers investigated PSD and chemical-mineralogical composition of colloids and particles from a sinking stream and a connected karst spring (Atteia 1998; Atteia and Kozel 1997; Atteia *et al*. 1998). While PSD curves at the spring revealed large variations in the amount and size distribution of particles, they were generally composed of two distinct parts with a break point at 4 to 5 µm. Smaller particles appeared to be mostly affected by chemical factors, as demonstrated by the influence of pH. In contrast, larger particles were mainly controlled by physical factors represented by spring discharge. The break point was consequently interpreted as the limit between colloidal and particle behaviour in the studied karst aquifer system, although this limit is typically defined at 1 µm. However, PSD and its relation to faecal indicator bacteria in karst groundwater have not yet been assessed in detail.

The main objectives of this study were: (*i*) to identify and characterise autochthonous and allochthonous turbidity events occurring at karst springs; (*ii*) to better understand the occurrence, transport and behaviour of particles and faecal bacteria in karst groundwater flow systems; and (*iii*) to point out a surrogate parameter for possible faecal contamination that can be measured online and continuously. In order to achieve these goals, the Yverdon-les-Bains karst aquifer system was monitored for various physico-chemical parameters, PSD and faecal indicator bacteria from January 2005 to December 2007. To accurately examine the short-term, high-amplitude variations of karst groundwater quality, event-based, high-frequency monitoring programs have been implemented along with a classical long-term follow-up. Furthermore, two comparative tracer tests (particulate and solute tracers) were carried out in order to investigate particle transport. Finally, additional monitoring of specific hydrological events was undertaken at the Noiraigue karst aquifer system from August 2006 to January 2007. Mainly results from the Yverdon-les-Bains test site will be presented and discussed here.

3.2 METHODOLOGY

3.2.1 Material and methods

Discharge, temperature, electrical conductivity, turbidity and TOC were monitored continuously (time step: 10 min), as described in Chapter 2, at the Feurtille swallow hole and the

Moulinet and Cossaux springs (Yverdon-les-Bains karst aquifer system). Daily precipitation data were provided by MeteoSwiss. A similar monitoring program was also put in place at the Noiraigue spring (Noiraigue karst aquifer system).

On-site PSD measurements were carried out twice-monthly to monthly during the investigation period and continuously (time step: 10 min) during selected hydrological events. PSD was analysed with a portable particle counter (Abakus mobil fluid, Klotz, Unterhaugstett, Germany) that counts suspended particles in the range of 0.9 to 139 µm in a sample volume of 10 mL and groups them into up to 32 pre-definable size classes. Based on preliminary field analyses, particle-size classes were defined with increasing size intervals as follows: an initial class from 0.9 to 1.5 µm, 0.5 µm intervals from 1.5 to 6.0 µm, 1.0 µm intervals from 6.0 to 14.0 µm, 2.0 µm intervals from 14.0 to 20.0 µm, 5.0 µm intervals from 20.0 to 40.0 µm, 10.0 µm intervals from 40.0 to 70.0 µm and an ultimate class from 70.0 to 139.0 µm. Simultaneously with the long-term follow-up of PSD measurements, pH was determined on-site using a portable pH-meter (826 pH mobile, Metrohm, Herisau, Switzerland).

During the above-mentioned selected hydrological events, water samples were collected hourly by automatic samplers (6712C Sampler, Teledyne ISCO, Lincoln, USA) in sterilised bottles for microbiological and chemical analyses. Samples were processed within 6 h (for the latest sample) to 30 h (for the earliest sample). Control analyses showed that this approach did not falsify the results. Bacteria were enumerated using standard cultivation techniques (APHA, AWWA and WEF 2005), and results are alternately single and duplicate determinations. As it is increasingly recognised that total coliforms and mesophilic aerobic bacteria have low sanitary significance (Doyle and Erickson 2006; Leclerc *et al.* 2001), the high-resolution monitoring presented here focused on *E. coli* and enterococci. Samples for major ion chemistry were analysed as described in Chapter 2.

Two comparative tracer tests were carried out at the Yverdon-les-Bains karst aquifer system during different hydrological conditions. For each tracer test, 1 kg of uranine and $2.28 \cdot 10^{11}$ fluorescent 1-µm spheres (Fluoresbrite Polychromatic Red Microspheres 1.0 µm, Polysciences, Inc., Warrington, USA), dissolved in 10 L of water, were injected simultaneously at the Feurtille swallow hole. Uranine breakthrough at the springs was monitored continuously as described in Chapter 2. For microsphere quantification, water samples were collected every 30 min to 1 h by automatic samplers. Analyses were done in the laboratory according to Käss (1998): a 100 mL water sample volume, previously homogenised by sonication, was filtered through 0.8 µm cellulose nitrate membranes (Sartorius, Göttingen, Germany); and using an epifluorescence microscope (Leica Microsystems, Wetzlar, Germany), microspheres were identified, according to the size, shape and specific fluorescence, and counted.

3.2.2 Preliminary remark to PSD representation and characterisation

PSD measurements contain a large amount of information (e.g. 29 particle-size classes with varying class sizes were defined in this study). Therefore, their representation is crucial for the interpretation. PSD data may either be represented as distributive functions (number of particles per size class per volume) or cumulative functions (sum of particles equal or smaller to a size class per volume). In the present study, temporal changes in particle concentrations of selected

size classes were directly taken from the distributive PSD function, whereas PSD curves were plotted as absolute and relative cumulative functions ($\sum n \leq Ø$ [n/water volume] and $\sum n \leq Ø / \sum n$ [%], respectively). These latter are not only insensitive to class size variations but also allow obtaining smoothed curves, which facilitates the interpretation.

Furthermore, two additional parameters were derived from PSD data: the $d_{95\%}$ and the d_{max} values. The $d_{95\%}$ value, deduced from relative cumulative PSDs, represents the particle diameter such that 95 % of the total particle number has a diameter of this value or less. The d_{max} value is defined as the size at which the distributive PSD gives a concentration of 10 particles per mL (Atteia and Kozel 1997). As the latter parameter is affected by class size variations, the distributive PSD data were expressed in $n \cdot mL^{-1} \cdot \mu m^{-1}$.

3.3 AUTOCHTHONOUS AND ALLOCHTHONOUS TURBIDITY EVENTS IN KARST SYSTEMS

A typical response of the Yverdon-les-Bains karst aquifer system to an intense rainfall event was monitored in October 2007 (Fig. 3.1). As a long dry period of two months preceded this intense rainfall event, the latter occurred in a general context of low- to medium-flow conditions. Discharge of the stream sinking into the Feurtille swallow hole increased rapidly from 20 to over 200 L/s (Fig. 3.1a), followed by recession. Large quantities of particulate matter (turbidity) and TOC were mobilised (up to 180 NTU and 14 mg/L, respectively) and entered the swallow hole during this event.

Responses of suspended matter to rainfall events at the springs coincide with those of flow and solute transport and may thus be synthesised in the three phases discussed in Section 2.5:

I. an initial phase, representing pre-storm conditions with low and stable values for all parameters and lasting until spring discharge increases;

II. a pulse-through phase, starting at the moment of flow increase and lasting until the arrival of runoff-event recharge. Stable pre-event levels of typical natural tracers of the swallow hole component, such as TOC and nitrate, are monitored during this period;

III. a flow-through phase, principally characterised by the arrival and breakthrough of contaminated storm-derived water that entered the swallow hole. During this phase, increased levels of TOC and nitrate are monitored at the springs.

During the initial phase (*I*), turbidity, as well as TOC, remained stable at low pre-storm levels at the Moulinet and the Cossaux springs (Fig. 3.1b and c). However, during phase *II*, while TOC still remained stable at its low level, a first turbidity signal (T_{auto}) occurred at both springs during the rising limb of the hydrograph. Turbidity increased from 0.2 to 0.3 NTU at the Cossaux spring and 0.2 to about 10 NTU at the Moulinet spring and then decreased to about 0.25 and 0.5 NTU, respectively. The high variability of flow velocities during the rising limb of spring hydrograph induces pronounced hydrological shear stress and leads to scouring and resuspension of intrakarstic particulate material. These first turbidity responses represent, consequently, typical autochthonous or pulse-through turbidity events.

About three days after the rainfall, when discharge was in the recession stage, a second increase of turbidity (T_{allo}) was observed at the springs (Fig. 3.1b and c). These secondary signals,

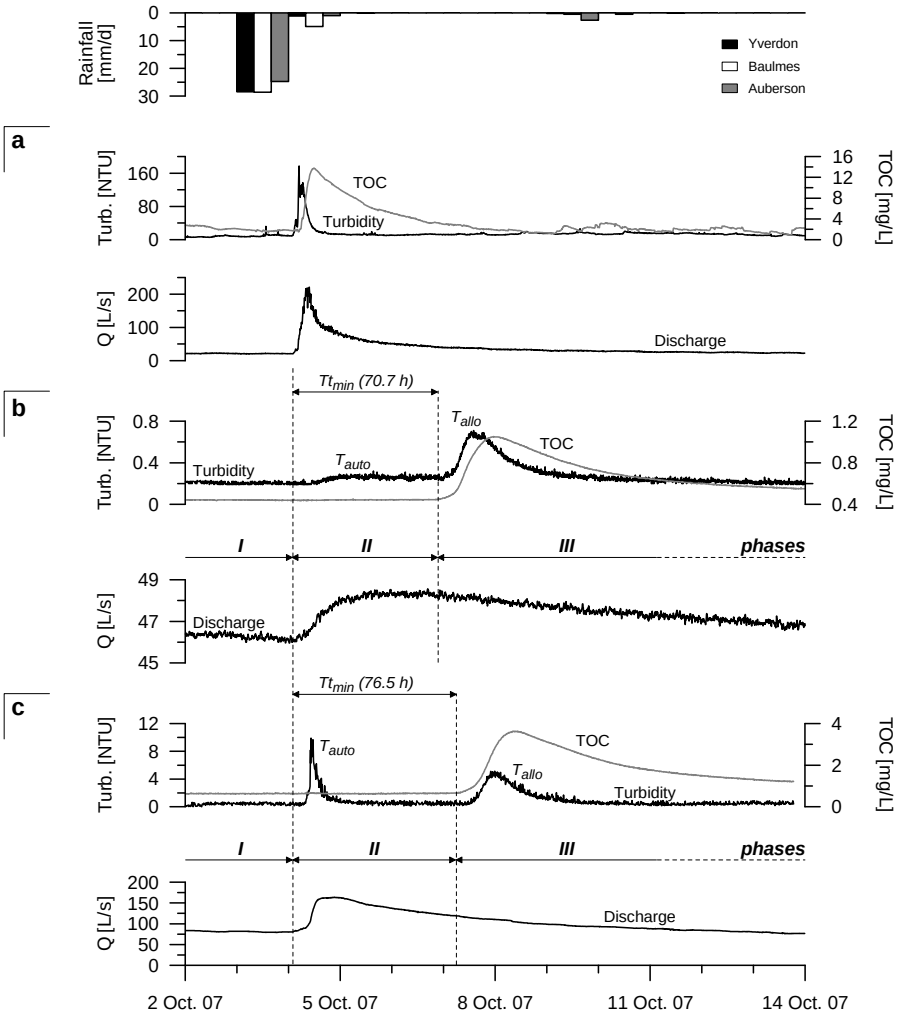

Fig. 3.1 Typical autochthonous (T_{auto}) and allochthonous (T_{allo}) turbidity signals occurring at the Cossaux and Moulinet karst springs after an intense rainfall event monitored in October 2007. The storm event was preceded and followed by long dry periods. (**a**) Feurtille swallow hole, (**b**) Cossaux spring and (**c**) Moulinet spring. Phases *I*, *II* and *III* are described in the text. Q: discharge; Turb.: turbidity; Tt_{min}: minimum swallow hole – spring transit time.

which reached maximums of about 0.7 and 5 NTU at the Cossaux and Moulinet springs, respectively, are attributed to the arrival of turbid storm-derived water (phase *III*) that entered the swallow hole. This is also corroborated by the simultaneous increase of TOC (Cossaux spring: 0.4 to 1.1 mg/L; Moulinet spring: 0.6 to 3.6 mg/L). Furthermore, the time lags between the infiltration event at the swallow hole and the arrival at the springs (Tt_{min}) corresponded well to the discharge-dependent transit times obtained by tracer tests (Fig. C.1, Appendix C). These secondary turbidity signals represent therefore typical allochthonous or flow-through turbidity events.

A combined increase of turbidity and TOC at the springs is thus indicative for an allochthonous particle origin, whereas an increase of turbidity alone during the rising limb of the hydrograph is indicative for an autochthonous particle origin. This behaviour is neither specific to the Yverdon-les-Bains karst aquifer system, nor to its hydrogeological setting. Similar observations were also made at the Noiraigue karst aquifer system (Fig. C.2, Appendix C), which

is characterised by important allochthonous point recharge (i.e. swallow hole), and at the Milandre karst system (Switzerland), which is characterised by diffuse recharge (Fig. C.3, Appendix C; unpublished data by L. Savoy).

Finally, the analysis of this single event makes it possible to better understand and resolve the response of the aquifer system to more complex conditions, such as multiple rainfall events or rainfall and snowmelt.

3.4 PSD MONITORING IN KARST SYSTEMS

3.4.1 Colloid and particle abundance in karst systems

PSD data of the Feurtille swallow hole and the Moulinet and Cossaux springs, collected during the long-term follow-up (twice-monthly to monthly measurements), not only showed a wide range of total particle concentrations but revealed also highly variable size distributions. A set of PSD curves for each observation point is shown in Fig. 3.2.

Total particle concentrations, with particle sizes between 0.9 and 139 µm, ranged from $1.2 \cdot 10^5$ (*PSD1*) to $2.2 \cdot 10^7$ n/10 mL (*PSD4*) at the Feurtille swallow hole (Fig. 3.2a). At the springs, the ranges of total particle concentrations were about one order of magnitude lower than at the swallow hole; they varied from $3.8 \cdot 10^4$ (*PSD5*) to $7.8 \cdot 10^6$ n/10 mL (*PSD8*) and $2.4 \cdot 10^4$ (*PSD9*) to $1.1 \cdot 10^6$ n/10 mL (*PSD12*) at the Moulinet (Fig. 3.2c) and Cossaux (Fig. 3.2e) springs, respectively. These values are comparable to those observed in other karst systems (Atteia and Kozel 1997; Mahler and Lynch 1999).

Particles entering the swallow hole and discharging at the springs were poly-dispersed (i.e. large amounts of particles were detected over the whole analysed size range) but largely dominated by the smaller size classes: 0.9 to about 20.0 µm for the swallow hole (Fig. 3.2b) and 0.9 to about 10.0 µm for the springs (Fig. 3.2d and f). This was also manifested by the $d_{95\%}$ and d_{max} values: the $d_{95\%}$ value ranged between 3.5 and 13.0 µm at the swallow hole and between 2.5 and 6.5 µm and 3.0 and 5.0 µm at the Moulinet and Cossaux springs, respectively; whereas the d_{max} value varied from the 12.0 – 13.0 to the 40 – 50 µm size class at the swallow hole, from the 8.0 – 9.0 to the 35.0 –40.0 µm size class at the Moulinet spring and from the 7.0 – 8.0 to the 20.0 – 25.0 µm size class at the Cossaux spring. However, despite this abundance of smaller particles, PSD data revealed a high variability of the relative size distributions among these finer size classes. This is particularly marked by the fraction of particles smaller than 1.5 µm (colloids) with respect to total particle concentrations. These fractions varied between 38 % (*PSD3*) and 80 % (*PSD2*) at the swallow hole, 58 % (*PSD7*) and 84 % (*PSD6*) at the Moulinet spring and 60 % (*PSD11*) and 80 % (*PSD10*) at the Cossaux spring.

Among all monitored environmental variables, the most influential parameter on PSD data was the effect of discharge on the d_{max} value. Similar observations have also been reported by Atteia and Kozel (1997). The d_{max} parameter increased more or less linearly with the discharge of both springs (Fig. 3.3a and b), independently of total particle number or its relative size distribution. Larger particles remain thus in suspension and are transported if flow velocity, which is directly linked to the system discharge in the case of the Yverdon-les-Bains karst aquifer system (Fig. C.1, Appendix C), in the whole system is sufficient.

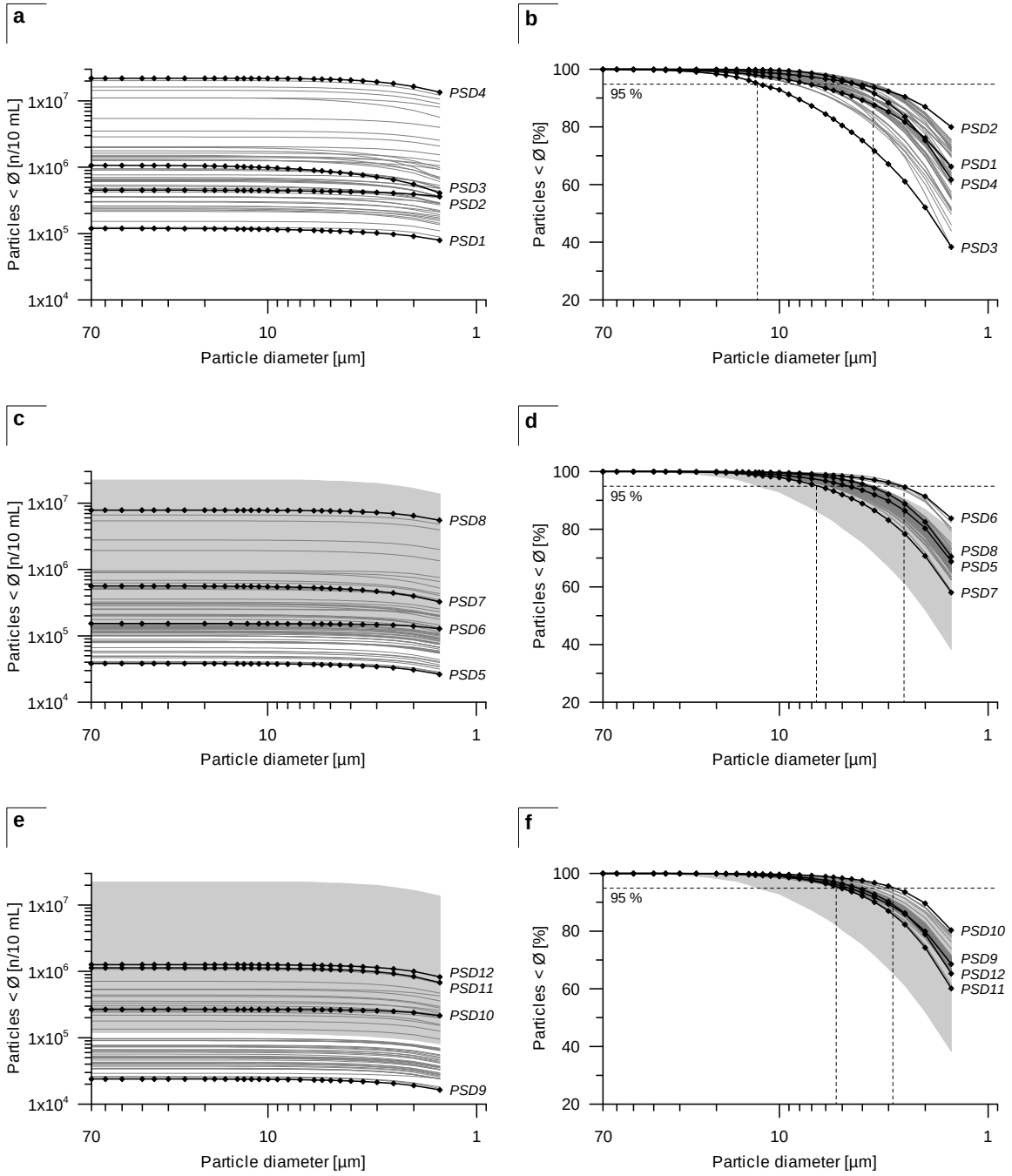

Fig. 3.2 Typical PSD curves (for particle sizes ranging from 0.9 to 139 µm) obtained at (**a** and **b**) the Feurtille swallow hole, (**c** and **d**) the Moulinet spring and (**e** and **f**) the Cossaux spring. Left (**a**, **c** and **e**): absolute cumulative PSDs ($\sum n \leq Ø$); and right (**b**, **d** and **f**): relative cumulative PSDs ($\sum n \leq Ø / \sum n$, expressed in %). The dotted lines (**b**, **d** and **f**) represent the range of the $d_{95\%}$ values and the grey shaded areas (**c** – **f**) represent the extension of swallow hole data.

When considering the system discharge (Fig. 3.4), this correlation was even improved for data collected at the Cossaux spring. Moreover, the slopes of the regression models of both springs were nearly identical. These facts suggest that the dynamics of larger particles and their occurrence at the springs is principally controlled by the flow conditions within the system, i.e. the flow dynamics of the karst groundwater component and the Feurtille swallow hole

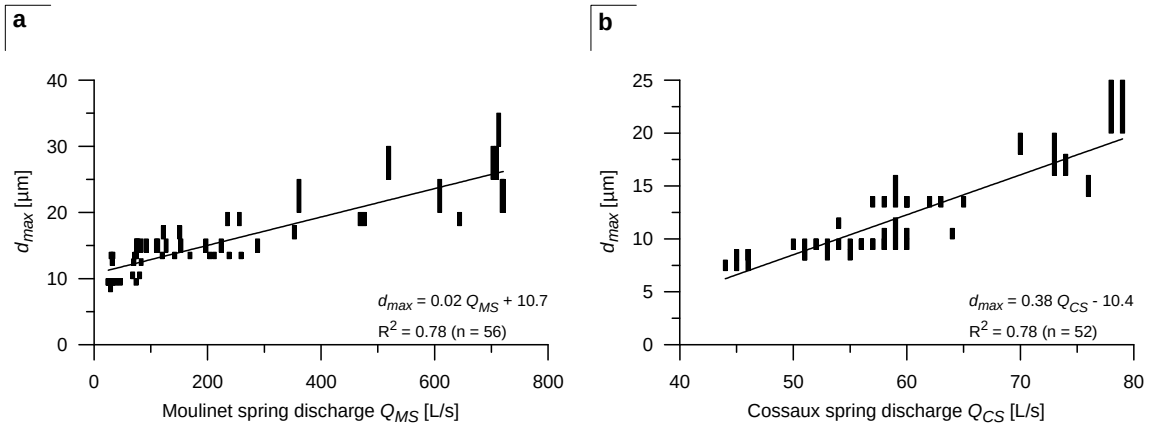

Fig. 3.3 Relation between d_{max} and spring discharge. (**a**) Moulinet spring and (**b**) Cossaux spring. The height of the rectangles expresses the size range of the particle class.

component. The very slow dynamics of the deep and thermal groundwater component, which particularly affects the Cossaux spring and principally results in a lower intercept for the d_{max} – system discharge relation due to a dilution effect, strengthen this hypothesis.

Besides the d_{max} – discharge relation, the analysis of single PSD curves did not allow establishing relations between total particle concentrations, their relative size distributions and monitored environmental parameters. However, high total particle concentrations were always associated with high-flow conditions and mostly storm events, whereas low total particle concentrations occurred during base-flow conditions. Indeed, the lowest total particle concentrations at the springs (Fig. 3.2, *PSD5* and *PSD9*) were measured following a long period of extreme low-flow conditions and the nearly absence of any swallow hole contribution.

Data presented here demonstrate the high variability of PSD data. Colloids and particles can directly act as transport "vehicles" for contaminants, it is therefore crucial to get a better insight into particle dynamics and behaviour in karst systems. As about the totality of sediment transport occurs during or following storm events, PSD was, consequently, monitored continuously during several selected hydrological events.

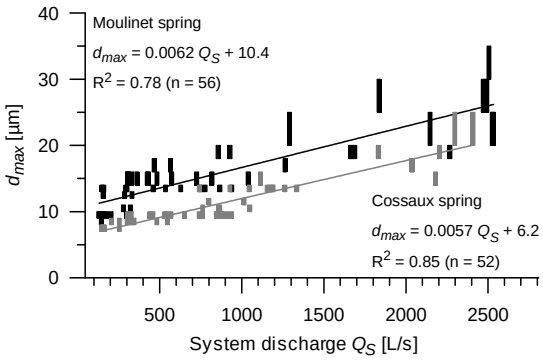

Fig. 3.4 Relation between d_{max} and system discharge (Q_S). Black rectangles: Moulinet spring data; grey rectangles: Cossaux spring data. The height of the rectangles expresses the size range of the particle class.

3.4.2 Temporal changes in PSD during rainfall events

Several storm events were monitored in order to investigate the temporal changes in PSD at the Yverdon-les-Bains karst aquifer system. Two of them, representing rainfall events during low- and high-flow conditions, are discussed in detail below. The other results are shown throughout Chapter 3 (Fig. 3.11 and 3.12) or in Appendix C (Fig. C.4 – C.7).

RAINFALL EVENT DURING LOW-FLOW CONDITIONS

Following a long dry period of about 6 weeks, resulting in stable base-flow conditions in the karst system, the response to a multiple rainfall event was monitored in February 2006 (Fig. 3.5). The discharge of the stream sinking into the Feurtille swallow hole showed several successive distinct increases, followed by rapid recession (Fig. 3.5a). During this period, high levels of turbidity and TOC (up to 140 NTU and 11.2 mg/L, respectively) entered the swallow hole.

The response of suspended matter at the Moulinet spring during this event (Fig. 3.5b) was consistent with the different phases described earlier. During pre-storm conditions (phase *I*), all parameters remained stable at low levels; discharge was about 30 L/s and turbidity and TOC showed low levels at 0.2 NTU and 0.8 mg/L, respectively. Next, almost immediately in response to the rainfall event, the discharge of the Moulinet spring increased to about 220 L/s. During the rising limb of the spring hydrograph, turbidity displayed a narrow peak of about 8.2 NTU (*T1*), while TOC still remained stable at its low pre-storm level (phase *II*). Consequently, *T1* represents thus typical autochthonous turbidity. In the following days, while turbidity had decreased to about 0.8 NTU, several successive overlapping turbidity signals, with a maximum of about 8.1 NTU (*T2*), were monitored (phase *III*). As the occurrence of these latter was simultaneous with an increase of TOC content, they correspond thus to the breakthrough of turbid storm-derived water that entered the swallow hole and are therefore of allochthonous origin. The time lag between the infiltration of turbid water at the swallow hole and its arrival at the spring, which was about 65 h, corresponded well to the discharge-dependent transit time obtained by tracer tests (Fig. C.1, Appendix C).

PSD measurements yielded more detailed information of the turbidity signals (Fig. 3.5b). During pre-storm conditions, PSD remained stable at low levels for all size classes and was dominated by finer particles ($d_{95\%}$: 4 µm). Total particle concentration was about $4.0 \pm 0.3 \cdot 10^4$ n/10 mL. The autochthonous turbidity signal was caused by simultaneous particle concentration increases over the whole range of monitored size classes (from 0.9 to 139 µm). Maximum total particle concentration reached about $9.0 \cdot 10^5$ n/10 mL, and the most important increases were observed for the smaller size classes. Nevertheless, the relative increases of particle concentrations with respect to pre-storm conditions among the different size classes were differing. At the moment of maximum autochthonous turbidity (*T1*), the concentration of 0.9 – 1.5 µm particles was 18 times the pre-storm value (*T0*), against 41 times for the 8.0 – 9.0 µm particle-size class. Maximum relative increase was obtained for the 11.0 – 12.0 µm size class (58 times the pre-storm value). The increasing $d_{95\%}$ value, which showed a slight shift towards larger particles (6 µm), corroborates this tendency. It is hypothesised that this behaviour results from a relative higher availability of larger particles in the active conduit network of the karst system with respect to smaller particles (colloids), which have less tendency to settle down during low-flow conditions. The abundance of smaller particles with respect to total particle number discharging at the spring during stable low-flow conditions (e.g. *T0*) strengthens this hypothesis.

During the allochthonous turbidity signal, maximum total particle concentration was similar to the one during the autochthonous turbidity event, i.e. $9.2 \cdot 10^5$ n/10 mL. However, only concentrations of the smaller particle-size classes showed increases. This resulted consequently in a decrease of the $d_{95\%}$ value below its initial level (2.5 µm). In terms of both absolute and relative

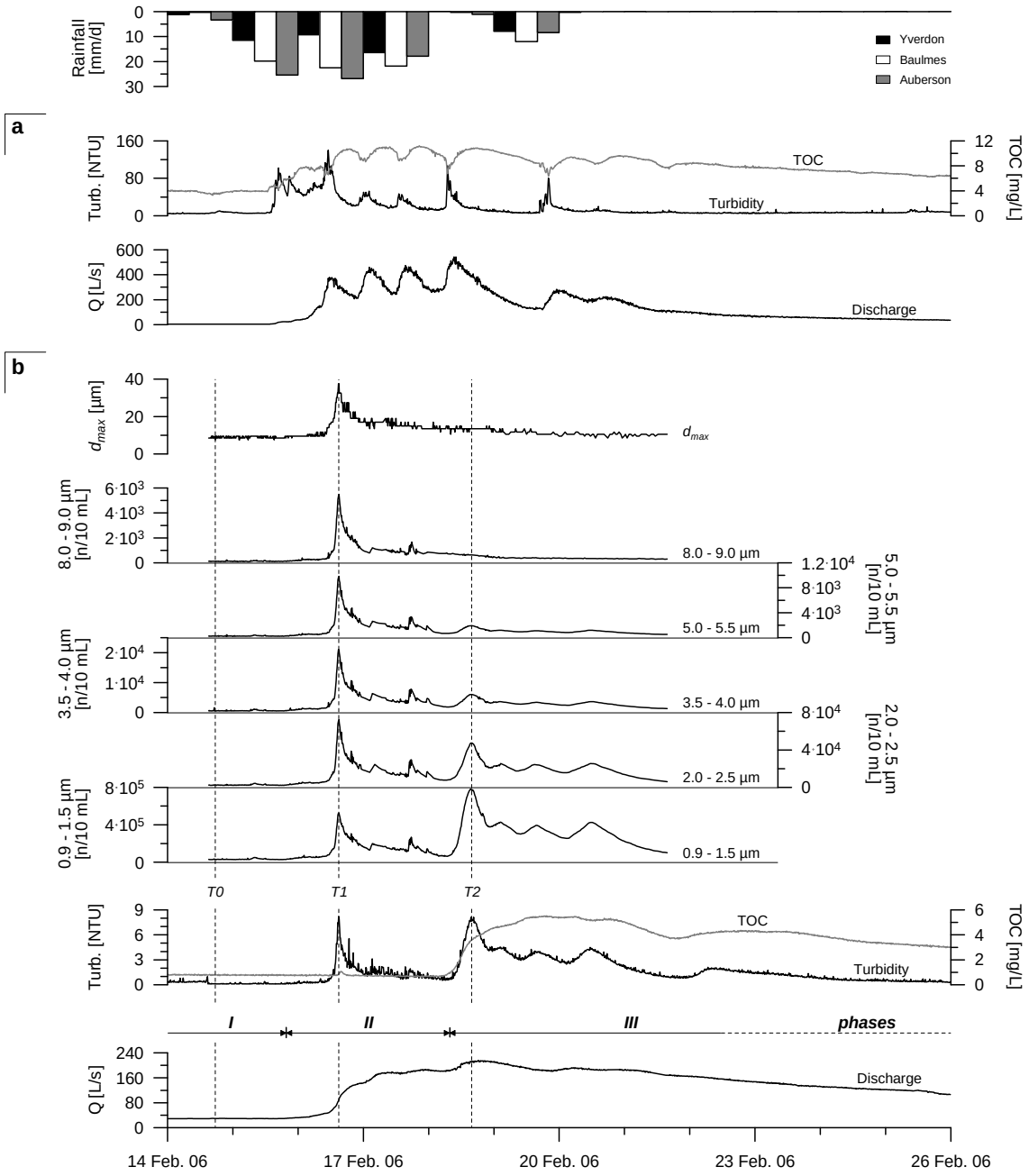

Fig. 3.5 Temporal changes in PSD at the Moulinet spring in response to the February 2006 storm event, which occurred during a period of low-flow conditions. (**a**) Feurtille swallow hole and (**b**) Moulinet spring. Phases *I*, *II* and *III* are described in the text. Q: discharge; Turb.: turbidity; *T0*: pre-storm conditions; *T1*: maximum autochthonous turbidity; *T2*: maximum allochthonous turbidity.

(i.e. with respect to pre-storm values) concentrations, the increase was highest for the finest particle-size class (0.9 – 1.5 µm) and decreased gradually towards larger size classes. Flow-through turbidity was completely unapparent for particles larger than 7.0 µm. At the moment of maximum allochthonous turbidity (*T2*), the concentration of 0.9 – 1.5 µm particles was 27 times the pre-storm value (*T0*), against 5 to 6 times for particles larger than 7.0 µm. It is suggested that the larger particles discharging at the spring, in this case particles larger than 7.0 µm, represent strictly the dynamics of autochthonous turbidity.

RAINFALL EVENT DURING HIGH-FLOW CONDITIONS

Autochthonous and allochthonous turbidity signals at karst springs may partly overlap due to the shorter transit times during high-flow conditions. The response of a storm rainfall of about 60 mm was therefore monitored at the Feurtille swallow hole and the Moulinet spring in April 2006 (Fig. 3.6). At that time, the flow conditions within the system were relatively stable and high due to the snowmelt on the south-eastern slope of the Jura Mountains.

At the Feurtille swallow hole (Fig. 3.6a), the discharge of the sinking stream showed a sharp increase from 200 to over 1000 L/s. Water entering the swallow hole was turbid (> 150 NTU) and rich in TOC (up to 11.7 mg/mL). Turbidity entering the swallow hole showed strong particle concentration increases among all particle-size classes. However, different behaviours were observed among the size classes; the concentrations of larger particles peaked before the smaller ones (*T1'* and *T2'*, respectively). This general behaviour may be explained by different particle origins within the catchment basin of the swallow hole. Large particles mostly originate from erosion in the stream channel and at the soil surface and are mainly mobilised by the first flush in the stream and by surface runoff. In contrast, small particles mostly result from water percolation through the soil towards the network of artificial drainage tubes. This hypothesis is further supported by electrical conductivity, TOC and nitrate data, which decreased during the rising limb of the hydrograph untill *T1'* (dilution by precipitation water), and then suddenly increased (participation of soil water). Nevertheless, in terms of both absolute and relative concentrations, smaller particles dominated the input at the swallow hole. Indeed, at moments *T1'* and *T2'*, particle concentrations of the 0.9 – 1.5 µm size class were 72 and 170 times the pre-storm value (*T0'*), against 44 and 19 times for the 14.0 – 16.0 µm size class, respectively.

The response of suspended matter at the Moulinet spring (Fig. 3.6b) could again be divided in the three phases mentioned before. During phase *I* (pre-storm conditions), a high and relatively stable flow rate of ~ 610 L/s was established due to previous snowmelt. Turbidity level was stable at about 2 NTU, and TOC was in a slow recession phase. Phase *II* was characterised by increasing turbidity from 2 to 5 NTU due to an increasing flow rate at the spring, while TOC content was still decreasing. This corresponds thus to a typical autochthonous signal. Phase *III* started about 22 hours after the first response of the spring. All parameters displayed sudden increases, with a turbidity maximum of about 40 NTU (*T2*), clearly originating from the swallow hole (allochthonous).

Again, PSD measurements yielded more detailed information about the turbidity pulses. During pre-storm conditions, total particle concentration was about $2.8 \cdot 10^5$ n/10 mL with a predominance of finer particles. During the pulse-through phase (phase *II*), all particle-size classes showed a similar evolution and increased steadily. At the moment of maximum strictly autochthonous turbidity (*T1*), total particle concentration was with $5.6 \cdot 10^5$ n/10 mL about twice as high as the pre-storm value. From the moment when the water from the swallow hole first arrived (phase *III*), total particle concentration increased abruptly and reached about $7.9 \cdot 10^6$ n/10 mL at the moment of maximum allochthonous turbidity (*T2*). The different particle-size classes evolved, however, differently during this flow-through event. The 0.9 – 1.5 µm particle-size class displayed an abrupt break point and a sharp concentration increase. This break point was progressively attenuated with increasing size classes until the 14.0 – 16.0 µm size class, which

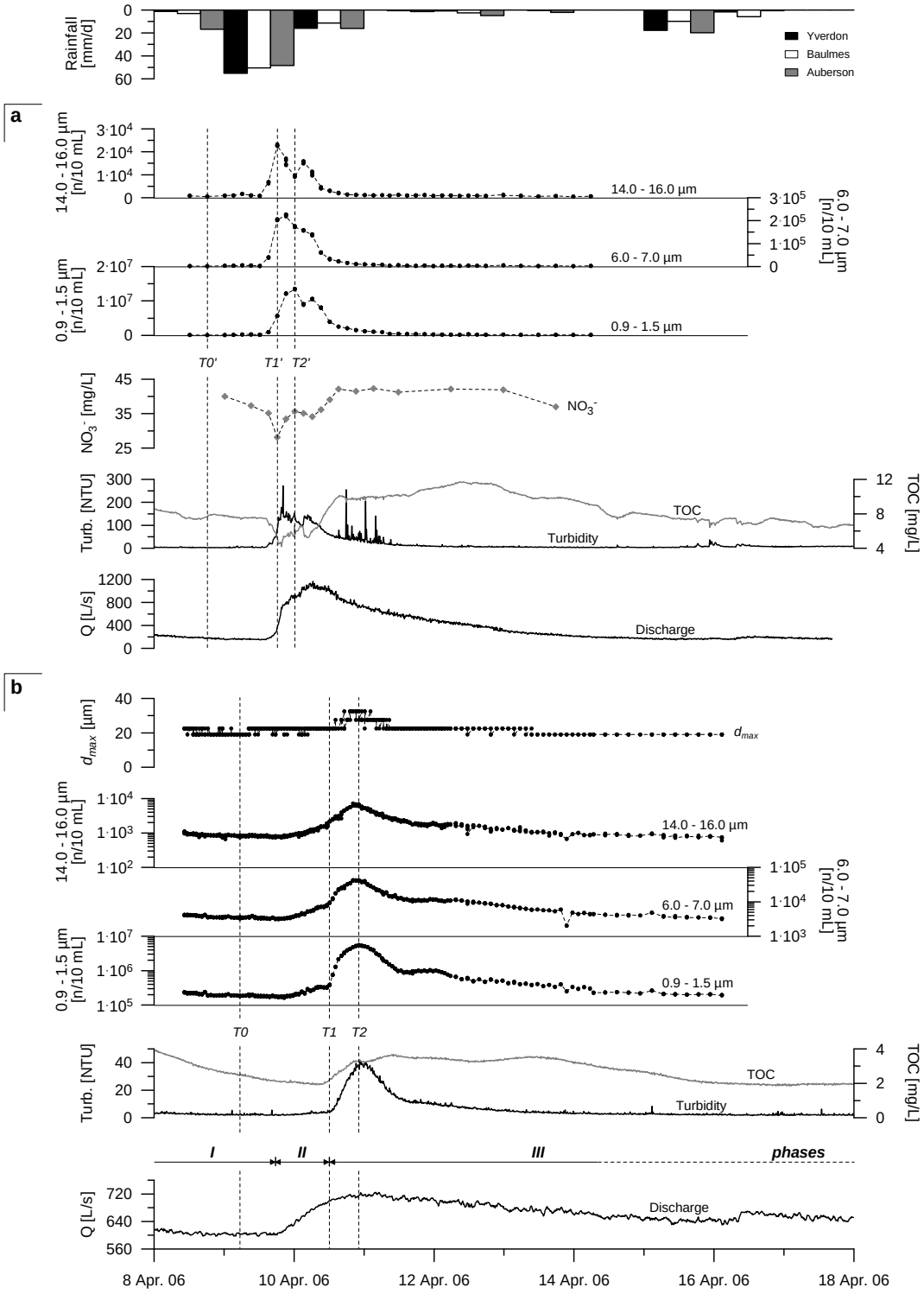

Fig. 3.6 Temporal changes in PSD at (**a**) the Feurtille swallow hole and (**b**) the Moulinet spring during the April 2006 storm event, which occurred during a period of high-flow conditions. Phases *I*, *II* and *III* are described in the text. Q: discharge; Turb.: turbidity; *T0*: pre-storm conditions; *T1*: maximum strictly autochthonous turbidity; *T2*: maximum allochthonous turbidity.

continued to increase steadily. The larger particles (> 14.0 µm) are strictly attributed to the resuspension and scouring of intrakarstic particulate material, whereas the finer particles mainly

originate from the swallow hole. As for the storm event during low-flow conditions, relative concentrations of the different size classes with respect to pre-storm conditions were differing during the autochthonous and allochthonous turbidity signals. At moment *T1*, the concentration of the 14.0 – 16.0 µm particles was 2.6 times the pre-storm value (*T0*), against 1.8 times for the 0.9 – 1.5 µm particles. Conversely, at moment *T2*, the concentrations were 8 and 31 times the pre-storm conditions, respectively.

GENERAL COMMENTS

As already stated in the introduction, the comparison of turbidity and PSD showed that turbidity is a global parameter. For instance, maximum autochthonous and allochthonous turbidity values at the Moulinet spring during the February 2006 storm event (Fig. 3.5) were almost identical (8.2 and 8.1 NTU, respectively). However, the first turbidity rise was mainly due to increases of particles over the whole analysed size range, whereas only the smaller particles accounted for the turbidity in the second part of the event. Hence turbidity indicates the presence of particles, but it is neither significant to define a particle size nor to determine its origin. Conversely, continuous PSD monitoring alone allowed identifying turbidity origin: the flow-pulses following rainfall events thus remobilise and scour particles of a wide range of diameters within the karst system, while only small particles are transported along the entire pathway from the sinking stream to the springs. This differentiation between autochthonous and allochthonous turbidity signals using PSD was even possible when they were partially superimposed. Data from other monitored storm events at the Moulinet spring, as well as those from the Cossaux spring, were in agreement with the examples described above.

3.4.3 Dynamics of autochthonous turbidity events at karst springs

The autochthonous turbidity signals at the Moulinet spring during both events were differing. Pulse-through turbidity displayed a narrow, high-amplitude peak during the February 2006 storm event (Fig. 3.5), against a wide, low-amplitude signal during the April 2006 storm event (Fig. 3.6). While both types of signals were monitored at the Moulinet spring, the autochthonous turbidity episodes at the Cossaux spring displayed always wide, low-amplitude signals (Fig. 3.1b). The response of the Moulinet spring to two rainfall events, the January 2006 and March 2006 storm events, provides insight into these different behaviours of pulse-through turbidity episodes (Fig. 3.7).

The January 2006 storm event occurred during low-flow conditions. During this event, autochthonous turbidity displayed a narrow, high-amplitude signal (Fig. 3.7a). Of particular note, maximum pulse-through turbidity was monitored during the steepest part of the rising limb of spring discharge and preceded by approximately 10 hours peak discharge. Thus autochthonous turbidity seems to be related to flow acceleration in the system ($m^2 \cdot m/s^2$), which can be quantified by the first derivative of the spring hydrograph (flow velocity, $m^2 \cdot m/s$). This increasing flow acceleration leads to increasing turbulences and hydrological shear stress in the active conduit network, resulting in significant sloughing off and remobilisation of particles into the water phase. Time delay between maximum flow acceleration and maximum autochthonous turbidity was short (~ 20 min), signifying that large amounts of suspended matter discharging at the spring during this episode originated from locations close to this latter. The different pulse-through turbidity signals

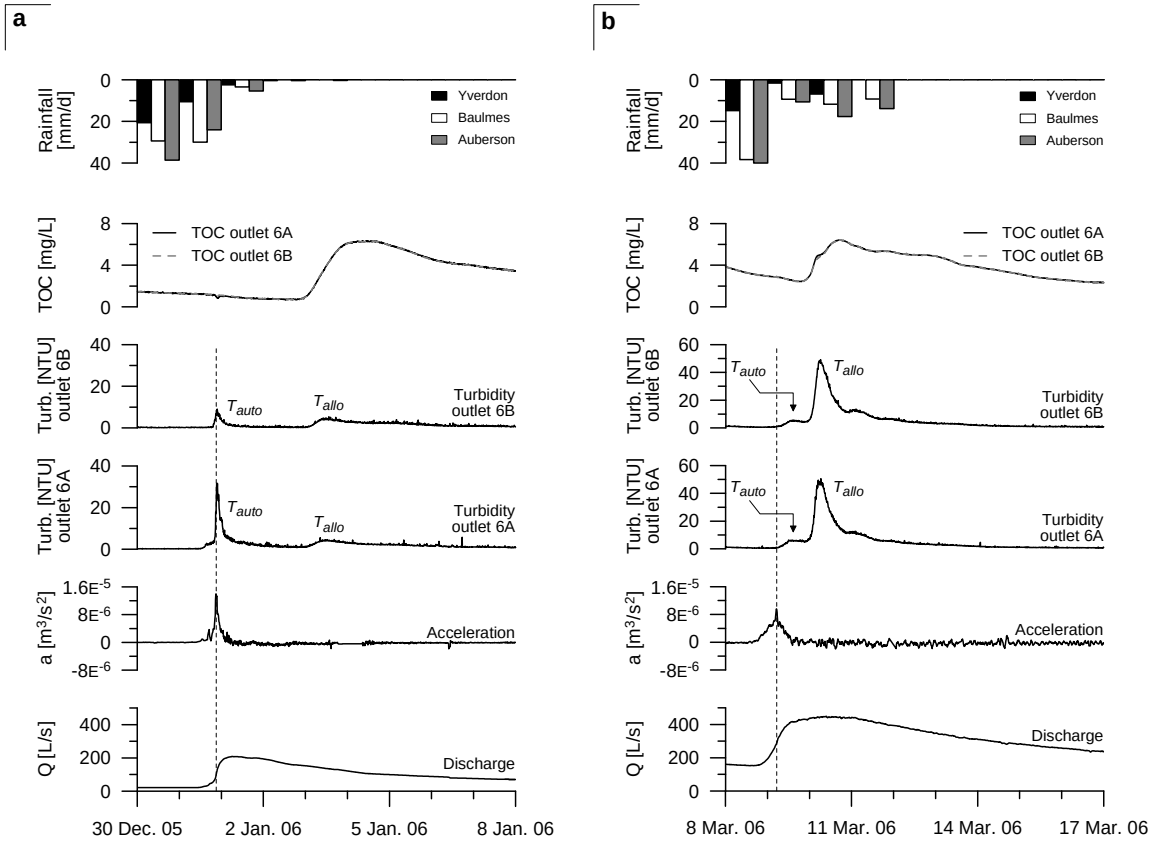

Fig. 3.7 Occurrence of autochthonous turbidity episodes at the Moulinet spring during storm events preceded by (**a**) long dry periods (January 2006 storm event) and (**b**) short dry periods (March 2006 storm event). Q: discharge; a: acceleration; Turb.: turbidity; T_{auto}: autochthonous turbidity; T_{allo}: allochthonous turbidity.

monitored at the outlets 6A and 6B of the Moulinet spring in response to this storm event (Fig. 3.7a) confirmed the "local" origin of these autochthonous particles. Furthermore, the rapid turbidity decrease, while discharge was still rising, suggests that flow velocities were not sufficient to transport particulate matter mobilised in deeper parts of the system, i.e. particles were affected by sedimentation.

This general behaviour is also reflected in the temporal variations of d_{max} during such events (Fig. 3.5). The increasing hydrological shear stress and turbulences during the rising limb of the spring hydrograph mobilised a wide range of particles up to the 35.0 – 40.0 µm size class. These d_{max} values exceeded clearly those for similar discharges during stable flow conditions (Fig. 3.8). The rapidly decreasing d_{max} after peak flow acceleration further confirms that flow velocities in the system were not sufficient to transport larger particles towards the outlet of the system.

Conversely, for the March 2006 storm event, which occurred during a period of medium- to high-flow conditions, autochthonous turbidity displayed a wide, low-amplitude signal (Fig. 3.7b). During this event, turbidity started to increase simultaneously with spring discharge, whereas its maximum peaked about 11 hours after maximum flow acceleration. Hence, the autochthonous particles discharging during this event originated mainly from deeper parts of the aquifer. This was not only confirmed by the identical pulse-through turbidity signals monitored at the outlets

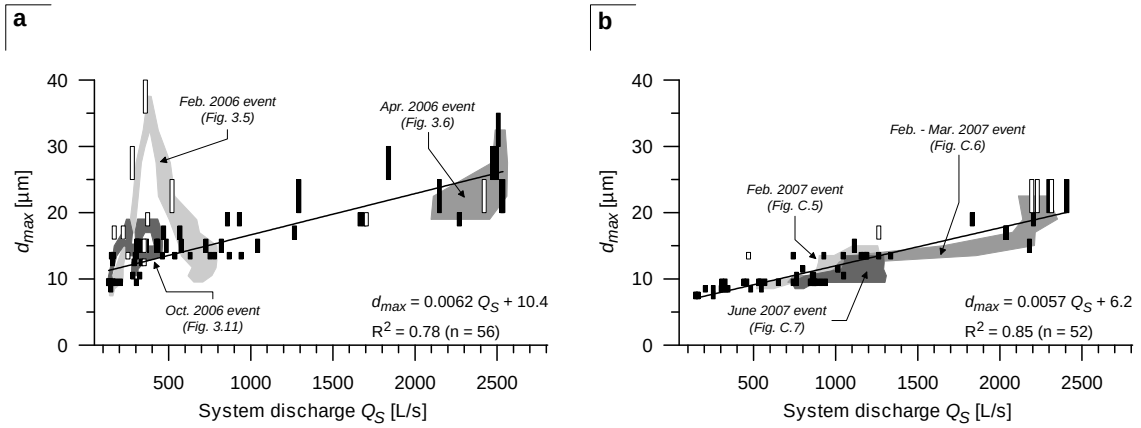

Fig. 3.8 Relation between d_{max} and system discharge (Q_S). (**a**) Moulinet spring and (**b**) Cossaux spring. Open rectangles: data collected during the rising limb of the spring hydrograph; filled rectangles: data collected during other periods. The height of the rectangles expresses the size range of the particle class. Grey shaded areas represent the extension of d_{max} monitored continuously during storm events (temporal evolution is clockwise).

6A and 6B in response to this storm event (Fig. 3.7b) but also by the temporal variation of d_{max} during such events (Fig. 3.6), which did not exceed the d_{max} values for similar discharges during stable flow conditions (Fig. 3.8). The absence of a turbidity pulse synchronous to maximum flow acceleration is explained by the fact that substantial amounts of suspended matter were already washed out of the system during the previous storm event that occurred 5 days earlier.

The presented data show that the amount of autochthonous particulate material released at the springs during storm events is dependent on antecedent flow conditions within the system. The time lag between storm events influences the weathering state of the aquifer substrate and the amount of sediments accumulated in the system. It further suggests also that mobilisation of intrakarstic particulate material is governed by flow acceleration, whereas its transport is governed by flow velocity.

Finally, it is assumed that the autochthonous suspended matter discharging at the Cossaux spring, which displayed wide, low-amplitude signals, originates mainly from deeper parts of the aquifer. The very low flow acceleration at the Cossaux spring, due to the lower discharge variations, and the fact that the spring is captured by drillings, which prevent important sediment accumulation close to the outlet, further supports the lack of narrow, high-amplitude turbidity episodes at the spring.

3.4.4 Particle vs. solute transport in the active conduit network of karst systems

Both at the swallow hole and the springs, the allochthonous turbidity signals preceded the TOC signals and were narrower than those. These observations are consistent with the findings of studies from porous media, which revealed faster transport of colloids with respect to solutes due to exclusion processes (Bradford *et al.* 2003; Grolimund *et al.* 1998; Keller *et al.* 2004; Sirivithayapakorn *et al.* 2003). In the present case, the time lag between turbidity and TOC maxima at the swallow hole can be attributed to differential transport processes in the catchment area of the stream sinking into the swallow hole. The longer time lags observed at the springs

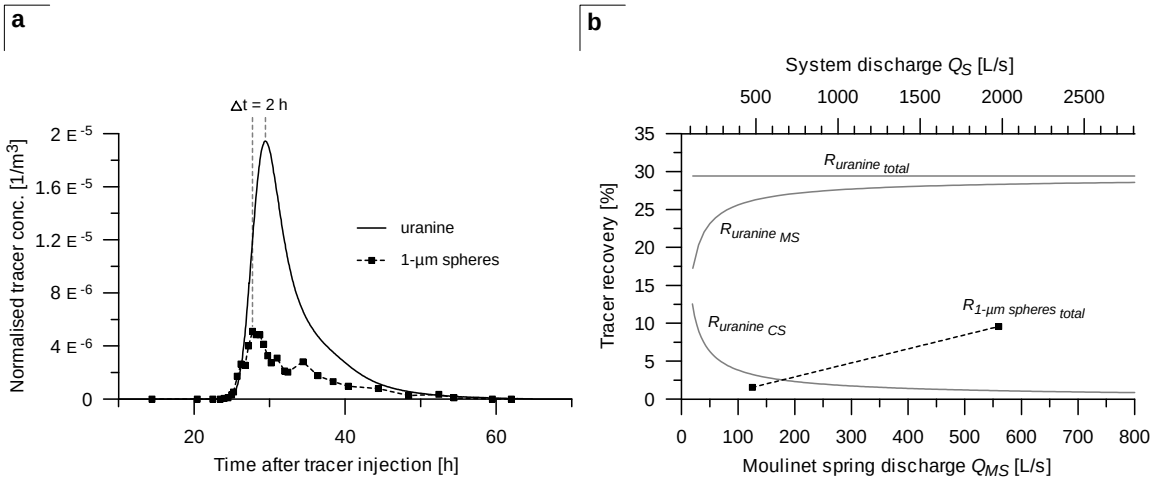

Fig. 3.9 (**a**) Uranine and 1-µm spheres breakthrough at the Moulinet spring during the April 2006 comparative tracer test. All other breakthrough curves are shown in Fig. C.9, and main results are summarised in Table C.1 (Appendix C). (**b**) Uranine and 1-µm spheres recovery rates as function of the system discharge. Only the total 1-µm spheres recovery rates of both springs are shown, as they are nearly identical to those obtained at the Moulinet spring (recoveries at the Cossaux spring were very low). The straight dashed line linking 1-µm spheres recovery rates is for a visual aspect and may not necessarily reflect a linear relation.

suggest that similar processes also operate in the active conduit network of karst aquifers and indicate higher mean velocities for suspended particles. Results of the comparative tracer experiments, which showed an earlier peak breakthrough of the 1-µm spheres with respect to uranine (Fig. 3.9a), further confirmed these observations. This behaviour can be explained by exclusion processes, i.e. particles travel along the fastest flow lines while solutes sample the entire fluid volume, and / or time-dependent loss functions, i.e. fast particles arrive at the spring, while slow particles are removed.

During the comparative tracer experiments, the total recovery rates of the 1-µm spheres at the springs were lower than those for uranine (Fig. 3.9b). These results show that particles are affected by removal mechanisms such as attachment, sedimentation and filtration processes. Nevertheless, recoveries of the microspheres increased with increasing flow conditions in the system suggesting that particle sedimentation in low flow-velocity regions may play an important role. This was further also confirmed by the decreasing maximum diameter of the flow-through particles at the springs (i.e. originating from the swallow hole and mobilised during storm events) with decreasing flow conditions (Fig. 3.10).

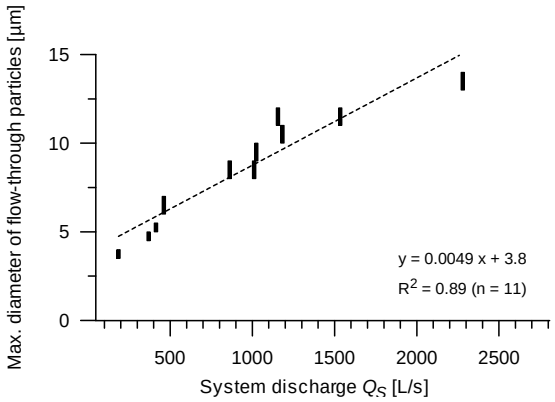

Fig. 3.10 Relation between system discharge (Q_S) and the maximum diameter of flow-through particles at the springs. Data were retrieved from the continuous PSD monitoring during storm events. The height of the rectangles expresses the size range of the particle class.

3.5 OCCURRENCE OF FAECAL INDICATOR BACTERIA IN KARST SYSTEMS

Several storm events were monitored at the Yverdon-les-Bains karst aquifer system in order to investigate the temporal dynamics of faecal indicator bacteria and their relation to PSD measurements. Two of them, again representing rainfall events during low- and high-flow conditions, are treated below in detail. Results of similar investigations during other storm events are shown in Fig. C.4, C.5 and C.7 (Appendix C).

RAINFALL EVENT DURING LOW-FLOW CONDITIONS

Two shortly successive rainfall events were monitored in autumn 2006 (Fig. 3.11). This multiple rainfall event, which was preceded by a dry period of about 6 weeks, occurred during low-flow conditions. The discharge of the sinking stream showed two distinct peaks, followed by rapid recession (Fig. 3.11a). Discharge increased from 7 to 97 L/s on the 1st of October and from 30 to 280 L/s on the 3rd of October. Consequently, high levels of turbidity (max.: 90 NTU) and TOC (max.: 14 mg/L) entered the swallow hole (data not shown). Moreover, a sample collected on the 4th of October revealed high concentrations of *E. coli* (> 3000 CFU/100 mL), suggesting that large amounts of faecal bacteria entered the system during these events.

The discharge of the Moulinet spring increased almost immediately in response to the rainfall events from 26 L/s to a first maximum of 63 L/s and a second maximum of 119 L/s (Fig. 3.11b). During the rising limbs of these discharge pulses, turbidity displayed two distinct peaks (*T1a / b*) of about 2 NTU. Both peaks were characterised by particle concentration increases over a large range of size classes (0.9 to 70 µm), with maximum relative increases for the 9.0 – 10.0 µm size class. These turbidity signals thus result from the remobilisation and scouring of autochthonous particulate material inside karst conduits due to increasing flow rates. TOC and *E. coli* counts remained at their low pre-storm levels (0.5 mg/L and 0 to 4 CFU/100 mL, respectively).

During the following days, when the spring was in a recession period, two successive increases of turbidity (*T2a / b*) and TOC were monitored. The turbidity signals, which reached maximums of 1 and 2.5 NTU, respectively, were characterised by particle concentration increases of the smaller size classes only (0.9 to 5.0 µm). Larger particles were in a recession period. These turbid episodes, which are attributed to the arrival of turbid and contaminated water that infiltrated during the two rainfall events, are thus of allochthonous origin. The time lags between the two discharge increases at the swallow hole and the corresponding arrivals at the spring were 95 and 85 h, respectively, which fell in the range of the tracer results (Fig. C.1, Appendix C). The higher mean discharge during the second phase explains the shorter transit time.

Simultaneously with the arrival of the allochthonous swallow hole component, *E. coli* content in spring water started to increase. Within a few hours (approximately 10 h), *E. coli* concentrations rose by 2 and 3 log units, reaching maximum concentrations of 362 (*T2a*) and 1088 CFU/100 mL (*T2b*). During these faecal bacteria contamination events, allochthonous particles and *E. coli* displayed a nearly perfect parallel evolution.

At the Cossaux spring, all parameters evolved similarly, but at lower levels. Turbidity and TOC maxima (0.9 NTU and 0.9 mg/L, respectively) did not exceed the water quality standards of 1 NTU and 1 mg/L, respectively. However, *E. coli* contents reached two distinct maximum levels of 116 and 383 CFU/100 mL during phases *T2a* and *T2b*, respectively. It is suggested that the

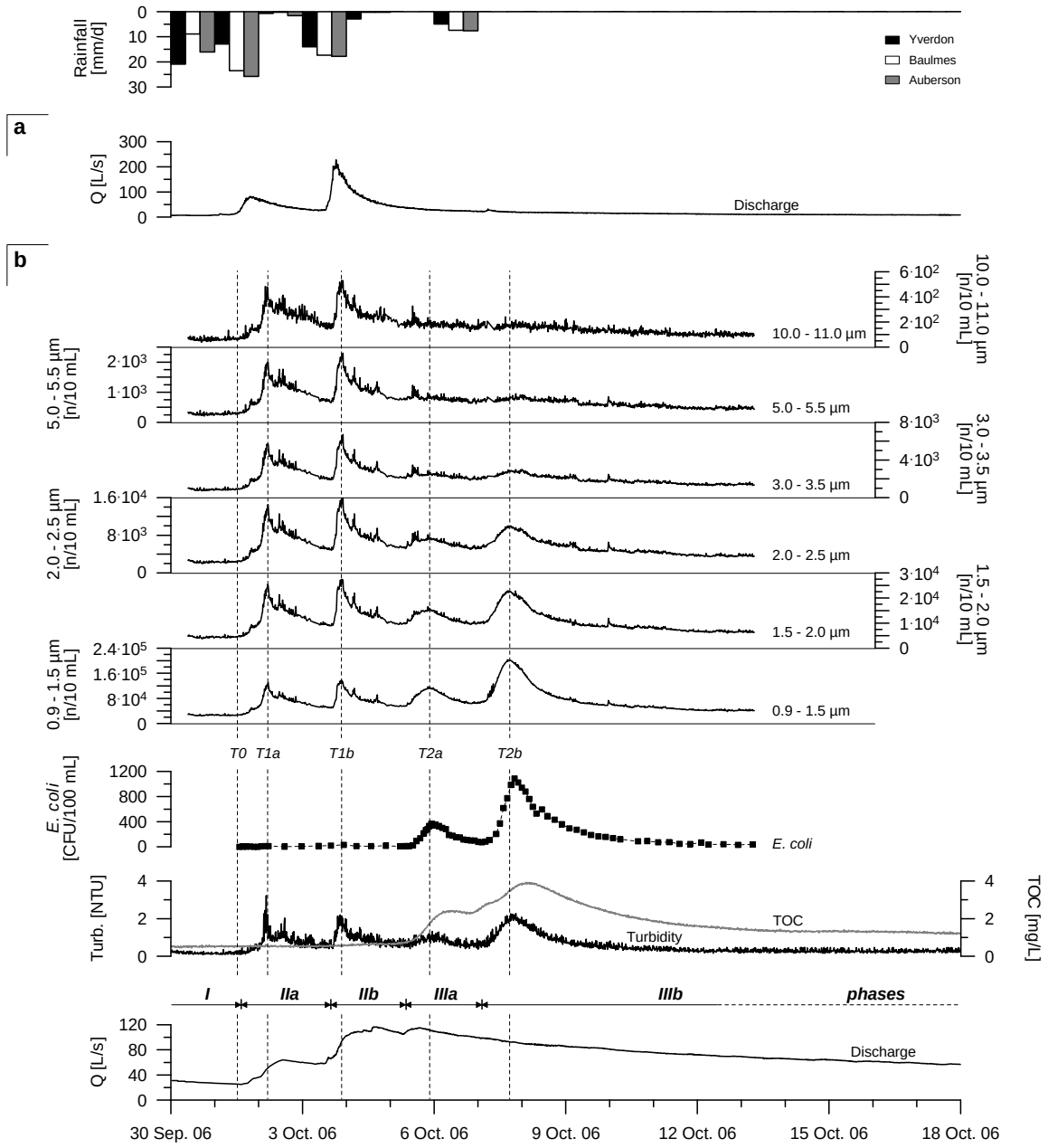

Fig. 3.11 Temporal changes in *E. coli* content and PSD at the Moulinet spring during two successive storm events in October 2006. (**a**) Feurtille swallow hole and (**b**) Moulinet spring. Q: discharge; Turb.: turbidity; *T0*: pre-storm conditions; *T1a* / *b*: autochthonous turbidity signals of the first / second storm event; *T2a* / *b*: allochthonous turbidity signals of the first / second storm event.

high sensitivity of PSD analysis to identify allochthonous particle contributions would probably have detected these microbial contamination events.

RAINFALL EVENT DURING HIGH-FLOW CONDITIONS

The occurrence of faecal indicator bacteria at the Moulinet spring was also monitored during the April 2006 storm event (Fig. 3.12), which occurred during a period of high-flow conditions. The dynamics of suspended matter during this storm event are discussed in Section 3.4.2.

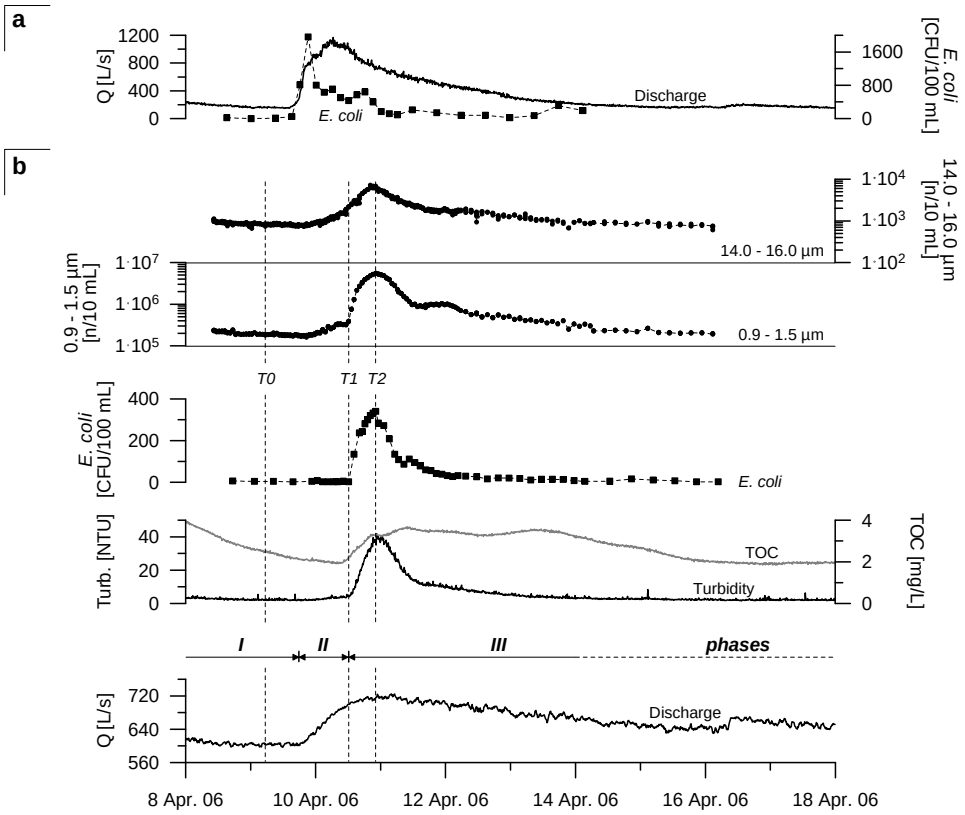

Fig. 3.12 Temporal changes in *E. coli* content and PSD at the Moulinet spring during the April 2006 storm event. (**a**) Feurtille swallow hole and (**b**) Moulinet spring. Q: discharge; Turb.: turbidity; *T0*: pre-storm conditions; *T1*: maximum strictly autochthonous turbidity / first arrival of allochthonous turbidity and *E. coli* from the swallow hole; *T2*: maximum allochthonous turbidity.

Simultaneously with the infiltration of turbid storm-derived water, increased levels of *E. coli* content entered the swallow hole (Fig. 3.12a) and reached about 2000 CFU/100 mL. During the rising limb of the spring hydrograph at the Moulinet spring and when autochthonous particles discharged at the spring (*T0* to *T1*), *E. coli* content was constantly low at 0 to 2 CFU/100 mL (Fig. 3.12b). However, as for the rainfall event during low-flow conditions, simultaneously with the arrival of storm-derived water, indicated by a sudden TOC increase and characterised by typical allochthonous turbidity breakthrough, *E. coli* counts started to increase abruptly (*T1*). The latter reached its maximum concentration of 340 CFU/100 mL at the moment of maximum allochthonous turbidity (*T2*), approximately 10 h after the first arrival of the allochthonous component. Finally, as for the October 2006 storm events, the breakthrough of allochthonous particles and *E. coli* showed a nearly perfect parallel evolution.

GENERAL COMMENTS

Results of other monitored storm events at the Yverdon-les-Bains karst aquifer system were in agreement with the observations described above. The occurrence of faecal indicator bacteria at the springs was intimately related to the breakthrough of allochthonous particles. The absence of faecal indicator bacteria content increases during autochthonous turbidity events suggests further

that enteric bacteria originating from periodical contamination (in this case from the Feurtille swallow hole) are unlikely to persist in the karst aquifer system. Similar observations have also been reported by Personné *et al.* (1998).

Faecal indicator bacteria, which have sizes of about 0.5 – 2 µm, were highly correlated to allochthonous particles of similar sizes, i.e. the 0.9 – 1.5 µm size class. Indeed, the correlation coefficients (R^2) for all events were higher than 0.92, except during the December 2005 storm event (Fig. C.4, Appendix C) for which the coefficient was 0.86. These high correlations suggest that allochthonous bacteria are mainly transported attached to or together with suspended particles as proposed by Hipsey *et al.* (2006) and Mahler *et al.* (2000). Consequently, similar transport and deposition processes for bacteria and the fine natural particles / colloids in karst aquifers are suggested. This hypothesis is further supported by the recovery rate for *E. coli* of 21 % at the Moulinet spring during the April 2006 storm event (mean discharge ~ 670 L/s), which is in general agreement with the increasing recovery rates of the 1-µm fluorescent microspheres with increasing flow conditions within the system.

However, despite the strong correlation between fine allochthonous particle and faecal indicator bacteria breakthrough at the springs for each storm event, no universal and absolute relation exists between both parameters. Bacterial input at the swallow hole is strongly dependent on the land use. PSD monitoring at karst springs allows thus identifying periods potentially contaminated by allochthonous microorganisms, but it does not permit inferring the level of contamination.

Finally, results of monitoring of selected hydrological events undertaken at the Noiraigue karst aquifer system confirmed the feasibility of PSD monitoring as tool for identifying potential microbial contamination of karst groundwater (Fig. C.2, Appendix C).

3.6 PSD AS INDICATOR FOR FAECAL BACTERIA CONTAMINATION AT KARST SPRINGS

In the foregoing section, it was shown that faecal bacteria contamination occurred during allochthonous turbidity events, while autochthonous turbidity events were hygienically safe. In the simplest case, a combined increase of turbidity and TOC indicates the arrival of faecal bacteria. A complication arises from the fact that very low increases of both parameters, sometimes even below the water quality standards (which was often the case at the Cossaux spring), may coincide with high allochthonous bacteria levels. Therefore, the decision imputed to drinking water purveyors based solely on turbidity and TOC may be very complicated.

PSD monitoring allowed discriminating clearly autochthonous from allochthonous turbidity and thus better identifying periods of microbial contamination. Autochthonous turbidity consisted of particle concentration increases over a wide range of particle sizes, while allochthonous turbidity and bacterial contamination periods were characterised by a predominance of finer particles. However, in absolute numbers, finer particles were always more abundant than larger ones.

These differences in size distributions among autochthonous and allochthonous turbidity events are clearly expressed in a graphic representation of the relative cumulative size distributions, i.e. percent of particles smaller than a given diameter vs. particle diameter

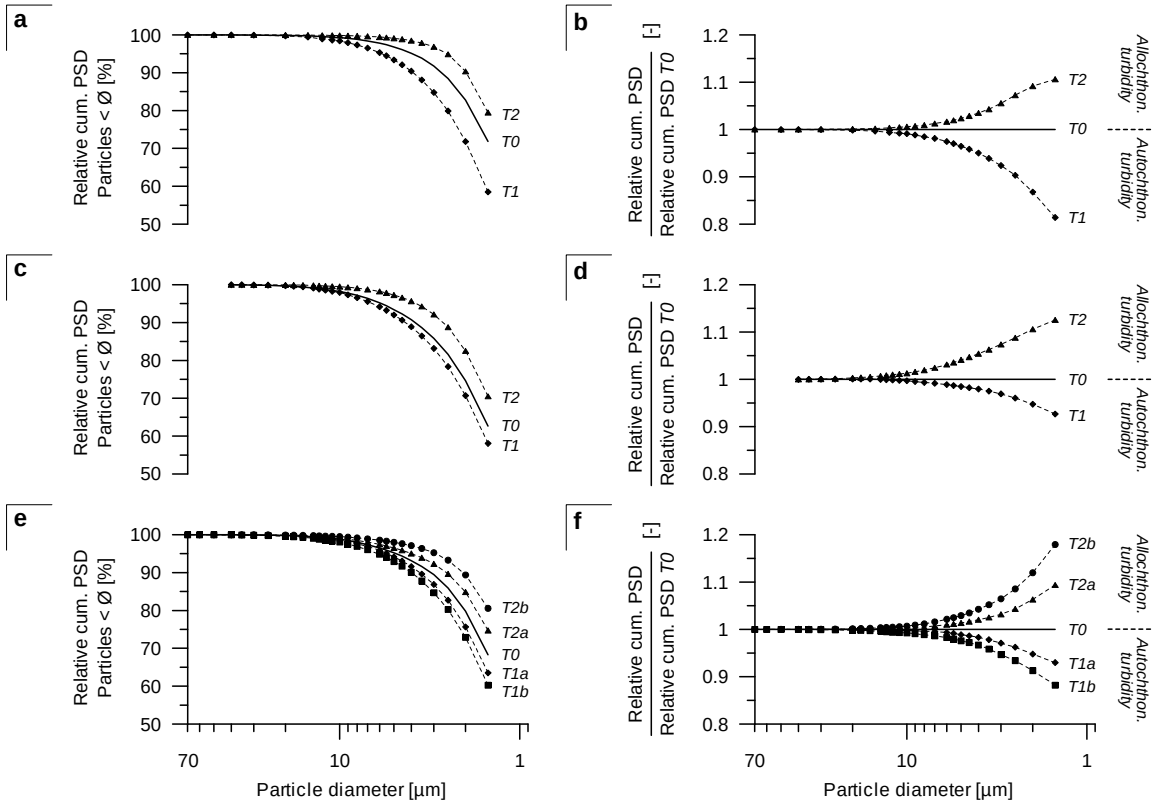

Fig. 3.13 Analysis of selected PSD curves from the Moulinet spring during (**a** and **b**) the February 2006 storm event (sampling times *T* are shown in Fig. 3.5), (**c** and **d**) the April 2006 storm event (Fig. 3.6 and 3.12) and (**e** and **f**) the October 2006 storm event (Fig. 3.11). A relative decrease of finer particles (0.9 to 10 µm) with respect to pre-storm reference PSDs (*T0*) is indicative of autochthonous turbidity (*T1*), while a relative increase of finer particles characterises allochthonous turbidity (*T2*) and thus the possible presence of faecal bacteria contamination. Similar analyses of PSD curves from the Cossaux spring are shown in Fig. C.8 (Appendix C).

(Fig. 3.13a, c and e). In this representation, PSD curves of pre-storm conditions are plotted as reference curves (*T0*). The PSD of autochthonous turbidity events (*T1*) lies below this reference curve, while the PSD of allochthonous turbidity periods (*T2*) lies above, indicating a relative predominance of finer particles. The difference becomes even more evident when all PSD curves are normalised by the pre-storm PSD (Fig. 3.13b, d and f). In this representation, the reference PSD (*T0*) is a horizontal line (y = 1), while finer particle-size classes display values < 1 for autochthonous turbidity and > 1 for allochthonous turbidity.

The analysis of storm event PSD curves gave also very similar results using one unique reference PSD. This reference PSD, which corresponds to the PSD measurement showing the lowest particle concentration (Fig. 3.2, *PSD5* and *PSD9* for the Moulinet and Cossaux springs, respectively), was measured during a prolonged period of extreme low-flow conditions with almost complete absence of any allochthonous swallow hole contribution.

An important feature of such analysis is the sensitivity to detect an allochthonous particle contribution. For all monitored storm events, this analysis allowed detecting an allochthonous contribution, and thus a potential microbial contamination of spring water, within 2 hours. For example, the results of the April 2006 storm event (Fig. 3.12), which showed an important overlap

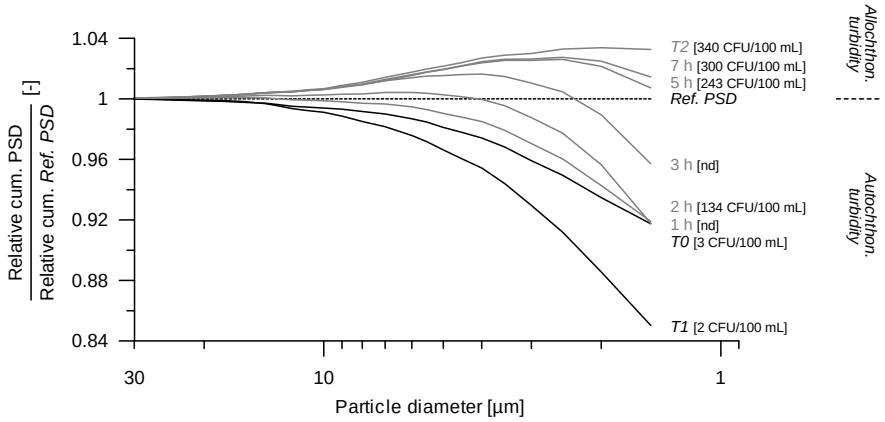

Fig. 3.14 Analysis of selected PSD curves of the Moulinet spring during the rising limb of the allochthonous turbidity signal during the April 2006 storm event (Fig. 3.12). *T0*: pre-storm conditions; *T1*: maximum strictly autochthonous turbidity / last measurement preceding the first arrival of the allochthonous swallow hole component; *T2*: maximum allochthonous turbidity; other sample labels: time in hours after *T1*. Corresponding *E. coli* contents are given in brackets (nd: not determined).

of both turbidity signals, are shown in Fig. 3.14. In this case, PSD during pre-storm conditions (*T0*) showed an important strictly autochthonous signal. This is not surprising as high-flow conditions prevailed during this period. *T1*, which corresponded to the maximum of strictly autochthonous turbidity (last measurement preceding the first arrival of the allochthonous swallow hole component), showed also a strictly autochthonous signal. The first detection of an allochthonous turbidity contribution, using this type of analysis, was observed 1 hour after *T1*.

3.7 CONCLUSION

Following rainfall events, microbial quality of karst spring water may drastically deteriorate within very short time periods (less than 24 h at the Yverdon-les-Bains karst aquifer system). Therefore, classical microbiological survey programs are often inadequate to prevent contaminated water entering the distribution network. A surrogate indicator for possible microbial pollution would thus be of high utility for drinking water purveyors. The present study investigated therefore the occurrence, dynamics and behaviour of faecal indicator bacteria and particles in karst aquifers.

Turbidity events at karst springs either results from the remobilisation and scouring of intrakarstic particulate material, i.e. autochthonous turbidity, and / or from the direct transfer of suspended matter from the land surface entering the system following rainfall events, i.e. allochthonous turbidity. The occurrence of autochthonous turbidity was strongly related to the changing hydrodynamic conditions (i.e. flow acceleration) within the karst aquifer, whereas the breakthrough of allochthonous particles was related to the sediment input at the swallow hole and the flow-through time (i.e. flow velocity). This second turbidity type coincided with increased levels of microbial contamination originating from agricultural and other activities at the land surface.

Particle-size distribution (PSD) monitoring of karst spring waters made it possible to discriminate clearly autochthonous from allochthonous turbidity; autochthonous turbidity was characterised by significant particle concentration increases over a wide range of size classes, ranging from colloidal sizes up to about 0.1 mm, whereas allochthonous turbidity was characterised by increases of the finer size classes only, ranging from 0.9 to approximately 10.0 µm. PSD measurements can thus be used as an "early-warning" surrogate for real-time monitoring of possible faecal bacteria contamination of groundwater from karst springs. Moreover, as PSD can be monitored continuously online and as its sensitivity to detect an allochthonous particle contribution is very high, PSD represents therefore a new data resource for assessing microbial water quality in karst aquifers.

REFERENCES

Ahn J.H. and Grant S.B. 2007. Size distribution, sources, and seasonality of suspended particles in southern California marine bathing waters. Environmental Science & Technology 41 (3): 695-702.

American Public Health Association, American Water Works Association and Water Environment Federation (APHA, AWWA and WEF). 2005. Standard methods for the examination of water and wastewater, 21st Edition. Water Environment Federation, Alexandria, VA.

Amraoui F., Razack M. and Bouchaou L. 2003. Turbidity dynamics in karstic systems. Example of Ribaa and Bittit springs in the Middle Atlas (Morocco). Hydrological Sciences Journal – Journal des Sciences Hydrologiques 48 (6): 971-984.

Atteia O. 1998. Evolution of size distributions of natural particles during aggregation: modelling versus field results. Colloids and Surfaces A-Physicochemical and Engineering Aspects 139 (2): 171-188.

Atteia O. and Kozel R. 1997. Particle size distributions in waters from a karstic aquifer: from particles to colloids. Journal of Hydrology 201 (1-4): 102-119.

Atteia O., Perret D., Adatte T., Kozel R. and Rossi P. 1998. Characterization of natural colloids from a river and spring in a karstic basin. Environmental Geology 34 (4): 257-269.

Auckenthaler A., Raso G. and Huggenberger P. 2002. Particle transport in a karst aquifer: natural and artificial tracer experiments with bacteria, bacteriophages and microspheres. Water Science and Technology 46 (3): 131-138.

Bakalowicz M. 2005. Karst groundwater: a challenge for new resources. Hydrogeology Journal 13 (1): 148-160.

Bradford S.A., Simunek J., Bettahar M., van Genuchten M.T. and Yates S.R. 2003. Modelling colloid attachment, straining, and exclusion in saturated porous media. Environmental Science & Technology 37 (10): 2242-2250.

Brookes J.D., Hipsey M.R., Burch M.D., Regel R.H., Linden L.G., Ferguson C.M. and Antenucci J.P. 2005. Relative value of surrogate indicators for detecting pathogens in lakes and reservoirs. Environmental Science & Technology 39 (22): 8614-8621.

Doyle M.P. and Erickson M.C. 2006. Closing the door on fecal coliform assay. Microbe 1 (4): 162-163.

Drew D. and Hötzl H. 1999. Karst hydrogeology and human activities. Impacts, consequences and implications. International Contributions to Hydrogeology (IAH), Balkema, Rotterdam.

Dussart-Baptista L., Massei N., Dupont J.P. and Jouenne T. 2003. Transfer of bacteria-contaminated particles in a karst aquifer: evolution of contaminated materials from a sinkhole to a spring. Journal of Hydrology 284 (1-4): 285-295.

Edberg S.C., LeClerc H. and Robertson J. 1997. Natural protection of spring and well drinking water against surface microbial contamination. II: Indicators and monitoring parameters for parasites. Critical Reviews in Microbiology 23 (2): 179-206.

Ford D. and Williams P. 2007. Karst hydrogeology and geomorphology. Wiley, New York.

Grolimund D., Elimelech M., Borkovec M., Barmettler K., Kretzschmar R. and Sticher H. 1998. Transport of in situ mobilized colloidal particles in packed soil columns. Environmental Science & Technology 32 (22): 3562-3569.

Herwaldt B.L., Craun G.F., Stokes S.L. and Junanek D.D. 1992. Outbreaks of waterborne disease in the United States – 1989-90. Journal American Water Work Association 84 (4): 129-135.

Hipsey M.R., Brookes J.D., Regel R.H., Antenucci J.P. and Burch M.D. 2006. In situ evidence for the association of total coliforms and *Escherichia coli* with suspended inorganic particles in an Australian reservoir. Water Air and Soil Pollution 170 (1-4): 191-209.

Käss W. 1998. Tracing technique in geohydrology. Balkema, Rotterdam.

Keller A.A., Sirivithayapakorn S. and Chrysikopoulos C.V. 2004. Early breakthrough of colloids and bacteriophage MS2 in a water-saturated sand column. Water Resources Research 40 (8), article n°: W08304.

Kralik M. 2001. Strategie zum Schutz der Karstwassergebiete in Österreich. Report BE-189, Environment Agency, Vienna.

Kramer M.H., Quade G., Hartemann P. and Exner M. 2001. Waterborne diseases in Europe 1986-1996. Journal American Water Works Association 93 (1): 48-53.

Lacroix M., Rodet J., Wang H.Q., Massei N. and Dupont J.P. 2000. Origine des matières en suspension dans un système aquifère karstique: apports de la granulométrie. Comptes Rendus de l'Académie des Sciences, Sciences de la Terre et des Planètes 330 (5): 347-354.

LeClerc H., Mossel D.A.A., Edberg S.C. and Struijk C.B. 2001. Advances in the bacteriology of the coliform group: their suitability as markers of microbial water safety. Annual Review of Microbiology 55: 201-234.

Lisle J.L. and Rose J.B. 1995. *Cryptosporidium* contamination of water in the USA and UK: a minireview. Journal of Water Supply: Research and Technology-AQUA 44 (3): 103-117.

Mahler B.J. and Lynch F.L. 1999. Muddy waters: temporal variation in sediment discharging from a karst spring. Journal of Hydrology 214 (1-4): 165-178.

Mahler B.J., Personné J.C., Lods G.F. and Drogue C. 2000. Transport of free and particulate-associated bacteria in karst. Journal of Hydrology 238 (3-4): 179-193.

Massei M., Wang H.Q., Dupont J.P., Rodet J. and Laignel B. 2003. Assessment of direct transfer and resuspension of particles during turbid floods at a karstic spring. Journal of Hydrology 275 (1-2): 109-121.

Montgomery M.A. and Elimelech M. 2007. Water and sanitation in developing countries: including health in the equation. Environmental Science & Technology 41 (1): 17-24.

Nebbache S., Loquet M., Vinceslas-Akpa M. and Feeny V. 1997. Turbidity and microorganisms in a karst spring. European Journal of Soil Biology 33 (2): 89-103.

Personné J.C., Poty F., Vaute L. and Drogue C. 1998. Survival, transport and dissemination of *Escherichia coli* and enterococci in a fissured environment. Study of a flood in a karstic aquifer. Journal of Applied Microbiology 84 (3): 431-438.

Ryan M. and Meiman J. 1996. An examination of short-term variations in water quality at a karst spring in Kentucky. Ground Water 34 (1): 23-30.

Sirivithayapakorn S. and Keller A.A. 2003. Transport of colloids in saturated porous media: a pore-scale observation of the size exclusion effect and colloid acceleration. Water Resources Research 39 (4), article n°: 1109.

Tallon P., Magajna B., Lofranco C. and Leung K.T. 2005. Microbial indicators of faecal contamination in water: a current perspective. Water Air and Soil Pollution 166 (1-4): 139-166.

White W.B. 1988. Geomorphology and hydrology of karst terrains. Oxford University Press, New York.

Zwahlen F. (ed.) 2004. Vulnerability and risk mapping for the protection of carbonate (karst) aquifers, final report (COST action 620). European Commission, Brussels.

4

Percolation and particle transport in the unsaturated zone of karst aquifers*

ABSTRACT

Recharge and contamination of karst aquifers mainly occur via the unsaturated zone, but the functioning of this zone, principally with regard to the transfer of particles and the associated microbial contaminants, has not yet been fully understood. Therefore, irrigation and tracer experiments, along with monitoring of rainfall events, were used to examine water percolation and the transport of solutes, particles and faecal bacteria between the land surface and water outlets in shallow caves. Monitored parameters included discharge, electrical conductivity, organic carbon, turbidity, particle-size distribution (PSD), faecal indicator bacteria and artificial tracers. Results demonstrated that, following rainfall or irrigation, water percolation and the dynamics of suspended matter could be subdivided into three phases: a lag phase, which showed no response at the outlet; a piston-flow phase, characterised by the release of epikarst storage water by pressure transfer and a pulse-through turbidity signal due to remobilisation of particles from fractures; and a mixed-flow phase, characterised by an increasing contribution of freshly infiltrated water and a flow-through turbidity signal caused by direct particle transfer from the soil. PSD allowed differentiation between the two types of turbidity. Furthermore, during the mixed-flow phase, which started between 20 min and a few hours after the start of recharge event, the breakthrough of fine flow-through particles (0.9 –1.5 µm) coincided well with the breakthrough of faecal indicator bacteria. These findings helped to quantify water storage and percolation in the epikarst and to better understand contaminant transport and attenuation. The use of PSD as "early-warning" parameter for microbial contamination in karst waters was confirmed.

4.1 INTRODUCTION

The unsaturated zone of karst aquifers, consisting of the soil, epikarst and a transmission zone, plays a crucial role for groundwater recharge and contaminant attenuation. Significant amounts of (plant-accessible) water and contaminants can be stored in this zone for prolonged periods of

* This chapter is based on the paper:

Pronk M., Goldscheider N., Zopfi J. and Zwahlen F. 2009. Percolation and particle transport in the unsaturated zone of a karst aquifer. Ground Water 47 (3): 361-369.

time, allowing for biodegradation and other attenuation processes to operate. However, due to flow concentration in the epikarst, water and contaminants can also be rapidly transported downwards to the active conduit network, often via vertical shafts, mainly during storm rainfall (Klimchouk 2004; Williams 2008).

Not only water and solutes but also different types of organic and inorganic particles and colloids can be transported through karst systems. Sediments in karst systems can act as reservoirs for contaminants, such as dense non-aqueous phase liquids (DNAPL), pesticides and toxic metals. During storm events, they can be mobilised and transported towards springs or wells (Loop and White 2001; Vesper and White 2003, 2004). Particles and colloids also act as transport vectors for microbial pathogens, generally originating from human activities at the land surface, such as agriculture or wastewater releases (Mahler *et al*. 2000; Ryan and Meiman 1996).

Suspended particles and colloids are often measured as turbidity. Turbidity at karst springs may either result from the remobilisation of intrakarstic sediments due to increased flow velocities, i.e. pulse-through or autochthonous turbidity, and / or from direct particle transfer from the land surface, i.e. flow-through or allochthonous turbidity (e.g. Mahler and Lynch 1999; Massei *et al*. 2003). Pulse-through turbidity episodes often occur shortly after rainfall events, generally during increasing flow conditions in the system, while flow-through turbidity signals may arrive hours to several days later, depending on the flow-through time, often during the recession phase (Pronk *et al*. 2006). Turbidity is a bulk optical parameter, while particle-size distribution (PSD) measurements (Atteia and Kozel 1997; Mahler and Lynch 1999) and mineralogical analyses (Atteia *et al*. 1998; Herman *et al*. 2007) yield more detailed information about the number, size and composition of particles in karst spring water.

Recently, it has been demonstrated that continuous monitoring of PSD in karst spring water could also be used to differentiate between both types of turbidity (Pronk *et al*. 2007). Pulse-through turbidity was characterised by particle concentration increases over a wide range of particle-size classes, from colloidal sizes up to hundreds of micrometers. In contrast, flow-through turbidity was identified by increases of only smaller particles, ranging between 0.9 and approximately 10 µm, which are not or only little affected by sedimentation. Faecal bacteria contamination was often associated with this type of turbidity, as they also originate from the land surface, so that PSD was proposed as an "early-warning" parameter for microbial contamination of karst spring water. Artificial tracer tests with solutes and colloids / particles also confirmed that particles of a size similar to that of bacteria (~ 1 µm) and *Cryptosporidium* oocysts (3 to 7 µm) can travel over large distances in karst systems, even during low-flow conditions (e.g. Auckenthaler *et al*. 2002; Göppert and Goldscheider 2008).

In general, the role of sediments in contaminant storage, attenuation and transport in karst aquifers has not been sufficiently investigated and would require more research (White 2002). The few available studies cited earlier mainly deal with sediment transport in the main conduit network of karst aquifers, while investigations of the vadose zone in karstified limestone formations mostly focused on the percolation of water and solute transport (Perrin *et al*. 2003; Savoy 2007). Colloid / particle transport, on the other hand, was mostly studied in porous media, whereas there is little knowledge about the behaviour of colloids / particles and associated contaminants in the unsaturated zone of karst aquifers (McCarthy and McKay 2004).

Therefore, the objectives of the present study were: (*i*) to characterise and differentiate the two principal components – storage water and freshly infiltrated water – contributing to percolation in the unsaturated zone of karst aquifers; (*ii*) to investigate the temporal variations of sediment particles in this zone in response to recharge events, with the main focus on the mobilisation and transfer of particles and the associated microbial contaminants; (*iii*) to identify the processes governing particle dynamics and transport; and (*iv*) to further confirm (or refute) the use of PSD as an "early-warning" parameter for microbial contamination, as it can be done for karst spring water.

In order to achieve these goals, several irrigation and tracing experiments were carried out between 2005 and 2007 at three sites in the Swiss Jura Mountains: the artificial galleries near Gänsbrunnen (Canton Solothurn) and the Grand-Bochat and the Vers-chez-le-Brandt caves (Canton Neuchâtel). Moreover, the latter was also continuously monitored to observe the response of natural parameters at the cave outlet to rainfall events. Ready access and the simple settings make these caves and galleries suitable sites for this type of investigation. The most complete and insightful results were obtained at the Vers-chez-le-Brandt cave and the artificial galleries near Gänsbrunnen; therefore, mainly the findings from these two test sites will be presented and discussed here.

4.2 TEST SITES

For reminder, the nearly horizontal Vers-chez-le-Brandt cave is developed in unsaturated limestone beneath relatively flat pasture land (Fig. 4.1). About 1 to 2 m of soil / loess and 30 m of limestone overlie the approximately 200-m-long cave. A perennial vadose flow issuing from a fracture at the cave roof was monitored and sampled. The base flow of this water outlet is approximately 0.6 L/min.

The artificial galleries near Gänsbrunnen are located beneath a forested hilltop and are overlaid by an approximately 10-m-thick sequence of unsaturated limestone. The Gänsbrunnen test site mainly differs from the Vers-chez-le-Brandt test site by the nearly absence of soil, i.e. less than 10 cm. The monitored water outlet, issuing from a fissure in the wall, is only activated during rainfall events and runs rapidly dry.

Finally, in terms of soil, land use and lithology, these settings are quite typical for large parts of the unsaturated zone in the Jura Mountains.

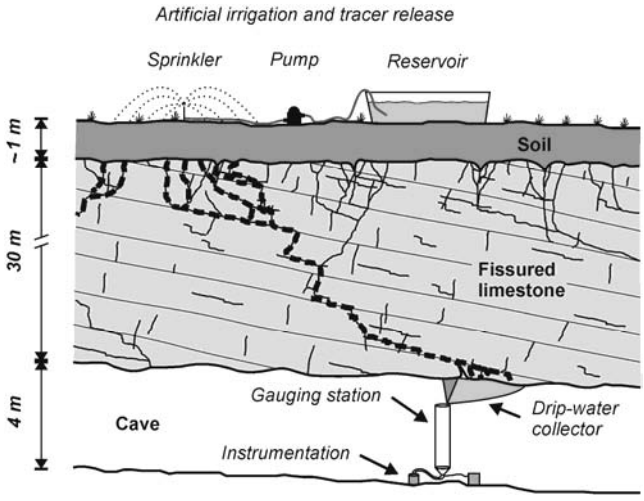

Fig. 4.1 Schematic cross-section of the Vers-chez-le-Brandt test site and illustration of the experimental set-up (an identical experimental set-up was put in place at the Gänsbrunnen test site).

4.3 MATERIAL AND METHODS

4.3.1 Experiments, experimental set-up and instrumentation

Investigation at the test sites reported in this chapter consisted essentially of four elements; each of them having different objectives:

1. continuous monitoring of natural parameters at the water outlet in the Vers-chez-le-Brandt cave for several months. This monitoring allowed observing the response of the unsaturated zone to natural recharge events;

2. a long-term (steady-state) irrigation experiment with a constant concentration of a conservative solute tracer in irrigation water. This experiment, carried out at the Vers-chez-le-Brandt test site, intended at characterising flow conditions within the unsaturated zone;

3. comparative tracer tests (particulate and solute tracers), performed during steady-state flow regime established by long-term irrigation. These tracer tests aimed at investigating particle and solute transport in the unsaturated zone and were carried out both at the (***3a***) Vers-chez-le-Brandt and the (***3b***) Gänsbrunnen test sites;

4. a short-term (transient) irrigation experiment with a constant concentration of a non-reactive solute tracer in irrigation water. This experiment, conducted at the Vers-chez-le-Brandt test site, was designed to study the behaviour of particles, TOC and faecal bacteria in the unsaturated zone with an irrigation scenario similar to natural rain events.

To study the response of the unsaturated zone to natural rainfall events (***1***), discharge, temperature, electrical conductivity, turbidity and total organic carbon (TOC) were monitored continuously at the water outlet in the Vers-chez-le-Brandt cave from June to November 2007. Discharge was measured by collecting water from the fracture on a plastic sheet draining towards a flow gauge containing a pressure probe (RTC28, Kistler, Winterthur, Switzerland), and temperature and electrical conductivity were monitored using a conductivity probe (340i, WTW, Weilheim, Germany). Data of both probes were recorded every 2 min by a data logger (DT50, dataTaker, Rowville, Australia). Turbidity and TOC were measured every 30 s with a GGUN-FL30 flow-through field fluorometer (Schnegg and Costa 2003) as described in Chapter 2.

The irrigation (and tracer) experiments (***2***, ***3*** and ***4***) were done using garden sprinklers connected to a pump and a reservoir of 6 m^3. The irrigated areas, some tens of square meters, were chosen according to previous studies, which established the catchment areas of the monitored outlets by means of tracer tests (Savoy 2007; unpublished report by Pochon 2004). With respect to the typical scale of regional fracture frequencies and epikarst development, these irrigation areas are supposed to be sufficiently large to obtain results that are representative for larger areas. Furthermore, for tracer release at the land surface (***3***), 35 L of water containing the tracers was pumped through the irrigation device, and the irrigation was continued afterwards. During all experiments, in addition to the above-mentioned standard monitoring program, PSD was determined every 2 min with a portable particle counter (Abakus mobil fluid, Klotz, Unterhaugstett, Germany). The latter groups the particles into 32 pre-definable size classes, ranging from 0.9 to 139 µm (see Chapter 3 for details). Fluorescent dyes were monitored continuously with the aforementioned field fluorometer at a time step of 30 s, and water samples

were collected manually for analyses of major ion chemistry and faecal indicator bacteria (*E. coli* and enterococci). Major ion chemistry was analysed by ion chromatography (IC DX-120, Dionex, Sunnyvale, USA), and faecal indicator bacteria were determined, within maximum 20 h following sampling, using standard cultivation techniques (APHA, AWWA and WEF 2005).

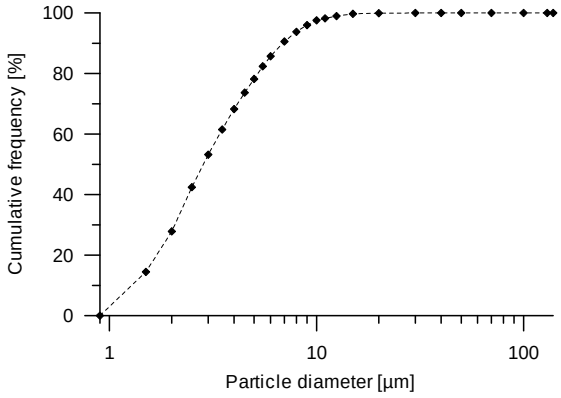

Fig. 4.2 Cumulative percentage frequency of PSD (between 0.9 and 139 µm) of the clayey loam suspension released at the Vers-chez-le-Brandt test site for the comparative tracer test during the long-term irrigation experiment.

The long-term irrigation experiment performed at the Vers-chez-le-Brandt test site (***2***) was combined with a comparative tracer test (***3a***). An area of approximately 28 m^2 (which is only a part of the outlet catchment) was irrigated for 13.2 hours at a constant irrigation rate of 7.1 L/min, corresponding to an intensity of about 15 mm/h or 200 mm of rain. The irrigation water contained a constant chloride concentration of 13.4 mg/L. When stable flow conditions were reached at the outlet, two successive tracer tests were carried out: for the first tracer test, 386 g of sodium bromide (corresponding to 300 g of Br^-) were released 3.3 h after start of irrigation, whereas for the second test, 518 mg of uranine and 3.6 L of clayey loam suspension were released simultaneously 7.1 h after start of irrigation. The clayey loam suspension was obtained from sediments at a karst spring in the region (Moulinet spring, Yverdon-les-Bains, Switzerland). PSD of the injected suspension was determined in the laboratory (Fig. 4.2); the suspension, dominated by small particles (0.9 to 10 µm), included a total number of approximately $7.9 \cdot 10^{11}$ particles.

For the comparative tracer test conducted at the Gänsbrunnen test site (***3b***), an area of approximately 17 m^2 was irrigated for 11.3 h at a constant irrigation rate of 6.1 L/min. This irrigation rate corresponds to an intensity of about 22 mm/h. When steady-state flow conditions were reached at the outlet, 51 g of sodium bromide (39.6 g of Br^-) and 0.2 L of clayey loam suspension ($4.3 \cdot 10^{10}$ particles) were released at the land surface. PSD of the suspension was identical to the one of the suspension used at the Vers-chez-le-Brandt test site.

During the short-term irrigation experiment carried out at the Vers-chez-le-Brandt test site (***4***), a volume of 670 L of water with a constant chloride concentration of 9.2 mg/L was irrigated over an approximately 28-m^2 plot during 1.5 h at a constant rate of 7.4 L/min. This watering corresponds to an intensity of about 16 mm/h and a total rainfall of 24 mm.

Long dry periods of minimum 8 days preceded all irrigation experiments. This resulted in outlet discharges close to its base flow at the Vers-chez-le-Brandt test site prior to the watering, while the outlet at the Gänsbrunnen test site was dry. For all experiments, tap water was used for irrigation; it had a pH of 7.2 to 7.6, an electrical conductivity of 500 to 600 µS/cm and very low background levels of the parameters monitored at the outlets (turbidity: 0.2 to 0.4 NTU, TOC: 0.6 to 0.8 mg/L, *E. coli* and enterococci: 0 to 1 CFU/100mL).

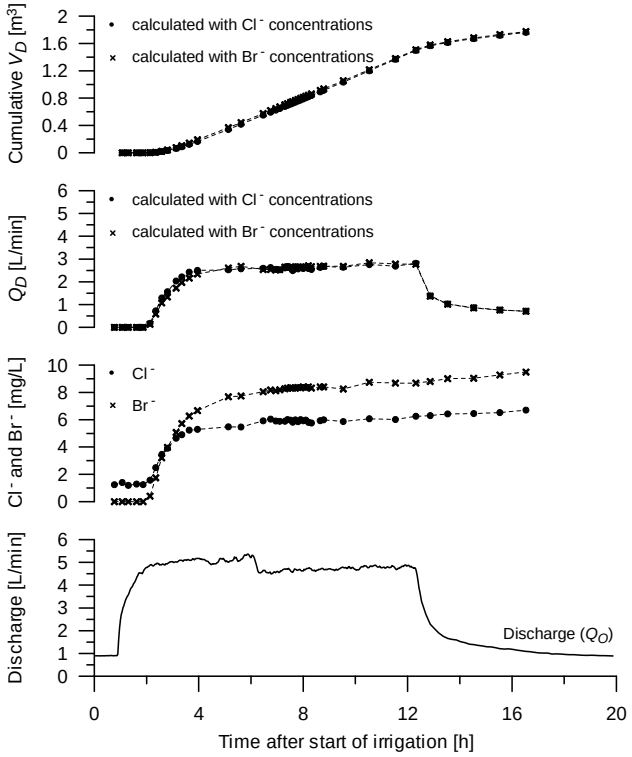

Fig. 4.3 Quantification of infiltration water discharging at the outlet (Q_D) during the October 2007 long-term irrigation experiment at the Vers-chez-le-Brandt test site. Q_D was calculated by means of chloride and bromide concentrations. Both methods gave highly similar results. For both tracers, the calculated total volume of infiltration water discharged at the outlet (V_D) during this experiment was 1.8 m^3. Cl^- in infiltration water: 9.6 mg/L; Cl^- in storage water: 1.3 mg/L; Br^- in infiltration water: 14.7 mg/L; Br^- in storage water: 0.0 mg/L.

4.3.2 Hydrograph separation

It is assumed that the outlet discharge Q_O is the result of mixing of two components: storage water, noted as Q_S, that is released by gravity drainage and pressure transfer; and freshly infiltrated water that directly percolates from the soil surface through the unsaturated zone and discharges at the outlet, noted as Q_D. Two equations (Eq. 4.1 and 4.2) describe the water fluxes and the corresponding natural tracer concentrations (c_O, c_S and c_D):

$$Q_O = Q_S + Q_D \qquad (4.1)$$

$$Q_O c_O = Q_S c_S + Q_D c_D \qquad (4.2)$$

For conservative tracers, c_D is equal to the concentration in the infiltration water (c_I). Combining equations 4.1 and 4.2 makes it possible to quantify, at any instant in time, the contribution of freshly infiltrated water to the discharge at the outlet via direct transfer (Eq. 4.3):

$$Q_D = \frac{c_O - c_S}{c_D - c_S} Q_O \qquad (4.3)$$

The corresponding water volumes (V_O, V_D, V_S and V_I) were calculated by integrating the respective discharges over time. In this study, chloride was used as a conservative tracer, which is present both in the irrigation water and in the natural system. This approach assumes that the chloride concentration of the storage component (c_S) remains constant throughout the experiment. A preliminary irrigation experiment, using constant bromide (absent in storage water) and chloride concentrations in the irrigation water, demonstrated the validity of this hypothesis (Fig. 4.3).

4.4 NATURAL RAINFALL EVENTS

The responses of the water outlet in the Vers-chez-le-Brandt cave to a small rainfall event (2.8 mm during 1.5 h) and to a major rainfall event (19.1 mm in 8 h) are shown in Fig. 4.4. As

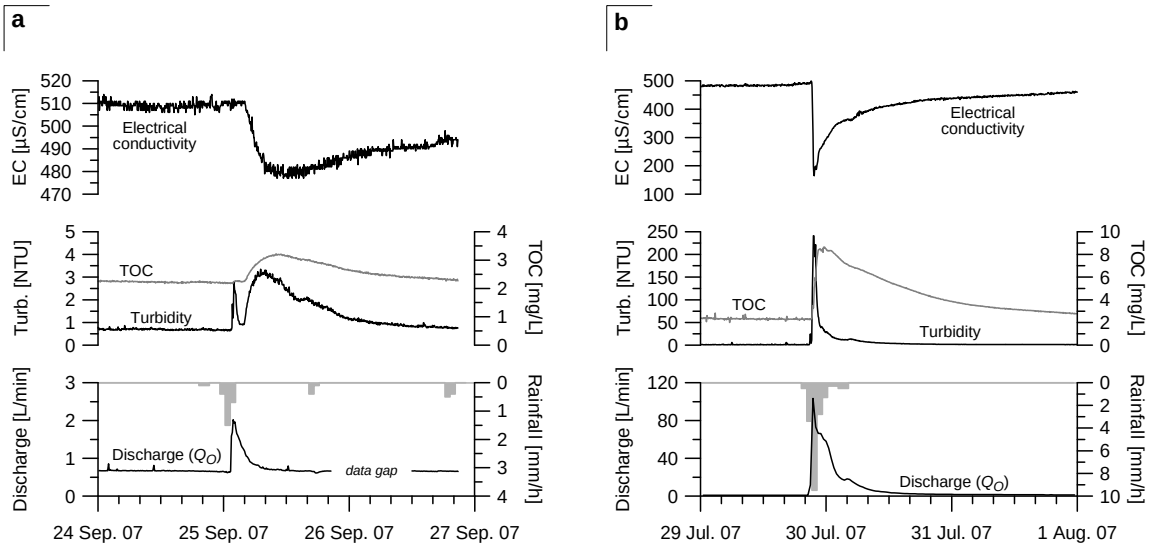

Fig. 4.4 Responses to natural rainfall events monitored at the water outlet in the Vers-chez-le-Brandt cave. (**a**) small rainfall event (2.8 mm) and (**b**) abundant rainfall event (19.1 mm). Turb.: turbidity; EC: electrical conductivity.

both events were preceded by dry periods of 5 days, the initial discharge of the outlet was close to its base flow at 0.7 L/min. The hydrographs showed a rapid increase, starting about 2 h after the start of the rain, followed by slow recession. The maximum discharge was 2.0 L/min during the small rainfall and about 100 L/min during the intense rainfall event.

The arrival of freshly infiltrated rainwater at the outlet, indicated by sudden decreases in electrical conductivity, occurred about 160 and 20 min after the initial discharge increases for the small and intense rainfall events, respectively. These flow-through times corresponded well to the discharge-dependent transit time relationship obtained from natural and artificial tracer tests (Fig. 4.5). Simultaneously with the arrival of fresh infiltration water, TOC, principally originating from the soil, started to increase. Flow variations in the unsaturated zone may thus be divided into three phases:

I. a lag phase, where rainfall has already occurred, but the outlet shows no reaction. The duration of this phase depends largely on the initial saturation of the soil;

II. a piston-flow phase, starting at the moment of discharge increase and lasting until the arrival of fresh infiltration water. Water discharging during this phase originates from the epikarst, released by a pressure pulse produced by increasing hydraulic head;

III. a mixed-flow phase, where water discharging at the outlet is a mixture of epikarst water, soil water and rainwater.

The volumes of the different components feeding the outlet are difficult to quantify. However, the volume of epikarst water discharging at the outlet represented at least 73 % and 26 % (calculated during phase *II*) of the total water volume discharged during the small and large precipitation events, respectively. This high contribution of storage water during rainfall events has also been observed in other studies (Lee and Krothe 2001; Perrin *et al.* 2003), where it represented about 70 to 90 %.

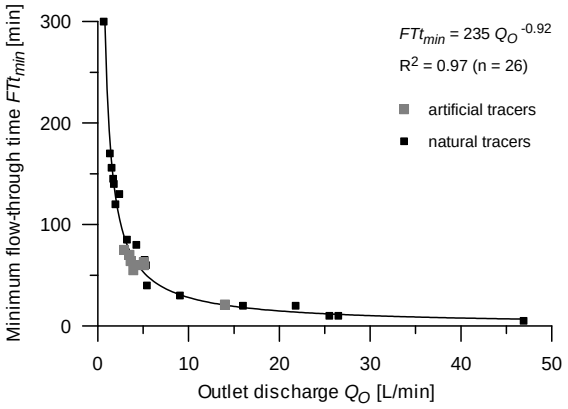

Fig. 4.5 Relationship between the outlet discharge (Q_O) and the minimum flow-through time (FTt_{min}) at the Vers-chez-le-Brandt test site, obtained from tracer tests and monitoring of TOC and electrical conductivity during rainfall events. Minimum flow-through times are spans of time between the moment of discharge increase at the outlet (for natural parameters), or the time of injection (for artificial tracers during long-term irrigation experiments), and the time when the respective parameter started to vary at the outlet.

Turbidity variations during both events differed significantly. During the small rainfall event (Fig. 4.4a), two distinct successive turbidity episodes were observed: a first narrow signal during the rising limb of the hydrograph while electrical conductivity and TOC remained stable at pre-event levels; and a second much wider signal during flow recession, accompanied by simultaneous electrical conductivity and TOC variations. The first signal is attributed to the mobilisation and scouring of particles inside fractures, close to the outlet, by increasing flow velocities and turbulences resulting from pressure transfer, i.e. pulse-through turbidity. The second signal indicates the arrival of freshly infiltrated rainwater that mobilised soil particles by hydrodynamic shear, i.e. flow-through turbidity.

During the major rainfall event (Fig. 4.4b), turbidity seemed to display only one large signal increasing simultaneously with discharge. However, observing the turbidity graph in detail, two turbidity events can be distinguished as during the small rainfall event. A first signal, i.e. pulse-through turbidity, reached a maximum of 24 NTU about 10 min after the start of discharge increase and recessed rapidly to 4 NTU. Simultaneously with the arrival of freshly infiltrated water, only about 20 min after the initial discharge increase, a flow-through turbidity signal increased and reached a maximum of 240 NTU about 15 min after peak discharge. Therefore, the very large and early flow-through turbidity signal largely masked the much smaller pulse-through turbidity signal. Substantial amounts of sediments may thus be released from the soil and epikarst zones during intense and abundant rainfall events and rapidly transported towards the active conduit network of karst aquifers.

During both events, sediment particles transported by infiltration water (flow-through turbidity) preceded the corresponding TOC signals, although both flow-through turbidity and TOC originate from the soil. This observation is consistent with findings from other studies, which revealed faster transport of particles and colloids with respect to solutes due to exclusion mechanisms in porous media (e.g. Sirivithayapakorn and Keller 2003), fractures (e.g. Zvikelsky and Weisbrod 2006) and karst conduits (e.g. Göppert and Goldscheider 2008).

4.5 CHARACTERISATION OF FLOW IN THE UNSATURATED ZONE

The response of the water outlet in the Vers-chez-le-Brandt cave to the long-term irrigation experiment (Fig. 4.6) allowed for the characterising and quantifying of flow within the unsaturated zone (the results of the tracer test carried out during this experiment will be discussed

in Section 4.6). Several phases, reflecting the changes in flow conditions and contributing components, were distinguished and enabled a "phase-by-phase" conceptual model to be proposed (Fig. 4.7). The model considers three types of fissures / fractures differing in their hydrological function resulting mainly from the aperture width, and it is based on the different types of water flow occurring in the unsaturated zone (Klimchouk 2004; Kogovšek 1997): (1) small fissures, which have not been affected by dissolution processes. They are always saturated with water that can only move by pressurised flow and are characterised by vadose seepage; (2) medium fissures, which are saturated during high recharge conditions and allow for moderately fast percolation or vadose flow; and (3) large fractures, which are never fully saturated

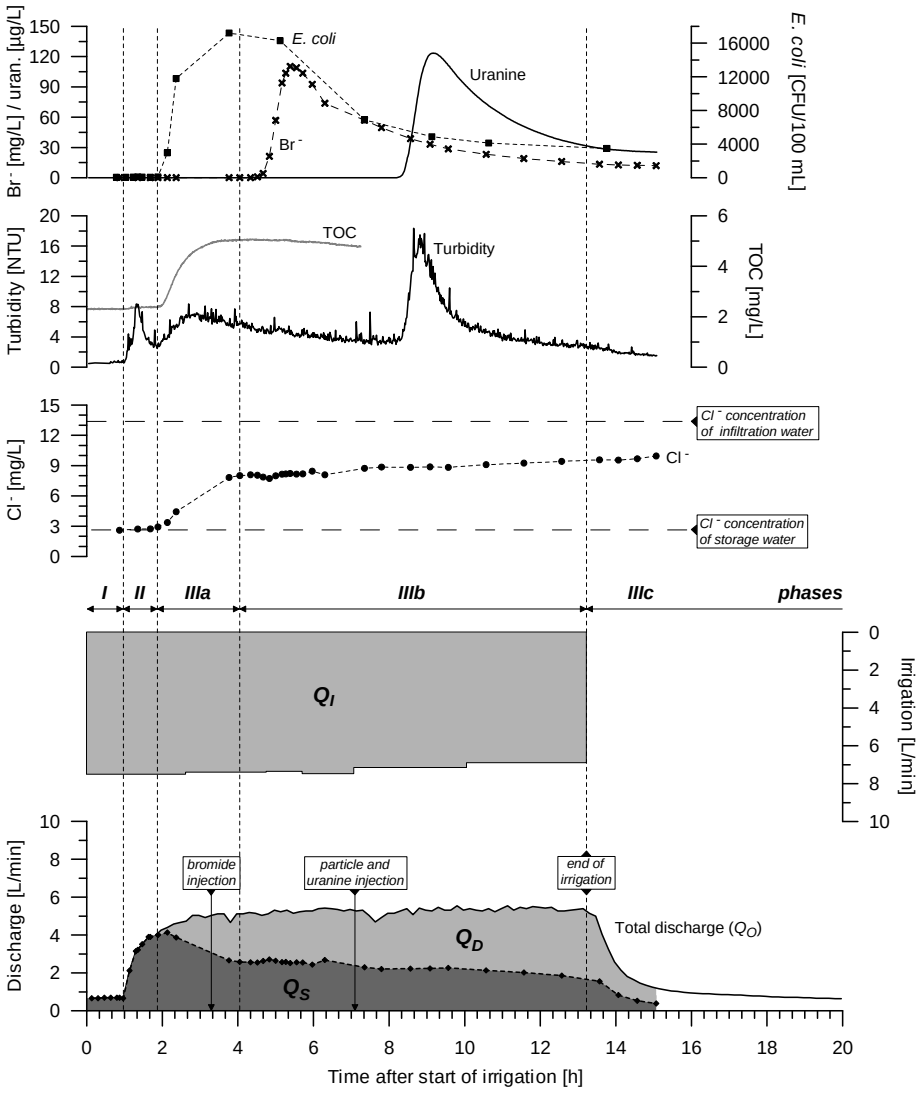

Fig. 4.6 Results of the September 2005 long-term irrigation experiment at the Vers-chez-le-Brandt test site. The response of the water outlet in the cave can be divided into several phases distinguished by different flow conditions and contributions of storage water (Q_S) and direct transfer of infiltration water (Q_D), which were separated using chloride concentrations. The turbidity signal occurring between 8 and 12 h after start of irrigation corresponds to the breakthrough of the clayey loam suspension released at the land surface 7.1 h after irrigation started (see Section 4.6 and Fig. 4.8).

and allow for rapid gravitational percolation or shaft flow. The outlet in the cave is connected to such a solutionally enlarged fracture.

As the experiment was preceded by a long dry period, the discharge of the outlet (0.7 L/min) was stable and close to its base-flow value. It is thus hypothesised that the soil water was immobile, i.e. the soil water content was less than field capacity. Therefore, the water percolating at the outlet results from the slow gravity drainage of epikarst water (*Qs*) from medium fractures via large fractures towards the outlet. When irrigation started, all parameters remained stable at pre-experimental levels (Fig. 4.6, phase *I*). During this lag phase, the irrigation water is essentially used to replenish the soil water deficit (Fig. 4.7a).

The piston-flow phase (Fig. 4.6, phase *II*) started after 0.9 h of irrigation with a sudden discharge increase from 0.7 to 3.9 L/min, while chloride and TOC remained stable, indicating that the water discharging at the outlet is still entirely composed of epikarst storage water (*Qs*). This is attributed to a pressure pulse from the soil-water column, causing water transfer from small and medium fissures into larger fissures (Fig. 4.7b). Turbidity increased simultaneously with discharge, reached a maximum of 8.4 NTU before the discharge maximum, and then decreased to 2.5 NTU. This pulse-through turbidity results from the mobilisation and scouring of particles in the large fractures near the outlet due to increasing flow velocities.

The mixed-flow phase (Fig. 4.6, phase *III*) is characterised by a mixed contribution of epikarst and soil storage water (Q_S) and direct transfer of freshly infiltrated water (Q_D). Phase *III* can further be subdivided into three stages.

Phase *IIIa* started after 1.9 h of irrigation and was defined by the first arrival of infiltration water, demonstrated by an increase of chloride, and soil water, demonstrated by an increase of TOC. The still increasing discharge and the rapidly changing chloride concentration at the outlet demonstrate the transient character of this phase. Such a fast direct transfer of water (approximately 16 m/h) is only possible via large fractures (Fig. 4.7c). The decreasing storage water (Q_S) discharging at the outlet is explained by a decreasing drainage of the medium and small fissures into the larger fractures, possibly resulting from a hydraulic gradient inversion. Furthermore, simultaneously with the first arrival of fresh infiltration water, a second turbidity episode was monitored at the outlet. Turbidity reached a maximum of 7.1 NTU after 2.8 h of irrigation and then decreased until the end of the experiment. This is clearly flow-through turbidity, i.e. direct transfer of eroded soil particles from the land surface and the soil compartment, also confirmed by a dramatic increase of faecal bacteria levels (up to 17000 CFU/100 mL of *E. coli*).

Transition between phases *IIIa* and *IIIb* was marked by a sudden decrease in the slope of the increasing chloride concentration, coinciding with a stabilisation of the outlet discharge at about 5.2 L/min (Fig. 4.6). This observation suggests the establishment of steady-state flow conditions with a high level of water saturation in the soil and well-organised flow routes through a network of small, medium and large fractures (Fig. 4.7d). The continuing gradual increase of chloride concentrations, suggesting a slightly decreasing drainage of storage water and an increasing contribution of infiltration water, expresses the effect of mixing between storage and infiltration water in the medium and smaller fissures.

Phase *IIIc* corresponded to the recession period after irrigation was stopped (Fig. 4.6). The discharge decreased rapidly due to decreasing hydraulic heads. These progressively decreasing hydraulic heads result in a decreasing water contribution to the outlet of the small and medium fissures, which are mainly characterised by pressurised flow, with respect to the large fractures, characterised by gravitational percolation (Fig. 4.7e). Moreover, the still slightly increasing chloride concentration at the outlet further confirms the higher degree of drainage of the large fractures, which mainly include irrigation water rich in chloride, with respect to drainage of the medium and small fissures containing a mixture of infiltration water and storage water, which includes less chloride.

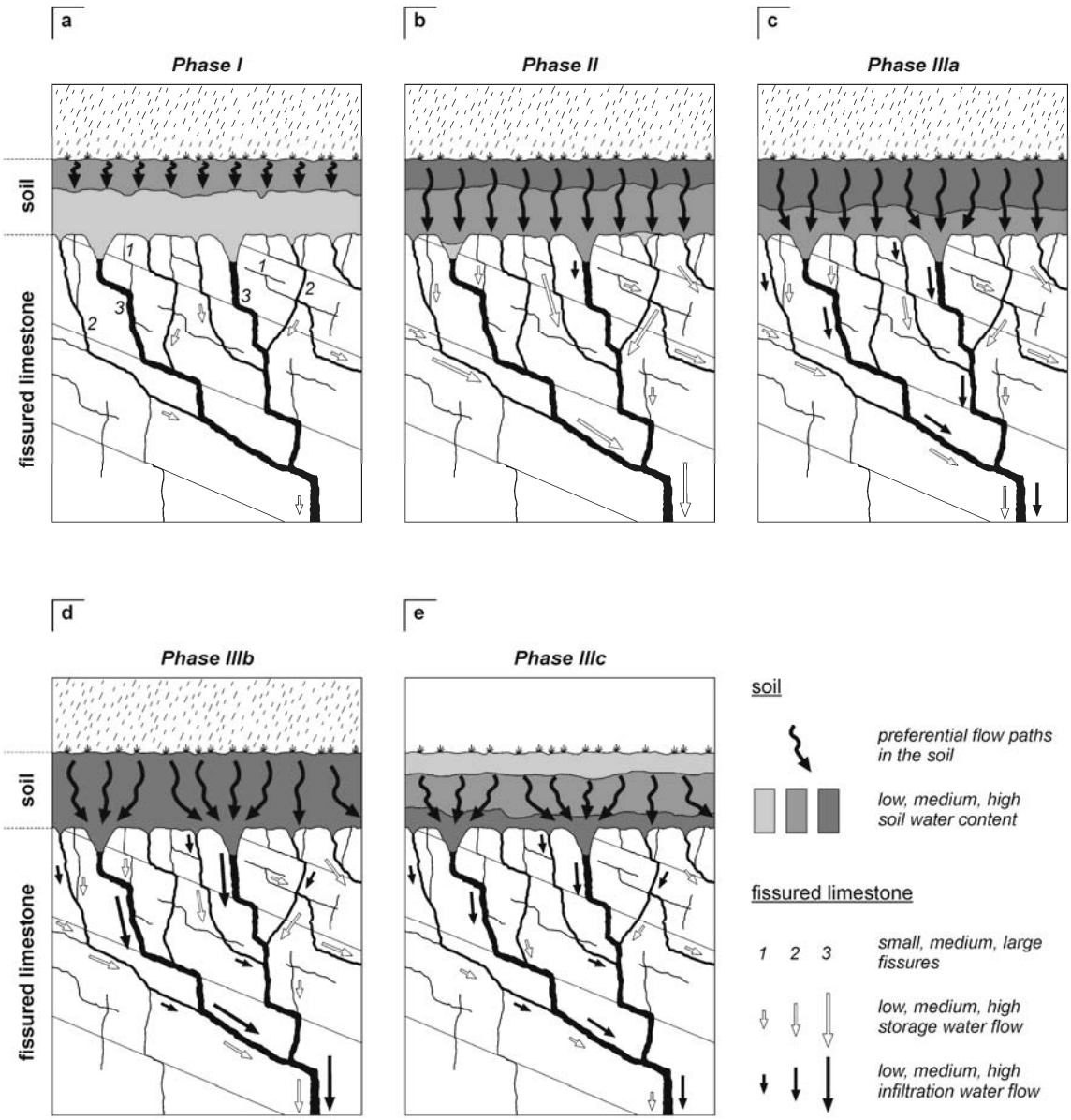

Fig. 4.7 Conceptual model of flow routes and percolation conditions during the long-term irrigation experiment (or during very long and abundant rainfall events). Phases (**a**) *I*, (**b**) *II*, (**c**) *IIIa*, (**d**) *IIIb* and (**e**) *IIIc* are described in the text.

The discharge at the outlet (Q_O) during steady-state flow conditions (phase *IIIb*) represented about 73 % of the irrigation rate (Q_I). Obviously, the missing 27 % of water used another, unmonitored percolation pathway, presumably laterally bypassing the cave. During another long-term irrigation experiment at this site, with a smaller irrigation area, the outlet discharge corresponded approximately to the infiltration rate, suggesting a more focused percolation with nearly no lateral losses.

During the entire experiment, 36 % of the irrigated water volume (V_I) reached the cave via direct transfer (V_D, obtained by integration of Q_D). This value is very close to the recovery of bromide, which was injected as a conservative artificial tracer during the experiment: 39 % (Fig. 4.6). The total volume of infiltration water that reached the outlet via direct transfer (V_D) was approximately 2.0 m^3, and the volume of storage water (V_S) was also approximately 2.0 m^3. Redistributed on 28 m^2 (surface of the irrigation area), this corresponds to 70 mm of water storage. Extrapolation of the linear chloride and discharge trends makes it possible to estimate the total volume of storage water: 3.1 m^3 or 110 mm. Based on degradation rate calculations of reactive compounds, Savoy (2007) obtained similar estimates of storage water volume at the Vers-chez-le-Brandt test site.

4.6 COMPARATIVE TRACER TESTS DURING STEADY-STATE FLOW REGIME

During the long-term irrigation experiment described above, when steady-state flow conditions were reached in the system (Fig. 4.6, phase *IIIb*), a mixture of uranine and clayey loam suspension was released at the land surface 7.1 h after the experiment began, and its breakthrough was monitored at the outlet (Fig. 4.8). Uranine was first detected at the outlet 1.1 h after tracer release and reached a maximum of 123 µg/L after 2.1 h. The uranine breakthrough curve showed a long tail, and the tracer was still detectable at the end of the monitoring period. Monitored uranine recovery reached 22 %. However, extrapolation of the breakthrough curve suggests that the total uranine recovery should approach the bromide recovery, about 39 %.

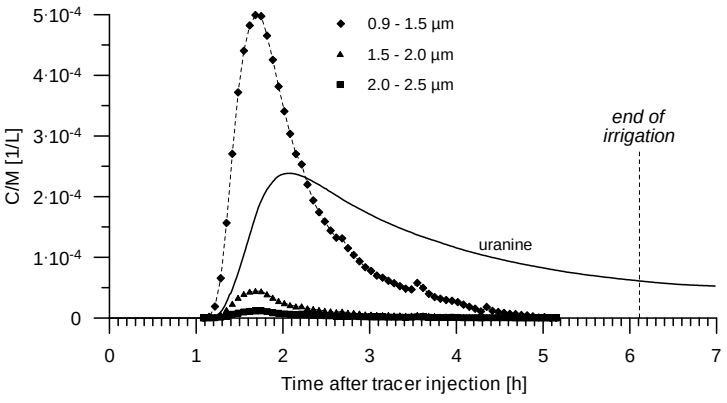

Fig. 4.8 Results of the comparative tracer test carried out during steady-state flow regime of the September 2005 long-term irrigation experiment at the Vers-chez-le-Brandt test site. C/M (ordinate) expresses concentrations normalised to mass input (uranine) and particle number input (clayey loam suspension).

All particle-size classes between 0.9 and 8.0 µm showed a positive response to the release of the suspension. However, particles larger than 3.5 µm showed irregular breakthrough curves at very low levels, which may be due to the low injection quantities (the suspension mostly consisted of small particles, Fig. 4.2). Therefore, the analysis will focus on smaller particles (0.9 to 3.5 µm) that were grouped into five size classes: 0.9 – 1.5, 1.5 – 2.0,

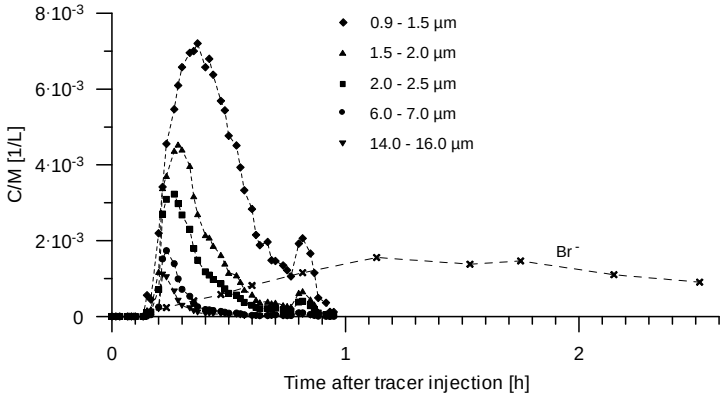

Fig. 4.9 Results of the comparative tracer test carried out during steady-state flow regime of the November 2006 long-term irrigation experiment at the Gänsbrunnen test site. C/M (ordinate) expresses concentrations normalised to mass input (bromide) and particle number input (clayey loam suspension).

2.0 – 2.5, 2.5 – 3.0 and 3.0 – 3.5 µm. The first detection of these particles occurred 1.1 h after tracer release, simultaneously with first uranine detection. Maximum concentrations of all particle-size classes occurred simultaneously after 1.7 h, preceding the uranine peak by 26 min. The different size classes displayed short tails, diminishing with increasing particle size. The recovery rates of the injected particles decreased substantially with increasing particle size: 16.5 %, 1.3 %, 0.4 %, 0.2 % and 0.1 % recovery for the five different particle-size classes mentioned earlier, respectively.

The earlier peak time of the 0.9 – 1.5 µm particles with respect to uranine is attributed to different transport processes, i.e. particles are affected by exclusion processes. Zhang *et al*. (2001) pointed out that an earlier peak time of particles with respect to solutes may also be an artefact due to a time-dependent particle-loss function (i.e. removal mechanisms) by attachment and deposition. However, in the present case, the higher normalised concentrations of the finest particles with respect to uranine clearly demonstrate that particles are effectively transported at higher velocities than solutes. In porous media, particle mobility is constrained to the pore centres (size exclusion) and to accessible pore networks (pore exclusion) where flow velocities are highest, while solutes sample the entire pore volume. This results in an earlier breakthrough of particles (e.g. Ryan and Elimelech 1996; Sirivithayapakorn and Keller 2003). Similar transport processes also seem to occur in the soil and unsaturated zone of karst aquifers, i.e. preferred particle transport in the centres of the larger pores and fractures. Furthermore, the higher recovery for uranine with respect to particles and more specifically the decreasing particle recovery with increasing particle size suggest an increasing effectiveness of particle removal mechanisms, such as mechanical filtration and straining (Bradford *et al*. 2006; McDowellboyer *et al*. 1986).

Similar results were also obtained during the comparative tracer test carried out at the Gänsbrunnen test site (Fig. 4.9), that is: a simultaneous first detection for both tracers about 10 min after tracer release; earlier peak times and higher normalised concentrations for the particulate tracer with respect to the solute tracer; and a higher recovery rate for the solute tracer (~ 40 %) than for the particulate tracer (0.9 – 1.5 µm: 24.3 %, 1.5 – 2.0 µm: 10.1 %, 2.0 – 2.5 µm: 6.3 %, 6.0 – 7.0 µm: 1.9 % and 14.0 – 16.0 µm: 0.8 %).

However, despite these similarities among results of both tracer experiments, peak concentration times of the size classes differed during both tests. While the breakthrough curves of the different size classes peaked simultaneously during the tracer test at the Vers-chez-le-Brandt test site, the tracing experiment carried out at the Gänsbrunnen test site resulted in earlier

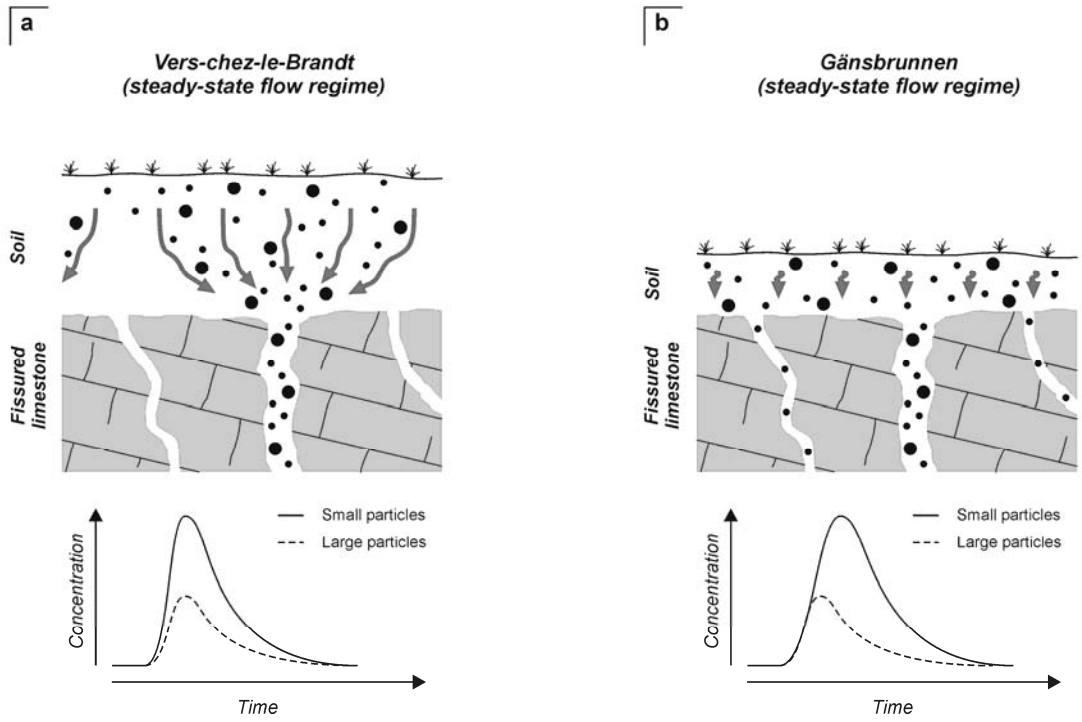

Fig. 4.10 Conceptual model of particle transport and observed breakthrough curves during the tracer tests carried out during steady-state flow conditions at (**a**) the Vers-chez-le-Brandt and (**b**) the Gänsbrunnen test sites.

breakthroughs of the larger particles with respect to fine particles. Indeed, maximum particle concentration of the 14.0 – 16.0, 6.0 – 7.0, 2.0 – 2.5 and 1.5 – 2.0 µm size classes preceded by 10, 8, 6 and 4 min, respectively, peak concentration of the 0.9 – 1.5 µm size class. These observations suggest that, during steady-state flow conditions, the presence (Vers-chez-le-Brandt test site) or the nearly absence (Gänsbrunnen test site) of a soil cover has a significant influence on preferential particle transport, which in turn will influence exclusion mechanisms (Fig. 4.10).

The 1-m-thick soil cover, present at the Vers-chez-le-Brandt test site, probably leads to preferential flow routes with important sub-lateral components towards the larger fractures, which act as drains (Fig. 4.10a). Those particles reaching the soil-epikarst boundary are thus principally transported towards and then through these main drains, resulting in similar breakthrough curves for the small and large particles at the outlet. Such preferential flow and particle transport towards fractures / fissures has also been observed at laboratory scale in fractured sand columns (Toran and Palumbo 1992). In contrast, the nearly absence of a soil cover at the Gänsbrunnen test site does not allow important lateral flow. Particles reaching the soil-epikarst boundary are therefore distributed more or less homogeneously over this boundary, and thus also over a wide range of fractures / fissures varying in aperture widths and flow velocities (Fig. 4.10b). Given that the small particles may be transported through all types of fractures / fissures, whereas the large particles are mainly constrained to the large fractures, the response at the outlet results in an earlier breakthrough of the large particles with respect to small particles.

Data presented above showed that particulate tracers from colloidal sizes up to a few micrometers travel rapidly through the vadose zone of karst aquifers. Furthermore, results

demonstrate that these particulate tracers may also be delivered at faster rates and higher normalised concentrations than solute tracers to the active conduit network of karst aquifers.

4.7 DYNAMICS OF NATURAL PARTICLES AND FAECAL BACTERIA DURING TRANSIENT FLOW REGIME

The response of the water outlet in the Vers-chez-le-Brandt cave to the short-term irrigation experiment (Fig. 4.11), which was designed to simulate a natural rainfall event, has provided further insights into the transport of sediment particles, faecal bacteria and TOC during transient flow conditions. The hydrograph and the temporal changes in turbidity, TOC and faecal indicator bacteria (*E. coli* and enterococci) could also be divided into the three phases described previously: a lag period with stable pre-experimental flow conditions and low levels of turbidity, TOC and bacteria (lag phase, *I*); a discharge increase, strictly composed of epikarst storage water, coming

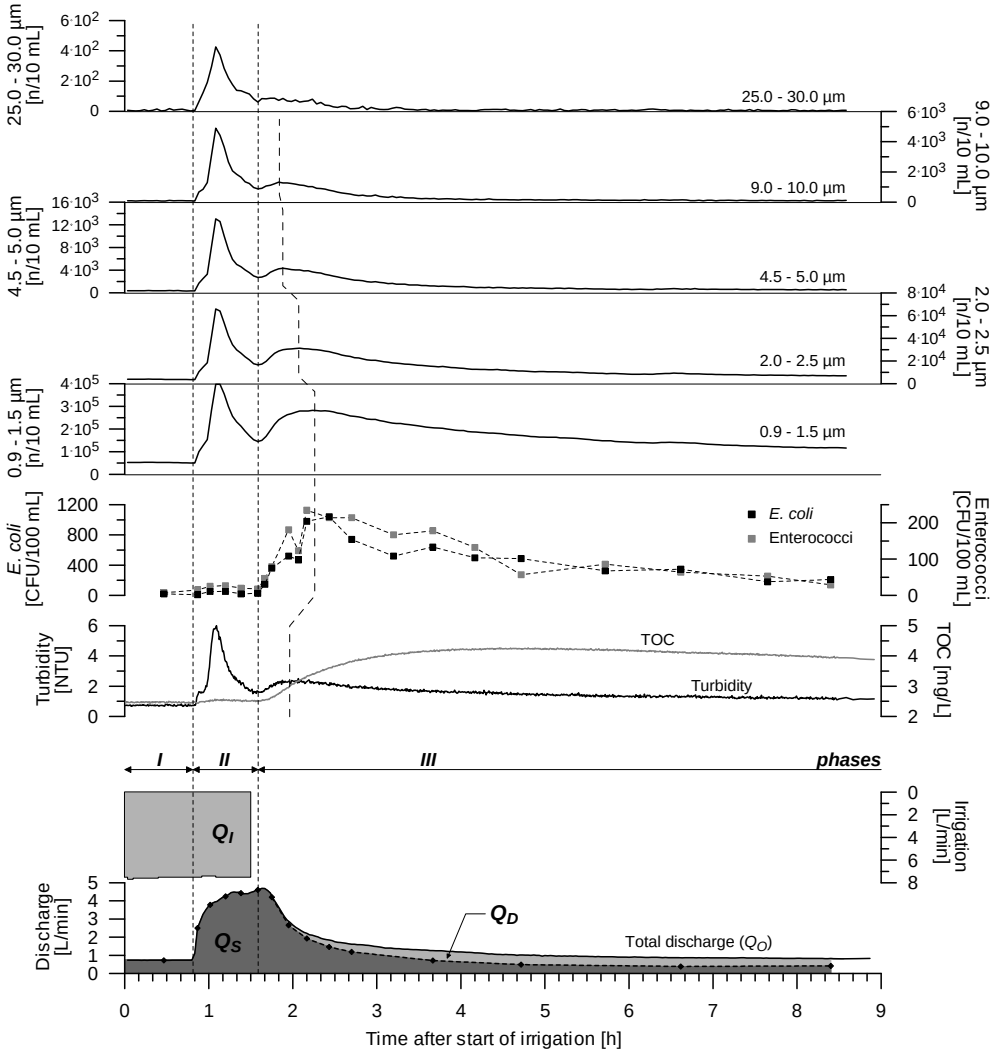

Fig. 4.11 Temporal changes in *E. coli* and enterococci contents and PSD at the water outlet in the Vers-chez-le-Brandt cave during the October 2007 short-term irrigation experiment. Pulse-through turbidity is characterised by increases of all particle-size classes (phase *II*), while flow-through turbidity mainly shows increases of small particles (phase *III*).

along with a pulse-through turbidity peak but still stable low levels of TOC and bacteria (piston-flow phase, *II*); and a mixed-flow period (epikarst storage water, soil water and infiltration water) showing increases of turbidity (flow through), TOC, *E. coli* and enterococci (mixed-flow phase, *III*). As no steady-state flow regime was attained during this experiment, phase *III* could not be further subdivided.

PSD measurements allowed more detailed analyses of the turbidity signals. The pulse-through turbidity signal was characterised by a simultaneous evolution of all particle-size classes between 0.9 and 139 µm. In contrast, the flow-through turbidity episode was mainly composed of fine particles. This signal was blurred with larger size classes and no longer discernible at particle sizes larger than 12.0 µm.

The peak times of the flow-through particles (phase *III*) preceded the TOC maximum, which is consistent with the findings of the artificial tracer experiments with particles and uranine described earlier. However, in this case, the peak times of the different particle-size classes increased systematically with decreasing particle size. Indeed, the maximum concentration of the 9.0 –10.0 µm particles occurred 25 min earlier than for the 0.9 – 1.5 µm particles, i.e. large particles seem thus to travel at higher peak velocities (phase *III*). This finding suggests that the flow conditions in the unsaturated zone – steady-state or transient state – also influence particle transport and exclusion mechanisms. As the steady-state flow regime was not attained during this experiment, water percolated more or less vertically through the soil cover. Therefore, it is hypothesised that the soil remobilised particles were distributed more or less homogeneously over the soil-epikarst boundary and thus also over a wide range of fractures / fissures varying in aperture widths and flow velocities.

E. coli and enterococci, which have sizes of about 1 µm, were highly correlated to 0.9 – 1.5 µm particles during the flow-through turbidity period (R^2 = 0.85 and 0.87 for *E. coli* and enterococci, respectively). Similar observations were also made from the monitoring of natural parameters during the long-term irrigation experiments (Fig. D.1 and D.2, Appendix D). These results suggest similar origin, transport and deposition processes for faecal bacteria and fine natural particles / colloids in the unsaturated zone. The same correlation was also observed at karst springs (Pronk *et al*. 2007). A relative increase of fine particles can thus be used as an "early-warning" parameter for faecal contamination.

4.8 CONCLUSION

The protection and management of water resources in karst aquifers require the understanding of water and contaminant transfer from the land surface through the entire hydrogeological system towards springs or other drinking water abstraction points. The present study investigated the storage and percolation of water and transport processes in the unsaturated zone, with a particular focus on particles and faecal bacteria, which represent the most important contaminants in many karst water supplies.

Results confirmed that, during rainfall events and irrigation experiments, most of the water initially discharging at the base of the unsaturated zone originates from the epikarst and is remobilised by a pressure pulse; this finding is in agreement with previous studies (Lee and Krothe 2001; Perrin *et al*. 2003). The substantial quantity of water stored in the soil and epikarst

(110 mm in this case) can either contribute to groundwater recharge (downward movement during precipitation periods) or be used by plants (upward movement during dry spring and summer periods). With increasing rainfall or irrigation intensity and duration, an increasing amount of freshly infiltrated water contributes to deep percolation; this water can transport considerable amounts of sediments and associated contaminants from the land surface and soil zone towards the active conduit network.

Particles discharging at the base of the unsaturated zone have two distinct origins. Pulse-through turbidity, which is a result of the suspension and scouring of particles from the fractures close to the observation point, is highly dependent on the hydrodynamics in the epikarst and transmission zone. Its PSD is characterised by significant increases of all particle-size classes, ranging from colloidal sizes up to 0.1 mm or more. Conversely, flow-through turbidity, which corresponds to the arrival of soil particles mobilised especially during the first flush of storm rainfall events, is dependent on the flow-through time. Its PSD is characterised by increases of the finer size classes, up to a few micrometer. This flow-through turbidity is often associated with high levels of faecal bacteria and TOC, which also originate from the land surface and underlying soil horizons.

Comparative tracer tests with clayey loam suspension and non-reactive solutes revealed that mineral particles tend to travel at faster rates and have shorter overall travel times than solutes. Similarly, faecal bacteria often reach their maximum concentration before TOC. These findings indicate that exclusion processes and removal mechanisms, which are known from saturated porous media, also occur in the soil and unsaturated zone of karst aquifers.

Faecal bacteria, which have sizes of about 1 µm, are very well correlated with fine particles (0.9 – 1.5 µm) during flow-through turbidity periods ($R^2 > 0.8$). A similar correlation was also observed in saturated conduit networks, at karst springs affected by microbial contamination from swallow holes (Pronk *et al*. 2007). Results presented in this study thus confirm the use of continuous PSD monitoring as a reliable and sensitive “early-warning” parameter for microbial contamination of karst water, particularly if this contamination results from agricultural or other activities at the land surface and is flushed into the aquifer during storm rainfall events. The applicability of this approach to other type of microbial contamination, such as permanent wastewater releases via leaking sewers or septic tanks, still needs to be tested.

REFERENCES

American Public Health Association, American Water Works Association and Water Environment Federation (APHA, AWWA and WEF). 2005. Standard methods for the examination of water and wastewater, 21st Edition. Water Environment Federation, Alexandria, VA.

Atteia O. and Kozel R. 1997. Particle size distributions in waters from a karstic aquifer: from particles to colloids. Journal of Hydrology 201 (1-4): 102-119.

Atteia O., Perret D., Adatte T., Kozel R. and Rossi P. 1998. Characterization of natural colloids from a river and spring in a karstic basin. Environmental Geology 34 (4): 257-269.

Auckenthaler A., Raso G. and Huggenberger P. 2002. Particle transport in a karst aquifer: natural and artificial tracer experiments with bacteria, bacteriophages and microspheres. Water Science and Technology 46 (3): 131-138.

Bradford S.A., Simunek J., Bettahar M., van Genuchten M.T. and Yates S.R. 2006. Significance of straining in colloid deposition: Evidence and implications. Water Resources Research 42 (12), article n°: W12S15.

Göppert N. and Goldscheider N. 2008. Solute and colloid transport in karst conduits under low- and high-flow conditions. Ground Water 46 (1): 61-68.

Herman E.K., Tancredi J.H., Toran L. and White W.B. 2007. Mineralogy of suspended sediment in three karst springs. Hydrogeology Journal 15 (2): 255-266.

Klimchouk A. 2004. Towards defining, delimiting and classifying epikarst: Its origin, processes and variants of geomorphic evolution. Speleogenesis and Evolution of Karst Aquifers 2 (1): 1-13.

Kogovšek J. 1997. Water tracing tests in vadose zone. In: Tracer Hydrology 97, Kranjc A. (ed.), Balkema, Rotterdam.

Lee E.S. and Krothe N.C. 2001. A four-component mixing model for water in a karst terrain in south-central Indiana, USA. Using solute concentration and stable isotopes as tracers. Chemical Geology 179 (1-4): 129-143.

Loop C.M. and White W.B. 2001. A conceptual model for DNAPL transport in karst ground water basins. Ground Water 39 (1): 119-127.

Mahler B.J. and Lynch F.L. 1999. Muddy waters: temporal variation in sediment discharging from a karst spring. Journal of Hydrology 214 (1-4): 165-178.

Mahler B.J., Personné J.C., Lods G.F. and Drogue C. 2000. Transport of free and particulate-associated bacteria in karst. Journal of Hydrology 238 (3-4): 179-193.

Massei N., Wang H.Q., Dupont J.P., Rodet J. and Laignel B. 2003. Assessment of direct transfer and resuspension of particles during turbid floods at a karstic spring. Journal of Hydrology 275 (1-2): 109-121.

McCarthy J.F. and McKay L.D. 2004. Colloid transport in the subsurface: past, present and future challenges. Vadose Zone Journal 3 (2): 326-337.

McDowellboyer L.M., Hunt J.R. and Sitar N. 1986. Particle-transport through porous media. Water Resources Research 22 (13): 1901-1921.

Perrin J., Jeannin P.Y. and Zwahlen F. 2003. Epikarst storage in a karst aquifer: a conceptual model based on isotopic data, Milandre test site, Switzerland. Journal of Hydrology 279 (1-4): 106-124.

Pronk M., Goldscheider N. and Zopfi J. 2006. Dynamics and interaction of organic carbon, turbidity and bacteria in a karst aquifer system. Hydrogeology Journal 14 (4): 473-484.

Pronk M., Goldscheider N. and Zopfi J. 2007. Particle-size distribution as indicator for fecal bacteria contamination of drinking water from karst springs. Environmental Science and Technology 41 (24): 8400-8405.

Ryan J.N. and Elimelech M. 1996. Colloid mobilization and transport in groundwater. Colloids and Surfaces A-Physicochemical and Engineering Aspects 107: 1-56.

Ryan M. and Meiman J. 1996. An examination of short-term variations in water quality at a karst spring in Kentucky. Ground Water 34 (1): 23-30.

Savoy L. 2007. Use of natural and artificial reactive tracers to investigate the transfer of solutes in karst systems. PhD thesis, Centre of Hydrogeology, University of Neuchâtel, Switzerland.

Schnegg P.A. and Costa R. 2003. Tracer tests made easier with field fluorometers. Technical note. Bulletin d'Hydrogéologie 20: 89-91.

Sirivithayapakorn S. and Keller A.A. 2003. Transport of colloids in saturated porous media: A pore-scale observation of the size exclusion effect and colloid acceleration. Water Resources Research 39 (4), article n°: 1109.

Toran L. and Palumbo A.V. 1992. Colloid transport through fractured and unfractured laboratory sand columns. Journal of Contaminant Hydrology 9 (3): 289-303.

Vesper D.J. and White W.B. 2003. Metal transport to karst springs during storm flow: an example from Fort Campbell, Kentucky / Tennessee, USA. Journal of Hydrology 276 (1-4): 20-36.

Vesper D.J. and White W.B. 2004. Spring and conduit sediments as storage reservoirs for heavy metals in karst aquifers. Environmental Geology 45 (4): 481-493.

White W.B. 2002. Karst hydrology: recent developments and open questions. Engineering Geology 65 (2-3): 85-105.

Williams P.W. 2008. The role of the epikarst in karst and cave hydrogeology: a review. International Journal of Speleology 37 (1): 1-10.

Zhang P., Johnson W.P., Piana M.J., Fuller C.C. and Naftz D.L. 2001. Potential artifacts in interpretation of differential breakthrough of colloids and dissolved tracers in the context of transport in a zero-valent iron permeable reactive barrier. Ground Water 39 (6): 831-840.

Zvikelsky O. and Weisbrod N. 2006. Impact of particle size on colloid transport in discrete fractures. Water Resources Research 42 (12), article n°: W12S08.

5

Microbial communities in karst groundwater and their potential use for biomonitoring*

ABSTRACT

The structure, diversity and dynamics of microbial communities from a swallow hole draining agricultural land and two connected karst springs (Yverdon-les-Bains karst aquifer system, Switzerland) were investigated using molecular microbiological methods and related to hydrological and physico-chemical parameters. Storm responses and an annual hydrological cycle were monitored to determine the short- and long-term variability, respectively, of bacterial communities. Statistical analysis of bacterial genetic fingerprints (16S rDNA PCR-DGGE profiles) of spring water samples revealed several clusters that corresponded well with different levels of the allochthonous swallow hole contribution. Microbial communities in spring water samples highly affected by the swallow hole showed low similarities among them, reflecting the high temporal variability of the bacterial communities in the water entering the swallow hole. Conversely, high similarities among samples with low allochthonous contribution provided evidence for a stable autochthonous endokarst microbial community. Furthermore, three spring water samples, representative for low, intermediate and high swallow hole contribution, were analysed by cloning / sequencing in order to identify the major bacterial groups in the communities. The autochthonous endokarst microbial community was mainly characterised by *δ-Proteobacteria*, *Acidobacteria* and *Nitrospira* species. However, the high percentage of unknown sequences (i.e. sequences revealing similarities lower than 97 % to already known sequences) suggests that many karst aquifer bacteria are still undiscovered and illustrates further the distinctiveness of karst aquifer ecosystems. Finally, the potential use of groundwater biomonitoring using microbial communities is discussed.

5.1 INTRODUCTION

Biomonitoring is widely used to evaluate the quality of surface waters and appears to be an interesting approach for groundwater. This reasoning is also reflected in the Swiss Water Protection Ordinance (GSchV 1998), which demands, in order to improve water quality standards,

* This chapter is based on the paper:

Pronk M., Goldscheider N. and Zopfi J. 2009. Microbial communities in karst groundwater and their potential use for biomonitoring. Hydrogeology Journal 17 (1): 37-48.

that the biocenoses in groundwater should be in a natural state, adapted to the habitat and characteristic of water that is not or only slightly contaminated.

Unlike chemical analyses, biomonitoring may give indications about unknown contaminants and substances which are usually not analysed routinely. Furthermore, biomonitoring may also deliver temporally integrated information. Two main approaches to groundwater biomonitoring exist: active biomonitoring, where standardised organisms such as trout or the crustacean Daphnia are introduced into the water and their responses are observed (e.g. Green *et al*. 2003); and passive biomonitoring, which uses naturally occurring organisms such as invertebrate fauna (e.g. Hahn and Friedrich 1999; Malard *et al*. 1996; Vervier and Gibert 1991).

In the last years, aquifers are increasingly considered as ecosystems harbouring their proper biocenoses (Danielopol *et al*. 2003; Griebler and Mösslacher 2003; Hancock *et al*. 2005), and the potential use of microbial communities for biomonitoring has been raised (Goldscheider *et al*. 2006; Mösslacher *et al*. 2001; Steube *et al*. 2009). This approach seems promising as bacteria are abundant and ubiquitous, thriving even in extreme habitats such as contaminated, anoxic or thermal aquifers (for a review, see Griebler and Lueders 2009).

To date, most studies on karst microbiology have focused on caves within the unsaturated zone (e.g. Barton and Northup 2007; Chelius and Moore 2004), percolation water with extreme chemical compositions (e.g. Hose *et al*. 2000; Macalady *et al*. 2006, 2007) and on the role of specific bacteria in geochemical processes (e.g. Canaveras *et al*. 1999; Northup and Lavoie 2001). Few studies, however, have investigated the structure, diversity and activity of microbial communities in pristine karst aquifers.

Karst systems are characterised by different bacterial habitats (Goldscheider *et al*. 2006) including the soil-vegetation compartment from where bacteria may reach the aquifer by diffuse percolation or via swallow holes (i.e. allochthonous origin), the unsaturated zone (fissures, fractures, cavities) and the saturated zone where bacteria live in groundwater, attached to rock surfaces or sediment particles (i.e. autochthonous origin). However, karst systems are rarely accessible; their investigation is therefore often limited to spring water samples. Several studies have reported that groundwater samples from porous aquifers do not always accurately reflect aquifer microbiology due to a high ratio of attached versus suspended cells (Alfreider *et al*. 1997; Lehman 2007). However, the high variability of flow velocities in karst systems induces pronounced hydrological shear stress and leads to scouring and resuspension of intrakarstic particulate material and associated bacteria. Storm events appear not only to be key periods in scouring these aquifer biofilms but also in transporting allochthonous soil bacteria into karst aquifers (Simon *et al*. 2001). Particle-size distribution (PSD) measurements at karst springs have allowed distinguishing between autochthonous and allochthonous particles, i.e. a relative predominance of finer particles, for example, suggests an allochthonous origin and is often associated with faecal indicator bacteria contamination (Pronk *et al*. 2007).

Personné *et al*. (2004) have studied bacterial colonisation of introduced substrates in a karst aquifer and concluded that enteric bacteria from periodical contamination with wastewater were unlikely to persist in the system. Rusterholtz and Mallory (1994) have further described the bacterial community from Mammoth cave (Kentucky, USA) sediments as highly diverse with no dominant species. Based on bacterial fingerprinting and sequencing of alpine karst spring water,

Farnleitner *et al*. (2005) have provided first evidence for the presence of stable and autochthonous endokarst microbial communities. Most of the retrieved bacterial sequences were affiliated with *Proteobacteria* and the *Cytophaga – Flexibacter – Bacteroides* group. However, more than 95 % of the 28 sequences revealed similarities lower than 97 % to already known bacteria and were thus considered as new species.

The main objectives of this study were: (*i*) to explore structure, diversity and temporal variability of microbial communities in karst groundwater; (*ii*) to differentiate between allochthonous bacteria from the land surface and autochthonous, endokarstic bacteria; and (*iii*) to characterise the autochthonous microbial community by identifying the most abundant bacterial components. In order to achieve these goals, the Yverdon-les-Bains karst aquifer system was investigated on short- (storm events) and long-term scales (annual hydrological cycle). Physico-chemical monitoring at the Feurtille swallow hole and the Moulinet and Cossaux karst springs was combined with PSD measurements and the genetic characterisation of bacterial communities by PCR-DGGE (polymerase chain reaction - denaturing gradient gel electrophoresis) and cloning / sequencing.

5.2 16S rDNA ANALYSES: WHAT CAN THESE MOLECULAR TECHNIQUES TELL US?

Most bacteria do not grow on traditional culture media. Therefore, culture-independent, molecular biological techniques are employed to bridge the disparity between cultivable and *in-situ* diversity. PCR-DGGE and cloning / sequencing of the 16S rDNA (a universal marker gene allowing the identification of bacteria and inferring their phylogenetic relationship) are two of these techniques and are widely used in microbial ecology but increasingly also in hydrogeology, contaminant hydrology and related disciplines. The different techniques including their potentials and limitations have been recently reviewed (Goldscheider *et al*. 2006; Nocker *et al*. 2007; Weiss and Cozzarelli 2008).

5.2.1 PCR-DGGE

PCR-DGGE is a rapid fingerprinting technique that provides a simplified image of the bacterial community structure in a sample (e.g. Muyzer *et al*. 1993; Muyzer 1999; Nocker *et al*. 2007). Small PCR-amplified DNA products of about the same length are separated on a vertical acrylamide gel in a gradient of a denaturing agent. The direction of electrophoresis is parallel to the gradient; thus, as PCR products travel through the gel, increasing denaturing conditions start to separate the double-stranded DNA, resulting in a slower migration in the gel compared to the native conformation. The separation, or melting, of the double-stranded DNA occurs in discrete domains rather than in a zipper-like fashion and is strongly dependant on its GC (Guanine-Cytosine) content and nucleotide sequence. PCR-DGGE analysis of environmental samples containing different bacterial communities will result in a specific band pattern for each sample. Each band in the gel represents theoretically one bacterial species, and the band intensity is about proportional to its relative abundance in the sample. This fingerprinting technique is thus well suited to detect community structure changes in groundwater in response to aquifer conditions (e.g. seasonal variations, rain events, contamination). However, it is estimated that PCR-DGGE only detects bacterial populations representing at least 1 – 2 % of the microbial community (Muyzer *et al*. 1993).

5.2.2 Cloning / sequencing

In contrast to the PCR-DGGE method, the direct cloning / sequencing approach, which is rather laborious and time-consuming, is not a fingerprinting technique but offers the highest phylogenetic resolution of all molecular methods. Identification of bacterial species or determination of similarities to already known species (or to sequences of uncultivated microorganisms) is possible through the use of sequence databases. Cloning / sequencing of environmental samples allows thus a more complete picture of the microorganisms present in a sample to be obtained and provides also qualitative and quantitative information on the diversity (Chapelle 2001; Nocker *et al*. 2007).

5.3 MATERIAL AND METHODS

5.3.1 Monitoring and sampling program

Discharge, temperature, electrical conductivity, turbidity and total organic carbon (TOC) were monitored continuously (time step: 10 min), as described in detail in Chapter 2, at the Feurtille swallow hole and the Moulinet and Cossaux springs. Daily precipitation data were provided by MeteoSwiss.

The swallow hole and the springs were sampled consecutively (within approximately 4 h) and fortnightly during a complete annual hydrological cycle from March 2005 until February 2006 and daily during the April 2005 storm event for molecular biological analyses, water quality indicator bacteria enumeration and major ion chemistry. Sampling, sample processing and analytical methods for major ion chemistry and water quality indicator bacteria (including mesophilic aerobic bacteria, total coliforms, *E. coli* and enterococci) are described in detail in Chapter 2. Furthermore, simultaneously with sample collection, PSD was determined directly on-site with a portable particle counter (see Chapter 3 for details).

5.3.2 Molecular microbiological analyses

SAMPLING, SAMPLE PROCESSING AND DNA EXTRACTION

For molecular microbiological analyses, water samples were collected in two sterile 1 L Nalgene bottles, transported to the laboratory in cooling boxes and processed within maximum 6 h. Two volumes of 0.5 L water were filtered through 0.2 µm polycarbonate membranes (Cyclopore, Whatman, Maidstone, UK). Filters were then immediately stored at -80 °C until DNA extraction. Genomic DNA was extracted from the membranes with the FastDNA SPIN Kit (Bio101, Vista, USA) and a FastPrep bead-beating machine (Bio101) according to manufacturers' instructions.

POLYMERASE CHAIN REACTION – DENATURING GRADIENT GEL ELECTROPHORESIS

For DGGE analysis, a small DNA fragment (~ 180 bp) that covers the V3 region on the eubacterial 16S rDNA gene was PCR amplified with the forward primer GC-Eub338f (5'-ACTCCTACGGGAGGCAGCAG-3'), carrying a GC-clamp at the 5' end, and the reverse primer Univ518r (5'-ATTACCGCGGCTGCTGG-3'; Ovreas *et al*. 1997). PCR mixtures were prepared

in a total volume of 50 µl containing 25 µl of H_2O, 6 µl of $MgCl_2$ (25 mM), 10 µl of PCR buffer (5x), 1.25 µl of dNTPs (dATP, dCTP, dGTP and dTTP; 10 mM), 1.25 µl of each primer (10 µM), 0.25 µl of GO-*Taq* DNA polymerase (5 U/µl; Promega, Madison, USA) and 5 µl of template DNA. PCR was performed on a Peltier Thermal Cycler (PTC-200, MJ Research, Waltham, USA) by using the following cycle profile: initial denaturation at 95 °C for 2 min; 30 cycles of denaturation at 94 °C for 1 min, primer annealing at 55 °C for 30 s and chain extension at 72 °C for 1 min; and a final extension step at 72 °C for 10 min. Reactions were run in triplicate and then combined prior to further analyses.

DGGE was performed on the Dcode System (Bio-Rad, Vienna, Austria). Quantities of 600 ng of PCR products were loaded onto 1 mm thick 8 % (wt/vol) polyacrylamide gels (ratio of acrylamide to bisacrylamide: 37.5:1) with a linear denaturing gradient from 30 to 60 %; 100 % denaturant containing 7 M urea and 40 % (vol/vol) formamide. Additionally, two markers consisting of 7 clones were included in each gel (reference lanes). The outer two lanes of each gel were not used in order to avoid the "smiling effect". Electrophoresis was done for 4.5 h at 150 V and 60 °C. After migration, gels were stained in a 1:10 000 dilution SYBR Green I (Molecular Probes, Eugene, USA) bath for 20 min.

Standardisation and analysis of the obtained DGGE banding patterns was performed with the Gelcompar II software (Applied Maths, Sint-Martens-Latem, Belgium). Comparison of DGGE profiles was done by using band-based (Jaccard similarity coefficient) and curve-based (Pearson similarity coefficient) procedures. For individual gel analysis, both procedures gave very similar results. However, Jaccard analysis was performed if several gels were analysed together, as variable staining from one gel to the other may influence the band intensities used by the curve-based procedure.

Finally, the whole PCR-DGGE procedure (including standardisation and analysis of the DGGE image) was repeated for the samples collected at the Moulinet spring during the annual hydrological cycle in order to verify the results. The general sample arrangement and the clusters of both procedures were highly similar. However, sample arrangement within the clusters and the similarity values were slightly differing.

CLONING / SEQUENCING

For clone library construction, the nearly complete eubacterial 16S rDNA gene (~1400 bp) was PCR amplified using the primers GM3f (5'-AGAGTTTGATC(AC)TGGC-3') and GM4r (5'-TACCTTGTTACGACTT-3'; Muyzer *et al*. 1995). PCR mixtures were prepared in a total volume of 50 µl containing 25.75 µl of H_2O, 6 µl of $MgCl_2$ (25 mM), 10 µl of PCR buffer (5x), 1 µl of dNTPs (10 mM), 1 µl of each primer (10 µM), 0.25 µl of GO-*Taq* DNA polymerase (5 U/µl, Promega) and 5 µl of template DNA. PCR amplification was performed using following conditions: initial denaturation at 94 °C for 4.5 min; 24 cycles of denaturation at 94 °C for 30 s, annealing at 56 °C (minus 0.5 °C per cycle during the first 10 cycles, and then at 51 °C for the next 14 cycles) for 30 s and extension at 72 °C for 1 min; and a final extension step at 72 °C for 10 min. Reactions were run in triplicate and then combined prior to further analysis.

PCR products were purified using the Wizard SV clean-up system (Promega) and ligated into pGEM-T vectors (Promega) according to manufacturers' instructions. The plasmid vectors were

transformed into electrocompetent *E. coli* cells, which were then incubated overnight at 37 °C on Luria-Bertani (LB) plates that also contained 50 mg/mL ampicillin, 125 µl of IPTG (isopropyl-β-D-thiogalactopyranoside) and 50 µl X-Gal (5-bromo-4-chloro-3-indolyl-β-D-galactopyranoside). The presence of inserts of the expected size in the *E. coli* colonies was verified by PCR using the pGEM-T specific primers T7 and SP6 (Promega). PCR mixtures were prepared in a total volume of 10 µl containing 5.45 µl of H_2O, 1.33 µl of $MgCl_2$ (25 mM), 2.25 µl of PCR buffer (5x), 0.3 µl of dNTPs (10 mM), 0.3 µl of each primer (10 µM), 0.07 µl of GO-*Taq* DNA polymerase (5 U/µl; Promega) and template DNA. PCR conditions were as follows: initial denaturation at 94 °C for 4.5 min; 34 cycles of denaturation at 94 °C for 30 s, annealing at 51 °C for 30 s and extension at 72 °C for 1.5 min; and a final extension step at 72 °C for 5 min.

Colonies having the insert were grown overnight in 3 mL LB-broth containing 50 mg/mL ampicillin (37 °C, 180 rpm agitation). Plasmids were extracted with Wizard plus SV minipreps kits (Promega) and then sequenced by MWG-Biotech (Germany). A total of 134 different partial (~ 900 bp) and full length 16S rDNA gene sequences have been deposited in the EMBL (European Molecular Biology Laboratory) Nucleotide Sequence Database under the accession numbers AM991142 to AM991275 (only one representative of 100 % identical sequences was deposited).

Sequences were analysed by tools available at the Ribosomal Database Project (Cole *et al.* 2007), accessible online at http://www.rdp.cme.msu.edu. The analyses were last done on 6 March 2009 (RDP Release 10, Update 9, 6 March 2009, 800159 16S rRNA sequences). Sequences were tested for PCR anomalies by using the chimera check program. Classification of the sequences was done by using the Naive Bayesian rRNA Classifier (Version 2.0, July 2007; Wang *et al.* 2007), and the closest affiliations to the retrieved sequences were achieved by SeqMatch (Version 3, RDP Data: release 10.2). Prior to phylogenetic tree construction, sequences were aligned using the SILVA Aligner, accessible online at http://www.silva-arb.de. Phylogenetic trees were constructed with the MEGA4 software (Tamura *et al.* 2007), available online at http://www.megasoftware.net, by using the evolutionary distances (i.e. Jukes-Cantor distances), the neighbour-joining method and bootstrap analysis (1000 replicates).

Finally, as a 99 % similarity between two sequences was proposed as a discriminator of species versus strain differences (Sakano and Kerkhof 1998), sequences with a similarity equal to or larger than 99 % were considered to represent the same phylotype for statistical analysis and sequence population diversity. Coverage (*C*) was calculated according to (Eq. 5.1; Mullins *et al.* 1995):

$$C = 1 - \left(n_1 / N\right) \tag{5.1}$$

where n_1 is the number of phylotypes that occurred only once in the clone library and N is the total number of clones analysed. Rarefaction curves (Heck *et al.* 1975) were produced by using the Analytic Rarefaction (Version 1.3) software, available online at http://www.uga.edu/~strata/software/index.html.

5.4 LONG-TERM MONITORING: ANNUAL HYDROLOGICAL CYCLE

5.4.1 Hydrogeological conditions during the investigation period

Recorded hydrological conditions of the Yverdon-les-Bains karst aquifer system during the investigation period from March 2005 to February 2006 were in general agreement to other years. The investigated annual hydrological cycle was marked by several distinct periods of varying flow conditions within the karst aquifer system (Fig. 5.1): a period of high-flow conditions (March – May 2005) resulting from a combined influence of snowmelt and storm rainfall events; a long period of recession resulting in medium-flow conditions (June – July 2005) and low-flow conditions (August – November 2005); and again a period of medium-flow conditions (December 2005 – February 2006) caused by several intense rainfall events. The particularly dry summer and autumn resulted in a prolonged period of very low discharges at the springs and the stream sinking into the swallow hole. Compared to other years, the mean annual discharges were somewhat low at 99 and 49 L/s for the Moulinet and Cossaux springs, respectively, and 32 L/s for the Feurtille swallow hole (see Table 2.2). The latter fell even dry for a period of 2 to 3 weeks end November 2005.

For the investigation on the structure, diversity and temporal variability of the microbial communities, 20 swallow hole water samples and 22 water samples of each spring were selected. These sample sets covered the hydrological variability inherent to the three observation sites (Fig. 5.1) and are thus representative for all types of flow conditions. Moreover, water quality characteristics of these samples (Table 5.1) also covered approximately the whole range of

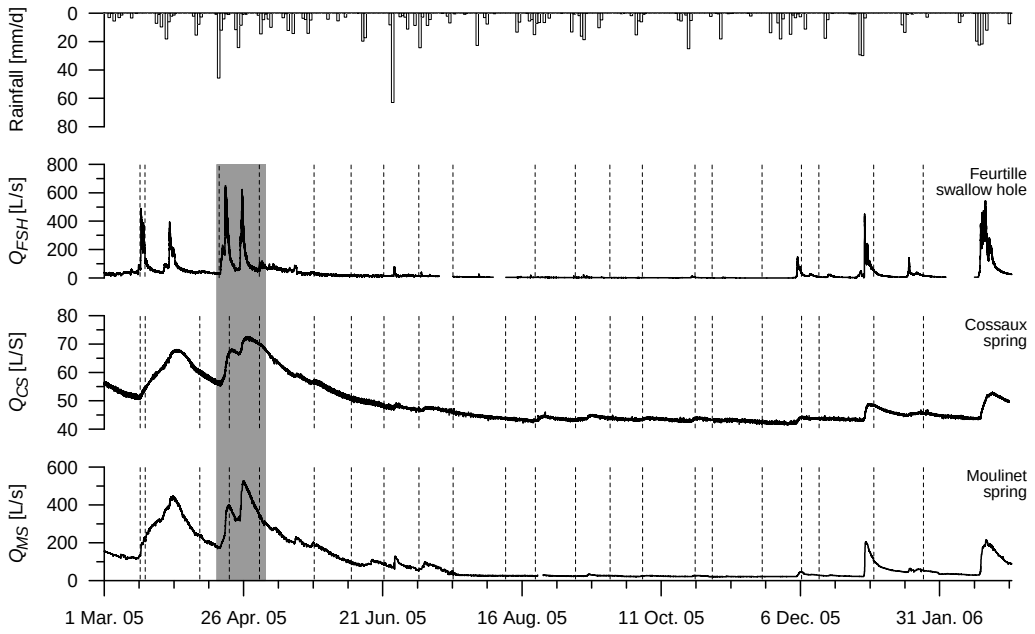

Fig. 5.1 Hydrological situation of the Feurtille swallow hole and the Moulinet and Cossaux springs during the investigation period (Mar. 2005 – Feb. 2006). Only precipitation data of the Baulmes station are shown. Sampling times are marked by dashed lines. The grey shaded area corresponds to the investigated storm event (see Section 5.5). Q_{MS}: discharge of the Moulinet spring; Q_{CS}: discharge of the Cossaux spring; Q_{FSH}: discharge of the stream sinking into the Feurtille swallow hole.

Table 5.1 General water quality characteristics of the samples collected during the annual hydrological cycle for molecular microbiological analyses.

Parameter	Unit	Feurtille swallow hole			Moulinet spring			Cossaux spring		
		n [a]	Median	Range	n [a]	Median	Range	n [a]	Median	Range
Discharge	[L/s]	20	15	0.2 - 123	22	51	21 - 403	22	46	43 - 70
Temperature	[°C]	20	8.6	3.4 - 14.6	22	11.1	9.5 - 11.6	22	13.3	12.8 - 13.4
EC [b]	[µS/cm]	20	720	596 - 962	22	443	398 - 580	22	463	443 - 506
TOC	[mg/L]	20	4.0	1.3 - 13.2	22	0.7	0.3 - 6.2	22	0.5	0.3 - 1.7
Turbidity	[NTU]	20	6.8	2.9 - 26.8	22	0.6	0.2 - 6.2	22	0.2	0.1 - 1.3
Nitrate	[mg/L]	19	25.6	14.5 - 48.6	20	7.0	4.4 - 31.0	20	7.0	5.4 - 14.5
MAB [c]	[CFU/mL]	20	608	120 - 4340	22	18	7 - 2564	22	7	1 - 1174
Tot. colif. [d]	[CFU/100 mL]	19	4310	600 - 65600	22	131	14 - 8680	22	30	3 - 2150
E. coli	[CFU/100 mL]	20	54	3 - 1990	22	3	0 - 648	22	1	0 - 183
Enterococci	[CFU/100 mL]	19	51	2 - 890	22	2	0 - 480	22	1	0 - 123

[a] Number of samples
[b] Electrical conductivity
[c] Mesophilic aerobic bacteria
[d] Total coliforms

observed physical, chemical and microbiological variations (see Tables 2.2 and 2.3). The contribution of the swallow hole to spring water quality deterioration is clearly discernable from chemical (e.g. TOC and nitrate) and microbiological parameters. Contamination was generally lower at the Cossaux spring than at the Moulinet spring. Moreover, water temperature was higher and all parameters showed less variations at the Cossaux spring. This behaviour is explained by a stable inflow at the Cossaux spring of clean, warm groundwater from greater depth, i.e. the thermal groundwater component.

5.4.2 Annual dynamics of microbial communities

Bacterial community profiles (i.e. V3 16S rDNA PCR-DGGE profiles) of Feurtille swallow hole water samples revealed the presence of a large number of bands with about 20 different intense bands (Fig. 5.2a). These results indicate that the microbial assemblages are diverse and dominated by the occurrence of a few abundant species. Although some bands were present in several samples, the general banding pattern changed drastically from one sampling date to the other. Microbial community composition in the water sinking into the swallow hole was thus highly dynamic throughout the observation period. This high degree of temporal variability was also reflected in the cluster analysis (Fig. 5.3a, cluster I), expressed by the low similarities among the swallow hole samples.

The general banding pattern of the DGGE fingerprints of Moulinet spring water samples was contrasting with the one of the Feurtille swallow hole water samples. Moulinet spring water DGGE profiles showed complex patterns with mostly faint bands (Fig. 5.2b), indicating that the microbial communities are diverse and consist of about equally abundant species. Several of these bands were present in all samples, which is consistent with an autochthonous endokarst microbial community as recently proposed by Farnleitner *et al*. (2005). Only those samples that were characterised by increased contents of TOC, nitrate and faecal indicator bacteria, i.e. samples

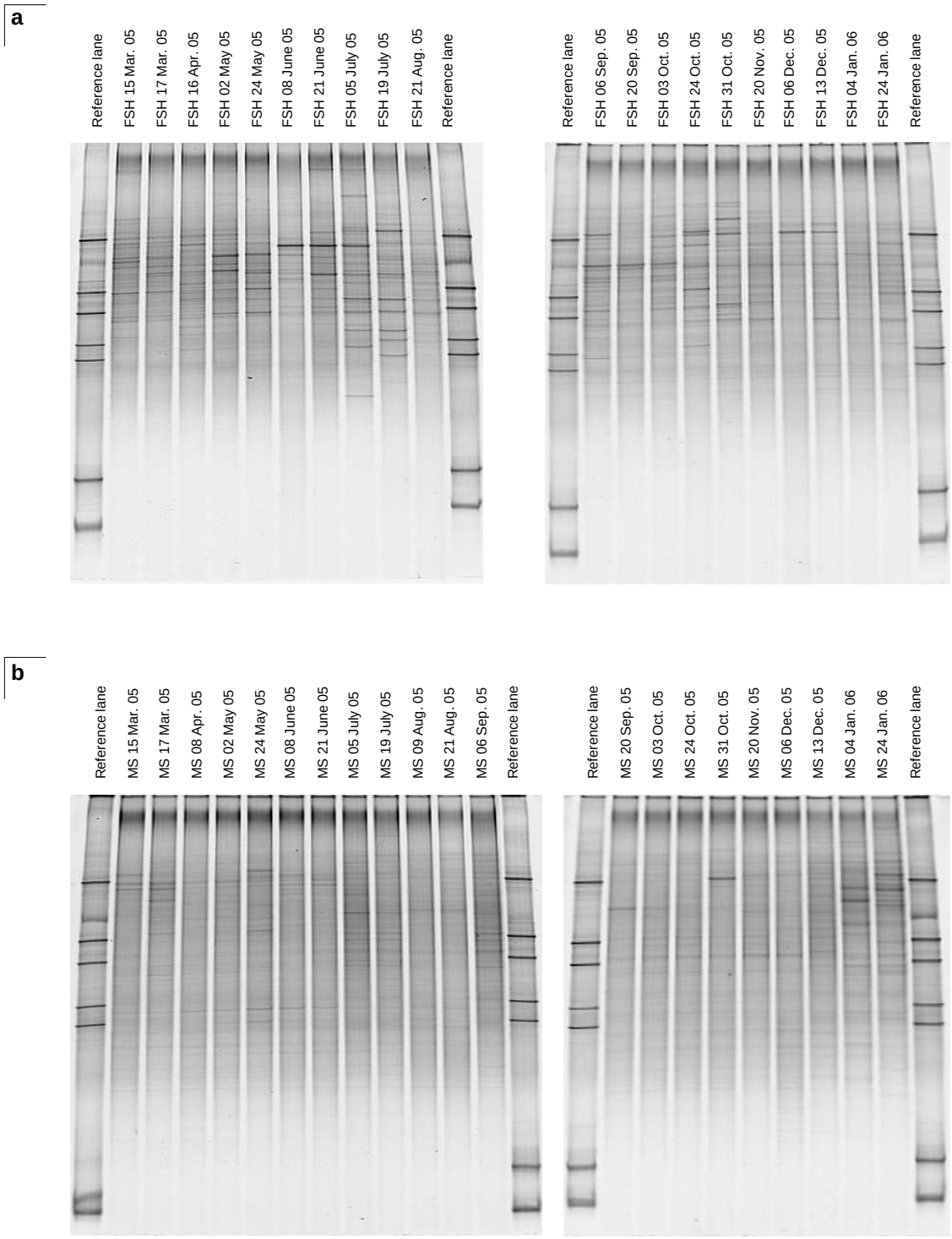

Fig. 5.2 16S rDNA PCR-DGGE profiles of microbial communities in (**a**) Feurtille swallow hole and (**b**) Moulinet spring water samples collected during the annual hydrological cycle. The DGGE profiles of bacterial communities in Cossaux spring water samples are shown in Fig. E.1 (Appendix E).

strongly affected by the allochthonous swallow hole component, displayed some few intense bands (e.g. samples "MS 04 Jan. 06" and "MS 24 Jan. 06"; Fig. 5.2b) representing dominant populations of bacteria.

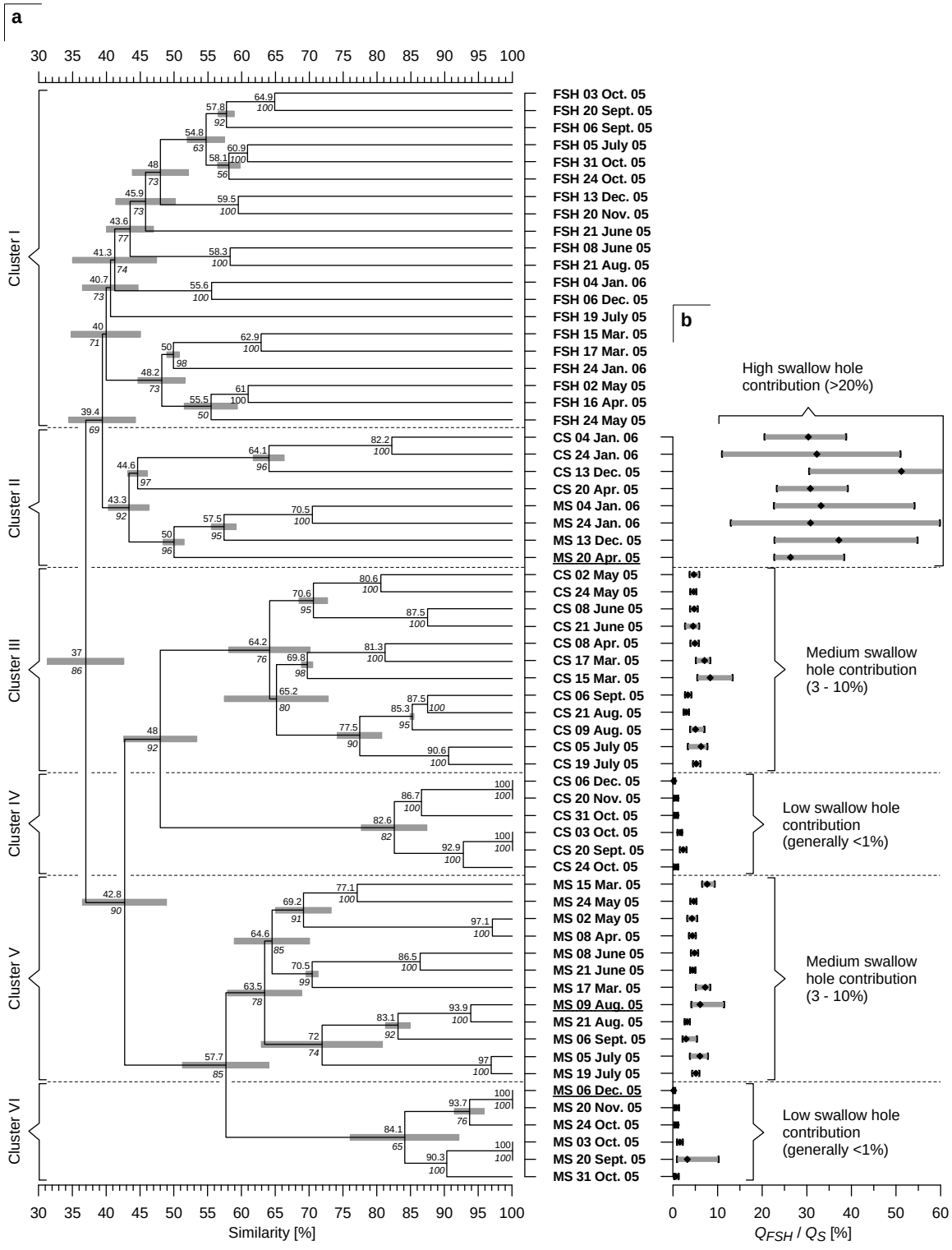

Fig. 5.3 (**a**) Hierarchical cluster analysis of bacterial community fingerprints (16S rDNA PCR-DGGE profiles) from swallow hole and spring water samples collected during the annual hydrological cycle (Jaccard correlation and unweighted pair group method with arithmetic mean). Error flags (grey bars), similarity (numbers) and cophenetic correlation coefficients (italic numbers) are shown. (**b**) Feurtille swallow hole contribution to the system discharge during the calculated infiltration time lag (Q_{FSH} / Q_S). Mean values (diamonds) with respective minimum and maximum values are shown. Sample labels (FSH: Feurtille swallow hole; MS: Moulinet spring; CS: Cossaux spring) and dates are given along the vertical axis. The underlined samples were chosen for clone library construction (see Section 5.6).

The DGGE band patterns of Cossaux spring water samples (Fig. E.1, Appendix E) were very similar to those observed for the Moulinet spring water samples. Differences between the microbial assemblages of both springs were nevertheless marked by the presence or absence of certain faint bands.

Hierarchical cluster analysis of all DGGE profiles from the three observation points revealed six separate and significant clusters (Fig. 5.3a): a cluster comprising all the Feurtille swallow hole water samples (cluster I); a mixed cluster with Moulinet and Cossaux spring water samples (cluster II); two clusters of Cossaux spring water samples (clusters III and IV); and two clusters of Moulinet spring water samples (clusters V and VI).

Cluster II was most closely related to cluster I, which comprised strictly swallow hole samples. This fits nicely with the calculated high swallow hole contribution to the total system discharge during the calculated infiltration time lag (Q_{FSH} / Q_S, calculated as described in Section 2.6) of at least 10 to 20 % (Fig. 5.3b). Moreover, all water samples of this cluster II were characterised by increased contents of TOC, nitrate and faecal indicator bacteria (Fig. E.2 and E.3, Appendix E) and showed also strictly allochthonous PSD curves. The relatively low similarities among the samples forming cluster II further mirror the high temporal variability of the bacterial communities entering the swallow hole (cluster I).

Clusters III (Cossaux samples) and V (Moulinet samples) were characterised by an intermediate swallow hole contribution (Q_{FSH} / Q_S) of about 3 – 10 %, while clusters IV (Cossaux samples) and VI (Moulinet samples) received only small amounts of water from the swallow hole (Q_{FSH} about 0 – 1 % of Q_S). Only one sample ("MS 20 Sept. 05") did not cluster in accordance with the degree of swallow hole contribution. Besides the swallow hole contribution, for the spring water clusters III through VI no clear relation to the monitored natural parameters was observed (Fig. E.2 and E.3, Appendix E).

The calculated similarities between clusters equally affected by the swallow hole (clusters III and V and clusters IV and VI) were low at just 42.8 %. It is hypothesised that the additional inflow of the deep and warm groundwater component at the Cossaux spring, which was estimated to contribute at about 66 to 75 % to the discharge of the spring (see Section 2.4.3), could explain these differences. Nevertheless, the almost identical arrangement of Cossaux spring samples (clusters II, III and IV) and Moulinet spring samples (clusters II, V and VI) in the dendrogram suggests that the deep and warm groundwater component harbours a stable autochthonous microbial community. Finally, the frequently high similarities among samples within low swallow hole affected clusters (clusters IV and VI) provide additional evidence for an autochthonous endokarst microbial community and suggest further also a temporal constancy of this community.

5.5 SHORT-TERM MONITORING: STORM EVENT

5.5.1 Hydrogeological analysis of the storm event

The physical, chemical and microbial response of two successive rainfall events was monitored in April 2005 (Fig. 5.4). The discharge of the Feurtille swallow hole increased shortly after the rainfall events and showed two distinct peaks followed by rapid recession (Fig. 5.4a). High levels of turbidity (max.: 60 NTU), TOC (max.: 12 mg/L), faecal indicator bacteria (max.:

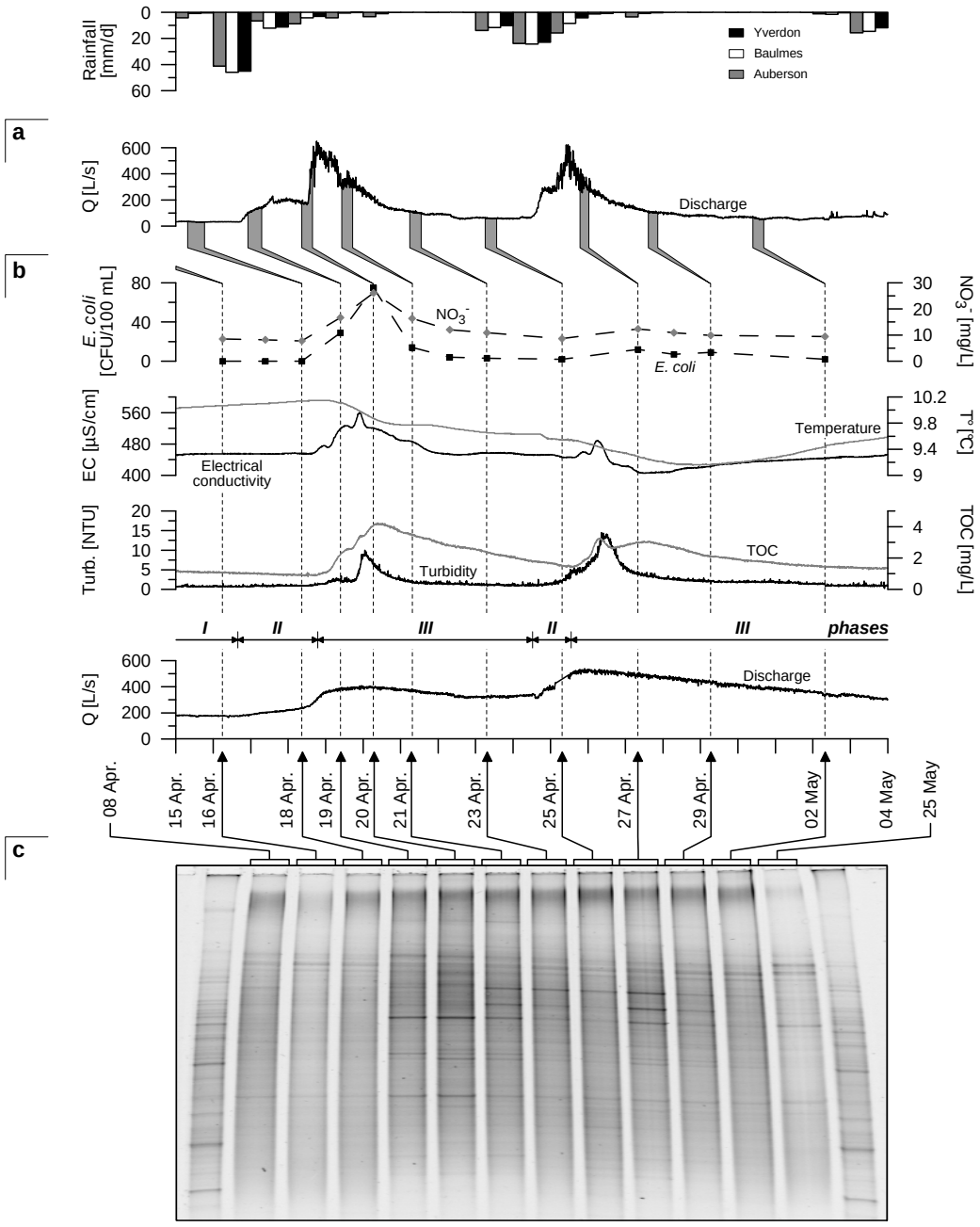

Fig. 5.4 Temporal variations of physical, chemical and microbiological parameters during the April 2005 storm event. (**a**) Feurtille swallow hole, (**b**) Moulinet spring and (**c**) 16S rDNA PCR-DGGE profiles of bacterial communities in Moulinet spring water samples (the two external profiles are reference lanes). The grey shaded areas under the swallow hole hydrograph indicate the calculated moments of infiltration at the swallow hole for each spring water sample. Phases *I*, *II* and *III* are described in the text. Q: discharge; Turb.: turbidity; EC: electrical conductivity; T°: temperature.

~ 500 CFU/100 mL of *E. coli*) and nitrate (max.: 55 mg/L) entered the swallow hole (data not shown).

The response at the Moulinet spring showed also two distinct events (Fig. 5.4b). A typical response to a storm event at the spring is divided into three phases (see Sections 2.5 and 3.3):

I. an initial phase, representing pre-storm conditions with low and stable values for all parameters and lasting until spring discharge increases (Fig. 5.4b);

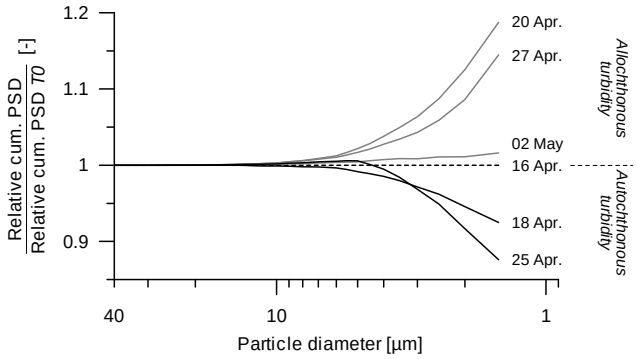

Fig. 5.5 Analysis of selected PSD curves of Moulinet spring water samples collected during the April 2005 storm event. Relative cumulative PSDs ($\sum n \leq Ø / \sum n$, expressed in %) were normalised to pre-storm conditions (sample "16 Apr.", see Chapter 3 for further details).

II. a pulse-through phase, characterised by the rising limb of the spring hydrograph and the remobilisation of autochthonous particulate material due to increasing flow velocities in the system. TOC, nitrate and faecal indicator bacteria, which are typical natural tracers of the Feurtille swallow hole component, remain stable at pre-event levels. During both phases *II* of the two successive storm events of April 2005, turbidity increased from 0.7 to 1.4 NTU and from 0.9 to 4.6 NTU, respectively (Fig. 5.4b). These turbidity episodes were of typical autochthonous origin as demonstrated by PSD measurements (Fig. 5.5, samples "18 Apr." and "25 Apr."). As phase *I* was not reached again before the second rainfall event, the PSD of the "25 Apr." sample still showed a minor allochthonous contribution;

III. a flow-through phase, characterised by the arrival and breakthrough of allochthonous turbid and contaminated water, which enters the swallow hole during the rainfall events, and by the following storm event recession. During the monitored storm events, PSD of samples collected during phase *III* exhibited a clear allochthonous signature (Fig. 5.5, samples "20 Apr." and "27 Apr."), while the PSD of the "02 May" sample, which was collected at the end of the recession, tended again towards the pre-storm PSD signature. Moreover, maximum values of all physical, chemical and microbiological parameters were reached during this phase *III* (turbidity: 14 NTU, TOC: 4.2 mg/L, *E. coli*: 75 CFU/100 mL and nitrate: 26 mg/L).

5.5.2 Dynamics of microbial communities during storm events

The DGGE fingerprints of Moulinet spring water samples collected during the storm event (Fig. 5.4c) were consistent with those collected during the annual hydrological cycle and showed rather complex patterns with mostly faint bands. Several of these bands were present in all stages of the storm event, which is again consistent with the presence of a stable autochthonous endokarst microbial community. Only samples strongly affected by the allochthonous swallow hole component (samples of phase *III*) were characterised by several particularly thick bands, which represent dominant populations of bacteria and were not present in pre-storm event samples.

Statistical analysis of the storm event PCR-DGGE profiles was consistent with the above described observations and the results of the annual hydrological cycle. Indeed, the analysis resulted in two separate clusters (Fig. 5.6a), which were again characterised by different levels of

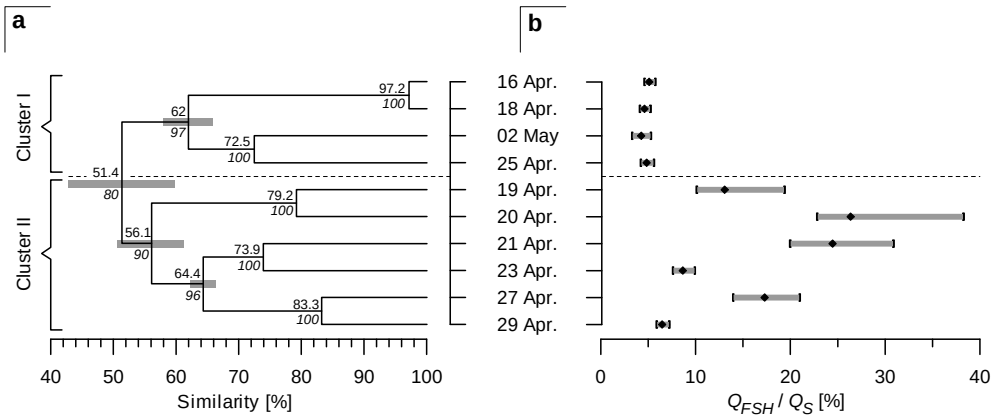

Fig. 5.6 (**a**) Hierarchical cluster analysis of storm event 16S rDNA PCR-DGGE profiles of Moulinet spring water samples (Jaccard correlation and unweighted pair group method with arithmetic mean). Error flags (grey bars), similarity (numbers) and cophenetic correlation coefficients (italic numbers) are shown. (**b**) Feurtille swallow hole contribution to the system discharge during the calculated infiltration time lag (Q_{FSH} / Q_S). Mean values (diamonds) with respective minimum and maximum values are shown. Sample dates are given along the vertical axis.

the allochthonous swallow hole contribution (Fig. 5.6b). Cluster I comprised samples belonging to different phases (phases *I* to *III*), but all samples were only weakly affected by the swallow hole component (Q_{FSH} / Q_S of about 4 to 5 %). In contrast, cluster II contained exclusively phase *III* water samples, which were characterised by a swallow hole contribution to the system discharge of 10 % to about 40 % and strictly allochthonous PSDs (Fig. 5.5). Only one sample ("29 Apr.") did not cluster in accordance with the degree of swallow hole contribution.

Of particular note is that samples collected before the swallow hole component arrival (i.e. samples "16 Apr." and "18 Apr.") and those collected towards the end of such events (i.e. samples "25 Apr." and "02 May") fell into the same cluster. Therefore, it appears that the microbial community in spring water regains its pre-event structure. This is seen as evidence for the non-persistence of allochthonous bacteria and may further suggest the stability of the autochthonous endokarst microbial community. Moreover, as suggested by the PCR-DGGE image, which showed continuous decreasing intensities of typical allochthonous bands (bacteria) during recession, the transition between samples with varying swallow hole contribution seems to occur in a rather smooth fashion. Finally, hierarchical cluster analysis of the storm event monitored at the Cossaux spring was consistent with the one for the Moulinet spring (Fig. E.4, Appendix E).

5.6 CLONE LIBRARIES AND SEQUENCE ANALYSIS: IDENTIFYING THE MICROORGANISMS IN THE KARST

5.6.1 Hydrogeological characteristics of the analysed samples

Based on PCR-DGGE results and hydrological parameters, three Moulinet spring water samples were chosen for clone library construction and sequence analysis. PSD analysis and physical, chemical and bacterial characteristics of the water samples are shown in Fig. 5.7 and summarised in Table 5.2, respectively.

- Library A encompasses sequences retrieved from sample "MS 06 Dec. 05" and is representative for all low swallow hole affected samples (Fig. 5.3). The sample was collected following a period of smowmelt and rainfall at the moment of maximum discharge (see Fig. C.4, Appendix C) and was characterised by a PSD typical for remobilised autochthonous particles. The direct swallow hole contribution was negligible as the stream sinking into the swallow hole was dry during the 16 days preceding the rainfall event. This sample is thus considered as the most appropriate for probing the autochthonous endokarst microbial community.

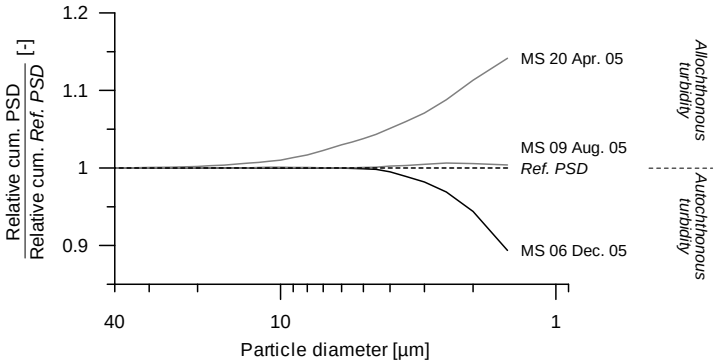

Fig. 5.7 Analysis of PSD curves of the three Moulinet spring water samples collected for clone library construction and sequence analysis. Relative cumulative PSDs ($\sum n \leq Ø / \sum n$, expressed in %) were normalised to the reference PSD ("*Ref. PSD*", see Chapter 3 for further details).

- Library B is composed of sequences retrieved from sample "MS 09 Aug. 05", which is characterised by an intermediate swallow hole contribution (Fig. 5.3) and a PSD indicating a minor impact of allochthonous particles.
- Library C comprises sequences retrieved from sample "MS 20 Apr. 05". The latter belongs to the samples strongly affected by the swallow hole component (Fig. 5.3, 5.4 and 5.6). The

Table 5.2 Physical, chemical and bacterial characteristics of the three Moulinet spring water samples collected for clone library construction and sequence analysis.

Parameter	Unit	MS 06 Dec. 05 *Clone libary A*	MS 09 Aug. 05 *Clone library B*	MS 20 Apr. 05 *Clone library C*
Discharge	[L/s]	45	27	403
Temperature	[°C]	11.4	11.0	9.9
EC [a]	[µS/cm]	422	438	519
TOC	[mg/L]	0.3	0.4	4.2
Turbidity	[NTU]	1.0	0.4	6.2
Q_{FSH} / Q_S	[%]	0	5 - 11	23 - 38
NO_3^-	[mg/L]	4.4	5.9	26.2
Cl^-	[mg/L]	2.0	2.5	6.1
SO_4^{2-}	[mg/L]	10.5	10.3	16.2
MAB [b]	[CFU/mL]	11	9	2564
Tot. colif. [c]	[CFU/100 mL]	158	69	7980
E. coli	[CFU/100 mL]	0	2	75
Enterococci	[CFU/100 mL]	0	0	50

[a] Electrical conductivity
[b] Mesophilic aerobic bacteria
[c] Total coliforms

sample is characterised by a PSD indicative for an important contribution of allochthonous particles that had entered the swallow hole during the preceding storm event. This high allochthonous contribution is also clearly discernable through the increased amounts of TOC, nitrate and water quality indicator bacteria (Table 5.2).

The library size, i.e. the number of retrieved 16S rDNA sequences, was 150 clones for library A, 104 clones for library B and 93 clones for library C.

5.6.2 Distribution of bacterial groups and phylogenetic analyses

The relative abundances of different phylogenetic groups were calculated for clone libraries A, B and C (Fig. 5.8), and phylogenetic trees were constructed for all phyla (Fig. 5.9, 5.10, 5.11 and 5.12). Complete listings of the retrieved sequences, their redundancy in clone library, their phylogenetic classification and their closest relatives are summarised in Tables E.1, E.2 and E.3 (Appendix E).

PROTEOBACTERIA

All libraries taken together, 166 of the 347 (~ 48 %) retrieved sequences were affiliated with the *Proteobacteria* phylum (Fig. 5.9 and 5.10). In all three water samples, the microbial communities were about equally dominated by *Proteobacteria*; the relative abundances varied between 42 and 52 %. These values are comparable to other aquatic and terrestrial ecosystems (e.g. Janssen 2006; Roesch *et al.* 2007). However, the relative proportion of the *Proteobacteria* subgroups varied greatly. While sequences belonging to the *α-Proteobacteria* were nearly absent in the low swallow hole affected sample (clone library A) and were replaced by *δ-Proteobacteria*, both swallow hole affected samples (clone libraries B and C) showed high abundances of *α-*, *β-*

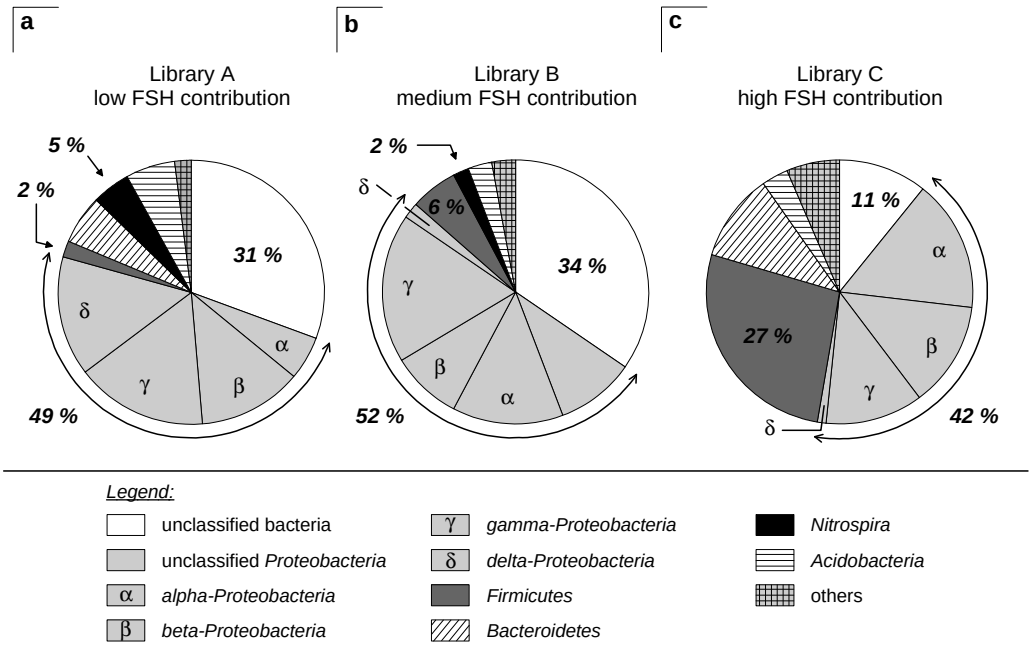

Fig. 5.8 Distribution in major phylogenetic groups (confidence threshold ≥ 95 %) of 16S rDNA bacterial genes of the Moulinet spring water samples with (**a**) low (library A), (**b**) medium (library B) and (**c**) high (library C) Feurtille swallow hole (FSH) contributions.

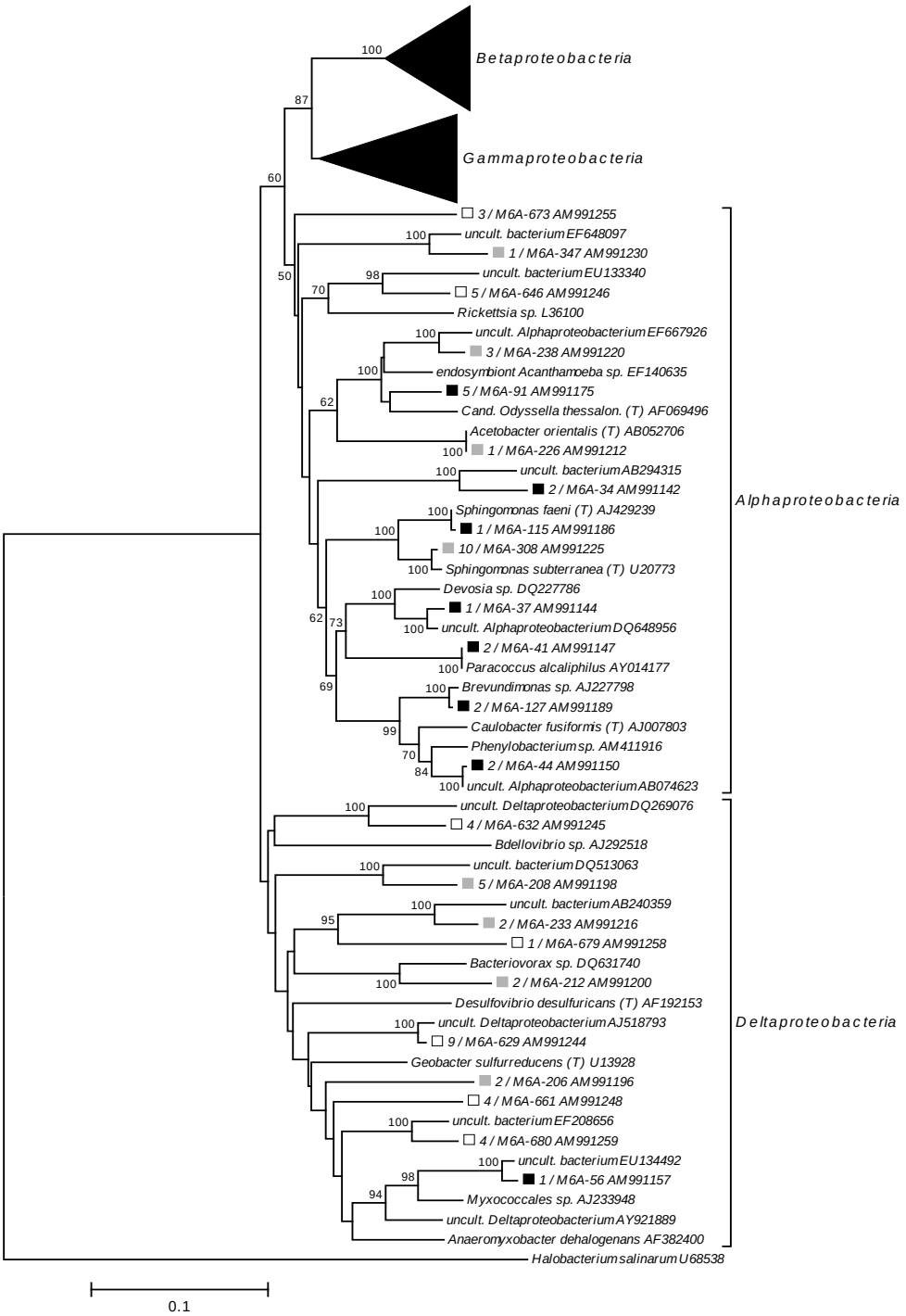

Fig. 5.9 Neighbour-joining tree showing phylogenetic relationships of 16S rDNA gene sequences from Moulinet spring water samples to closely related sequences belonging to the *α-Proteobacteria* and *δ-Proteobacteria* classes. *Halobacterium salinarum* was used as outgroup. Scale bar represents 10 % sequence difference. Bootstrap values higher than 50 % are shown. Clones from this study are coded as follows, with *3 / M6A-673 AM991255* as example: *3*, redundancy in clone library; *M6A-673*, sequence identifier; *AM991255*, accession number. White squares: sequences from library A (low FSH contribution); grey squares: sequences from library B (intermediate FSH contribution); black squares: sequences from library C (high FSH contribution).

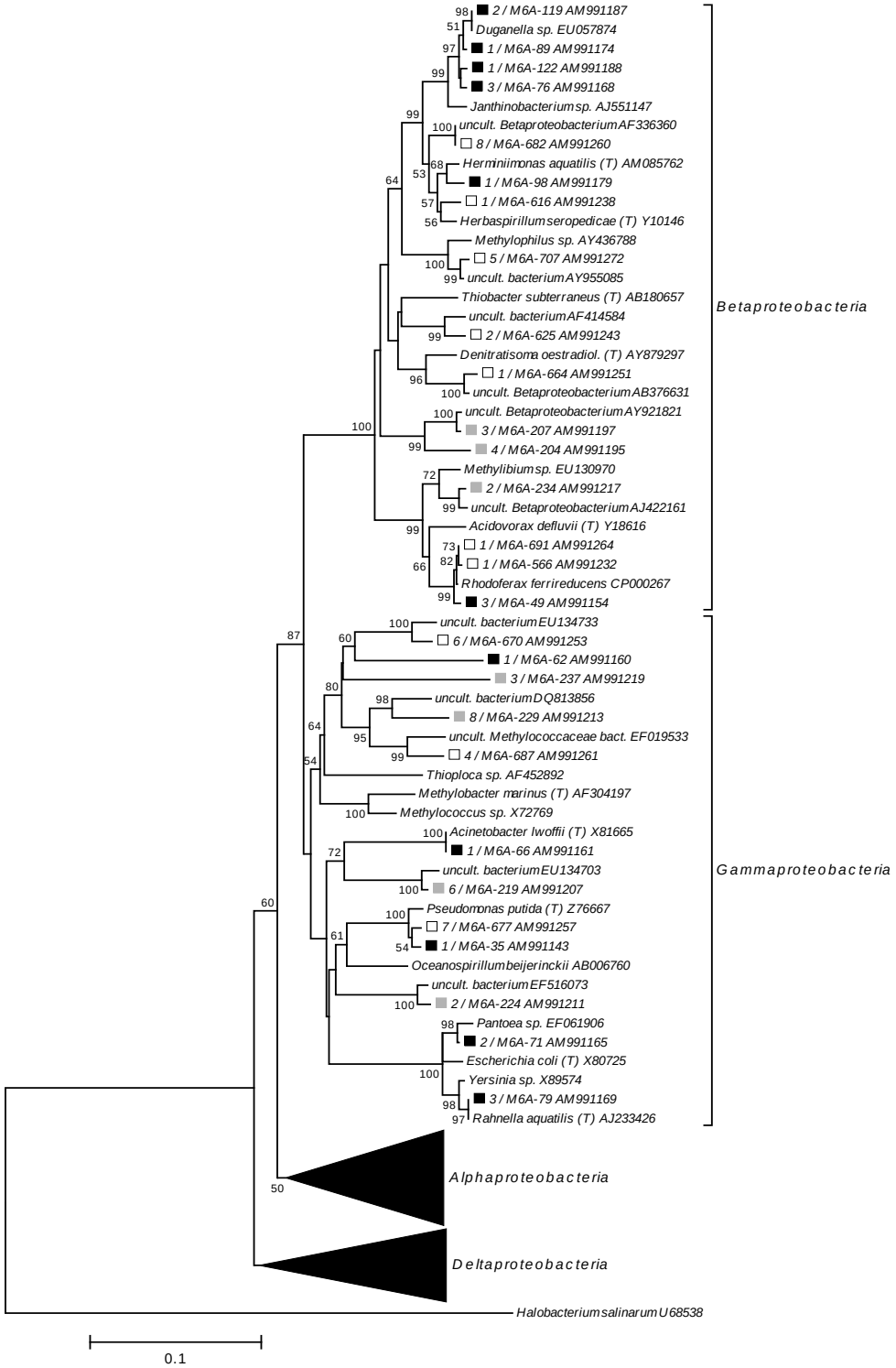

Fig. 5.10 Neighbour-joining tree showing phylogenetic relationships of 16S rDNA gene sequences from Moulinet spring water samples to closely related sequences belonging to the *β-Proteobacteria* and *γ-Proteobacteria* classes. *Halobacterium salinarum* was used as outgroup. Scale bar represents 10 % sequence difference. Bootstrap values higher than 50 % are shown. Clones from this study are coded as follows, with *2 / M6A-119 AM991187* as example: *2*, redundancy in clone library; *M6A-119*, sequence identifier; *AM991187*, accession number. White squares: sequences from library A (low FSH contribution); grey squares: sequences from library B (intermediate FSH contribution); black squares: sequences from library C (high FSH contribution).

and *γ-Proteobacteria*. *α-Proteobacteria* are an important, sometimes even dominant, subclass of *Proteobacteria* in soils (Felske *et al*. 1998; Hartmann and Widmer 2006; Roesch *et al*. 2007). Their low abundance in clone library A therefore further supports evidence for a specific intrakarstic microbial community. *β-* and *γ-Proteobacteria* are widespread in many habitats and were also frequently observed in groundwater environments (Griebler and Lueders 2009). As both classes were about equally abundant in all three clone libraries, it is difficult to draw any conclusion.

About 15 %, 2 % and 1% of the sequences retrieved from clone libraries A, B and C, respectively, were affiliated with the *δ-Proteobacteria* class. However, almost all sequences that were grouped as "unclassified *Proteobacteria*" using the RDP classifier (Fig. 5.8b) clustered with the *δ-Proteobacteria* class in the phylogenetic tree (Fig. 5.9). By this way, the frequency of this class in clone library B increased to approximately 10 %. As *δ-Proteobacteria*-like sequences were nearly absent in the high swallow hole affected sample, it is hypothesised that they are part of the autochthonous endokarst microbial community. The fact that *δ-Proteobacteria* are commonly found in aquifers further supports this hypothesis (Griebler and Lueders 2009). Although the *δ-Proteobacteria* class harbours most of the known aerobic sulphate-, sulphur- and iron-reducing bacteria, these metabolisms cannot be inferred for the retrieved sequences as most of them were only distantly related to any known organisms.

It is worth noting that no sequences belonging to the *ε-Proteobacteria* class were detected in any of the three clone libraries. *ε-Proteobacteria* have been frequently observed in sulfidic springs and caves (e.g. Meisinger *et al*. 2007), where they are believed to contribute to the karstification process by sulphide oxidation and concomitant sulphuric acid production (Engel 2007).

FIRMICUTES

A total of 3 sequences retrieved from the low swallow hole affected sample (clone library A), 6 sequences retrieved from the medium swallow hole affected sample (clone library B) and 25 sequences retrieved from the high swallow hole affected sample (clone library C) were affiliated with the *Firmicutes* phylum (Fig. 5.11). The increase of the relative abundance of *Firmicutes* from 2 to 27 % in clone libraries A to C seems to correlate with an increasing swallow hole contribution, suggesting that they are of allochthonous origin. Indeed, this phylum contains important soil bacteria such as *Bacillus* and *Clostridium* species but also many gut bacteria (e.g. *Enterococcus* sp.) and facultative pathogens (e.g. *Staphylococcus* sp. and *Streptococcus* sp.; Eckburg *et al*. 2005; Felske *et al*. 1998; Roesch *et al*. 2007). The allochthonous origin of the retrieved *Firmicutes* related sequences was further confirmed by the fact that almost all these sequences (except *M6A-671*, *M6A-102* and *M6A-213*) revealed similarities higher than 99 % to sequences in the database which were retrieved from environments such as wastewater and intestines of man, swine, cows and other mammals.

NITROSPIRA

The 9 sequences that were affiliated with *Nitrospira*, a phylum including nitrifying bacteria, clustered together and showed more than 99 % similarity among them (Fig. 5.12). The close association with *Nitrospira moscoviensis* (> 96 % similarity), which is obligatorily

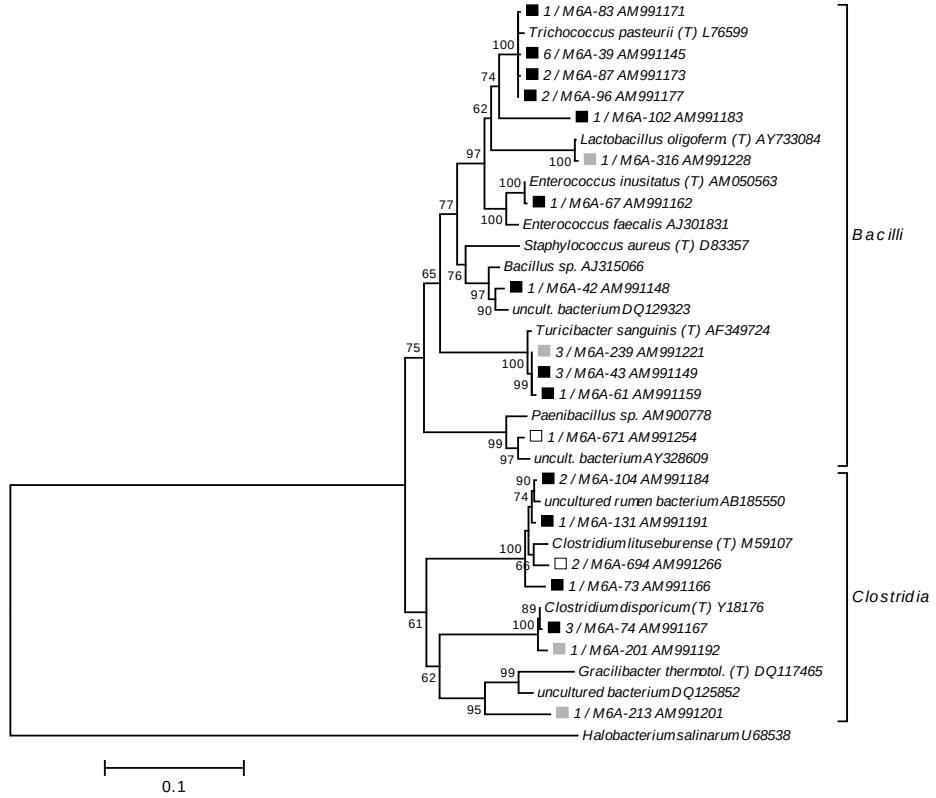

Fig. 5.11 Neighbour-joining tree showing phylogenetic relationships of 16S rDNA gene sequences from Moulinet spring water samples to closely related sequences belonging to the *Firmicutes* phylum. *Halobacterium salinarum* was used as outgroup. Scale bar represents 10 % sequence difference. Bootstrap values higher than 50 % are shown. Clones from this study are coded as follows, with *1 / M6A-83 AM991171* as example: *1*, redundancy in clone library; *M6A-83*, sequence identifier; *AM991171*, accession number. White squares: sequences from library A (low FSH contribution); grey squares: sequences from library B (intermediate FSH contribution); black squares: sequences from library C (high FSH contribution).

chemolithoautotrophic, may suggest a nitrite-oxidising metabolism for the corresponding organisms. The relative abundance of *Nitrospira* was highest in clone library A (5 %) and decreased with increasing swallow hole contribution. Although *Nitrospira* sequences have been retrieved from soils, geothermal and subsurface ecosystems (Hugenholtz *et al*. 1998; Roesch *et al*. 2007), they seem to be part of the autochthonous microbial community in the Yverdon-les-Bains karst aquifer system. The high similarities of the retrieved sequences (> 99 %) with a clone recovered from the Frasassi cave system in Italy (uncult. bacterium DQ499307, Fig. 5.12; Macalady *et al*. 2007), as well as the presence of *Nitrospira*-like sequences in an Austrian alpine karst aquifer (Farnleitner *et al*. 2005) and the Mammoth cave karst aquifer (Fowler, pers. comm.), further support this hypothesis.

ACIDOBACTERIA

A total of 15 sequences clustered with members of the genus *Gp6* of the *Acidobacteria* phylum (Fig. 5.12). Except for clone *M6A-230*, which was 5 % dissimilar to its closest relative, all

sequences revealed similarities higher than 98 % with environmental clones. *Acidobacteria* have been detected by molecular methods in diverse environments but seem to be particularly abundant in soils and sediments. However, little is known about their physiology and ecology as only a few

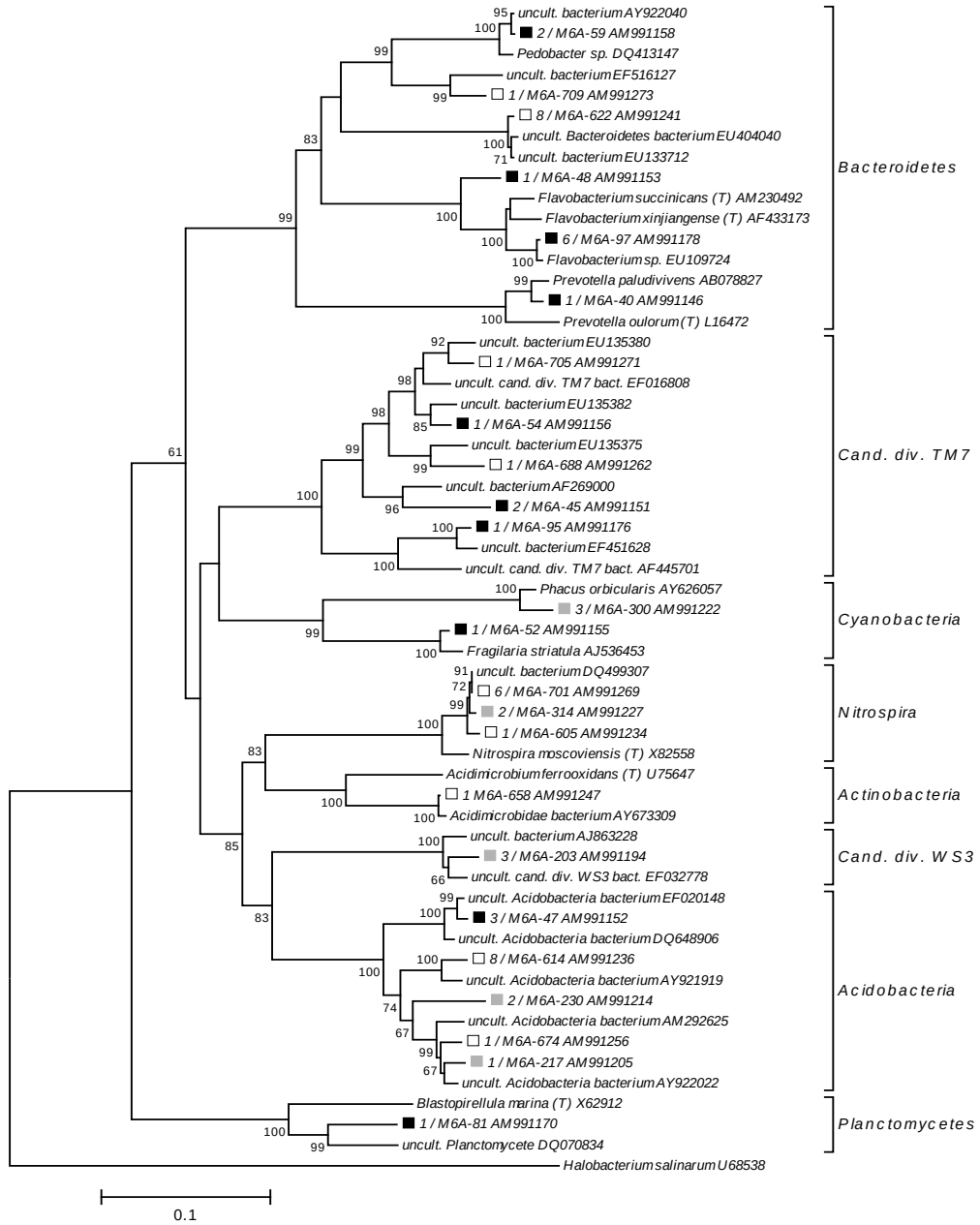

Fig. 5.12 Neighbour-joining tree showing phylogenetic relationships of 16S rDNA gene sequences from Moulinet spring water samples to closely related sequences belonging to the *Bacteroidetes*, *Nitrospira*, *Acidobacteria* and other phyla. *Halobacterium salinarum* was used as outgroup. Scale bar represents 10 % sequence difference. Bootstrap values higher than 50 % are shown. Clones from this study are coded as follows, with *2 / M6A-59 AM991158* as example: *2*, redundancy in clone library; *M6A-59*, sequence identifier; *AM991158*, accession number. White squares: sequences from library A (low FSH contribution); grey squares: sequences from library B (intermediate FSH contribution); black squares: sequences from library C (high FSH contribution).

species have been isolated and characterised (Barns *et al*. 2007). *Acidobacteria* sequences were found in all three samples, but particularly in clone library A, where they represented approximately 6 % of all retrieved sequences. These results suggest that this little known group may also dwell in karst systems. Moreover, *Acidobacteria* related sequences were also retrieved from sediments in the Mammoth cave karst aquifer (Fowler, pers. comm.).

BACTEROIDETES

The *Bacteroidetes* phylum was represented by 9 and 10 sequences in clone libraries A and C, respectively (Fig. 5.12). No sequences affiliated with this group were retrieved from the medium swallow hole affected sample (clone library B). *Bacteroidetes* are commonly found in diverse terrestrial and aquatic habitats, where they contribute to the degradation of organic matter (Hugenholtz *et al*. 1998).

OTHERS

Finally, all clone libraries taken together, 15 sequences clustered with various phylogenetic groups, such as *Actinobacteria*, *Cyanobacteria*, *Planctomycetes* and the candidate divisions *WS3* and *TM7* (Fig. 5.12). Among them, the candidate division *TM7* group was the most abundant and encompassed approximately 4 % of the sequences retrieved from the sample strongly affected by the allochthonous swallow hole component (clone library C). To date no representative of this phylum has been isolated, and therefore no conclusions about their physiology and ecological role can be drawn. It is also worth noting that only one sequence was affiliated with the *Actinobacteria* phylum, as *Actinobacteria* are typical and sometimes even dominant members of soil microbial communities (Hartmann and Widmer 2006).

UNCLASSIFIED BACTERIA

Of particular note, 31 to 34 % of the sequences retrieved from the low and the medium swallow hole affected samples (clone libraries A and B, respectively) remained unclassified using the RDP classifier, i.e. at least 5 % dissimilar to all currently known bacterial phyla (Fig. 5.8). The distinctiveness of these clone libraries becomes even more evident when looking at the similarities between all the sequences retrieved during this study and their closest relatives in databases (Table 5.3). For the high swallow hole affected sample (clone library C), 69.9 % of the retrieved sequences revealed similarities of more than 99 % to known bacteria. In contrast, only 27.3 % of the sequences recovered from the low swallow hole affected sample

Table 5.3 Number (n) and percentage (%) of sequences from libraries A, B and C revealing similarities higher than 99, 98, 97, 95, 90 and 80 % to known sequences in databases.

Similarities	Remark	Library A		Library B		Library C	
		n	%	n	%	n	%
≥ 99 %	Strain level	41	27.3	18	17.3	65	69.9
≥ 98 %		61	40.6	37	35.6	71	76.3
≥ 97 %	Species level	71	47.3	45	43.3	73	78.5
≥ 95 %	Genus level	83	55.3	53	51.0	81	87.1
≥ 90 %		140	93.3	87	83.7	92	98.9
≥ 80 %		149	99.3	98	94.2	93	100

(clone library A) showed similarities of more than 99 % to currently known sequences. At the species level, which is generally defined at a value of 97 % similarity (Stackebrandt 2004), 78.5 % of the sequences from clone library C were related to known sequences, against still only 47.3 % for sequences of clone library A. Many of the sequences retrieved from clone library A can thus be proposed as representatives of new species from an autochthonous endokarst microbial community.

This high proportion of unknown sequences suggests that many karst bacteria are yet to be discovered and illustrates further the uniqueness of the autochthonous microbial community of karst aquifers. Furthermore, it underscores the fact that microbial communities of karst aquifers are rarely investigated, that karst aquifers are unique habitats and that sequences from shallow subsurface ecosystems are currently underrepresented in databases.

DIVERSITY

In order to assess whether the microbial community in place has been sufficiently sampled to be representative, rarefaction curves were produced and coverage values were calculated. Rarefaction curves for all three clone libraries (Fig. E.5, Appendix E) did not reach saturation, although libraries A and B seemed to approach an asymptote, suggesting that the clones retrieved from the low and medium swallow hole affected samples were representative of the bacterial communities in place. Coverage values, which were 91, 93 and 76 % for clone libraries A, B and C, respectively, further supported this observation.

Finally, sequence analysis of the low swallow hole affected sample showed that the autochthonous endokarst microbial community was more or less evenly distributed, i.e. no

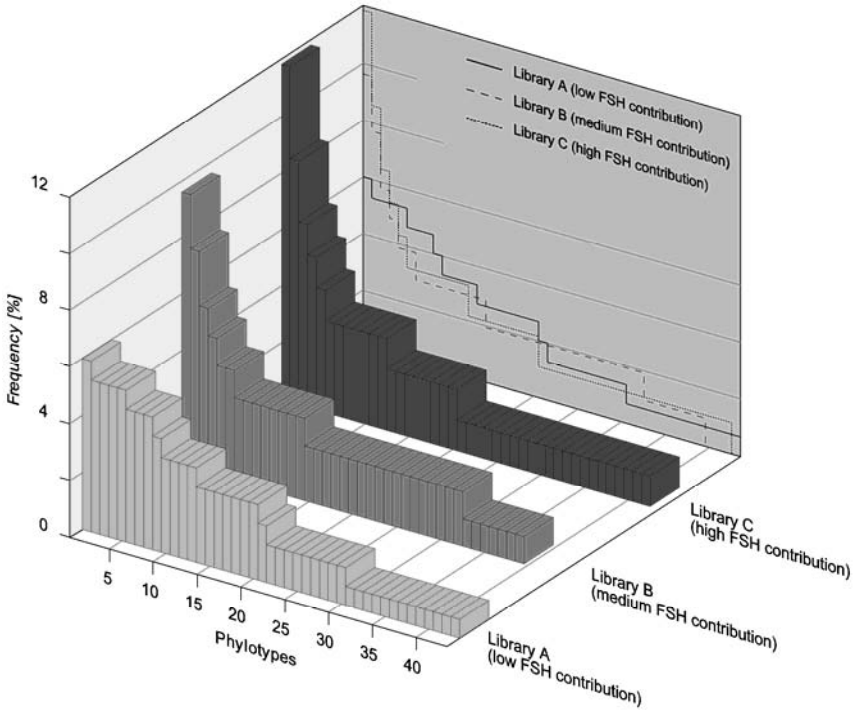

Fig. 5.13 Frequencies of phylotypes in clone libraries from Moulinet spring water samples with low, medium and high swallow hole (FSH) contributions.

dominant species were observed (Fig. 5.13). In contrast, during periods of high allochthonous input, several abundant species appeared and overprinted the autochthonous bacterial community. Similar conclusions were also drawn from the PCR-DGGE analysis. Furthermore, the abundant phylotypes observed during the high swallow hole affected sample corresponded principally to members of the *Firmicutes* phylum (e.g. genus *Trichococcus*).

5.7 CONCLUSION

5.7.1 Evidence for a stable community of endokarst microorganisms

PCR-DGGE and cloning / sequencing allowed the structure, diversity and temporal variability of microbial communities in karst groundwater to be investigated. The autochthonous endokarst microbial community is characterised by a high diversity with only a few dominant species and a high temporal constancy. *δ-Proteobacteria*, *Acidobacteria* and *Nitrospira* species are important members of this community, but the high proportion of unclassified sequences suggests that many karst bacteria are still undiscovered. Moreover, it highlights that pristine karst aquifers are rarely studied, unique habitats and that sequences from shallow subsurface ecosystems are currently underrepresented in databases.

Both molecular techniques revealed a clear relation between the bacterial community composition in spring water and the swallow hole contribution. During periods of high input of water from the swallow hole, the autochthonous microbial community is overprinted by allochthonous bacteria. Consequently, the high variability of bacterial communities in the spring water reflects the high fluctuations observed at the swallow hole. However, contamination of karst groundwater by allochthonous bacteria is unlikely to persist.

5.7.2 Particle-size distribution as tool to optimise sampling

Sampling strategy in karst aquifers should be based on hydrological conditions and focus on turbidity episodes. Autochthonous turbidity pulses at springs are the result of increasing flow rates in the aquifer. Due to higher shear stress, attached particles and cells are sloughed off the conduit surfaces and intrakarstic sediments are remobilised. Bacteria attached to these particles are thereby brought into the water phase and transported to the spring. Particle-size distribution measurements allow distinction between autochthonous and allochthonous turbidity episodes and represents therefore an important tool for identifying water samples that harbour endokarst microorganisms.

5.7.3 Potential use of microbial communities for groundwater biomonitoring

Biomonitoring is a valuable supplementary tool for controlling groundwater quality, as it delivers more integrated – but less quantitative – information than chemical analyses. Bacteria are the dominant organisms in aquifers, and their occurrence and activity is related to the biogeochemical conditions. The structures of microbial communities, individual marker organisms or even specific functional genes are therefore promising bioindicators. However, there is often a complex relation between water quality and microbial communities, and their response to specific contaminants is still poorly understood. Short-term microbial contamination at karst springs, such as those resulting from storm events, are easily detectable by *in-situ* monitoring of

natural physical and chemical parameters. However, the long-term monitoring of autochthonous endokarst microbial communities during years or even decades may be an interesting approach to assess the general water quality and to detect potential changes in ecosystem functioning due to chronic low level contamination or climate change. The applied molecular methodology does not have the required resolution and throughput for monitoring purposes yet, but new, promising techniques are continuously being developed (e.g. Chandler and Jarrell 2004; He *et al*. 2007; Roesch *et al*. 2007). This work represents therefore only a first step towards a better understanding of the microbial ecology in pristine karst aquifers and may serve as a starting point for developing biomonitoring tools.

REFERENCES

Alfreider A., Krössbacher M. and Psenner R. 1997. Groundwater samples do not reflect bacterial densities and activity in subsurface systems. Water Research 31 (4): 832-840.

Barns S.M., Cain E.C., Sommerville L. and Kuske C.R. 2007. *Acidobacteria* phylum sequences in uranium-contaminated subsurface sediments greatly expand the known diversity within this phylum. Applied and Environmental Microbiology 73 (9): 3113-3116.

Barton H.A. and Northup D.E. 2007. Geomicrobiology in cave environments: past, current and future perspectives. Journal of Cave and Karst Studies 69 (1): 163-178.

Canaveras J.C., Hoyos M., Sanchez-Moral S., Sanz-Rubio E., Bedoya J., Soler V., Groth I., Schumann P., Laiz L., Gonzales I. and Sainz-Jimenez C. 1999. Microbial communities associated with hydromagnesite and needle-fiber aragonite deposits in a karstic cave (Altamira, northern Spain). Geomicrobiology Journal 16 (1): 9-25.

Chandler D.P. and Jarrell A.E. 2004. Automated purification and suspension array detection of 16S rRNA from soil and sediment extracts by using tunable surface microparticles. Applied and Environmental Microbiology 70 (5): 2621-2631.

Chapelle F.H. 2001. Groundwater microbiology and geochemistry. Wiley, New York.

Chelius M.K. and Moore J.C. 2004. Molecular phylogenetic analysis of archaea and bacteria in Wind Cave, South Dakota. Geomicrobiology Journal 21 (2): 123-134.

Cole J.R., Chai B., Farris R.J., Wang Q., Kulam-Syed-Mohideen A.S., McGarrell D.M., Bandela A.M., Cardenas E., Garrity G.M. and Tiedje J.M. 2007. The ribosomal database project (RDP-II): introducing myRDP space and quality controlled public data. Nucleic Acids Research 35 (Database issue): D169-D172.

Danielopol D.L., Griebler C., Gunatilaka A. and Notenboom J. 2003. Present state and future prospects for groundwater ecosystems. Environmental Conservation 30 (2): 104-130.

Eckburg P.B., Bik E.M., Bernstein C.N., Purdom E., Dethlefsen L., Sargent M., Gill S.R., Nelson K.E. and Relman D.A. 2005. Diversity of the human intestinal microbial flora. Science 308 (5728): 1635-1638.

Engel A.S. 2007. Observations on the biodiversity of sulfidic karst habitats. Journal of Cave and Karst Studies 69 (1):187-206.

Farnleitner A.H., Wilhartitz I., Ryzinska G., Kirschner A.K.T., Stadler H., Burtscher M.M., Hornek R., Szewzyk U., Herndl G. and Mach R.L. 2005. Bacterial dynamics in spring water of alpine karst aquifers indicates the presence of stable autochthonous microbial endokarst communities. Environmental Microbiology 7 (8): 1248-1259.

Felske A., Wolterink A., van Lis R. and Akkermans A.D.L. 1998. Phylogeny of the main bacterial 16S rRNA sequences in Drentse A grassland soils (The Netherlands). Applied and Environmental Microbiology 64 (3): 871-879.

Goldscheider N., Hunkeler D. and Rossi P. 2006. Review: Microbial biocenoses in pristine aquifers and an assessment of investigative methods. Hydrogeology Journal 14 (6): 926-941.

Green U., Kremer J.H., Zillmer M. and Moldaenke C. 2003. Detection of chemical threat agents in drinking water by an early warning real-time biomonitor. Environmental Toxicology 18 (6): 368-374.

Griebler C. and Lueders T. 2009. Microbial diversity in groundwater ecosystems. Freshwater Biology 54 (4): 649-677.

Griebler C. and Mösslacher F. 2003. Grundwasser-Ökologie. Facultas UTB, Vienna.

GSchV. 1998. Water Protection Ordinance, SR 814.201, Swiss Federal Law, Bern.

Hahn H.J. and Friedrich E. 1999. Brauchen wir ein faunistisch begründetes Grundwassermonitoring und was kann es leisten? Grundwasser 4: 147-154.

Hancock P.J., Boulton A.J. and Humphreys W.F. 2005. Aquifers and hyporheic zone: towards an ecological understanding of groundwater. Hydrogeology Journal 13 (1): 98-111.

Hartmann M. and Widmer F. 2006. Community structure analyses are more sensitive to differences in soil bacterial communities than anonymous diversity indices. Applied and Environmental Microbiology 72 (12): 7804-7812.

He Z., Gentry T.J., Schadt C.W., Wu L., Liebich J., Chong S.C., Huang Z., Wu W., Gu B., Jardine P., Criddle C. and Zhou J. 2007. GeoChip: a comprehensive microarray for investigating biogeochemical, ecological and environmental processes. ISME Journal 1 (1): 67-77.

Heck K.L., Van Belle G. and Simberloff D. 1975. Explicit calculation of the rarefaction diversity measurement and the determination of sufficient sample size. Ecology 56 (6): 1459-1461.

Hose L.D., Palmer A.N., Palmer M.V., Northup D.E., Boston P.J. and DuChene H.R. 2000. Microbiology and geochemistry in a hydrogen-sulphide-rich karst environment. Chemical Geology 169 (3-4): 399-423.

Hugenholtz P., Goebel B.M. and Pace N.R. 1998. Impact of culture-independent studies on the emerging phylogenetic view of bacterial diversity. Journal of Bacteriology 180 (18): 4765-4774.

Janssen P.H. 2006. Identifying the dominant soil bacterial taxa in libraries of 16S rRNA and 16S rRNA genes. Applied and Environmental Microbiology 72 (3): 1719-1728.

Lehman R.M. 2007. Understanding of aquifer microbiology is tightly linked to sampling approach. Geomicrobiology Journal 24 (3-4): 331-341.

Macalady J.L., Jones D.S. and Lyon E.H. 2007. Extremely acidic, pendulous cave wall biofilms from the Frasassi cave system, Italy. Environmental Microbiology 9 (6): 1402-1414.

Macalady J.L., Lyon E.H., Koffman B., Albertson L.K., Meyer K., Galdenzi S. and Mariani S. 2006. Dominant microbial populations in limestone-corroding stream biofilms, Frasassi cave system, Italy. Applied and Environmental Microbiology 72 (8): 5596-5609.

Malard F., Plenet S. and Gibert J. 1996. The use of invertebrates in groundwater monitoring: a rising research field. Ground Water Monitoring and Remediation 16 (2): 103-113.

Meisinger D.B., Zimmermann J., Ludwig W., Schleifer K.H., Wanner G., Schmid M., Bennett P.C., Engel A.S. and Lee N.M. 2007. In situ detection of novel *Acidobacteria* in microbial mats from a chemolithoautotrophically based cave ecosystem (Lower Kane Cave, WY, USA). Environmental Microbiology 9 (6): 1523-1534.

Mösslacher F., Griebler C. and Notenboom J. 2001. Biomonitoring of groundwater systems: methods, applications and possible indicators among the groundwater biota. In: Griebler C., Danielopol D.L., Gibert J., Nachtnebel H.P. and Notenboom J. (eds.) Groundwater ecology: a tool for management of water resources. Office for Official Publications of the European Communities, Luxembourg.

Mullins T.D., Britschgi T.B., Krest R.L. and Giovannoni S.J. 1995. Genetic comparisons reveal the same unknown bacterial lineages in Atlantic and Pacific bacterioplankton communities. Limnology and Oceanography 40 (1): 148-158.

Muyzer G. 1999. DGGE / TGGE a method for identifying genes from natural ecosystems. Current Opinion in Microbiology 2 (3): 317-322.

Muyzer G., Dewaal E.C. and Uitterlinden A.G. 1993. Profiling of complex microbial-populations by denaturing gradient gel-electrophoresis analysis of polymerase chain reaction-amplified genes-coding for 16S ribosomal-RNA. Applied and Environmental Microbiology 59 (3): 695-700.

Muyzer G., Teske A., Wirsen C.O. and Jannasch H.W. 1995. Phylogenetic relationships of *Thiomicrospira* species and their identification in deep-sea hydrothermal vent samples by denaturing gradient gel electrophoresis of 16S rDNA fragments. Archives of Microbiology 164 (3): 165-172.

Nocker A., Burr M. and Camper A.K. 2007. Genotypic microbial community profiling: a critical technical review. Microbial Ecology 54 (2): 276-289.

Northup D.E. and Lavoie K.H. 2001. Geomicrobiology of caves: a review. Geomicrobiology Journal 18 (3): 199-222.

Ovreas L., Forney L., Daae F.L. and Torsvik V. 1997. Distribution of bacterioplankton in meromictic Lake Saelenvannet, as determined by denaturing gradient gel electrophoresis of PCR-amplified gene fragments coding for 16S rRNA. Applied and Environmental Microbiology 63 (9): 3367-3373.

Personné J.C., Poty F., Mahler B.J. and Drogue C. 2004. Colonization by aerobic bacteria in karst: laboratory and in situ experiments. Ground Water 42 (4): 526-533.

Pronk M., Goldscheider N. and Zopfi J. 2007. Particle-size distribution as indicator for fecal bacteria contamination of drinking water from karst springs. Environmental Science & Technology 41 (24): 8400-8405.

Roesch L.F., Fulthorpe R.R., Riva A., Casella G., Hadwin A.K.M., Kent A.D., Daroub S.H., Camargo F.A.O., Farmerie W.G. and Triplett E.W. 2007. Pyrosequencing enumerates and contrasts soil microbial diversity. ISME Journal 1 (4): 283-290.

Rusterholtz K.J. and Mallory L.M. 1994. Density, activity, and diversity of bacteria indigenous to a karstic aquifer. Microbial Ecology 28 (1): 79-99.

Sakano Y. and Kerkhof L. 1998. Assessment of changes in microbial community structure during operation of an ammonia biofilter with molecular tools. Applied and Environmental Microbiology 64 (12): 4877-4882.

Simon K.S., Gibert J., Petitot P. and Laurent R. 2001. Spatial and temporal patterns of bacterial density and metabolic activity in a karst aquifer. Archiv für Hydrobiologie 151 (1): 67-82.

Steube C., Richter S. and Griebler C. 2009. First attempts towards an integrative concept for the ecological assessment of groundwater ecosystems. Hydrogeology Journal 17 (1): 23-35.

Tamura K., Dudley J., Nei M. and Kumar S. 2007. MEGA4: Molecular evolutionary genetics analysis (MEGA) software version 4.0. Molecular Biology and Evolution 24 (8): 1596-1599.

Vervier P. and Gibert J. 1991. Dynamics of surface-water groundwater ecotones in a karstic aquifer. Freshwater Biology 26 (2): 241-250.

Wang Q., Garrity G.M., Tiedje J.M. and Cole J.R. 2007. Naïve bayesian classifier for rapid assignment of rRNA sequences into the new bacterial taxonomy. Applied and Environmental Microbiology 73 (16): 5261-5267.

Weiss J.V. and Cozzarelli I.M. 2008. Biodegradation in contaminated aquifers: incorporating microbial / molecular methods. Ground Water 46 (2): 305-322.

6

Summary and conclusion

6.1 PSD AS INDICATOR FOR FAECAL BACTERIA CONTAMINATION OF GROUNDWATER FROM KARST AQUIFERS

6.1.1 Summary

The protection and management of karst groundwater resources require the understanding of water and contaminant transfer from the land surface through the entire hydrogeological system towards springs or other drinking water abstraction points. Suspended matter and pathogenic microorganisms represent the most important contaminants in many karst water supplies. Therefore, the investigation of the dynamics and behaviour of particles and faecal bacteria in the unsaturated and saturated zones of karst aquifers, as well as the identification of an "early-warning" system for bacterial pollution, formed the backcloth of this work.

Turbidity events in karst systems are either derived from the aquifer itself, i.e. autochthonous or pulse-through turbidity, or from outside, i.e. allochthonous or flow-through turbidity. Autochthonous turbidity episodes results from the high and rapid variability of flow velocities in karst systems, which induces pronounced hydrological shear stress and leads to scouring and resuspension of intrakarstic particulate material. In contrast, allochthonous turbidity events results from the direct transfer of particles from the land surface. These particles are introduced into the aquifer during rainfall events, either diffusely by infiltration and percolation through shallow soil and the unsaturated zone or concentrated via sinking streams.

While turbidity alone does not allow identifying the origin of suspended matter, particle-size distribution (PSD) measurements make it possible to discriminate clearly autochthonous from allochthonous turbidity episodes. Autochthonous turbidity was characterised by significant particle concentration increases over a wide range of size classes, ranging from colloidal sizes up to about 0.1 mm, whereas allochthonous turbidity was characterised by increases of the finer size classes only, ranging from 0.9 to approximately 10.0 µm. The breakthrough of faecal bacteria originating from agricultural activities at the land surface were very well correlated with the finer particles (0.9 –1.5 µm) during flow-through turbidity periods ($R^2 > 0.8$). The sensitivity of PSD analysis to detect an allochthonous particle contribution being very high, PSD is consequently

proposed as an “early-warning” surrogate for real-time monitoring of possible microbial contamination of karst groundwater.

6.1.2 Limitations and perspectives

The presented method permits optimising water treatment and identifying periods when spring water must be rejected due to microbial contamination in the selected karst aquifer systems. The investigation at other karst aquifer systems, with combined inputs of faecal bacteria through shallow soils and the unsaturated zone and via sinking streams, would permit confirming (or refuting) the use of PSD as an “early-warning” parameter for faecal contamination. Furthermore, the applicability of this approach to other type of microbial contamination, such as permanent wastewater releases via leaking sewers or septic tanks, still needs to be tested.

In a similar vein, it would be interesting to test the use of PSD monitoring for other types of contaminants that absorb onto particulate material, such as polycyclic aromatic hydrocarbons (PAHs) and heavy metals.

Finally, PSD monitoring not only represents a new data resource to assess karst groundwater quality but also to further investigate particle transport and attenuation processes in karst aquifers. Indeed, to date, particle and colloid transport processes were mostly studied in porous media, while there is no consistent theory explaining such processes in karst aquifer systems. Rigorous laboratory studies would probably allow investigating these processes.

6.2 MICROBIAL COMMUNITIES IN KARST GROUNDWATER AND THEIR POTENTIAL USE FOR BIOMONITORING

6.2.1 Summary

Karst aquifers are increasingly considered as ecosystems harbouring their proper biocenoses, and the potential use of microbial communities for biomonitoring has been raised. However, microbial ecology research in such subsurface environments is still in an early stage and rather sparse. Therefore, another main objective of this work was to explore, by means of molecular biological methods, the structure, diversity and temporal variability of microbial communities in the Yverdon-les-Bains karst aquifer system.

During both the storm event and the annual hydrological cycle, statistical analysis of bacterial genetic fingerprints (16S rDNA PCR-DGGE profiles) of spring water samples revealed several clusters that corresponded well with different levels of the allochthonous swallow hole contribution. Bacterial assemblages in spring water samples highly affected by the swallow hole showed low similarities among them, reflecting the high temporal fluctuations of the microbial communities in the water entering the swallow hole. Conversely, high similarities among spring water samples with low allochthonous contribution provided evidence for a temporally constant autochthonous endokarst microbial community.

Microbial communities of spring water samples strongly affected by the allochthonous swallow hole component were highly diverse and displayed several dominant bacterial populations. The microbial community of such a sample was dominated by *Firmicutes* species, representing about 27 % of all retrieved sequences. The allochthonous origin of this bacterial

group was confirmed by the fact that the closest relatives of almost all these sequences were retrieved from environments such as wastewater and intestines of man, swine, cows and other mammals. In contrast, the autochthonous endokarst microbial community was characterised by a high diversity with the nearly absence of dominant species, i.e. the microbial community was more or less evenly distributed. *δ-Proteobacteria*, *Acidobacteria* and *Nitrospira* species were important members of this endokarstic community. However, the high percentage of unknown sequences (i.e. sequences revealing similarities lower than 97 % to already known sequences) suggests that many karst aquifer bacteria are still undiscovered. This highlights also that karst aquifer systems are rarely investigated, unique ecosystems and that sequences from shallow subsurface ecosystems are currently still underrepresented in databases.

Finally, both applied molecular microbiological methods (i.e. PCR-DGGE and cloning / sequencing) revealed a clear relation between the bacterial community composition in spring water and the allochthonous swallow hole contribution. During periods of high input of water from the swallow hole, the autochthonous endokarst microbial community is overprinted by allochthonous bacteria. However, contamination of karst groundwater by allochthonous bacteria is unlikely to persist.

6.2.2 Limitations and perspectives

Biomonitoring is a valuable supplementary tool for controlling groundwater quality, as it may deliver more integrated – but less quantitative – information than chemical analyses. Bacteria are the dominant organisms in aquifers, and their occurrence and activity is related to the biogeochemical conditions. The structures of microbial communities, individual marker organisms, or even specific functional genes are therefore promising bioindicators. However, there is often a complex relation between water quality and microbial communities, and their response to specific contaminants is still poorly understood. Short-term microbial contamination at karst springs, such as those resulting from storm events, are easily detectable by *in-situ* monitoring of natural physical and chemical parameters. However, long-term monitoring of autochthonous endokarst microbial communities during years or even decades may be an interesting approach to assess the general water quality and to detect potential changes in ecosystem functioning due to chronic low level contamination or climate change. The applied molecular methodology does not have the required resolution and throughput for monitoring purposes, but new, promising techniques are continuously being developed. This work represents therefore only a first step towards a better understanding of the microbial ecology in pristine karst aquifers and may serve as a starting point for developing biomonitoring tools.

Appendix A

Calibration of monitored parameters

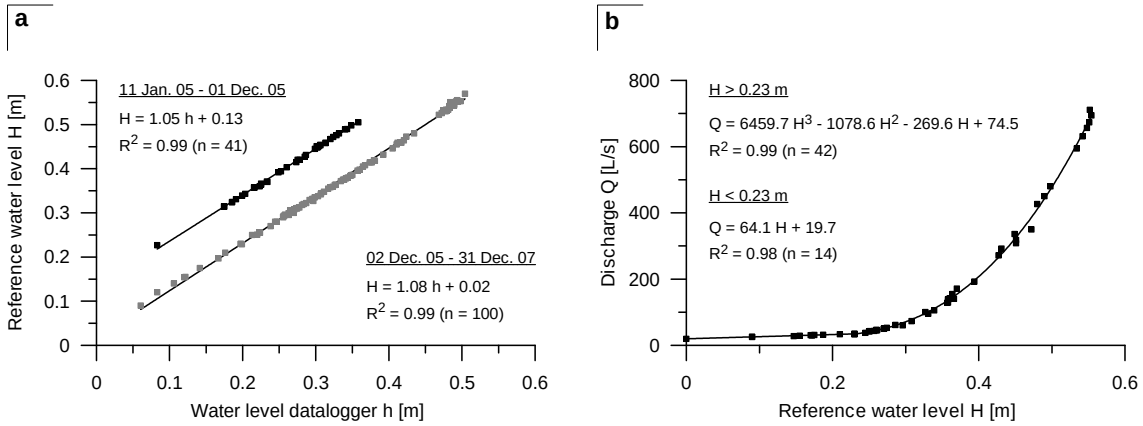

Fig. A.1 (**a**) Water level calibration curves and (**b**) stage-discharge rating curve for the Moulinet spring (junction of all eight Moulinet outlets, i.e. outlets 6A, 6B and 7A-F). The change in weir form at H = 0.23 m requires two equations.

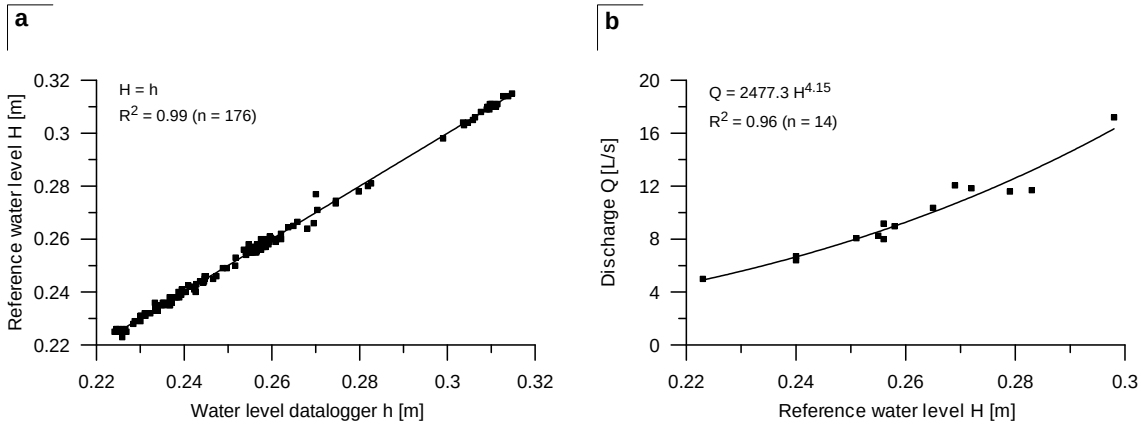

Fig. A.2 (**a**) Water level calibration curve and (**b**) stage-discharge rating curve for the Moulinet 6A outlet.

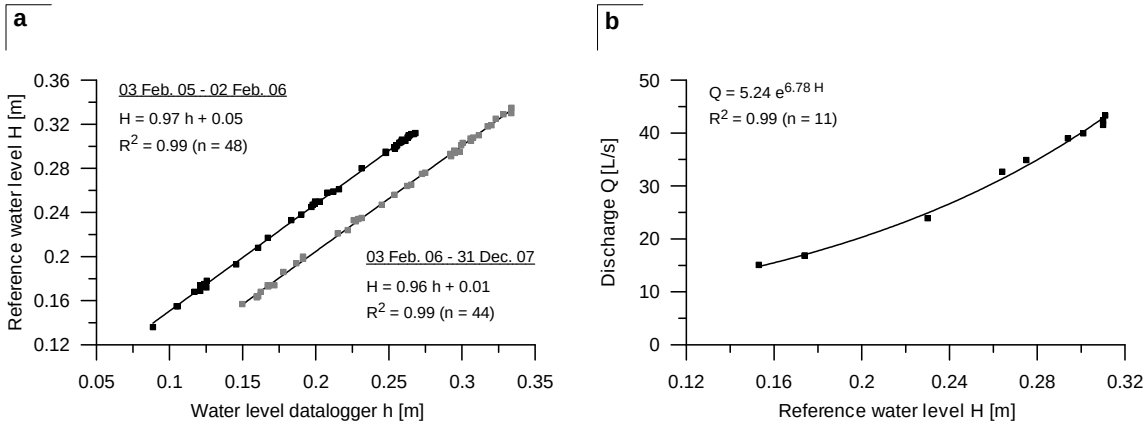

Fig. A.3 (**a**) Water level calibration curves and (**b**) stage-discharge rating curve for the Moulinet 6B outlet.

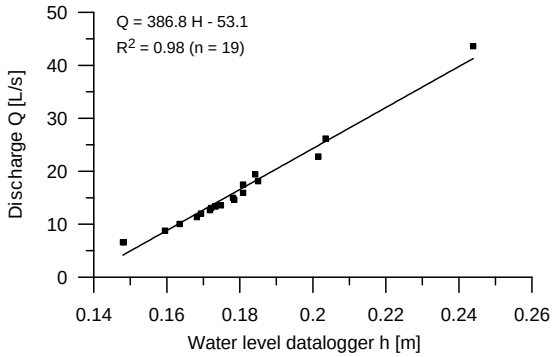

Fig. A.4 Stage-discharge rating curve for the Grange-Décoppet spring.

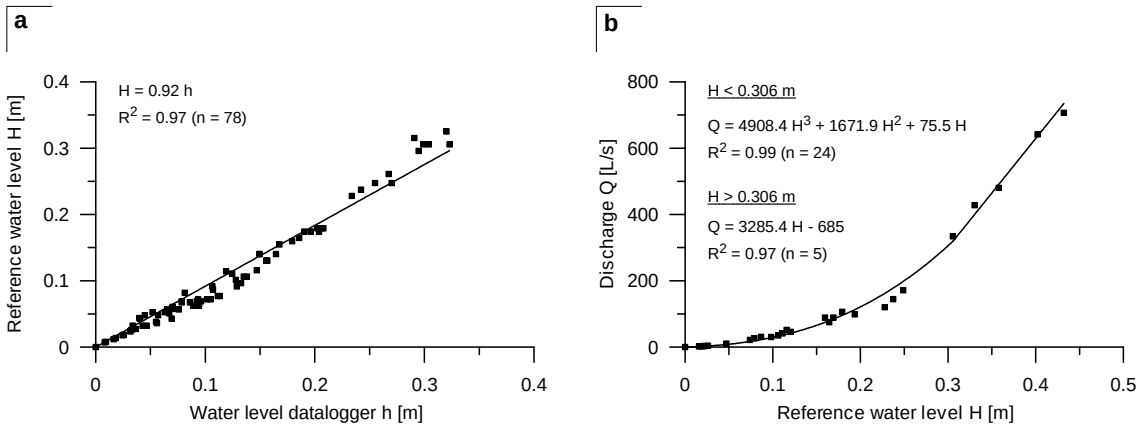

Fig. A.5 (**a**) Water level calibration curve and (**b**) stage-discharge rating curve for the Feurtille swallow hole. The change in weir form at H = 0.306 m requires two equations.

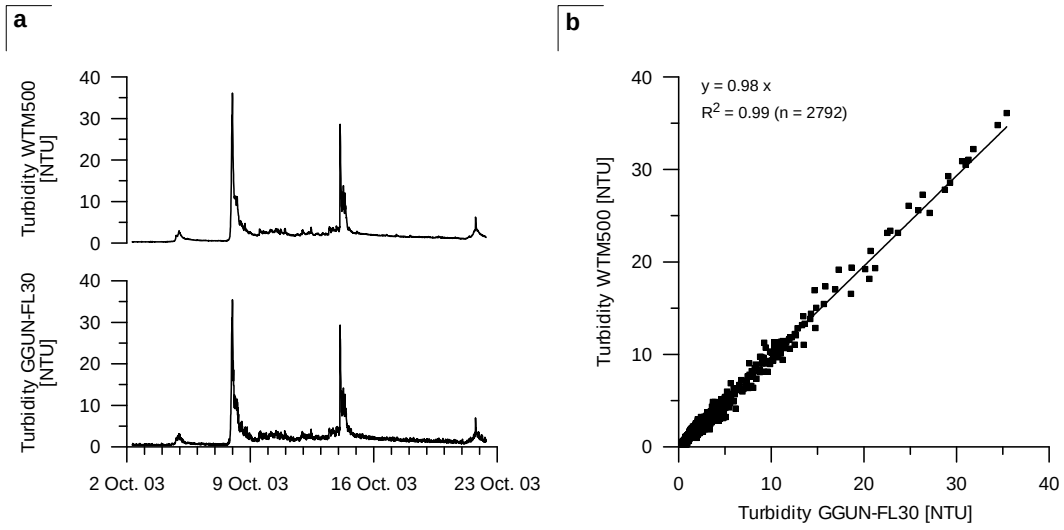

Fig. A.6 (**a**) Temporal changes in turbidity monitored at the Moulinet 6A outlet with both the GGUN-FL30 field fluorometer and the Sigrist-Photometer WTM500 turbidimeter. (**b**) Correlation of the data.

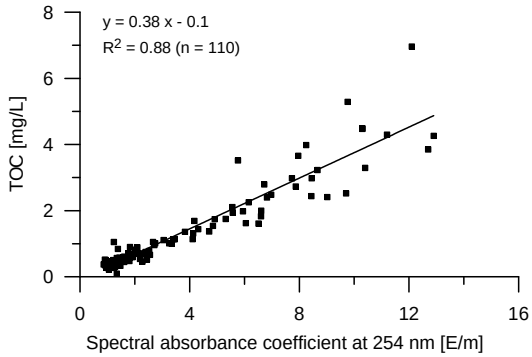

Fig. A.7 Correlation between the spectral absorbance coefficient at 254 nm, which was monitored continuously by the Sigrist-Photometer ColorPlus bypass absorptiometer at the Cossaux spring, and TOC content. Results are in accordance with manufacturer's instrument specification sheet (slope = 3/8 = 0.375).

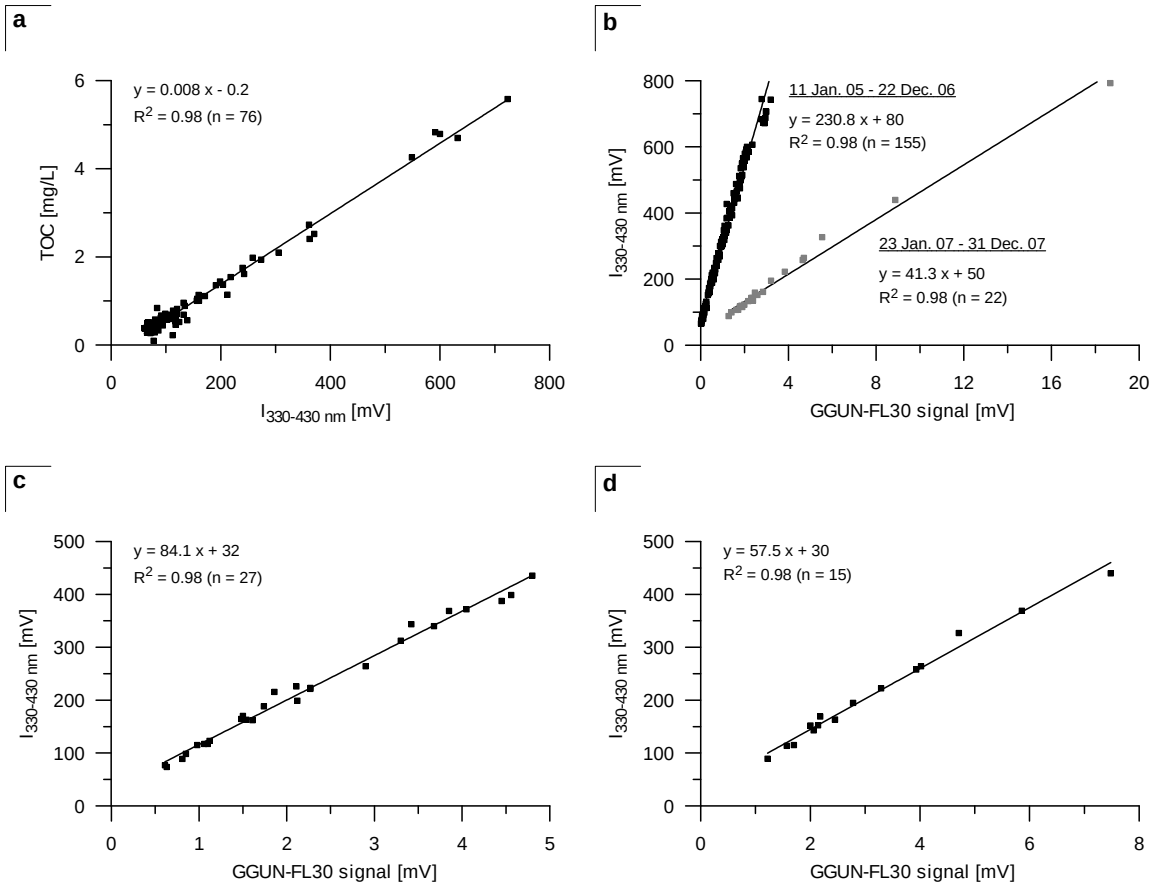

Fig. A.8 TOC calibration for the Moulinet 6A and 6B outlets and the Grange-Décoppet spring. (**a**) Correlation between maximum fluorescence intensity ($I_{330\text{-}430\ nm}$) obtained from synchronous excitation / emission scans (detection of fluorescence emission between 350 and 500 nm at 0.5 nm steps, using a constant delta lambda of 100 nm) and TOC content. (**b**, **c** and **d**) Correlation between the GGUN-FL30 fluorometer's signal and maximum fluorescence intensity ($I_{330\text{-}430\ nm}$) for the Moulinet 6A outlet, the Moulinet 6B outlet and the Grange-Décoppet spring, respectively.

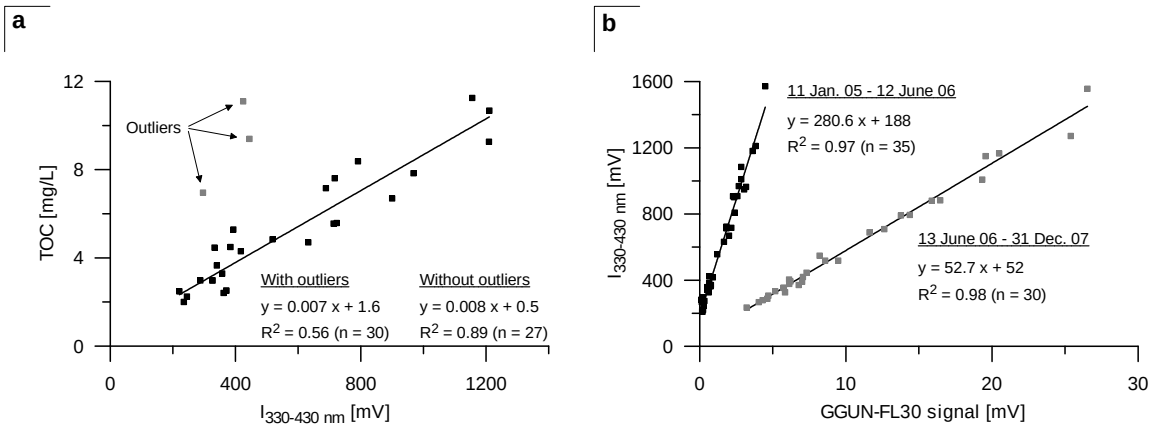

Fig. A.9 TOC calibration for the Feurtille swallow hole. (**a**) Correlation between maximum fluorescence intensity ($I_{330\text{-}430\ nm}$) obtained from synchronous excitation / emission scans (detection of fluorescence emission between 350 and 500 nm at 0.5 nm steps, using a constant delta lambda of 100 nm) and TOC content. (**b**) Correlation between the GGUN-FL30 field fluorometer's signal and maximum fluorescence intensity ($I_{330\text{-}430\ nm}$).

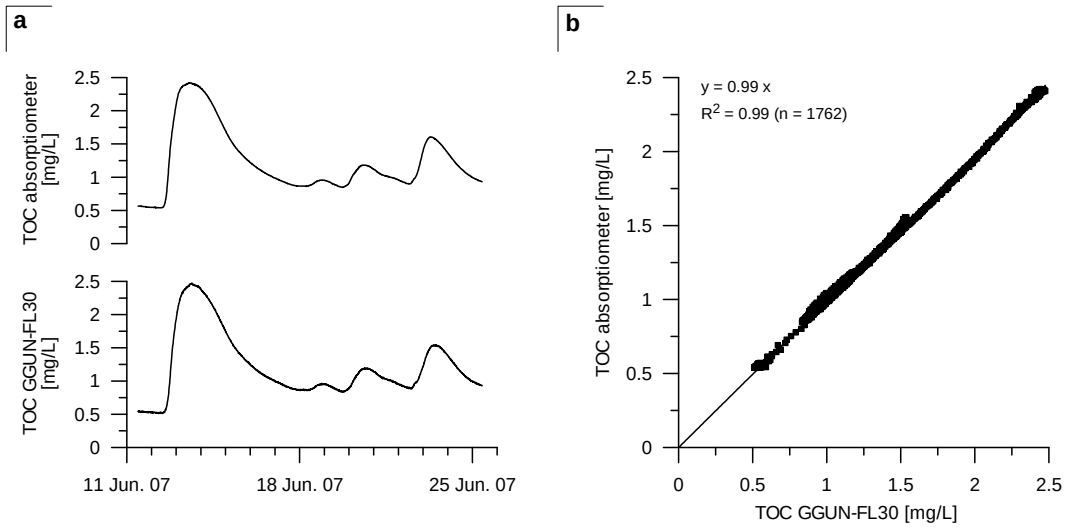

Fig. A.10 (**a**) Temporal changes in TOC content monitored at the Cossaux spring with both the GGUN-FL30 field fluorometer and the Sigrist-Photometer ColorPlus bypass absorptiometer. (**b**) Correlation of the data.

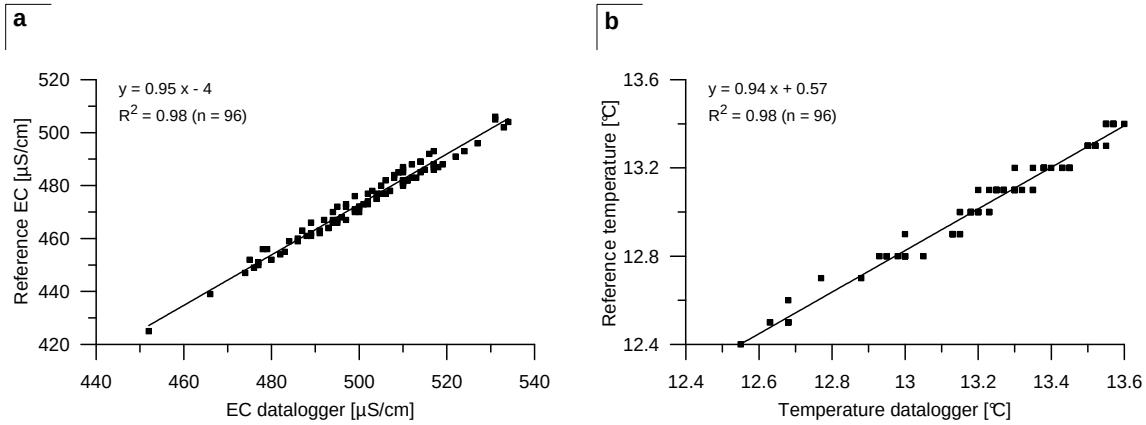

Fig. A.11 (**a**) Electrical conductivity (EC) and (**b**) temperature calibration curves for the Cossaux spring.

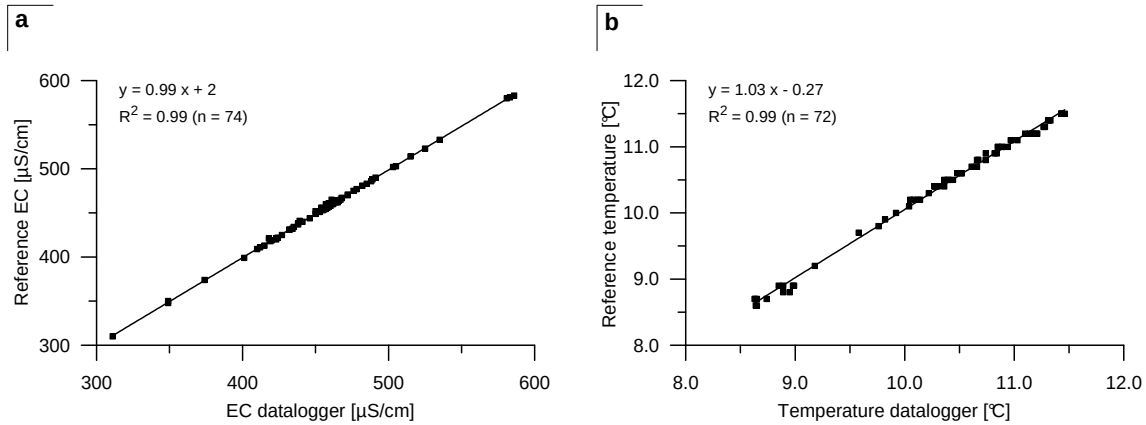

Fig. A.12 (**a**) Electrical conductivity (EC) and (**b**) temperature calibration curves for the Moulinet 6A outlet.

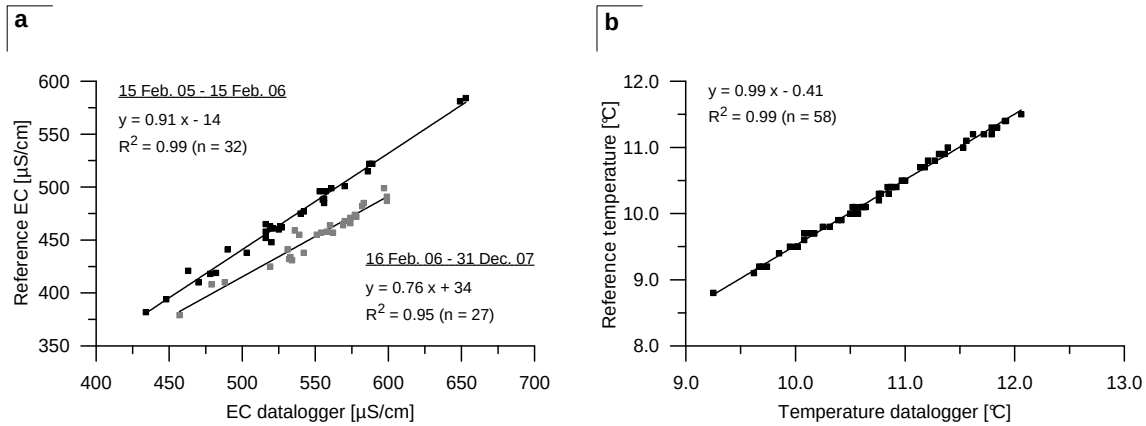

Fig. A.13 (**a**) Electrical conductivity (EC) and (**b**) temperature calibration curves for the Moulinet 6B outlet.

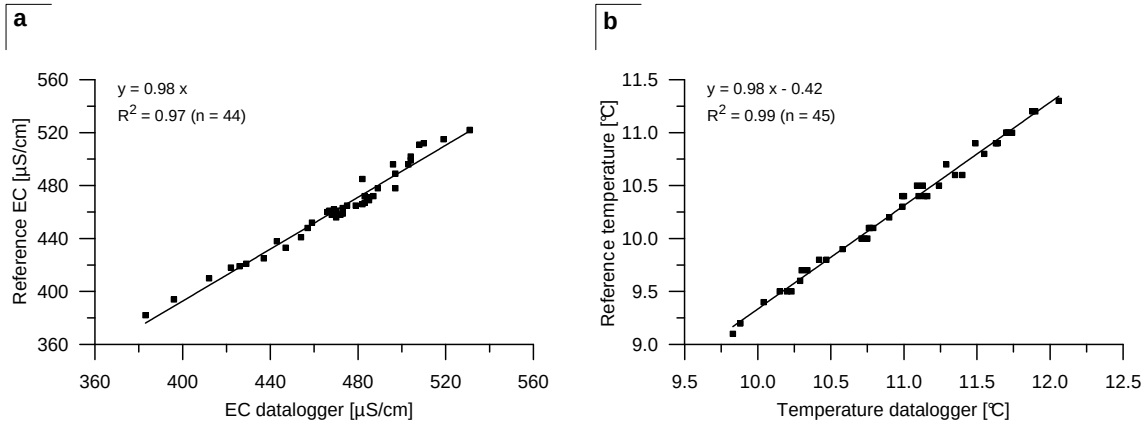

Fig. A.14 (**a**) Electrical conductivity (EC) and (**b**) temperature calibration curves for the Moulinet 7D and 7F outlets.

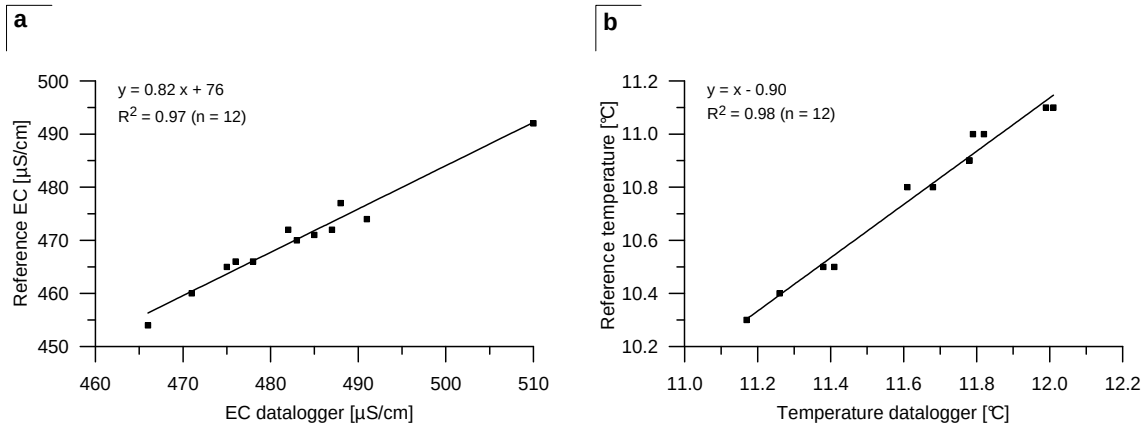

Fig. A.15 (**a**) Electrical conductivity (EC) and (**b**) temperature calibration curves for the Grange-Décoppet spring.

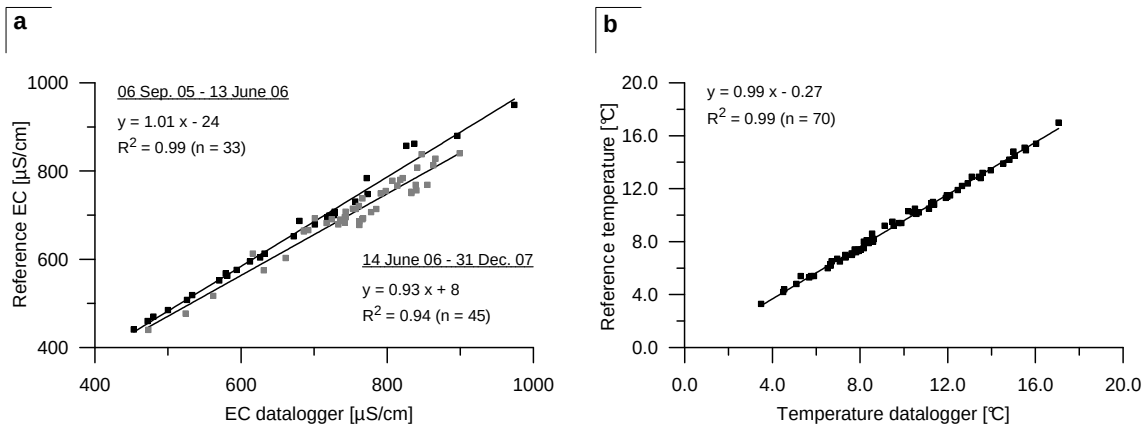

Fig. A.16 (**a**) Electrical conductivity (EC) and (**b**) temperature calibration curves for the Feurtille swallow hole.

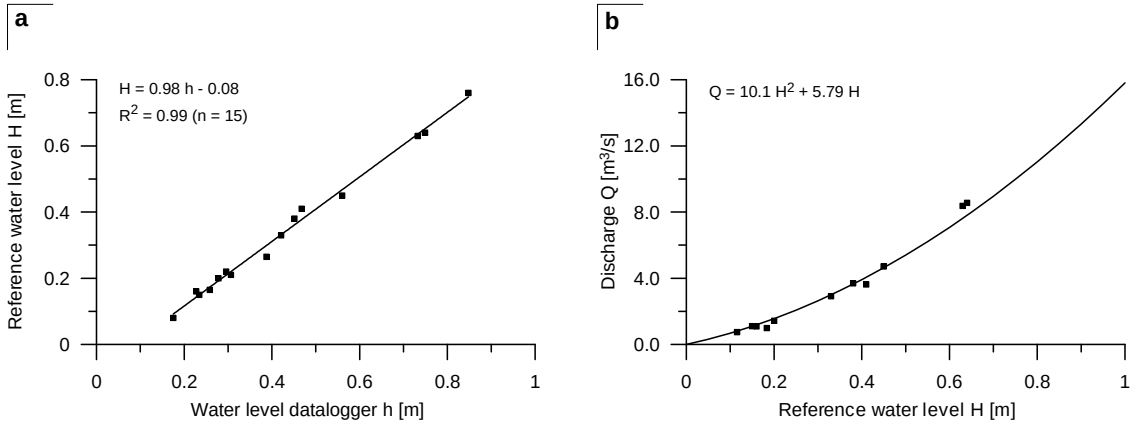

Fig. A.17 (**a**) Water level calibration curve and (**b**) stage-discharge rating curve for the Noiraigue spring. The stage-discharge rating curve was established in the 1970's by the SHGN (now FOEN, Federal Office for the Environment) and was verified by salt dilution gauging.

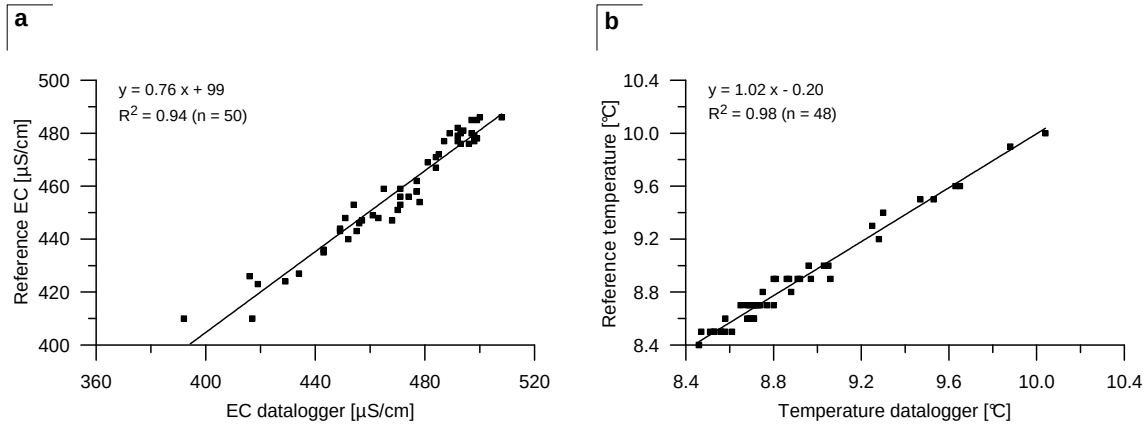

Fig. A.18 (**a**) Electrical conductivity (EC) and (**b**) temperature calibration curves for the Noiraigue spring.

Appendix B

From quantitative tracer tests towards a conceptual flow model of the Yverdon-les-Bains karst aquifer system

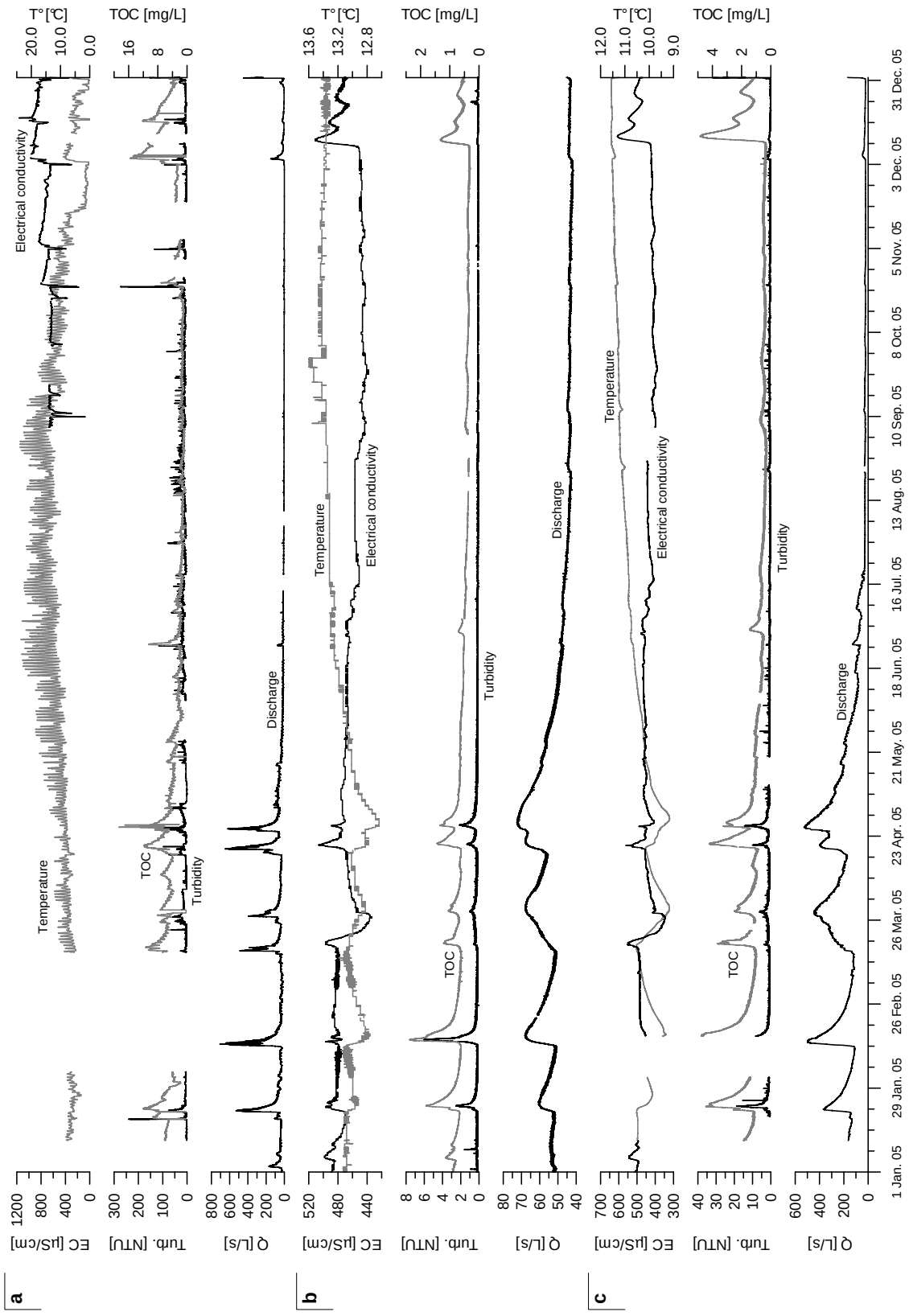

Fig. B.1 Temporal changes of discharge (Q), turbidity (Turb.), TOC, electrical conductivity (EC) and temperature (T°) at the Yverdon-les-Bains karst system during the year 2005. (**a**) Feurtille swallow hole, (**b**) Cossaux spring and (**c**) Moulinet spring.

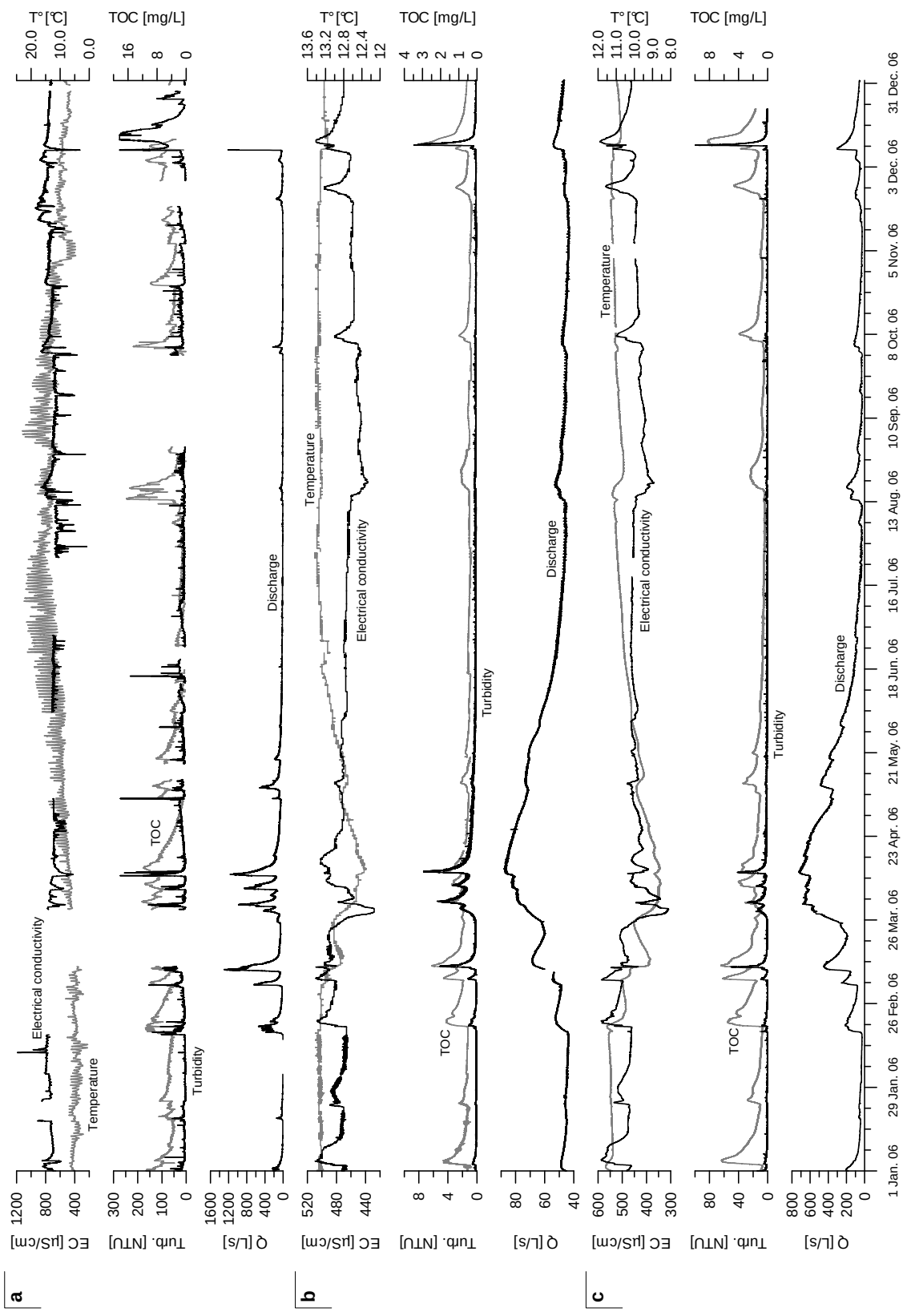

Fig. B.2 Temporal changes of discharge (Q), turbidity (Turb.), TOC, electrical conductivity (EC) and temperature (T°) at the Yverdon-les-Bains karst system during the year 2006. (**a**) Feurtille swallow hole, (**b**) Cossaux spring and (**c**) Moulinet spring.

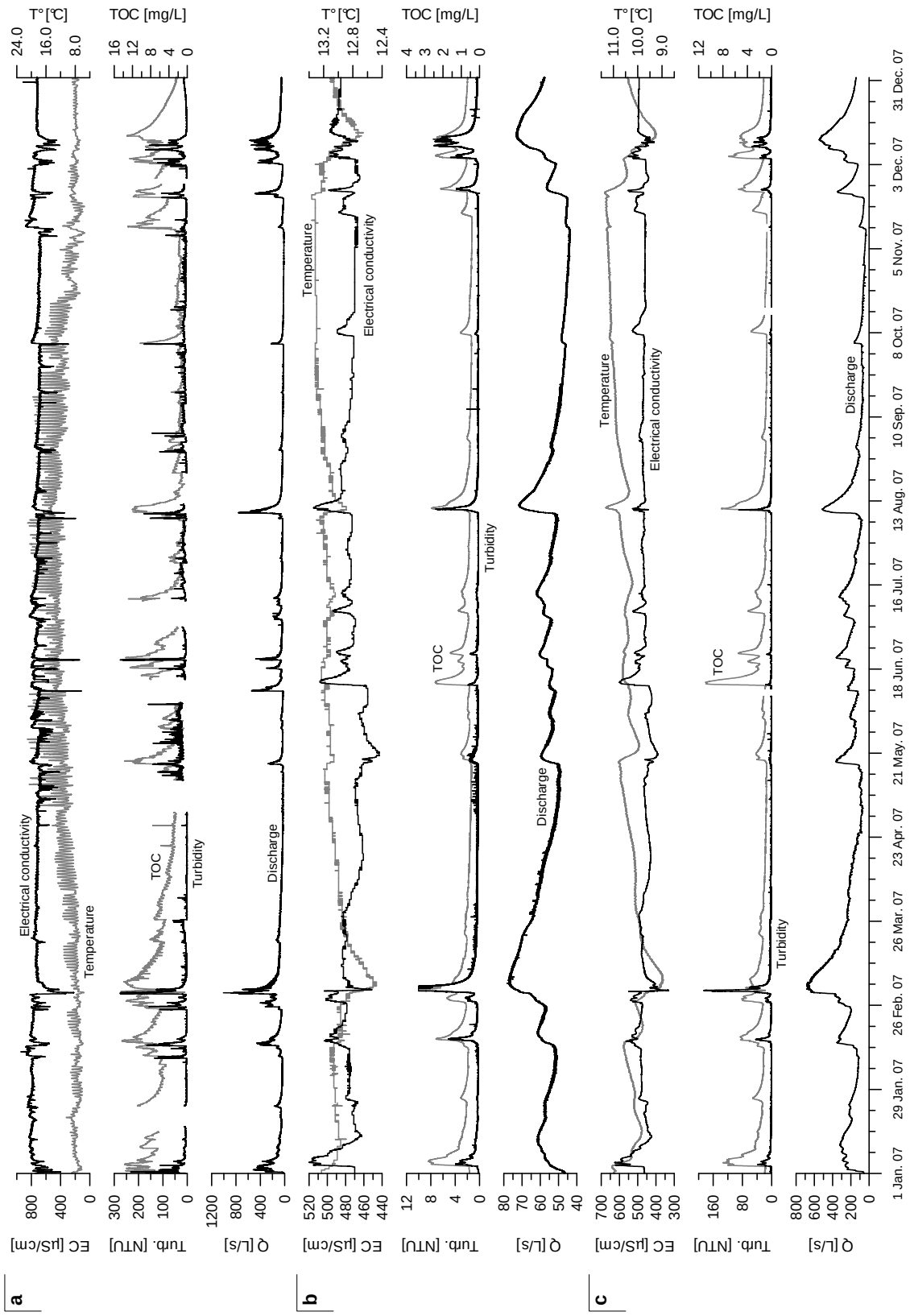

Fig. B.3 Temporal changes of discharge (Q), turbidity (Turb.), TOC, electrical conductivity (EC) and temperature (T°) at the Yverdon-les-Bains karst system during the year 2007. (**a**) Feurtille swallow hole, (**b**) Cossaux spring and (**c**) Moulinet spring.

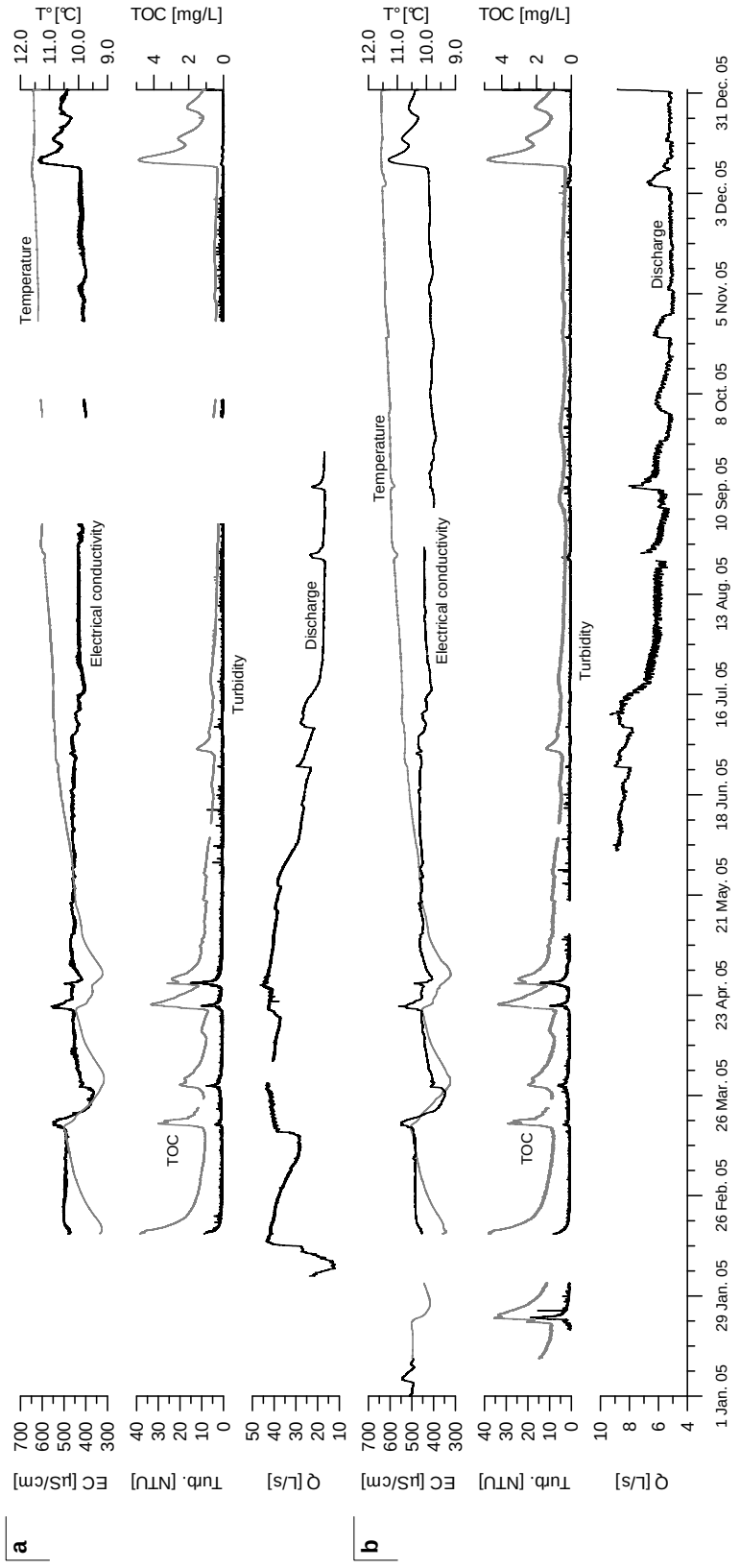

Fig. B.4 Temporal changes of discharge (Q), turbidity (Turb.), TOC, electrical conductivity (EC) and temperature (T°) at the outlets (**a**) 6B and (**b**) 6A of the Moulinet spring during the year 2005.

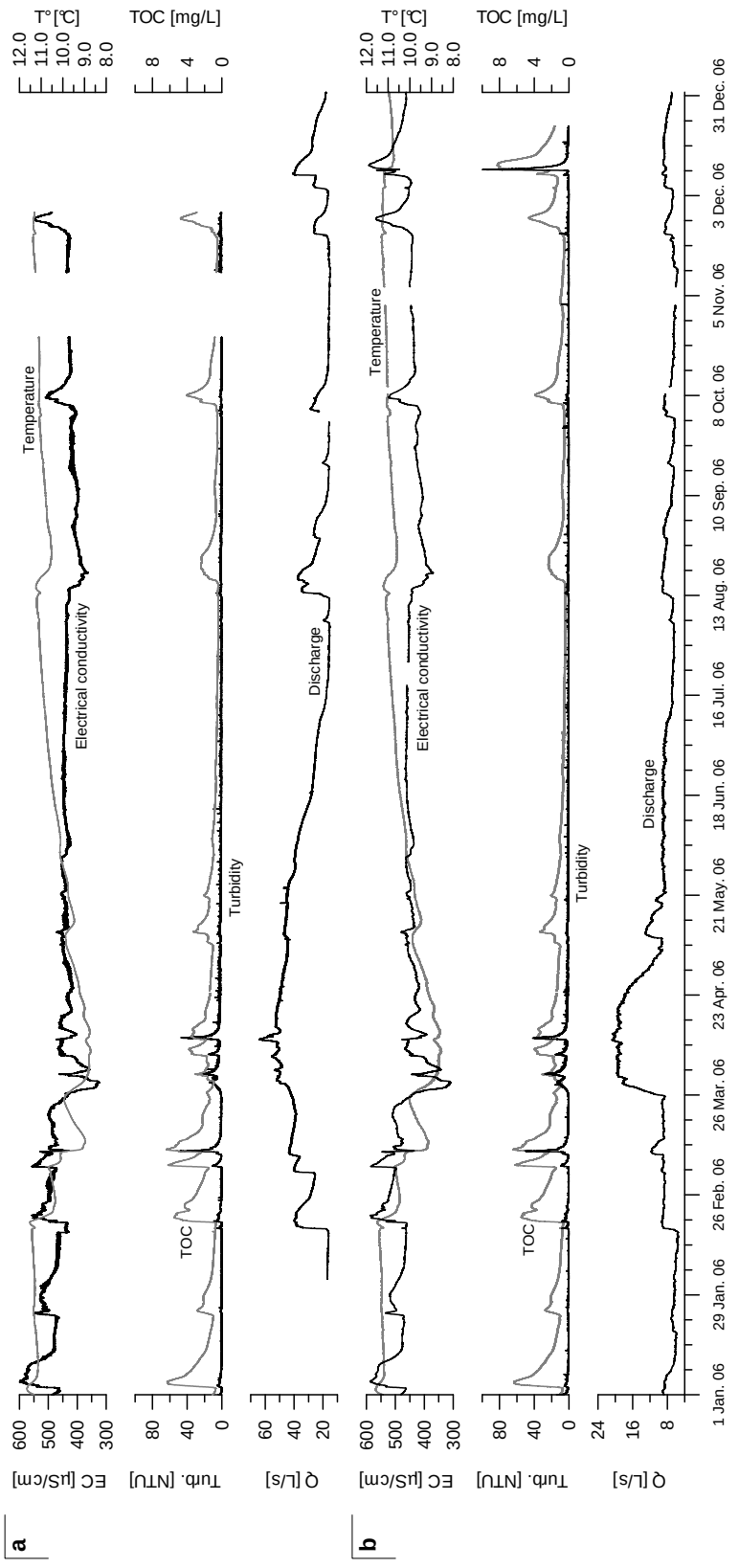

Fig. B.5 Temporal changes of discharge (Q), turbidity (Turb.), TOC, electrical conductivity (EC) and temperature (T°) at the outlets (**a**) 6B and (**b**) 6A of the Moulinet spring during the year 2006.

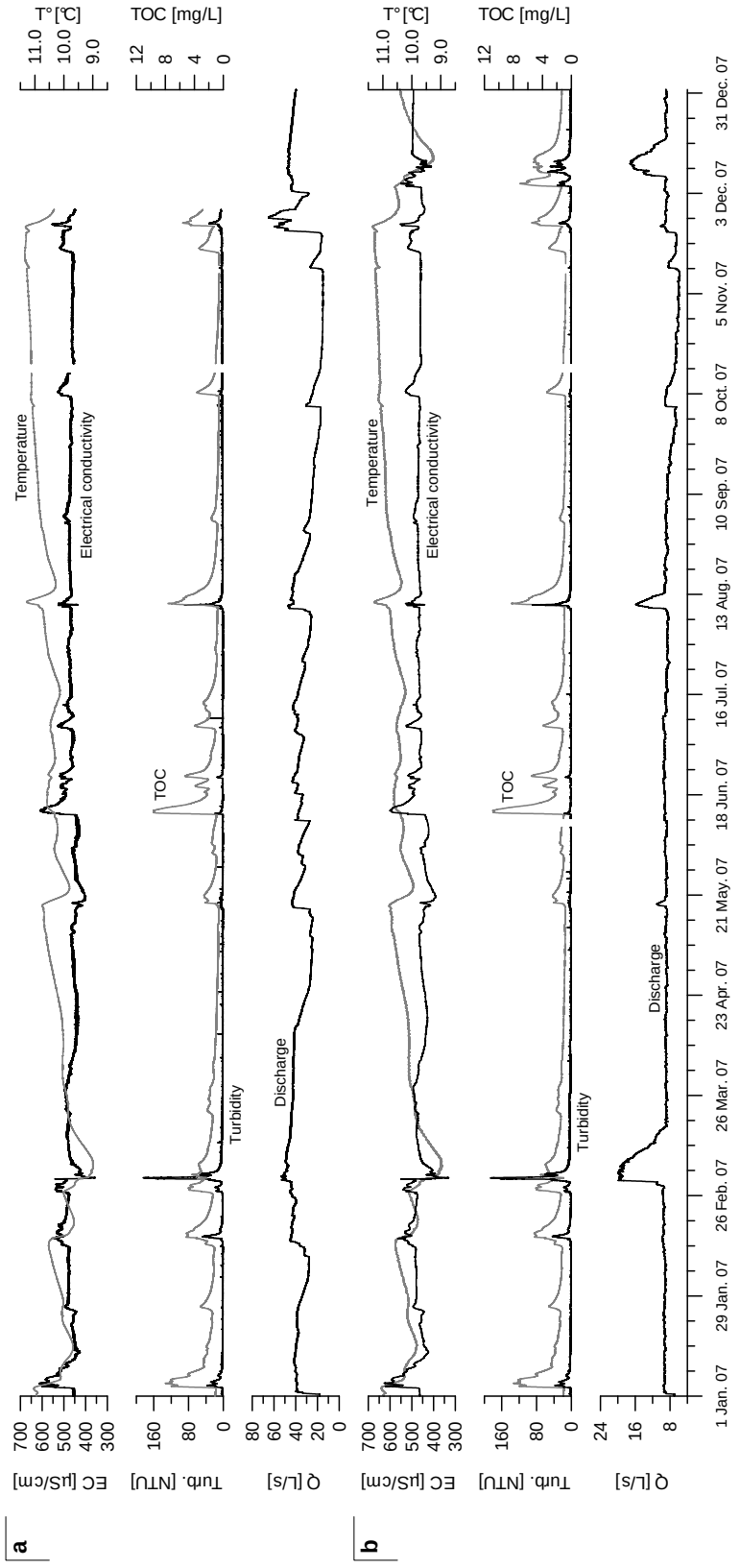

Fig. B.6 Temporal changes of discharge (Q), turbidity (Turb.), TOC, electrical conductivity (EC) and temperature (T°) at the outlets (**a**) 6B and (**b**) 6A of the Moulinet spring during the year 2007.

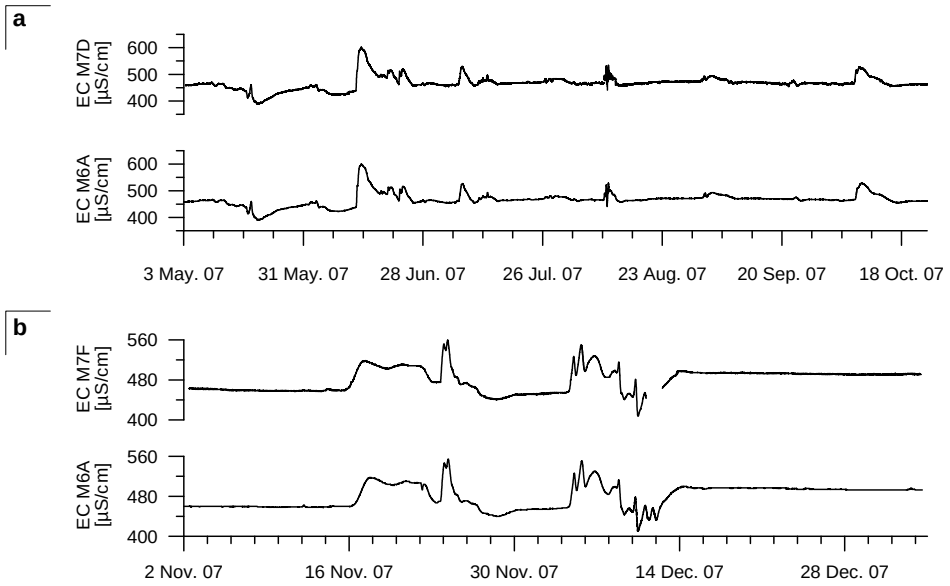

Fig. B.7 Temporal changes of electrical conductivity (EC) at several outlets of the Moulinet spring: (**a**) outlet 6A (M6A) vs. outlet 7D (M7D) and (**b**) outlet 6A (M6A) vs. outlet 7F (M7F).

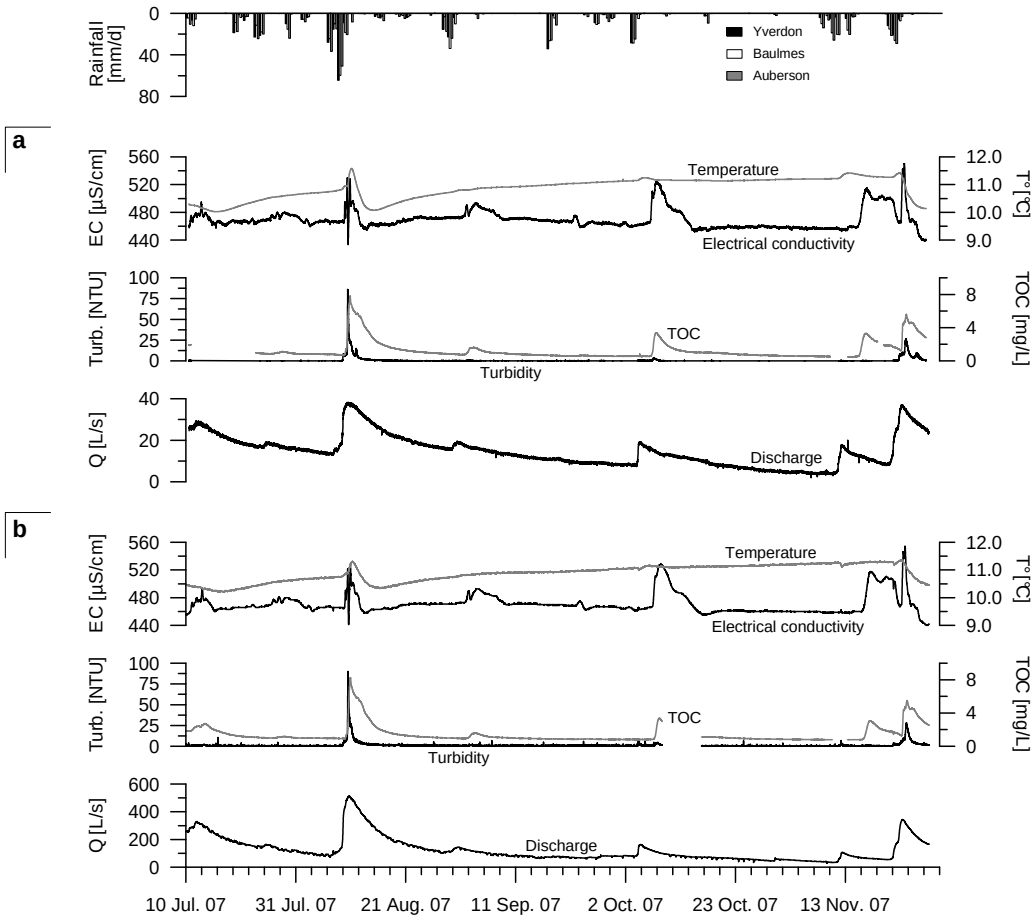

Fig. B.8 Temporal changes of discharge (Q), turbidity (Turb.), TOC, electrical conductivity (EC) and temperature (T°) at the (**a**) Grange-Décoppet and (**b**) Moulinet springs.

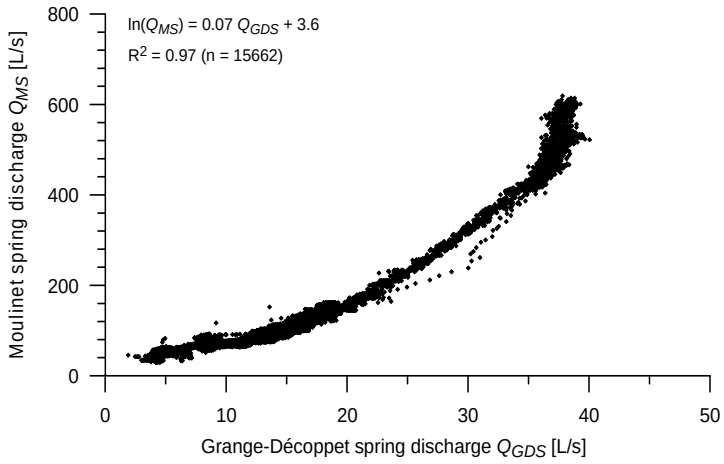

Fig. B.9 Grange-Décoppet spring discharge (Q_{GDS}) versus Moulinet spring discharge (Q_{MS}).

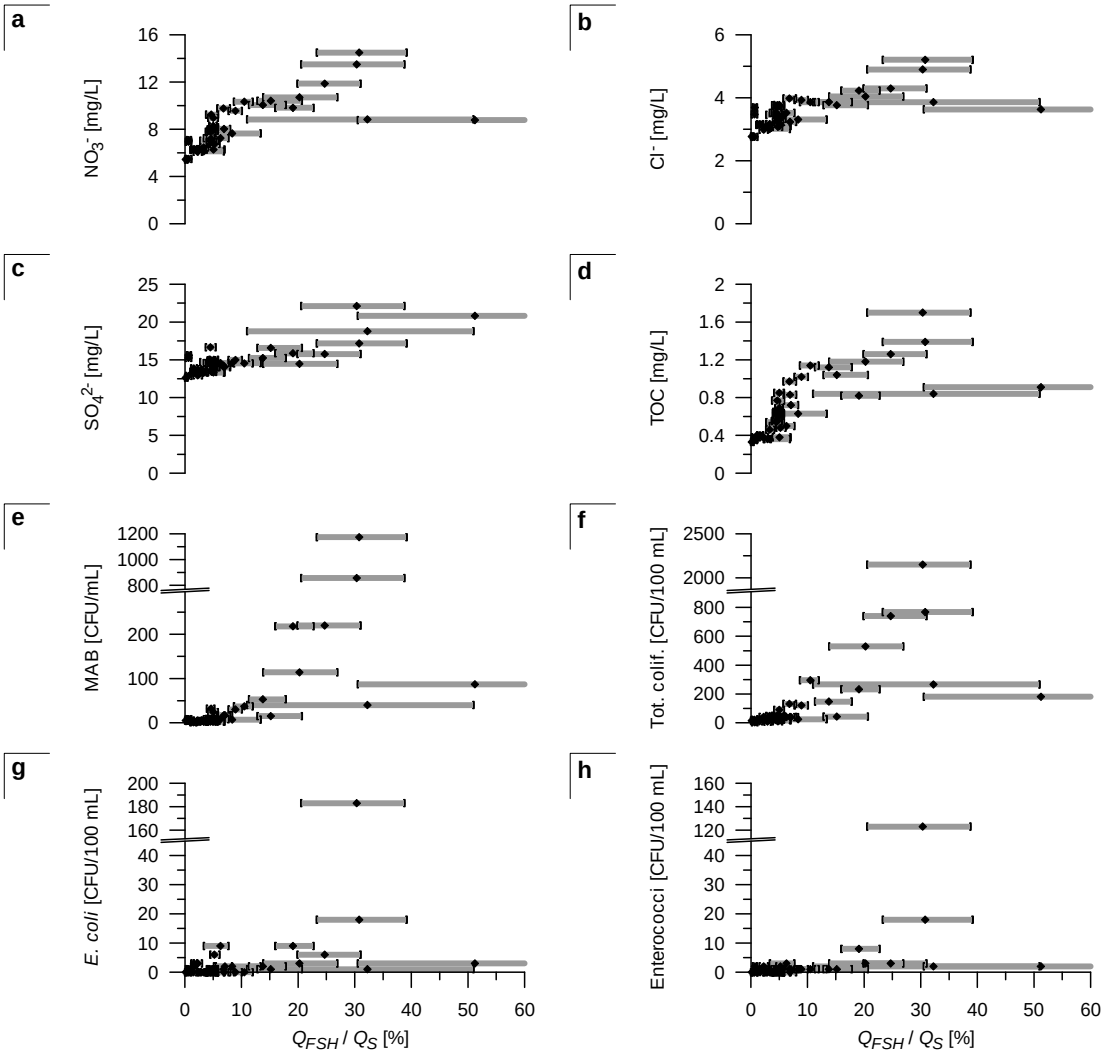

Fig. B.10 Feurtille swallow hole contribution to the system discharge during the calculated infiltration time lag (Q_{FSH} / Q_S) versus major ion and water quality indicator bacteria contents of samples collected at the Cossaux spring: (**a**) NO_3^-, (**b**) Cl^-, (**c**) SO_4^{2-}, (**d**) TOC, (**e**) mesophilic aerobic bacteria (MAB), (**f**) total coliforms (Tot. colif.), (**g**) *E. coli* and (**h**) enterococci. Mean values (diamonds) with respective minimum and maximum values are shown.

Table B.1 Overview of the monitoring programs of the tracer experiments carried out at the Yverdon-les-Bains karst aquifer system. c: continuous monitoring; as: automatic sampler; ms: manual sampling; is: integrative sampling (charcoal bags).

Observation point		Feurtille swallow hole					La Côte
		1 Sept. 03	21 Mar. 05	2 June 05	22 Apr. 06	2 Nov. 07	11 Apr. 07
Cossaux spring		c / ms	c / as / ms	c / as / ms	c / as / ms	c / as / ms	c / ms / is
Moulinet spring	Outlet 6A	c / ms	c / as / ms	c / as / ms	c / as / ms	c / as / ms	c / ms / is
	Outlet 6B	as / ms	c / ms	c / ms	c / ms	c / ms	c / ms
	Outlets 7A-7F	ms	ms	ms	ms	ms	ms / is
Grange-Décoppet spring		ms	ms	ms	ms	c/ms	c / ms / is
Observation period		*until end of tracer breakthrough*					*6 months*

Appendix C

Particle-size distribution as indicator for faecal bacteria contamination of groundwater from karst springs

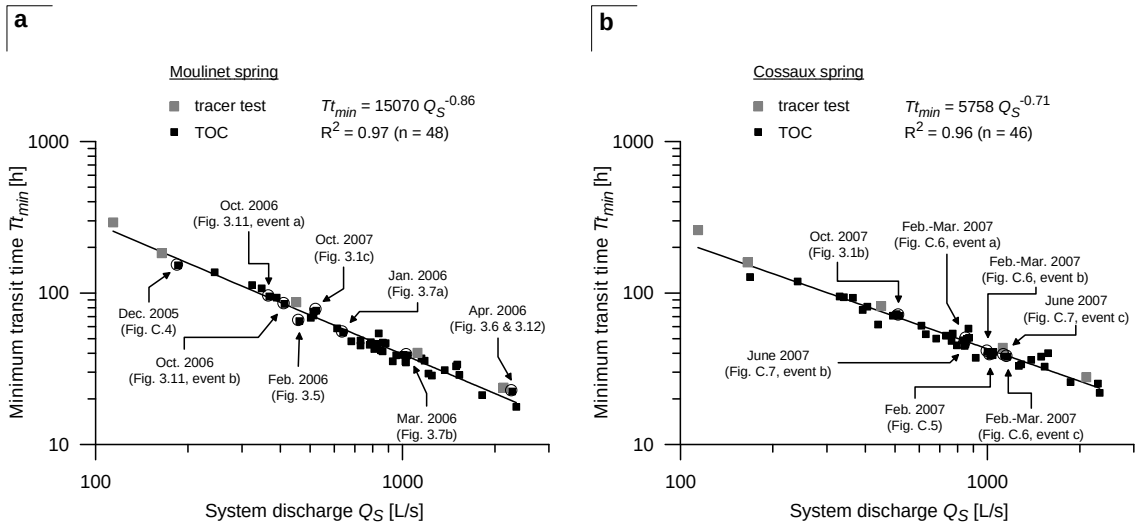

Fig. C.1 Minimum transit times (Tt_{min}) between the swallow hole and the (**a**) Moulinet and (**b**) Cossaux springs as function of the system discharge (Q_S). Results were obtained from tracer tests and monitoring of TOC following rainfall events. Minimum transit times are spans of time between the moment of injection (artificial tracers), or discharge increase at the swallow hole (TOC), and the time when the respective parameter started to increase at the springs.

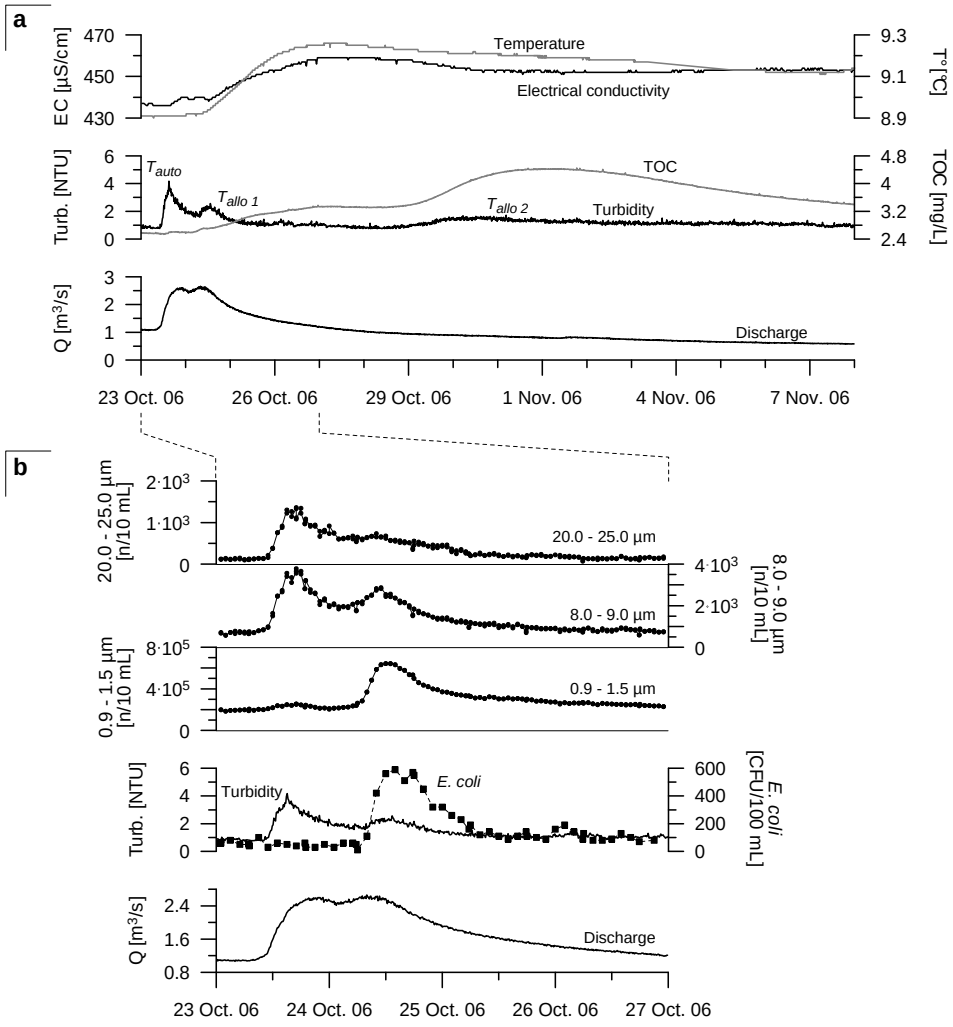

Fig. C.2 Dynamics of suspended matter and *E. coli* at the Noiraigue spring (Noiraigue karst aquifer system) following a rainfall event (10.3 and 13.5 mm on the 22nd and 23rd of October 2006, respectively). (**a**) Autochthonous (T_{auto}) and allochthonous (T_{allo}) turbidity signals. (**b**) Temporal changes in *E. coli* content and PSD. Q: discharge; Turb.: turbidity; EC: electrical conductivity; T°: temperature.

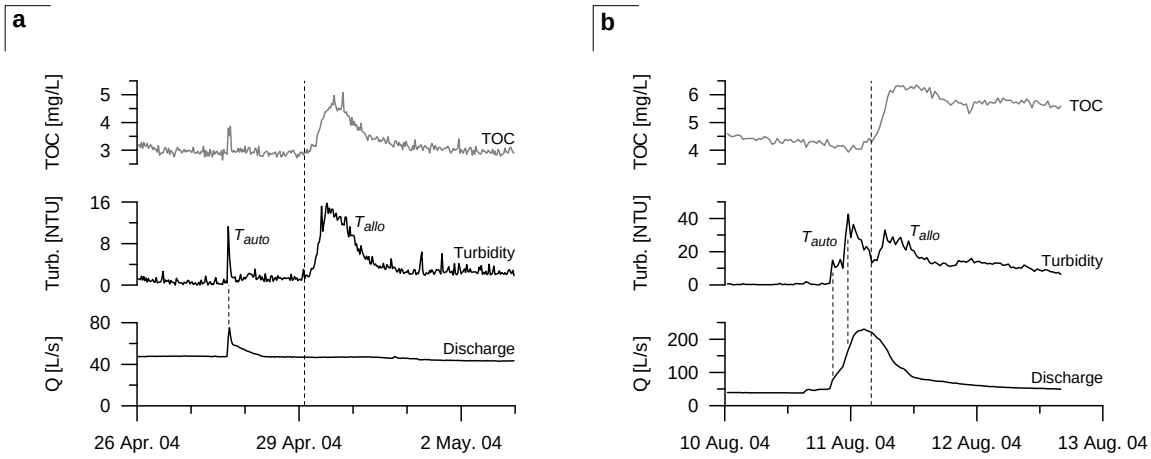

Fig. C.3 Autochthonous (T_{auto}) and allochthonous (T_{allo}) turbidity signals monitored at the "Milandrine upstream" station in the Milandre cave system, Switzerland: (**a**) response to a small rainfall event (3.7 mm on the 27th of April 2004) and (**b**) response to a major rainfall event (18.6 mm on the 10th of August 2004). Q: discharge; Turb.: turbidity. Data were provided by L. Savoy.

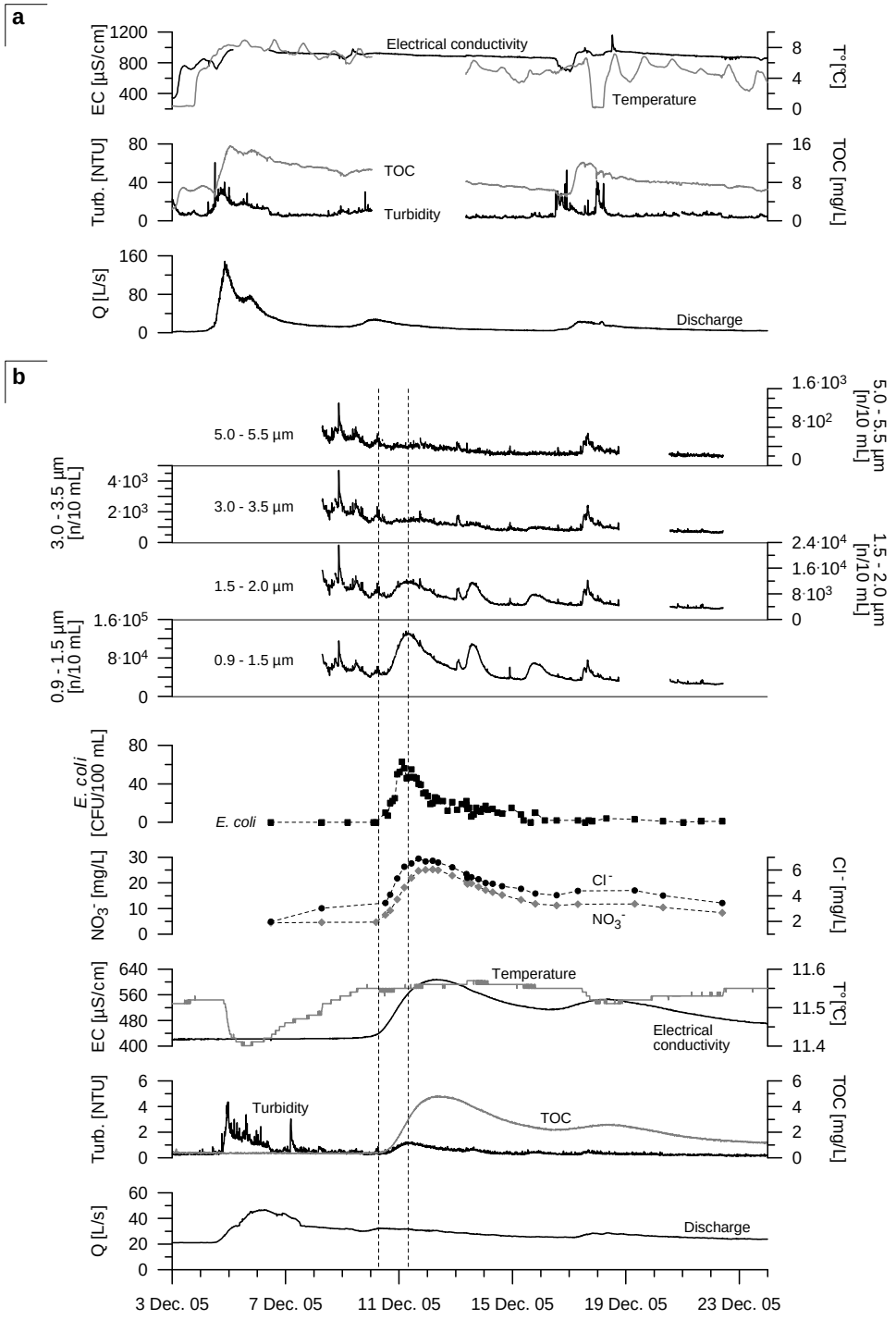

Fig. C.4 Temporal changes in *E. coli* content and PSD at the Moulinet spring following a period of snowmelt and rainfall in the recharge area of the Feurtille swallow hole. (**a**) Feurtille swallow hole and (**b**) Moulinet spring. Q: discharge; Turb.: turbidity; EC: electrical conductivity; T°: temperature.

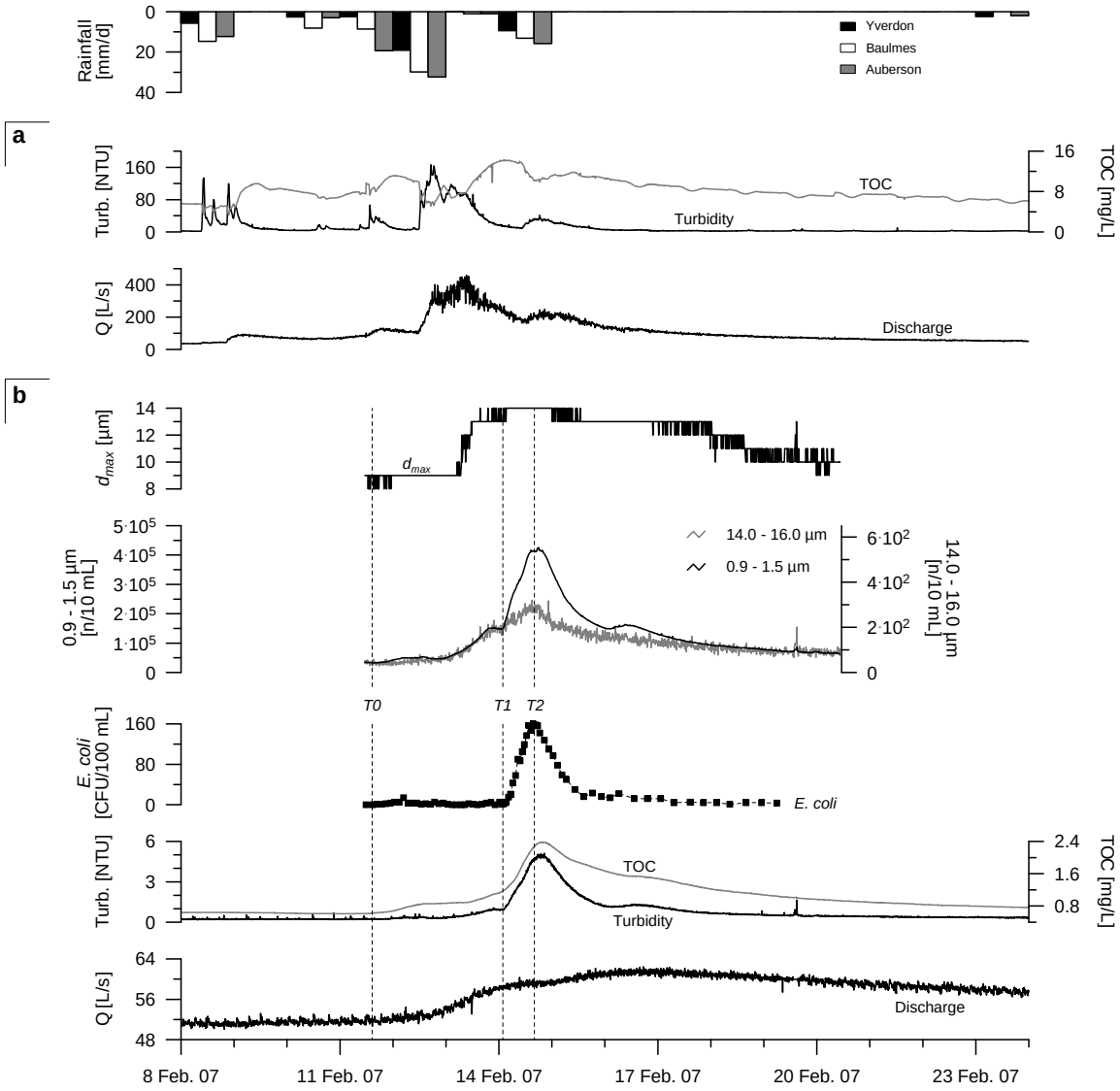

Fig. C.5 Temporal changes in *E. coli* content and PSD at the Cossaux spring in response to the February 2007 storm event. (**a**) Feurtille swallow hole and (**b**) Cossaux spring. Q: discharge; Turb.: turbidity; *T0*: pre-storm conditions; *T1*: maximum strictly autochthonous turbidity / first arrival of allochthonous turbidity and *E. coli* from the swallow hole; *T2*: maximum allochthonous turbidity.

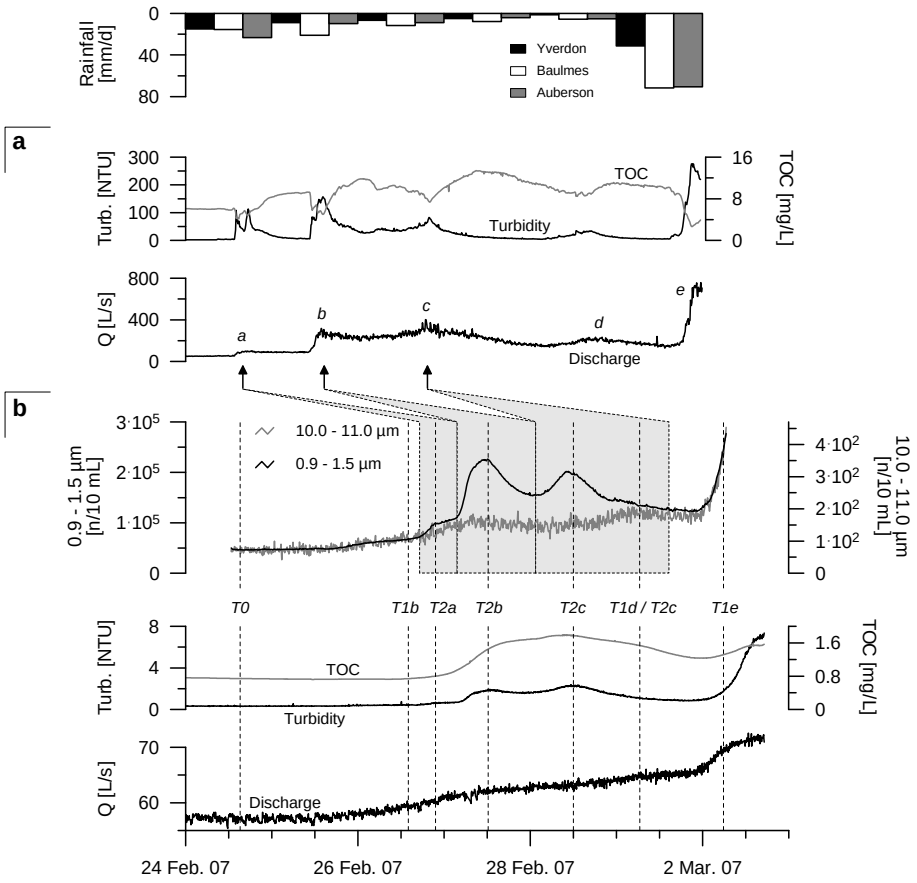

Fig. C.6 Temporal changes in PSD at the Cossaux spring in response to the February – March 2007 consecutive storm events. (**a**) Feurtille swallow hole and (**b**) Cossaux spring. Q: discharge; Turb.: turbidity; *T0*: pre-storm conditions; *T1*: autochthonous turbidity; *T2*: allochthonous turbidity.

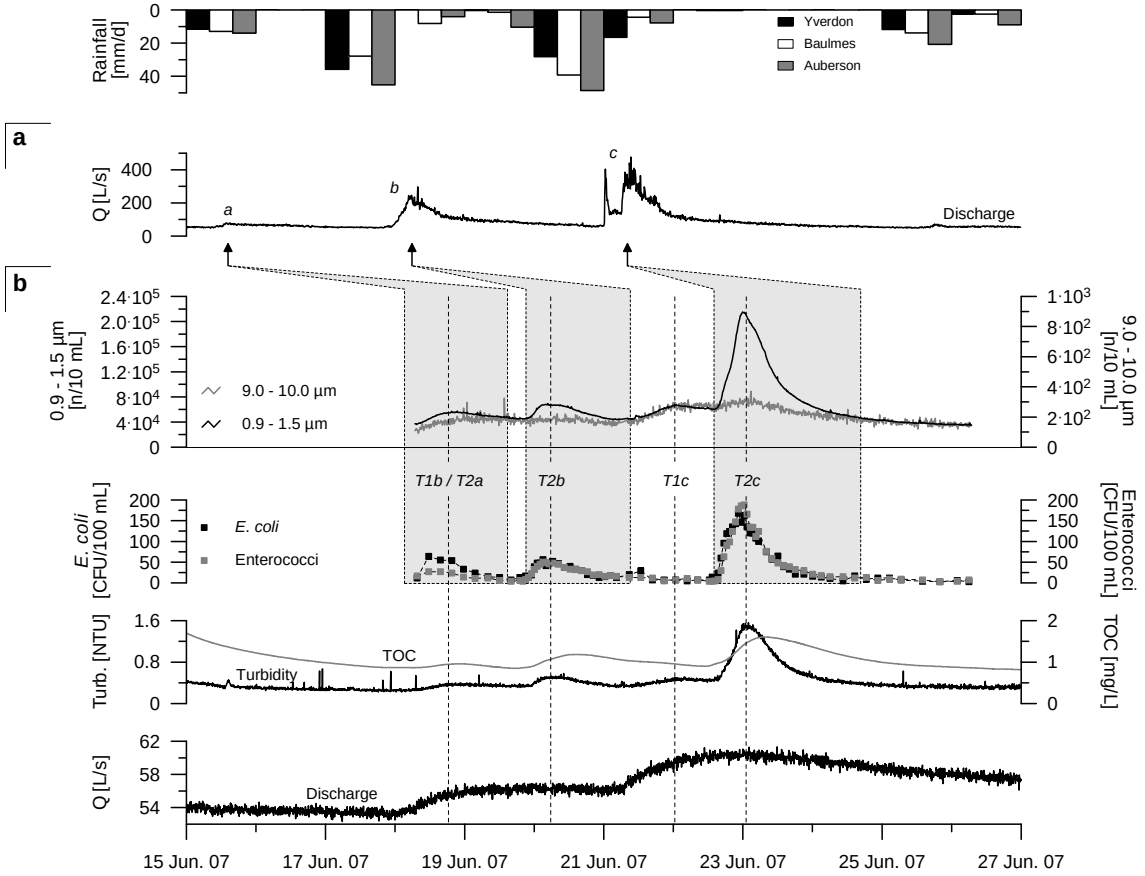

Fig. C.7 Temporal changes in *E. coli* and enterococci contents and PSD at the Cossaux spring in response to the June 2007 consecutive storm events. (**a**) Feurtille swallow hole and (**b**) Cossaux spring. Q: discharge; Turb.: turbidity; *T1*: autochthonous turbidity; *T2*: allochthonous turbidity.

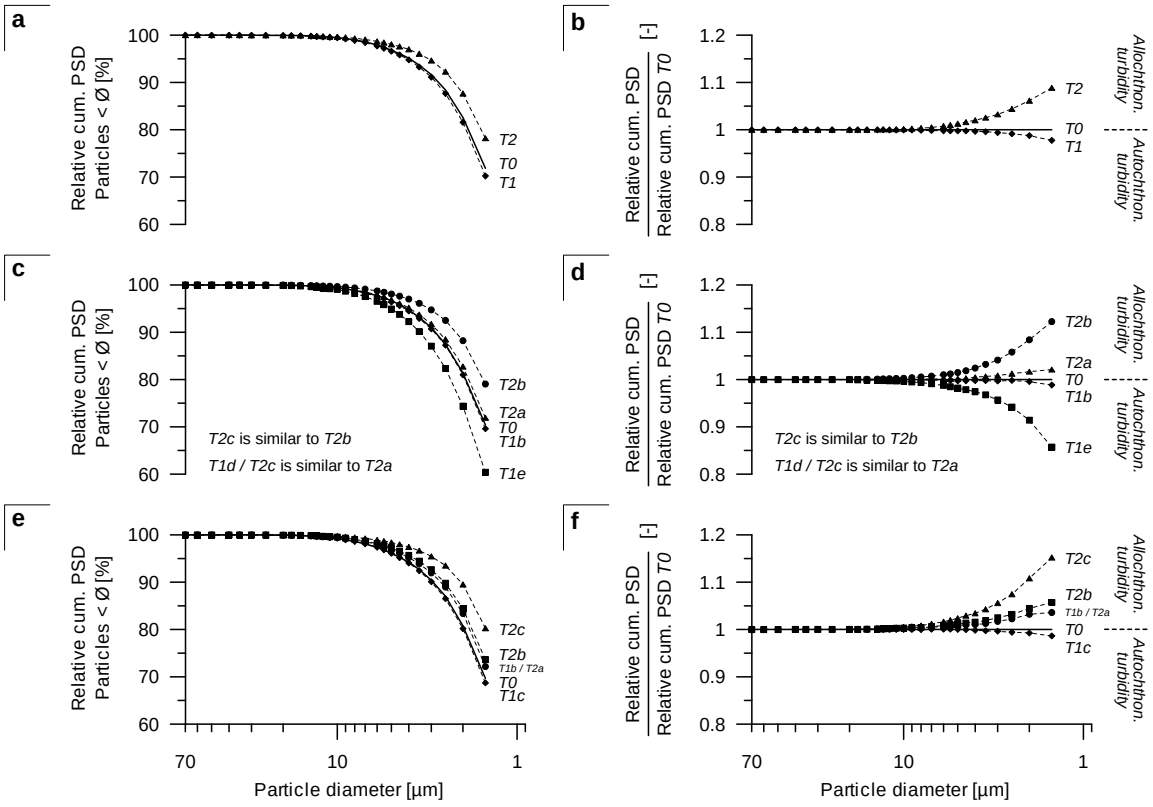

Fig. C.8 Analysis of selected PSD curves from the Cossaux spring during (**a** and **b**) the February 2007 storm event (sampling times *T* are shown in Fig. C.5, Appendix C), (**c** and **d**) the February – March 2007 consecutive storm events (Fig. C.6, Appendix C) and (**e** and **f**) the June 2007 consecutive storm events (Fig. C.7, Appendix C). A relative decrease of finer particles (0.9 to 10 µm) with respect to pre-storm reference PSDs (*T0*) is indicative of autochthonous turbidity (*T1*), while a relative increase of finer particles characterises allochthonous turbidity (*T2*) and thus the possible presence of faecal bacteria contamination.

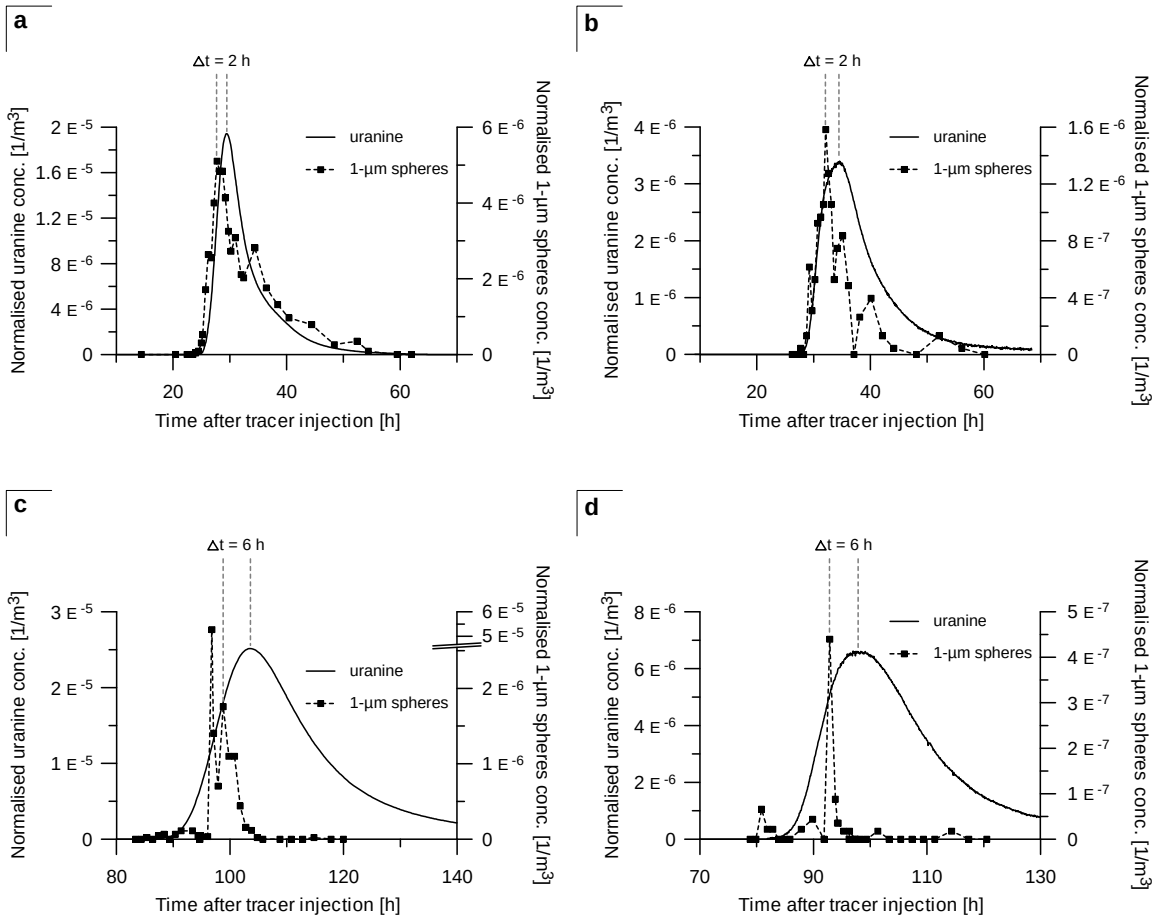

Fig. C.9 Breakthrough curves of the comparative tracer tests (1-µm spheres and uranine) performed at the Yverdon-les-Bains karst aquifer system during (**a** and **b**) high-flow conditions and (**c** and **d**) medium-flow conditions. (**a** and **c**) breakthrough curves monitored at the Moulinet spring and (**b** and **d**) breakthrough curves monitored at the Cossaux spring. Tracer concentrations were normalised to mass input (uranine) and particle number input (1-µm spheres).

Table C.1 Summary of the results of the comparative tracer tests performed at the Yverdon-les-Bains karst aquifer system.

Location	Property	Unit	2 June 05 tracer test		22 Apr. 06 tracer test	
			uranine	1-µm spheres	uranine	1-µm spheres
Moulinet spring (MS)	Discharge Q_{MS} [a]	[L/s]	125	125	560	560
	$t_{\text{first detection}}$ [b]	[h]	86.9	85.4	23.7	24.0
	$t_{\text{peak concentration}}$ [c]	[h]	103.5	96.8	29.4	27.7
	Recovery R_{MS}	[%]	26.1	1.5	28.8	9.4
Cossaux spring (CS)	Discharge Q_{CS} [a]	[L/s]	52	52	81	81
	$t_{\text{first detection}}$ [b]	[h]	81.9	80.9	27.8	27.7
	$t_{\text{peak concentration}}$ [c]	[h]	98.4	92.9	34.6	32.1
	Recovery R_{CS}	[%]	3.2	0.02	1.1	0.2
MS + CS	Total recovery	[%]	29.3	1.5	29.9	9.6

[a] Mean discharge during the tracer test

[b] Time of first detection

[c] Time of peak concentration

Appendix D

Percolation and particle transport in the unsaturated zone of karst aquifers

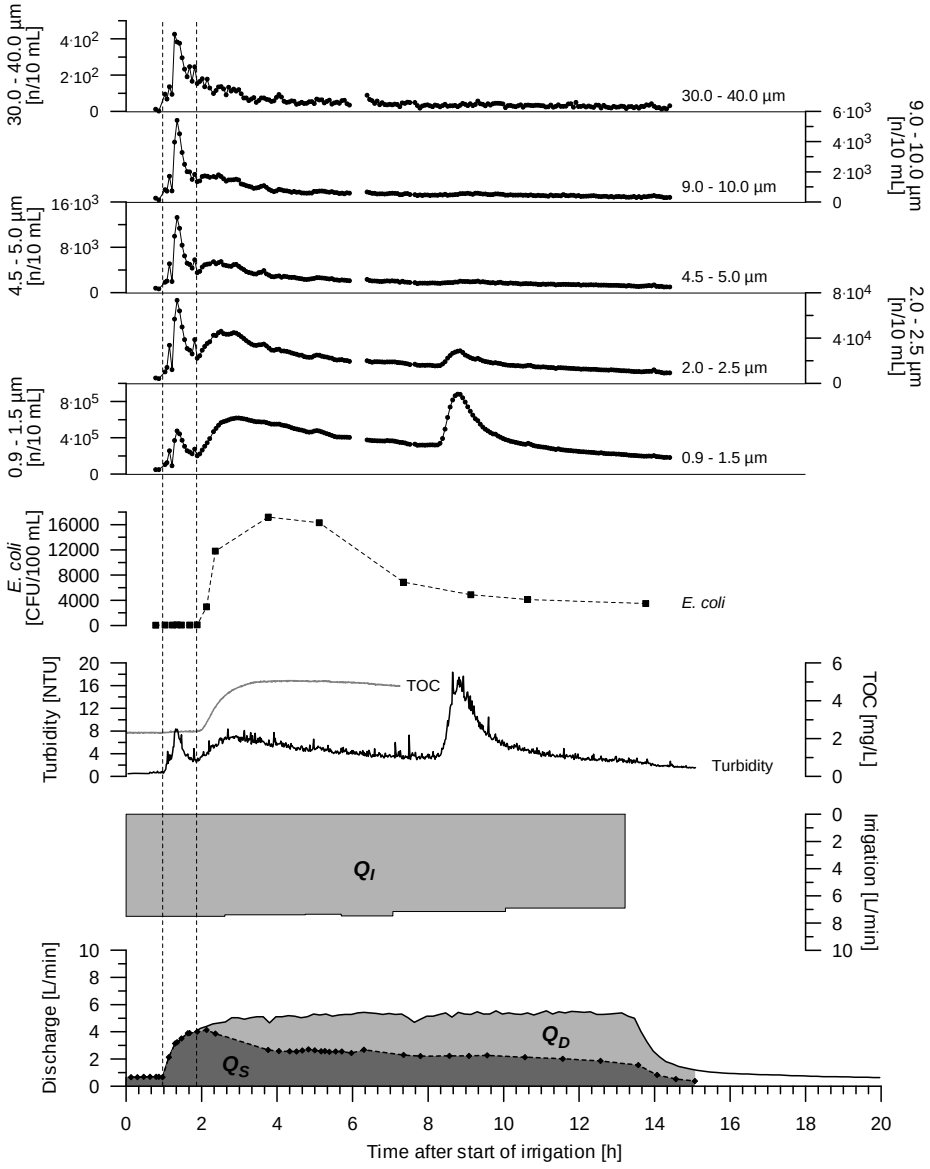

Fig. D.1 Temporal changes in *E. coli* content and PSD at the water outlet in the Vers-chez-le-Brandt cave during the September 2005 long-term irrigation experiment. Pulse-through turbidity is characterised by increases of all particle-size classes (0.9 to 139 µm), while flow-through turbidity mainly shows increases of small particles (0.9 to 12.0 µm). The turbidity signal occurring between 8 and 12 h after start of irrigation corresponds to the breakthrough of the clayey loam suspension, which was released at the land surface 7.1 h after irrigation started (for details see Section 4.6 and Fig. 4.8).

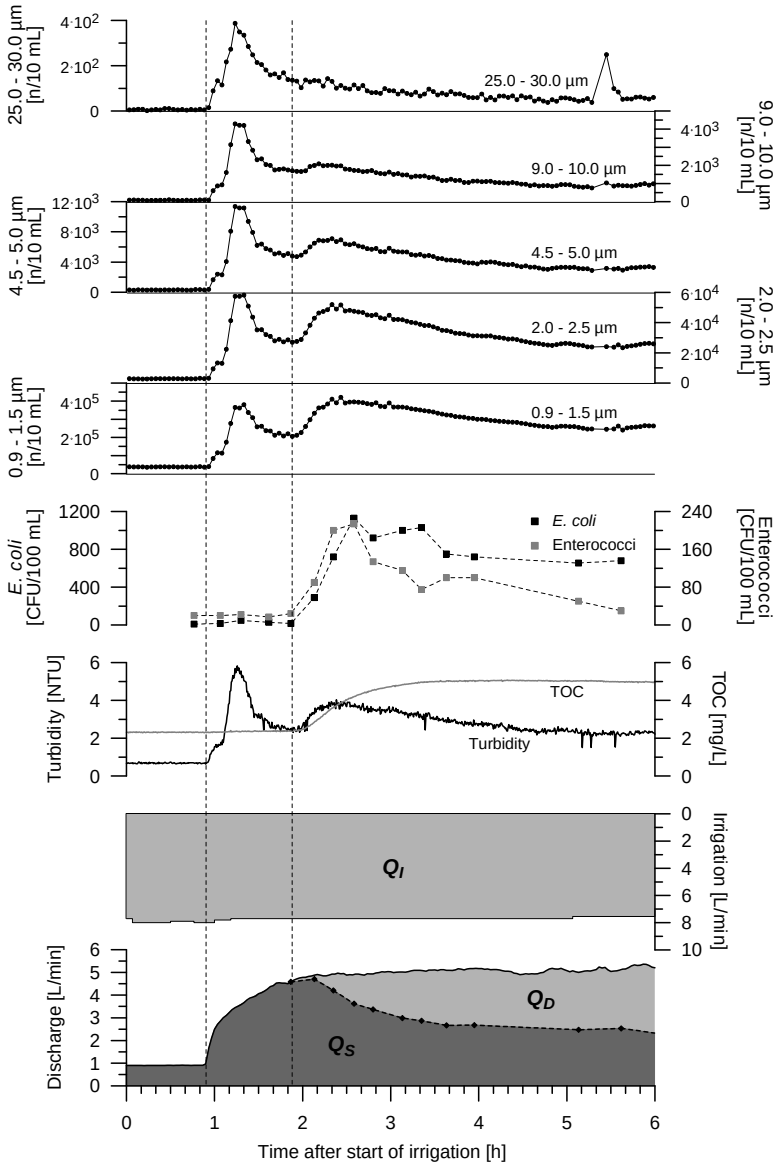

Fig. D.2 Temporal changes in *E. coli* and enterococci contents and PSD at the water outlet in the Vers-chez-le-Brandt cave during the October 2007 long-term irrigation experiment. Pulse-through turbidity is characterised by increases of all particle-size classes (0.9 to 139 µm), while flow-through turbidity mainly shows increases of small particles (0.9 to 12.0 µm).

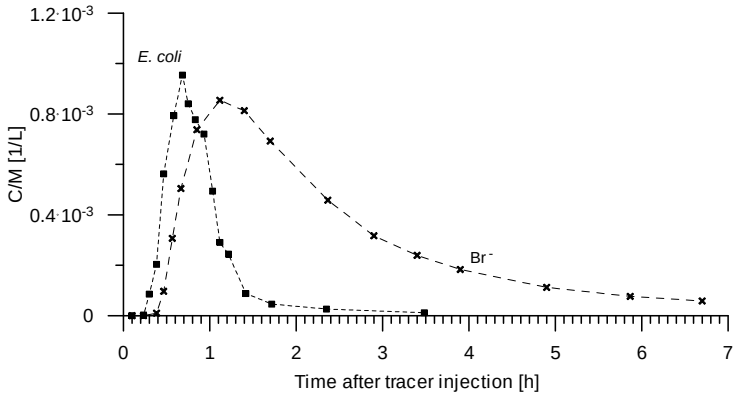

Fig. D.3 Results of the comparative tracer test carried out during steady-state flow regime at the Grand-Bochat cave site (September 2005 long-term irrigation experiment). C/M (ordinate) expresses concentrations normalised to bromide mass input and *E. coli* number input.

Appendix E

Microbial communities in karst groundwater and their potential use for biomonitoring

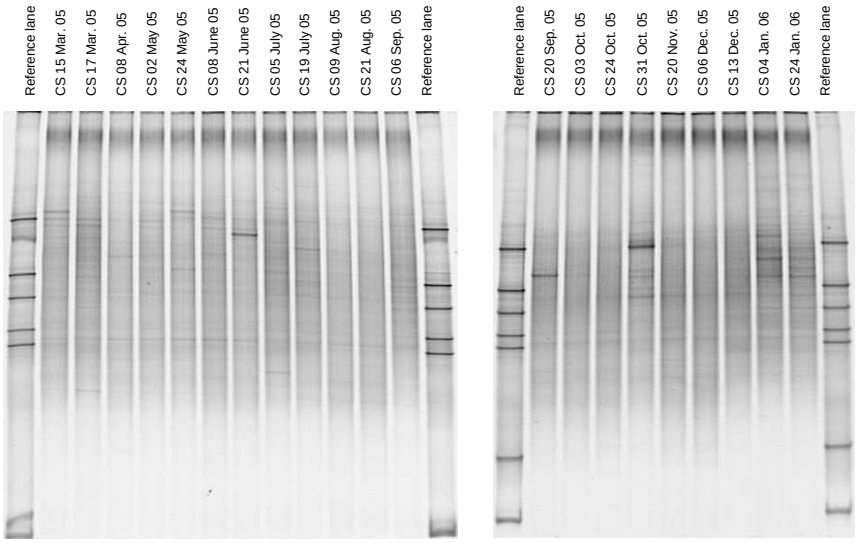

Fig. E.1 16S rDNA PCR-DGGE profiles of microbial communities in Cossaux spring (CS) water samples collected during the annual hydrological cycle.

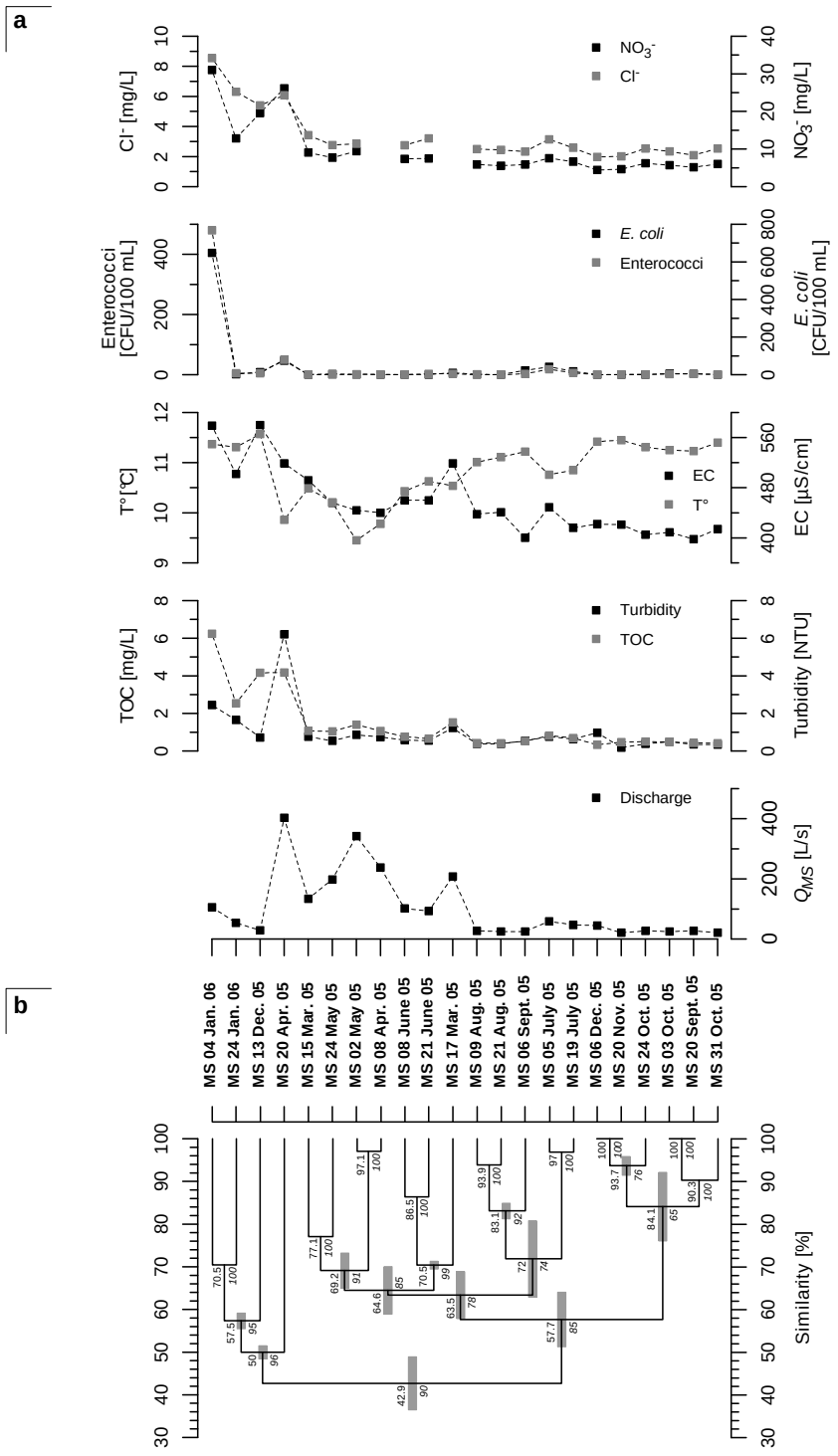

Fig. E.2 (**a**) Water quality characteristics of Moulinet spring water samples collected during the annual hydrological cycle. (**b**) Hierarchical cluster analysis of bacterial community fingerprints (16S rDNA PCR-DGGE profiles) from Moulinet spring water samples (Jaccard correlation and UPGMA). Error flags (grey bars), similarity (numbers) and cophenetic correlation coefficients (italic numbers) are shown. Q: discharge; EC: electrical conductivity; T°: temperature.

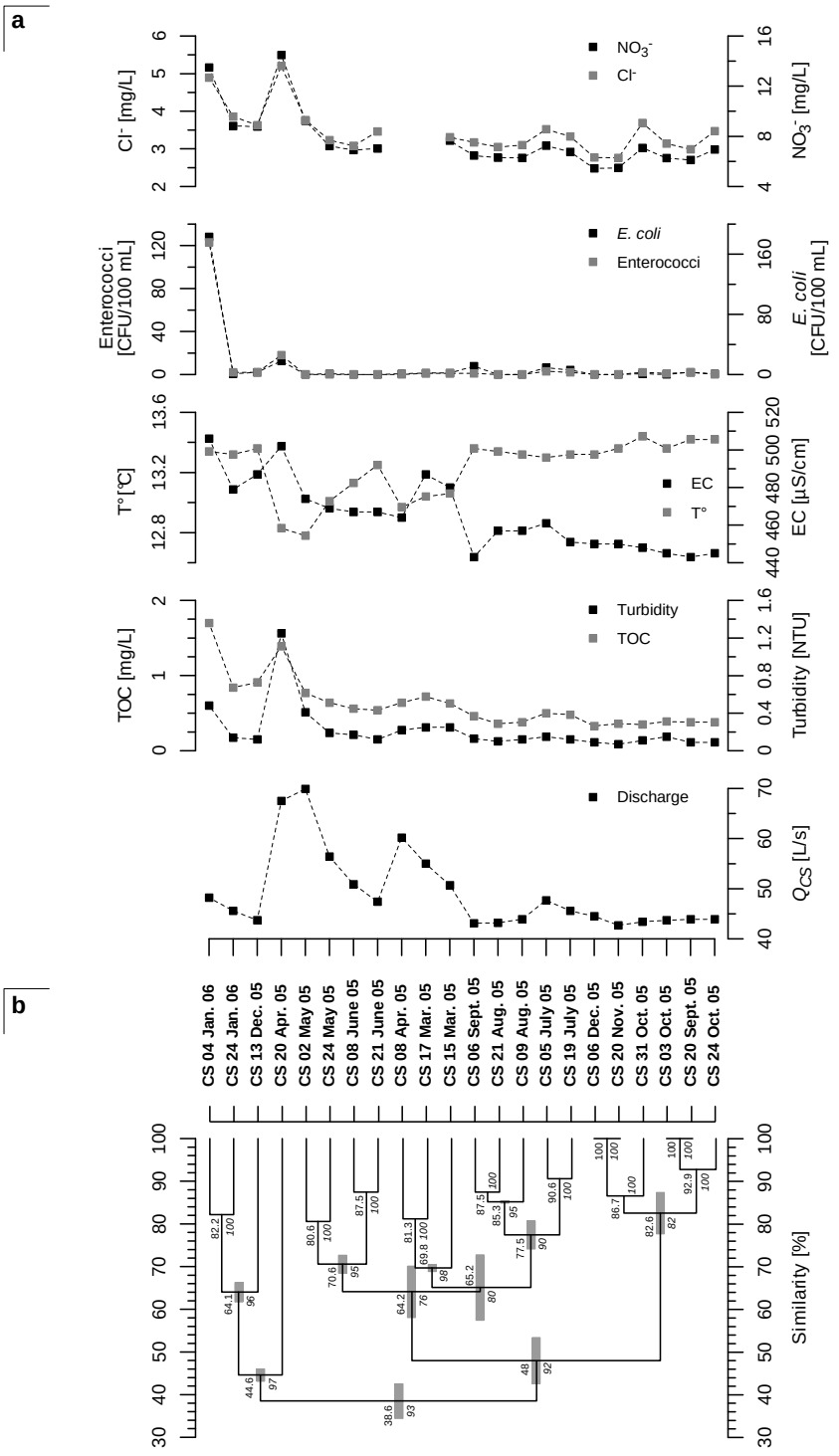

Fig. E.3 (**a**) Water quality characteristics of Cossaux spring water samples collected during the annual hydrological cycle. (**b**) Hierarchical cluster analysis of bacterial community fingerprints (16S rDNA PCR-DGGE profiles) from Cossaux spring water samples (Jaccard correlation and UPGMA). Error flags (grey bars), similarity (numbers) and cophenetic correlation coefficients (italic numbers) are shown. Q: discharge; EC: electrical conductivity; T°: temperature.

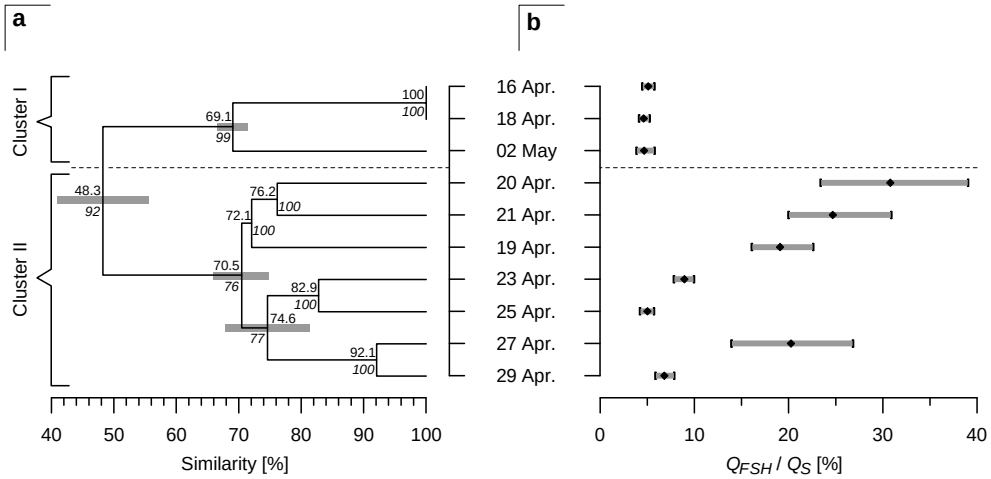

Fig. E.4 (**a**) Hierarchical cluster analysis of storm event 16S rDNA DGGE profiles of Cossaux spring water samples (Jaccard correlation and UPGMA). Error flags (grey bars), similarity (numbers) and cophenetic correlation coefficients (italic numbers) are shown. (**b**) Feurtille swallow hole contribution to the system discharge during the calculated infiltration time lag (Q_{FSH} / Q_S). Mean values (diamonds) with respective minimum and maximum values are shown. Sample dates are given along the vertical axis.

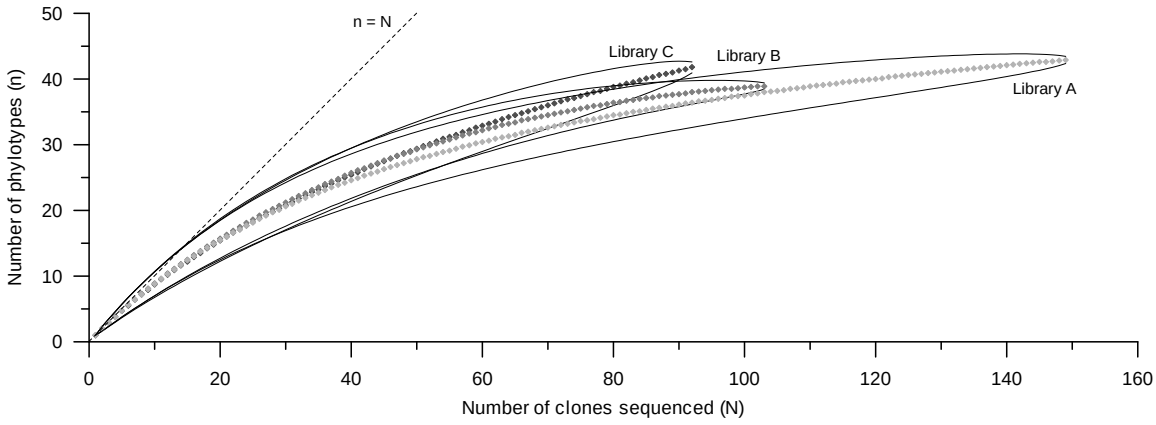

Fig. E.5 Rarefaction curves and 95 % confidence limits generated for 16S rDNA genes in clone libraries from Moulinet spring water samples. Library A: low swallow hole contribution; Library B: intermediate swallow hole contribution; Library C: high swallow hole contribution.

Table E.1 16S rDNA sequences recovered from spring water sample "MS 06 Dec. 05" (clone library A, low swallow hole contribution) and their closest affiliations.

Sequence	Redundancy [a]	Access. no.[b]	bp	Classification [c] / Closest affiliation [d]	S [e] [%]
M6A-455	1	AM991231	1392	domain unclassified *Bacteria* [100%] / uncultured bacterium KNA6-NB23 (AB179676)	94.0
M6A-566	1	AM991232	1461	class *Betaproteobacteria* [100%], family *Comamonadaceae* [100%] / *Betaproteobacterium* HIBAF001 (AB452981)	99.6
M6A-602	2	AM991233	931	domain unclassified *Bacteria* [99%] / uncultured organism MAT-CR-P3-C03 (EU246093)	93.2
M6A-605	1	AM991234	887	phylum *Nitrospira* [100%], genus *Nitrospira* [100%] / uncultured *Nitrospira* sp. Joinville8 (FJ236034)	99.6
M6A-607	4	AM991235	914	domain unclassified *Bacteria* [100%] / uncultured bacterium HDBW-WB69 (AB237732)	90.2
M6A-614	8	AM991236	1476	phylum *Acidobacteria* [100%], genus *Gp6* [100%] / uncultured *Acidobacteria* bacterium CM14G3 (EU132159)	98.6
M6A-615	7	AM991237	1466	class *Gammaproteobacteria* [100%], family *Xanthomonadaceae* [100%] / uncultured bacterium FFCH14140 (EU134748)	96.4
M6A-616	1	AM991238	1457	class *Betaproteobacteria* [100%], family *Oxalobacteraceae* [99%] / uncultured bacterium 12A-1 (DQ906892)	98.5
M6A-620	2	AM991239	1391	domain unclassified *Bacteria* [100%] / uncultured bacterium Elev_16S_392 (EF019223)	94.4
M6A-621	5	AM991240	1475	domain unclassified *Bacteria* [100%] / uncultured soil bacterium S042 (AF507707)	90.9
M6A-622	8	AM991241	1448	phylum unclassified *Bacteroidetes* [100%] / uncultured bacterium FFCH12595 (EU133712)	98.5
M6A-623	2	AM991242	1419	domain unclassified *Bacteria* [99%] / uncultured bacterium 82 (AB252962)	81.4
M6A-625	2	AM991243	1461	class unclassified *Betaproteobacteria* [100%] / uncultured bacterium P30B-60 (AF414584)	97.6
M6A-629	9	AM991244	890	class unclassified *Deltaproteobacteria* [98%] / uncultured bacterium KPF200711-168 (EU881160)	99.0
M6A-632	4	AM991245	1458	class unclassified *Deltaproteobacteria* [96%] / uncultured bacterium 080F71 (EU925875)	93.2
M6A-646	5	AM991246	1419	class unclassified *Alphaproteobacteria* [97%] / uncultured bacterium 5C231170 (EU803581)	93.2
M6A-658	1	AM991247	1443	phylum *Actinobacteria* [100%], class *Actinobacteria* [100%] / *Acidimicrobidae* bacterium Ellin7143 (AY673309)	98.9
M6A-661	4	AM991248	1482	class *Deltaproteobacteria* [100%], order *Myxococcales* [97%] / uncultured bacterium CI35cm.2.17a (EF208658)	91.8
M6A-662	1	AM991249	861	domain unclassified *Bacteria* [100%] / uncultured candidate division *OD1* bacterium Pav-OD6 (FJ482179)	99.4
M6A-663	2	AM991250	881	domain unclassified *Bacteria* [100%] / uncultured bacterium FFCH9380 (EU134908)	91.4
M6A-664	1	AM991251	1466	class *Betaproteobacteria* [100%], family *Rhodocyclaceae* [100%] / *Betaproteobacterium* KF033 (AB376631)	98.9
M6A-667	2	AM991252	877	domain unclassified *Bacteria* [100%] / uncultured bacterium 08 (AB252963)	92.5
M6A-670	6	AM991253	1469	class unclassified *Gammaproteobacteria* [100%] / uncultured bacterium FFCH11328 (EU134733)	97.4
M6A-671	1	AM991254	1469	phylum *Firmicutes* [100%], genus *Paenibacillus* [96%] / uncultured bacterium HOClCi60 (AY328609)	97.6
M6A-673	3	AM991255	926	class unclassified *Alphaproteobacteria* [100%] / uncultured *Rhizobium* sp. GI5-13-G07 (FJ192467)	88.2

[a] Number of identical sequences recovered from the "MS 06 Dec. 05" clone library

[b] Sequences are accessible at the EMBL Nucleotide Sequence Database under the respective accession numbers

[c] Classification was performed by using the Classifier algorithm (RDP). Respective confidence thresholds are given in brackets

[d] Closests affiliation was achieved by the SeqMatch algorithm (RDP). Accession numbers are given in parentheses

[e] Similarity to the closest affiliation calculated by the similarity matrix function (RDP)

Table E.1 *(cont.)* 16S rDNA sequences recovered from spring water sample "MS 06 Dec. 05" (clone library A, low swallow hole contribution) and their closest affiliations.

Sequence	Redundancy [a]	Access. no.[b]	bp	Classification [c] / Closest affiliation [d]	S [e] [%]
M6A-674	1	AM991256	938	phylum *Acidobacteria* [100%], genus *Gp6* [100%] / uncultured bacterium TX5A_32 (FJ152740)	98.7
M6A-677	7	AM991257	1463	class *Gammaproteobacteria* [100%], genus *Pseudomonas* [100%] / *Pseudomonas* sp. MFY138 (AY331366)	99.9
M6A-679	1	AM991258	1477	class unclassified *Deltaproteobacteria* [95%] / *Bacteriovorax* sp. R2IH3 (DQ631718)	84.1
M6A-680	4	AM991259	1483	class unclassified *Deltaproteobacteria* [97%] / uncultured bacterium CI35cm.2.14a (EF208656)	94.9
M6A-682	8	AM991260	888	class *Betaproteobacteria* [100%], family *Oxalobacteraceae* [100%] / uncultured bacterium FOOS7B_22 (EU431680)	100.0
M6A-687	4	AM991261	870	class unclassified *Gammaproteobacteria* [98%] / uncultured *Methylococcaceae* bacterium Elev_16S_1037 (EF019533)	95.7
M6A-688	1	AM991262	859	phylum *TM7* [100%], class *TM7_genera_incertae_sedis* [100%] / uncultured bacterium FFCH10712 (EU135375)	94.8
M6A-689	1	AM991263	935	domain unclassified *Bacteria* [100%] / uncultured bacterium 656064 (DQ404619)	79.5
M6A-691	1	AM991264	1461	class *Betaproteobacteria* [100%], family *Comamonadaceae* [100%] / *Betaproteobacterium* HIBAF001 (AB452981)	99.5
M6A-692	8	AM991265	844	domain unclassified *Bacteria* [100%] / uncultured bacterium 5C230825 (EU803277)	91.7
M6A-694	2	AM991266	920	phylum *Firmicutes* [100%], genus *Peptostreptococcaceae incertae sedis* [100%] / uncultured bacterium BH1_aao26b07 (EU466110)	99.9
M6A-696	5	AM991267	891	domain unclassified *Bacteria* [100%] / uncultured bacterium FFCH6028 (EU134390)	93.5
M6A-697	2	AM991268	896	domain unclassified *Bacteria* [100%] / uncultured soil bacterium S0145 (AF507709)	81.0
M6A-701	6	AM991269	865	phylum *Nitrospira* [100%], genus *Nitrospira* [100%] / uncultured bacterium CV64 (DQ499307)	100.0
M6A-704	1	AM991270	972	domain unclassified *Bacteria* [100%] / uncultured bacterium KNA6-NB14 (AB179670)	87.5
M6A-705	1	AM991271	733	phylum *TM7* [100%], class *TM7_genera_incertae_sedis* [100%] / uncultured bacterium FFCH13281 (EU135380)	97.0
M6A-707	5	AM991272	925	class *Betaproteobacteria* [100%], genus *Methylophilus* [100%] / uncultured bacterium 3C003274 (EU801895)	100.0
M6A-709	1	AM991273	1450	phylum unclassified *Bacteroidetes* [100%] / uncultured bacterium FCPS539 (EF516127)	95.1
M6A-713	4	AM991274	862	domain unclassified *Bacteria* [100%] / uncultured bacterium GIF19 (AF407207)	93.2
M6A-722	4	AM991275	1469	domain unclassified *Bacteria* [100%] / uncultured bacterium B39 (AM162486)	94.5

[a] Number of identical sequences recovered from the "MS 06 Dec. 05" clone library

[b] Sequences are accessible at the EMBL Nucleotide Sequence Database under the respective accession numbers

[c] Classification was performed by using the Classifier algorithm (RDP). Respective confidence thresholds are given in brackets

[d] Closests affiliation was achieved by the SeqMatch algorithm (RDP). Accession numbers are given in parentheses

[e] Similarity to the closest affiliation calculated by the similarity matrix function (RDP)

Table E.2 16S rDNA sequences recovered from spring water sample "MS 09 Aug. 05" (clone library B, intermediate swallow hole contribution) and their closest affiliations.

Sequence	Redundancy [a]	Access. no.[b]	bp	Classification [c] / Closest affiliation [d]	S [e] [%]
M6A-201	1	AM991192	919	phylum *Firmicutes* [100%], genus *Clostridium* [100%] / uncultured bacterium p-4786-2Wb2 (AF371838)	100.0
M6A-202	1	AM991193	1494	domain unclassified *Bacteria* [100%] / uncultured bacterium 2B-1 (DQ906782)	98.9
M6A-203	3	AM991194	1483	phylum *WS3* [100%], class *WS3_genera_incertae_sedis* [100%] / uncultured bacterium 21BSF64 (AJ863228)	97.8
M6A-204	4	AM991195	1465	class *Betaproteobacteria* [100%], genus *Thiobacter* [96%] / uncultured *Proteobacterium* EV221H2111601SAH33 (DQ223206)	98.1
M6A-206	2	AM991196	1469	phylum unclassified *Proteobacteria* [97%] / uncultured bacterium FFCH17316 (EU134330)	87.6
M6A-207	3	AM991197	893	class unclassified *Betaproteobacteria* [100%] / uncultured *Betaproteobacterium* AKYH490 (AY921821)	98.9
M6A-208	5	AM991198	895	phylum unclassified *Proteobacteria* [97%] / uncultured bacterium 1C226703 (EU799138)	91.6
M6A-211	2	AM991199	955	domain unclassified *Bacteria* [95%] / uncultured bacterium WM49 (DQ415768)	89.9
M6A-212	2	AM991200	1472	class *Deltaproteobacteria* [100%], genus *Bacteriovorax* [98%] / uncultured *Bacteriovorax* sp. MD2.17 (FJ403066)	92.4
M6A-213	1	AM991201	1439	phylum *Firmicutes* [100%], genus *Gracilibacter* [100%] / uncultured bacterium AKAU4083 (DQ125852)	93.2
M6A-214	3	AM991202	1450	domain unclassified *Bacteria* [100%] / uncultured bacterium Amb_16S_807 (EF018546)	92.8
M6A-215	4	AM991203	1499	domain unclassified *Bacteria* [99%] / uncultured bacterium GKS2-30 (AJ290044)	92.8
M6A-216	3	AM991204	1392	domain unclassified *Bacteria* [100%] / uncultured bacterium Won90(0625) (DQ839499)	83.8
M6A-217	1	AM991205	1481	phylum *Acidobacteria* [100%], genus *Gp6* [100%] / uncultured bacterium TX5A_37 (FJ152745)	98.3
M6A-218	2	AM991206	892	domain unclassified *Bacteria* [100%] / uncultured candidate division *OD1* bacterium MVP-5A-10 (DQ676436)	95.9
M6A-219	6	AM991207	947	class unclassified *Gammaproteobacteria* [98%] / uncultured bacterium FFCH6306 (EU134703)	98.6
M6A-220	2	AM991208	940	domain unclassified *Bacteria* [100%] / *Wolbachia* endosymbiont of *Onchocerca ochengi* (AJ010276)	74.9
M6A-222	2	AM991209	1377	domain unclassified *Bacteria* [100%] / uncultured candidate division *OP11* bacterium 49S1_2B_31 (DQ837245)	81.4
M6A-223	2	AM991210	1426	domain unclassified *Bacteria* [98%] / uncultured candidate division *OP11* bacterium RBE2CI-25 (EF111145)	98.5
M6A-224	2	AM991211	1471	class unclassified *Gammaproteobacteria* [98%] / uncultured bacterium FCPT525 (EF516073)	97.3
M6A-226	1	AM991212	1416	class *Alphaproteobacteria* [100%], genus *Acetobacter* [100%] / *Acetobacter orientalis* B-7SC (AB052707)	100.0
M6A-229	8	AM991213	947	class unclassified *Gammaproteobacteria* [100%] / uncultured bacterium aaa25h06 (DQ813856)	93.3
M6A-230	2	AM991214	888	phylum *Acidobacteria* [100%], genus *Gp6* [100%] / uncultured *Acidobacteria* bacterium TDNP_Wbc97_122_1_27 (FJ517004)	95.8
M6A-231	2	AM991215	884	domain unclassified *Bacteria* [100%] / uncultured archaeon Mn3b-B164 (FJ264554)	94.8
M6A-233	2	AM991216	1480	phylum unclassified *Proteobacteria* [100%] / uncultured bacterium B70 (FJ466056)	93.9

[a] Number of identical sequences recovered from the "MS 09 Aug. 05" clone library

[b] Sequences are accessible at the EMBL Nucleotide Sequence Database under the respective accession numbers

[c] Classification was performed by using the Classifier algorithm (RDP). Respective confidence thresholds are given in brackets

[d] Closests affiliation was achieved by the SeqMatch algorithm (RDP). Accession numbers are given in parentheses

[e] Similarity to the closest affiliation calculated by the similarity matrix function (RDP)

Table E.2 *(cont.)* 16S rDNA sequences recovered from spring water sample "MS 09 Aug. 05" (clone library B, intermediate swallow hole contribution) and their closest affiliations.

Sequence	Redundancy [a]	Access. no.[b]	bp	Classification [c] / Closest affiliation [d]	S [e] [%]
M6A-234	2	AM991217	925	class *Betaproteobacteria* [100%], family *Incertae sedis 5* [98%] / uncultured *Betaproteobacterium* Spb132 (AJ422163)	98.9
M6A-236	2	AM991218	923	domain unclassified *Bacteria* [100%] / uncultured candidate division *OP11* bacterium 49S1_2B_31 (DQ837245)	78.8
M6A-237	3	AM991219	954	class unclassified *Gammaproteobacteria* [100%] / uncultured bacterium MD2905-B8 (EU386120)	90.4
M6A-238	3	AM991220	1428	class *Alphaproteobacteria* [100%], genus *Odysella* [100%] / uncultured *Alphaproteobacterium* Hv(lakePohlsee)_38 (EF667926)	96.9
M6A-239	3	AM991221	1442	phylum *Firmicutes* [100%], genus *Turicibacter* [100%] / uncultured bacterium p-66-a5 (AF371535)	99.9
M6A-300	3	AM991222	940	domain unclassified *Bacteria* [100%] / *Phacus orbicularis* AICB 502 (AY626057)	97.0
M6A-303	2	AM991223	849	domain unclassified *Bacteria* [99%] / uncultured bacterium 655946 (DQ404818)	89.0
M6A-304	2	AM991224	1403	domain unclassified *Bacteria* [100%] / uncultured bacterium SK292 (AY882841)	77.1
M6A-308	10	AM991225	923	class *Alphaproteobacteria* [100%], genus *Novosphingobium* [100%] / uncultured bacterium EV818SWSAP5 (DQ337059)	99.9
M6A-310	2	AM991226	893	domain unclassified *Bacteria* [100%] / uncultured bacterium 82 (AB252962)	90.1
M6A-314	2	AM991227	1465	phylum *Nitrospira* [100%], genus *Nitrospira* [100%] / uncultured *Nitrospiraceae* bacterium D10_16 (EU266788)	99.7
M6A-316	1	AM991228	911	phylum *Firmicutes* [100%], genus *Lactobacillus* [100%] / *Lactobacillus oligofermentans* AMKR26 (AY733081)	99.6
M6A-343	2	AM991229	930	domain unclassified *Bacteria* [99%] / uncultured bacterium GKS2-30 (AJ290044)	92.3
M6A-347	1	AM991230	922	phylum unclassified *Proteobacteria* [97%] / uncultured bacterium HB108 (EF648097)	95.6

[a] Number of identical sequences recovered from the "MS 09 Aug. 05" clone library

[b] Sequences are accessible at the EMBL Nucleotide Sequence Database under the respective accession numbers

[c] Classification was performed by using the Classifier algorithm (RDP). Respective confidence thresholds are given in brackets

[d] Closests affiliation was achieved by the SeqMatch algorithm (RDP). Accession numbers are given in parentheses

[e] Similarity to the closest affiliation calculated by the similarity matrix function (RDP)

Table E.3 16S rDNA sequences recovered from spring water sample "MS 20 Apr. 05" (clone library C, high swallow hole contribution) and their closest affiliations.

Sequence	Redundancy [a]	Access. no.[b]	bp	Classification [c] / Closest affiliation [d]	S [e] [%]
M6A-34	2	AM991142	923	class unclassified *Alphaproteobacteria* [96%] / uncultured bacterium SWB04 (AB294315)	92.5
M6A-35	1	AM991143	1464	class *Gammaproteobacteria* [100%], genus *Pseudomonas* [100%] / *Pseudomonas fluorescens* Wuba22 (AF336349)	99.8
M6A-37	1	AM991144	1410	class *Alphaproteobacteria* [100%], genus *Devosia* [100%] / uncultured *Alphaproteobacterium* lhap9 (DQ648956)	98.4
M6A-39	6	AM991145	1484	phylum *Firmicutes* [100%], genus *Trichococcus* [100%] / *Trichococcus pasteurii* R-31594 (AM943044)	99.9
M6A-40	1	AM991146	1456	phylum *Bacteroidetes* [100%], genus *Prevotella* [100%] / uncultured *Bacteroidetes* bacterium ATB-LH-7189 (FJ535140)	99.0
M6A-41	2	AM991147	908	class *Alphaproteobacteria* [100%], genus *Paracoccus* [100%] / *Paracoccus alcaliphilus* ATCC 51199 (AY014177)	99.8
M6A-42	1	AM991148	881	phylum *Firmicutes* [100%], genus *Bacillus* [100%] / uncultured bacterium AKIW515 (DQ129323)	99.0
M6A-43	3	AM991149	930	phylum *Firmicutes* [100%], genus *Turicibacter* [100%] / uncultured bacterium p-66-a5 (AF371535)	99.9
M6A-44	2	AM991150	1372	class *Alphaproteobacteria* [100%], genus *Phenylobacterium* [100%] / uncultured *Alphaproteobacterium* APe9_7 (AB074623)	99.8
M6A-45	2	AM991151	918	phylum *TM7* [100%], class *TM7_genera_incertae_sedis* [100%] / uncultured bacterium SBR2013 (AF269000)	93.1
M6A-47	3	AM991152	911	phylum *Acidobacteria* [100%], genus *Gp6* [100%] / uncultured *Acidobacteria* bacterium lhad6 (DQ648904)	99.1
M6A-48	1	AM991153	890	phylum *Bacteroidetes* [100%], genus *Flavobacterium* [100%] / uncultured *Bacteroidetes* bacterium JG35-2-JT27 (AM084881)	96.5
M6A-49	3	AM991154	1461	class *Betaproteobacteria* [100%], family *Comamonadaceae* [100%] / uncultured bacterium SWB08 (AB294319)	99.4
M6A-52	1	AM991155	1406	phylum *Cyanobacteria* [100%], genus *Bacillariophyta* [100%] / uncultured bacterium KCLunmb_34_42 (FJ638599)	99.3
M6A-54	1	AM991156	1402	phylum *TM7* [100%], class *TM7_genera_incertae_sedis* [100%] / uncultured bacterium FFCH14101 (EU135382)	96.9
M6A-56	1	AM991157	897	class *Deltaproteobacteria* [100%], genus *Byssovorax* [94%] / uncultured bacterium FFCH16240 (EU134492)	98.1
M6A-59	2	AM991158	909	phylum *Bacteroidetes* [100%], genus *Pedobacter* [96%] / uncultured *Bacteroidetes* bacterium AKYG614 (AY922040)	99.5
M6A-61	1	AM991159	1443	phylum *Firmicutes* [100%], genus *Turicibacter* [100%] / uncultured bacterium AKIW620 (DQ129405)	99.9
M6A-62	1	AM991160	1461	class unclassified *Gammaproteobacteria* [99%] / uncultured bacterium 3BR-7DD (EU937896)	89.5
M6A-66	1	AM991161	926	class *Gammaproteobacteria* [100%], genus *Acinetobacter* [100%] / uncultured bacterium CE2_a08_2 (EU468005)	100.0
M6A-67	1	AM991162	917	phylum *Firmicutes* [100%], genus *Enterococcus* [100%] / *Enterococcus inusitatus* E2ET29 (AM050562)	100.0
M6A-68	1	AM991163	939	domain unclassified *Bacteria* [100%] / uncultured soil bacterium S1198 (AF507714)	91.5
M6A-70	3	AM991164	1470	class *Gammaproteobacteria* [100%], genus *Lysobacter* [100%] / *Lysobacter concretionis* (T) Ko07 (AB161359)	98.4
M6A-71	2	AM991165	953	class *Gammaproteobacteria* [100%], family *Enterobacteriaceae* [100%] / *Pantoea ananatis* JA04 (DQ365569)	100.0
M6A-73	1	AM991166	1427	phylum *Firmicutes* [100%], genus *Peptostreptococcaceae incertae sedis* [100%] / uncultured bacterium BH1_aao25c10 (EU773147)	99.9

[a] Number of identical sequences recovered from the "MS 20 Apr. 05" clone library

[b] Sequences are accessible at the EMBL Nucleotide Sequence Database under the respective accession numbers

[c] Classification was performed by using the Classifier algorithm (RDP). Respective confidence thresholds are given in brackets

[d] Closests affiliation was achieved by the SeqMatch algorithm (RDP). Accession numbers are given in parentheses

[e] Similarity to the closest affiliation calculated by the similarity matrix function (RDP)

Table E.3 *(cont.)* 16S rDNA sequences recovered from spring water sample "MS 20 Apr. 05" (clone library C, high swallow hole contribution) and their closest affiliations.

Sequence	Redundancy [a]	Access. no.[b]	bp	Classification [c] / Closest affiliation [d]	S [e] [%]
M6A-74	3	AM991167	1442	phylum *Firmicutes* [100%], genus *Clostridium* [100%] / uncultured bacterium SMC72 (AM183102)	99.6
M6A-76	3	AM991168	1455	class *Betaproteobacteria* [100%], family *Oxalobacteraceae* [100%] / uncultured *Proteobacterium* Elev_16S_731 (EF019469)	99.6
M6A-79	3	AM991169	918	class *Gammaproteobacteria* [100%], family *Enterobacteriaceae* [100%] / *Rahnella* sp. CDC 2987-79 (U88436)	99.9
M6A-81	1	AM991170	1453	phylum *Planctomycetes* [100%], family *Planctomycetaceae* [100%] / uncultured *Planctomycete* JdFBGBact_75 (DQ070834)	93.8
M6A-83	1	AM991171	892	phylum *Firmicutes* [100%], genus *Trichococcus* [100%] / uncultured bacterium B8 (EU234166)	99.9
M6A-85	1	AM991172	1444	domain unclassified *Bacteria* [100%] / uncultured bacterium 4C230497 (EU803079)	90.4
M6A-87	2	AM991173	1485	phylum *Firmicutes* [100%], genus *Trichococcus* [100%] / *Trichococcus pasteurii* R-31594 (AM943044)	99.9
M6A-89	1	AM991174	1457	class *Betaproteobacteria* [100%], family *Oxalobacteraceae* [100%] / uncultured *Proteobacterium* Elev_16S_731 (EF019469)	99.5
M6A-91	5	AM991175	1424	class *Alphaproteobacteria* [100%], genus *Odysella* [100%] / uncultured bacterium GW 15 (EU907894)	95.1
M6A-95	1	AM991176	1402	phylum *TM7* [100%], class *TM7_genera_incertae_sedis* [100%] / uncultured bacterium ARDRA0696 (EF451628)	98.8
M6A-96	2	AM991177	912	phylum *Firmicutes* [100%], genus *Trichococcus* [100%] / uncultured bacterium A59 (EU234092)	100.0
M6A-97	6	AM991178	901	phylum *Bacteroidetes* [100%], genus *Flavobacterium* [100%] / *Flavobacterium* sp. H7 (EU109724)	99.4
M6A-98	1	AM991179	942	class *Betaproteobacteria* [100%], genus *Herminiimonas* [100%] / *Herminiimonas fonticola* (T) S-94 (AY676462)	97.6
M6A-99	1	AM991180	1444	domain unclassified *Bacteria* [100%] / uncultured bacterium FCPT515 (EF516479)	97.6
M6A-100	2	AM991181	913	domain unclassified *Bacteria* [100%] / uncultured soil bacterium CWT ST01_F02 (DQ129144)	93.7
M6A-101	1	AM991182	889	domain unclassified *Bacteria* [100%] / uncultured bacterium SWB35 (AB294346)	96.8
M6A-102	1	AM991183	869	phylum *Firmicutes* [100%], genus *Trichococcus* [97%] / uncultured bacterium TSAS12 (AB186871)	94.3
M6A-104	2	AM991184	1429	phylum *Firmicutes* [100%], genus *Peptostreptococcaceae incertae sedis* [100%] / uncultured bacterium BH1_aao28e05 (EU466233)	99.6
M6A-106	3	AM991185	1489	domain unclassified *Bacteria* [100%] / uncultured bacterium FOOS7B_95 (EU431735)	99.4
M6A-115	1	AM991186	922	class *Alphaproteobacteria* [100%], genus *Sphingomonas* [100%] / *Sphingomonas faeni* (T) MA-olki (AJ429239)	99.9
M6A-119	2	AM991187	1457	class *Betaproteobacteria* [100%], genus *Duganella* [95%] / uncultured bacterium FD02G08 (FM873388)	99.9
M6A-122	2	AM991188	1455	class *Betaproteobacteria* [100%], family *Oxalobacteraceae* [100%] / uncultured *Proteobacterium* Elev_16S_731 (EF019469)	99.4
M6A-127	2	AM991189	1387	class *Alphaproteobacteria* [100%], genus *Brevundimonas* [100%] / *Brevundimonas* sp. FWC43 (AJ227798)	99.7
M6A-129	1	AM991190	1394	domain unclassified *Bacteria* [100%] / uncultured bacterium KNA6-NB23 (AB179676)	93.4
M6A-131	1	AM991191	1429	phylum *Firmicutes* [100%], genus *Peptostreptococcaceae incertae sedis* [100%] / uncultured bacterium gir_aah94h10 (EU775340)	99.8

[a] Number of identical sequences recovered from the "MS 20 Apr. 05" clone library

[b] Sequences are accessible at the EMBL Nucleotide Sequence Database under the respective accession numbers

[c] Classification was performed by using the Classifier algorithm (RDP). Respective confidence thresholds are given in brackets

[d] Closests affiliation was achieved by the SeqMatch algorithm (RDP). Accession numbers are given in parentheses

[e] Similarity to the closest affiliation calculated by the similarity matrix function (RDP)